UPPSALA
UNIVERSITET

Digital Comprehensive Summaries of Uppsala Dissertations from the Faculty of Science and Technology 76

Electromagnetic Interference in Distributed Outdoor Electrical Systems, with an Emphasis on Lightning Interaction with Electrified Railway Network

NELSON THEETHAYI

ACTA
UNIVERSITATIS
UPSALIENSIS
UPPSALA
2005

ISSN 1651-6214
ISBN 91-554-6301-0
urn:nbn:se:uu:diva-5889

Dissertation presented at Uppsala University to be publicly examined in Siegbahnsalen, Ångström Laboratory, Lägerhyddsvägen 1, Polacksbacken, Uppsala, Friday, September 30, 2005 at 13:30 for the degree of Doctor of Philosophy. The examination will be conducted in English.

Abstract
Theethayi, N. 2005. Electromagnetic Interference in Distributed Outdoor Electrical Systems, with an Emphasis on Lightning Interaction with Electrified Railway Network. (Elektromagnetisk interferens i distribuerade elektriska system för utomhusbruk, med fokus på växelverkan mellan blixtnedslag och elektrifierad järnväg). Acta Universitatis Upsaliensis. *Digital Comprehensive Summaries of Uppsala Dissertations from the Faculty of Science and Technology* 76. xxiv + 206 pp. Uppsala. ISBN 91-554-6301-0.

This thesis deals with the electromagnetic compatibility (EMC) problems of distributed electrical networks, especially that caused by lightning to electrified railway. Lightning transients were found to damage important devices that control train movements, causing traffic stoppage and delays. This thesis attempts to develop computational models for identification of parameters influencing the coupling phenomena between those devices and lightning. Some supporting experimental investigations are also carried out. This thesis forms the groundwork on the subject of lightning interaction with the electrified railway networks.

Lightning induces transient overvoltages in railway conductor systems such as tracks, overhead wires, and underground cables, either due to direct lightning strike to the system or due to the coupling of electromagnetic fields from remote strikes. Models based on multiconductor transmission line theory were developed for calculating the induced voltages and currents. A transmission line return stroke model, that can predict the remote electromagnetic fields comparable to experimental observations, is also developed.

Earlier works on modeling earth return impedances for transient studies in power distribution systems are not readily applicable for railways for lightning transients, in cases of low earth conductivities found in Sweden and for large variation in conductor heights. For the wires above ground, the ground impedance models were modified for wide range of frequencies, soil conductivities and wide spread of conductor heights. Influences of pole insulator flashovers, pole-footing soil ionizations and interconnections between the conductors on the lightning surge propagation are studied. Wave propagation in buried shielded and unshielded cables with ground return is studied. Simplified, valid and computationally efficient ground impedance expressions for buried and on-ground wires are proposed. A model for the coupling phenomena (transfer impedance) through multiple cable shields with multiconductor core is also proposed. Besides, experimental studies on lightning induced transients entering a railway technical house, failure modes of relay and rectifier units used in the train position/signaling applications for lightning transients are performed. A high frequency circuit model for the booster transformer for lightning interaction studies is developed. The simulation models are being converted to user-friendly software for the practicing engineers of the railway industry.

Keywords: Electromagnetic Compatibility (EMC), Lightning, Lightning Protection, Transmission Lines, Electromagnetic Wave Propagation, Underground Cables, Grounding, Electromagnetic Transients, Electromagnetic Interference, Shielding Effectiveness, Railway Systems

Nelson Theethayi, Department of Engineering Sciences, Box 534, Uppsala University, SE-75121 Uppsala, Sweden

ISSN 1651-6214
ISBN 91-554-6301-0
urn:nbn:se:uu:diva-5889 (http://urn.kb.se/resolve?urn=urn:nbn:se:uu:diva-5889)

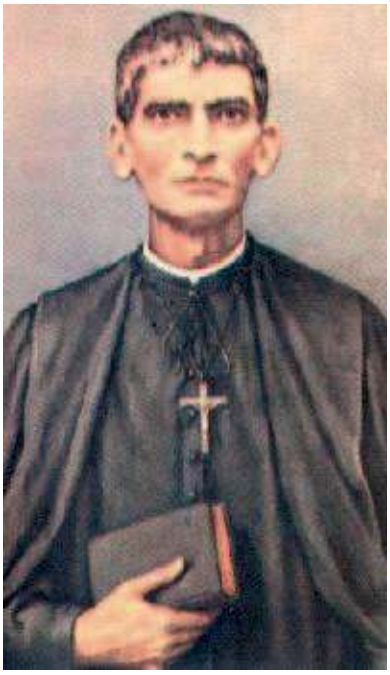

Venerable Fr. Agnelo Gustav de Souza (1869-1927)

Dedicated to his saintly life and to his important teachings.
His sayings has been an integral part of my academic life.
"One who fulfils his duties faithfully is on the way to perfection."
"One must not leave off a good action on account of the criticism of others."

2003 IEEE Bologna Power Tech
23-26 June, 2003

High Quality Paper Certificate

to

Nelson Theethayi

for the presentation of the paper "Parameters that Influence the Crosstalk in Multiconductor Transmission Line" by N. Theethayi, R. Thottappillil, Y. Liu and R. Montano

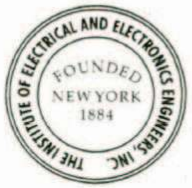

Carlo Alberto Nucci

Prof. Carlo Alberto Nucci
Chair, 2003 IEEE Bologna Power Tech

2003 IEEE Bologna Power Tech
23-26 June, 2003

High Quality Paper Certificate

to

Nelson Theethayi and Ms. Liu

for the presentation of the paper "Modeling Direct Lightning Attachment to Electrified Railway System in Sweden" by N. Theethayi, Y. Liu, R. Montano, R. Thottappillil,M. Zitnik, V. Cooray and V. Scuka

Prof. Carlo Alberto Nucci
Chair, 2003 IEEE Bologna Power Tech

List of Papers

The following papers (either published or under review) have resulted during the four year doctoral study. The main theme of this thesis is Electromagnetic compatibility (EMC) and Lightning Protection. Hence the papers listed below are directly or indirectly connected to the subject of the thesis.
The following nomenclature is adopted for a proper classification:
♣ : largely connected with the thesis - included in the thesis.
♢ : largely connected with the thesis - not included in the thesis.
♠ : popular subject and/or general knowledge/awareness in EMC and lightning - included in the thesis.
♡ : partially connected with the thesis - not included in the thesis.

I **Theethayi N**, Liu Y, Montano R and Thottappillil R, "On the influence of conductor heights and lossy ground in multiconductor transmission lines for lightning interaction studies in railway overhead traction systems", *Journal of Electric Power Systems Research*, Vol. 71, No. 2, 2004, pp. 186-193.♣ **[Paper-A available in Appendix-A]**

II **Theethayi N**, Thottappillil R, Liu Y and Montano R, "Importance of ground impedance in the study of parameters that influence crosstalk in multiconductor transmission line". *Paper in review at Journal of Electric Power Systems Research - first version*.♣ **[Paper-B available in Appendix-B]**

III **Theethayi N**, Thottappillil R, Liu Y and Montano R, "Parameters That Influence the Crosstalk in Multiconductor Transmission Line", *Proceedings of IEEE Bologna Power Tech. Conference*, Bologna, Italy, 2003.♢ **Received IEEE student paper award for high quality paper**.

IV **Theethayi N**, Liu Y, Montaño R and Thottappillil R, "Crosstalk in Multiconductor Transmission Line in the Presence of Finitely Conducting Ground", *Proceedings of the IEEE International Symposium on Electromagnetic Compatibility*, Istanbul, Turkey, 2003.♢

V **Theethayi N**, Liu Y, Montano R, Thottappillil R, Zitnik

M, Cooray V and Scuka V, "A Theoretical Study on the Consequence of a Direct Lightning Strike to Electrified Railway System in Sweden", *Journal of Electric Power Systems Research*, Vol. 74, No. 2, 2005, pp. 267 -280.♣ **[Paper-C available in Appendix-C]**

VI **Theethayi N**, Liu Y, Montano R, Thottappillil R, Zitnik M, Cooray V and Scuka V, "Modeling Direct Lightning Attachment to Electrified Railway System in Sweden", *Proceedings of IEEE Bologna Power Tech. Conference*, Bologna, Italy, 2003.♢ **Received IEEE student paper award for high quality paper**.

VII **Theethayi N** and Cooray V, "On the representation of the lightning return stroke process as a current pulse propagating along a transmission line", *IEEE Transactions on Power Delivery*, Vol. 20, No. 2, 2005, pp. 823 - 837.♣ **[Paper-D available in Appendix-D]**

VIII Thottappllil R, Uman M A and **Theethayi N**, "Electric and magnetic fields from a semi-infinite antenna above a conducting plane", *Journal of Electrostatics*, Vol. 61, No.3-4, 2004, pp. 209 - 221.♣ **[Paper-E available Appendix-E]**

IX **Theethayi N** and Cooray V, "Representation of the return stroke as a transmission line: the apparent return stroke velocity", *Proceedings of International Conference on Lightning Protection*, Avignon, France, 2004.♣,♠ **[Paper-F available in Appendix-F]**

X **Theethayi N** and Cooray V, "The transmission line model idealisation and reality", *Proceedings of IEEE Bologna Power Tech. Conference*, Bologna, Italy, 2003.♢

XI **Theethayi N**, Yirdaw T, Liu Y, Götschl T and Thottappillil R, "Experimental Investigation of Lightning Transients Entering a Swedish Railway Facility". *Paper in review at IEEE Transactions on Power Delivery - first version*.♣ **[Paper-G available in Appendix-G]**

XII **Theethayi N**, Liu Y, Thottappillil R, Götschl T, Montano R, Lindeberg P A and Hellstrom U, "Measurements of Lightning Transients Entering a Swedish Railway Facility", *Proceedings of International Conference on Lightning Protection*, Avignon, France, 2004.♢

XIII **Theethayi N** and Thottappillil R, "Lightning current pulse propagation in underground wires - a transmission line analysis: Part I-Simple expressions for external wire impedance and admittance". *Paper in review at IEEE Transactions on Power Delivery - second revised version*.♣ **[Paper-H available in Appendix-H]**

XIV **Theethayi N** and Thottappillil R, "Lightning current pulse propagation in underground wires - a transmission line analysis: Part II- Time domain simulations for sensitivity analysis". *Paper in review at IEEE Transactions on Power Delivery - second revised version*.♣ **[Paper-I available in Appendix-I]**

XV **Theethayi N** and Thottappillil R, "Pulse Propagation in Underground Wires-A Transmission Line Analysis", *Proceedings of RadioVetenskap och Kommunikation (RVK 05)*, Linkoping, Sweden, 2005.♣ **[Paper-J available in Appendix-J]**

XVI Thottappillil R and **Theethayi N**, "Lightning strikes to tall towers with implications to electromagnetic interference", *Proceedings of RadioVetenskap och Kommunikation (RVK 05)*, Linkoping, Sweden, 2005.♣,♠ **[Paper-K available in Appendix-K]**

XVII Thottappillil R, **Theethayi N**, Liu Y, Scuka V, Zitnik M, Lindeberg P A, Hellstrom U, "Computer simulation model for Swedish railway system for evaluating the effects of lightning and EMI", *World Congress on Railway Research*, Edinburgh, England, 2003.♣ **[Paper-L available in Appendix-L]**

XVIII Cooray V and **Theethayi N**, "The striking distance of lightning flashes and the early streamer emission (ESE) hypothesis", *Proceedings of International Conference on Lightning Protection*, Avignon, France, 2004 (recommended by ICLP committee for possible publication in Journal of Electrostatics).♠ **[Paper-M available in Appendix-M]**

XIX Cooray V, Rakov V and **Theethayi N**, "The relationship between the leader charge and the return stroke current - Berger's data revisited", *Proceedings of International Conference on Lightning Protection*, Avignon, France, 2004 (recommended by ICLP committee for possible publication in Journal of Electrostatics).♠ **[Paper-N available in Appendix-N]**

XX Liu Y, **Theethayi N**, Thottappillil R, Gonzalez R M and Zitnik M, "An improved model for soil ionization around grounding system and its application to stratified soil", *Journal of Electrostatics*, Vol. 60, No. 2-4, 2004, pp. 203 - 209.♢

XXI Liu Y, **Theethayi N** and Thottappillil R, "An engineering model for transient analysis under lightning strikes: Non - uniform transmission line approach", *IEEE Transactions on Power Delivery*, Vol. 20, No. 2, 2005, pp. 722 - 730.♢

XXII Cooray V, Montano R, **Theethayi N**, Zitnik M, Manyahi M and Scuka V, "A channel base current model to represent both negative and positive first return strokes with connecting leaders." *Proceedings of the International Conference on Lightning Pro-*

tection, Cracow, Poland, 2002.♡

Author's Request: This work, a result of the author's research during 2001-2005 for the doctoral degree in the Uppsala University, contains certain unpublished material. This has been marked accordingly in the thesis as ¶. The author reserves his right to publish it at appropriate times. If any of the unpublished material is taken for reproduction, further study or modification, it shall be duly acknowledged giving reference to this thesis.

Contents

1 Introduction 1
1.1 Background 1
1.2 How to begin this study? 6
1.3 Single track overhead traction system of the Swedish railways and the associated components 7
1.4 Skeleton of the thesis 10
2 Direct and Indirect Lightning Strikes to Outdoor Conductor System of Swedish Railways 15
2.1 Lightning current and electromagnetic field parameters 15
2.2 Direct strikes on the railway systems 18
2.3 Indirect strikes to railway systems 22
2.4 Conclusions 24
3 Genesis of Transmission Line Theory 27
3.1 What our good old masters did? 27
3.2 Wave propagation aspects 31
3.3 Transmission Line equations (Telegrapher's equations) 34
3.4 Circuit representation of transmission lines 40
3.5 Solutions to Two Conductor Transmission Line equations 44
3.6 Conclusions 46
4 Wave Propagation in Multiconductor Transmission Lines above Ground 47
4.1 Telegrapher's equations for MTLs 47
4.2 Internal losses in telegrapher's equations - conductor skin effect 50
4.2.1 Skin effect phenomena 50
4.2.2 Internal impedance for circular wires ¶ 51
4.2.3 Internal impedance in time domain ¶ 53
4.3 External loss in telegrapher's equations - dissipative or lossy ground 56
4.3.1 Ground impedance and its role in telegrapher's equations . 56
4.3.2 Earth's behavior to incident electromagnetic fields and the transmission line limit for wires above ground 59
4.3.3 Ground impedance expression for above ground wires - A comparative overview ¶ 60

4.3.4 Ground impedance in time domain - transient ground impedance ¶ 70
4.4 Solutions of telegrapher's equations in frequency and time domain 75
4.4.1 Frequency domain solution for MTLs 75
4.4.2 Time domain solutions for MTLs - FDTD method 78
4.5 Conclusions 84
5 Calculations of Lightning Induced Surges in Swedish Railway Overhead System 85
5.1 How are the Swedish railway traction and power line systems different from the conventional overhead power lines? 85
5.2 Parameters that influence lightning induced over voltage (LIOV) phenomena in MTLs 88
5.2.1 Current waveform used for the present study in the thesis for the sake of discussions 88
5.2.2 Direct strike pulse propagations on MTLs ¶ 89
5.2.3 Indirect strikes pulse propagation on MTLs 93
5.2.4 Application of the above modeling concepts to single-track railway system 108
5.3 Lightning strike to Swedish railway MTLs system: Incorporating non-linear phenomena and interconnection between the line conductors 110
5.3.1 Modeling interconnection 110
5.3.2 Modeling insulator flashover and soil ionization phenomena 113
5.3.3 Some important conclusions for a direct strike of $31kA$ to the auxiliary conductors of the single-track railway system from *Theethayi et al.* [74 **Paper-C**] 114
5.4 Conclusions 115
6 Measurements of lightning transients entering a Swedish railway facility 117
6.1 Measurement setup 117
6.2 Lightning induced events recorded by the measurement system ¶ 121
6.3 Conclusions 126
7 Current Pulse Propagation in Underground Wires - A transmission line analysis ¶ 127
7.1 Telegrapher's equations for the buried wires with earth as return 128
7.2 Ground impedance and admittance for buried wires 130
7.3 Limits of transmission line approximation 136
7.4 Validation of the proposed transmission line model 140
7.5 Ground impedance for wires on the surface of ground 142
7.6 Conclusions 145

8 Coupling to cable core through cable shields ¶ 147
8.1 Generalized double shield three core cable 148
8.1.1 Telegrapher's equations for shielded cables 148
8.1.2 Transmission line impedance and admittance parameters . 151
8.2 An example of RG-58 cable 155
8.3 An example of ELEK 3G 1.5 - three-conductor power cable . . 158
8.3.1 Line inductance and capacitance measurements 160
8.3.2 An experimental validation of the model 162
8.4 Can the transients entering to shield of the cable be diverted? . 164
8.5 Conclusions 167
9 Transient response of booster transformer and track circuit equipment 169
9.1 Booster transformer ¶ 169
9.1.1 Short circuit tests on booster transformer 170
9.1.2 Terminal model for the booster transformer 171
9.1.3 Fitting admittance functions 174
9.2 Track circuit withstand tests 177
9.3 Conclusions 180
10 My thesis: What else? 181
11 Sammanfattning 187
References 195

List of Tables

1.1 Conductor nomenclatures 8
1.2 Material properties 10

2.1 Electric and Magnetic fields associated with lightning [17 - 19] 18

3.1 Twenty variables originally used by Maxwell in his dynamical theory of the electromagnetic field adapted from [36] 29

4.1 Earth's behavior to incident electromagnetic waves corresponding to critical frequency ω_c 59

5.1 Impulse withstand voltages of the insulators for the single-track MTLs system 86
5.2 Geometrical details of the conductors used in single-track railway systems in Sweden 108

List of Figures

1.1 A typical traction conductor system layout, Source: http://www.railway-technical.com/etracp.html 2
1.2 Track circuits (relay and track feed) connection across the rails, Source: Banverket signalteknisk information, dokument nr. 95088, http://www.banverket.se 2
1.3 A typical traction power supply feeding system, Source: Indian Railways fan club, http://irfca.org 3
1.4 Different types of traction systems (Single Catenary (SC), Booster Transformer (BT) and Autotransformer (AT)) used in railways, Source: Indian Railways fan club, http://irfca.org . 4
1.5 Railway lines near Gistad, which shows the complexity of MTLs 8
1.6 Geometry of the single-track Swedish railway system (axes in meters) 9
1.7 Telecommunication cable used in Banverket systems 11
1.8 Typical booster transformer used in the Banverket systems . . . 12
1.9 Typical rectifier unit used in the track circuits 13
1.10 Typical relay unit used in the track circuits 13

2.1 Striking distance for a given conductor held by tower of given height 19
2.2 Collection surface offered by a single-track railway system to a descending stepped leader with prospective return stroke amplitude of $5kA$ and $100kA$ 20
2.3 Surface arcs (left panel) and penetration of stroke (right panel) into the ground (adapted from [21]) 22
2.4 Current waveforms measured at tower bottom for a flash with two subsequent strokes by Eriksson 23
2.5 Sketch showing field illumination phenomena due to return strokes and the consequent representation of field to wire coupling phenomena by means of distrib-uted voltage sources . . . 25

3.1 Uniform plane wave: propagation direction and direction of magnetic and electric fields 32

3.2 Application of Maxwell's curl equations for derivation of telegrapher's equation (adapted from [42]) 36
3.3 Distributed source locations on the line for incident field excitation (adapted from [42]) 39
3.4 Circuit representation of a two-wire transmission line 41
3.5 T model representation of the transmission line 44
3.6 Schematic of the transmission line under analysis for equation (3.42) 45

4.1 System of MTLs above a perfect ground plane 48
4.2 Plane solid conductor for demonstrating skin effect phenomena (adapted from [47]) 52
4.3 Internal impedance for rails and overhead wire using exact and approximate expression 54
4.4 Current responses at injection point, 400m and 800m using Wedepohl and Wilcox (solid red) and Nahman and Holt (dotted black) expressions for internal impedance for fast and slow impulse current injections 55
4.5 Single conductor above a dissipative semi-infinite earth (adapted from [42] and modified) 57
4.6 Allocation of conductors' k and l and their images k´ and l´ with a skin depth of p [57] 62
4.7 Ground impedance amplitude curves for a conductor at different heights and with different ground resistivity 67
4.8 Ground impedance argument response corresponding to conductor at (top) 0.5m height, $\sigma_g = 2mS/m$ and (below) 10m height, $\sigma_g = 0.1mS/m$ 68
4.9 Intrinsic impedance for various ground conductivities 69
4.10 Penetration depth of electromagnetic fields in the ground for various ground conductivities 70
4.11 Simulations for demonstrating the lack of importance of ground admittance for rail conductors above ground for fast (top) and slow (bottom) impulses, no change in rail current whether one uses ground admittance or not 75
4.12 Emitter and receptor setup for studying the induced voltage on the receptor for a current injection at the near end of the emitter 81
4.13 Simulations for the Case-R-UP (receptor height is 10m), with different number of exponential terms for transient ground impedance 82

4.14 Simulations for the Case-R-DOWN (receptor height is 0.5m), with different number of exponential terms for transient ground impedance 82
4.15 Responses at the near and far end loads of the receptor (0.5m height) - based on FD-IFFT and FDTD methods 83

5.1 Schematic diagram of insulators and the connection of the track to the pole footing [74] 87
5.2 Interconnection between conductors R5, R6, R1 87
5.3 A typical subsequent stroke current waveform and its derivative 89
5.4 Direct stroke to the midpoint of the emitter line 90
5.5 Induced voltage at the points S, M, L corresponding to direct strike at middle of emitter for various ground conductivities, for receptor height 10m and 0.5m 91
5.6 Vertical electric fields at ground level from subsequent strokes at 100km (adapted from [83]) 94
5.7 A typical example of vertical electric field at ground level (left) and the corresponding magnetic field (right) at 5km from the stoke (adapted from [82]), with return stroke field starting at t=0 95
5.8 A typical example of vertical electric field at ground level, at 50m distance from the stroke, with return stroke field starting at t=0, (triggered lightning experiment [84]) 95
5.9 A return stroke current segment in air and its image for the field calculations at any point in air medium 97
5.10 Electromagnetic fields from the return stroke transmission line model proposed by Theethayi and Cooray in [93] 101
5.11 Equivalent transmission line representation for lightning induced voltage calculation: Agrawal et al. [33] coupling model used for horizontal field contribution 102
5.12 Schematic showing an indirect lightning stroke at a horizontal distance of 50m from the point S on the line for induced voltage calculations 102
5.13 Vertical and Horizontal electromagnetic fields: stroke at r=50m and for different ground conductivities 104
5.14 Induced voltages due to indirect strike at the points S, M, L on the line, which is at a height of 10m above a perfect ground 105
5.15 Induced voltages due to indirect strike: line height h=10m, for various ground conductivities 107
5.16 Induced voltages due to indirect strike: line height h=0.5m, for various ground conductivities 109

5.17 Induced voltage on all the conductors of Fig. 1.6 at points S, M and L due to a direct strike on conductor R7 111
5.18 Induced voltage on all the conductors of Fig. 1.6 at points S, M and L due to an indirect strike at 50m horizontal distance from the line center of R7 112
5.19 Schematic shown an interconnection in MTLs system 113

6.1 Cable termination at the auxiliary power conductors 118
6.2 Inside technical house where the measurements are made, Ch0-Electric Field, Ch1-Voltage across Phase and neutral, Ch2-Phase Current and Ch3-local ground to S-rail current . . . 119
6.3 Vertical electric field measuring system for lightning 119
6.4 Terminations at the DAQ system 120
6.5 Line to neutral voltage and line current measurement point . . . 122
6.6 Local ground to S-rail connection 122
6.7 Location of the strokes corresponding to FLASH - 30 (each square has a size of 1sq.km) as per the Swedish lightning location network 123
6.8 Electric field waveform due to FLASH - 30 (magnitude in arbitrary units) 124
6.9 Line to neutral voltage and local ground to S-rail current waveforms for FLASH - 30 125

7.1 Schematic diagram of grounding conductors considering the tower and building as separate units (not to scale) 128
7.2 Bare and insulated conductor system in the soil under study . . 129
7.3 Per unit length transmission line representation for bare and insulated conductor system in the soil under study 129
7.4 Ground impedance comparisons between Sunde, Wait, Saad et al., Log and Log-Exp expressions: ground relative permittivity is 10 and wire buried at 0.5m depth 134
7.5 Ground impedance and admittance magnitude response for various ground conductivities for bare wire buried at 0.5m depth and ground relative permittivity is 10 135
7.6 Simulations demonstrating the importance of ground admittance in pulse propagations with ground conductivity 1mS/m and ground relative permittivity of 10 136
7.7 Penetration depth at which the currents return in the soil for underground wires and wavelength in the soil for ground relative permittivity of 10 and 40 for various ground conductivities 138
7.8 Verification - 1 simulated using the present transmission line model for buried bare wire 141

7.9 Verification - 1 simulated by the authors of [123] using complex electromagnetic field approach (left window) and complicated circuit approach (right window): figure is adapted from [123] 141
7.10 Influence of current rise time on effective length Verification-2 and Verification-3 143
7.11 Comparison between Sunde (7.16) and Modified-logarithmic formula (7.17) for the ground impedance of the wires on the surface of the earth 144

8.1 Generalized three-conductor cable arrangement for studying the coupling between the shields and internal conductors 149
8.2 Non twisted parallel conductor arrangement in the shield for MTL parameter estimation for multi-conductor cable adapted from [12, 41] 154
8.3 Triax setup for measuring the transfer impedance 157
8.4 Frequency domain response of the ratio of open circuit voltage and shield current for two shield thicknesses, Time domain response of the transfer impedance obtained from fitting the frequency response of the ratio of open circuit voltage and shield current - equivalent to convolution in time domain 159
8.5 Time domain response of the internal open circuit voltages for two shield thicknesses 160
8.6 Capacitance distribution in three conductor ELEK 3G-1.5 . . . 161
8.7 Various capacitance combinations for generalized independent equations (8.22) 161
8.8 Injected current into the shield for experiment 163
8.9 Comparison between experiment and simulation for three-conductor cable 164
8.10 Arrangement of cable and follow on earth wire 165
8.11 Example of 500m long cable showing the advantage of follow on earth wire for diverting the surge currents 166

9.1 The booster transformer positions and connections 170
9.2 Schematic showing the setup for short circuit transformer tests 171
9.3 Experimentally measured currents and voltages at the primary and secondary of the booster transformer for voltage injection in the primary 172
9.4 Schematic of a linear two-port network 173
9.5 π model of the booster transformer used for modeling 173
9.6 The RLCG model of the transformer adapted from [102, 136, 137] 174

9.7 Comparison between the actual driving point admittance function and its corresponding circuit representation in frequency domain 176
9.8 Comparison between the experiment and the simulations based on the π model circuit for the short circuit test 177
9.9 Configurations of tests conducted on the rectifier unit 178
9.10 Experimental setup for the I-Rail injection tests for the relay . 179

10.1 Client user interface window (top) and a typical client-server system 183
10.2 Edit geometry window, location and positioning the stroke, ground properties 184
10.3 The window showing the instruments and a typical simulation result 185

List of Important Symbols

r_s	Striking distance
r_w	Radius of the wire
h	Height in general
d	Depth in general
I_S	Prospective return stroke current
σ	Conductivity of medium or material in general
σ_g	Ground conductivity
μ	Permeability of medium or material in general
μ_0	Permeability of free space
ε	Permittivity of medium or material in general
ε_0	Permittivity of free space
ε_g	Ground permittivity
j	Imaginary unit with property $j = \sqrt{-1}$
$\Re$	Real part
$\Im$	Imaginary part
ω	Angular frequency
s	Laplace operator in Laplace transforms
λ	Wavelength
v	Velocity of the wave
γ	Wave propagation constant in general
γ_g	Ground wave propagation constant
α	Wave attenuation constant
β	Wave phase constant
∇	Gradient vector
$\vec{E}$	Electric field vector
$E_\_$	Magnitude of electric field in _ direction
$\vec{H}$	Magnetic field intensity vector
$H_\_$	Magnitude of magnetic field intensity in _ direction

$\vec{D}$	Electric flux density vector
$D_{\_}$	Magnitude of electric flux density in _ direction
$\vec{B}$	Magnetic flux density vector
$B_{\_}$	Magnitude of magnetic flux density in _ direction
$\vec{J}$	Current density vector
$J_{\_}$	Magnitude of current density in _ direction
$E^{inc/sca}$	Magnitude of incident/scattered electric field
$H^{inc/sca}$	Magnitude of incident/scattered magnetic field intensity
V	Voltage in general
I	Current in general
R	Resistance in general
$R_{DC/dc}$	DC resistance
L	Inductance in general
L_e	External inductance
L_i	Internal inductance
G	Conductance in general
C	Capacitance in general
C_e	External capacitance
Z	Impedance in general
Z_{iint}	Internal impedance of the conductor
$Z_{g...}$	Ground impedance in general
Z_{si}	Surface impedance of the ground
Z_T	Transfer impedance of the cable shield
Y	Admittance in general
Y_g	Ground admittance in general
Z_0	Characteristic impedance
ρ_L	Reflection coefficient
δ	Skin depth in a medium
δ_g	Ground penetration depth
η	Intrinsic impedance
η_g	Ground intrinsic impedance
ζ	Transient ground impedance
τ_s	Diffusion time of tubular shields
¶	See Author's Request on page x

1. Introduction

1.1 Background

Modern electrified railway networks have signaling, train control systems, rail communication systems and traction power systems that are highly automated. The signaling, train control systems and rail communication systems use digital electronics that can realize a great amount of intelligence and flexibility in the control functions and digital communications. The traction power systems include autotransformers/booster transformers and sub-station transformers and switchgear unit, for feeding the overhead catenary system that supply the power to traction locomotives.

The traction power systems use voltages for locomotives that are usually $15kV$ to about $25kV$. The frequencies could vary from DC to about $50Hz$. These voltages are obtained from substation transformers that are operating at even higher voltages. All the other systems like the signaling, train control systems and rail communication systems work at very low voltage levels typically at a few tens volts or $< 10V$, as they use electronic circuits and systems. Some of these equipments and their layout are shown in Figs. 1.1, 1.2 and 1.3. The track circuits and the relays are connected across tracks as shown in Fig. 1.2. A typical traction power supply feeding system is shown in Fig. 1.3. A sketch of how the currents are distributed in different traction systems during locomotive movements is shown in Fig. 1.4.

In the beginning, the design of signal and control network of railways in early times was not always done in accordance with the strict rules of Electromagnetic Compatibility (EMC). This created problems due to Electromagnetic Interference (EMI) when, old electro-mechanical signaling, control and communication systems were replaced by modern sensitive electronic circuits.

There are some studies on the EMC of railway systems in the literature. *Hill et al.* [1] derived detailed models for tracks for extremely low frequency (ELF) traction currents. The main emphasis of their work was to determine the rail-to-earth and rail-to-rail voltages that exist during the traction current flow. *Carpenter and Hill* [2] have also worked towards developing a suitable model for the track series impedance under ELF conditions that could help in designing track signaling equipment. Their main tool for modeling was using the *Finite Element Method (FEM)* [3]. *Hill and Carpenter* [4] have further

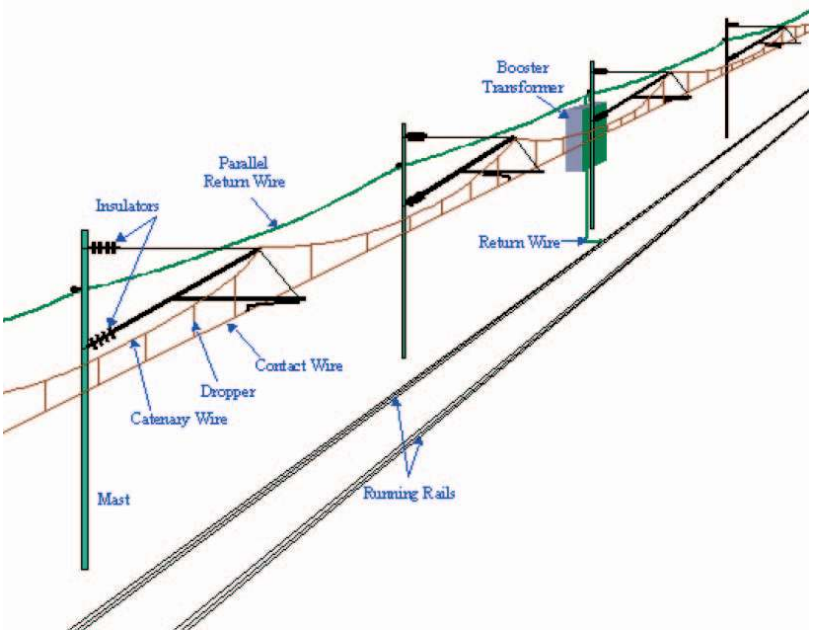

Figure 1.1: A typical traction conductor system layout, Source: http://www.railway-technical.com/etracp.html

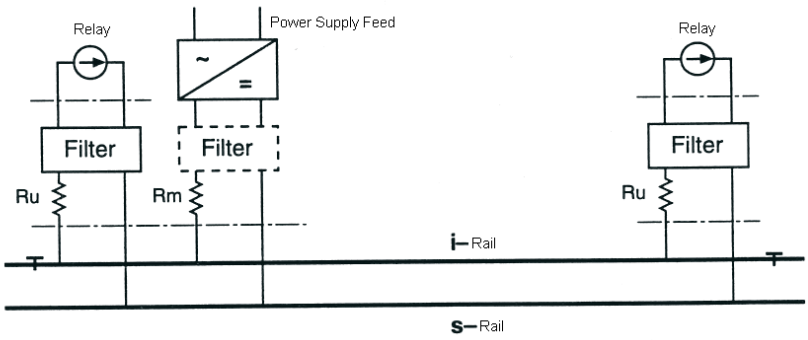

Figure 1.2: Track circuits (relay and track feed) connection across the rails, Source: Banverket signalteknisk information, dokument nr. 95088, http://www.banverket.se

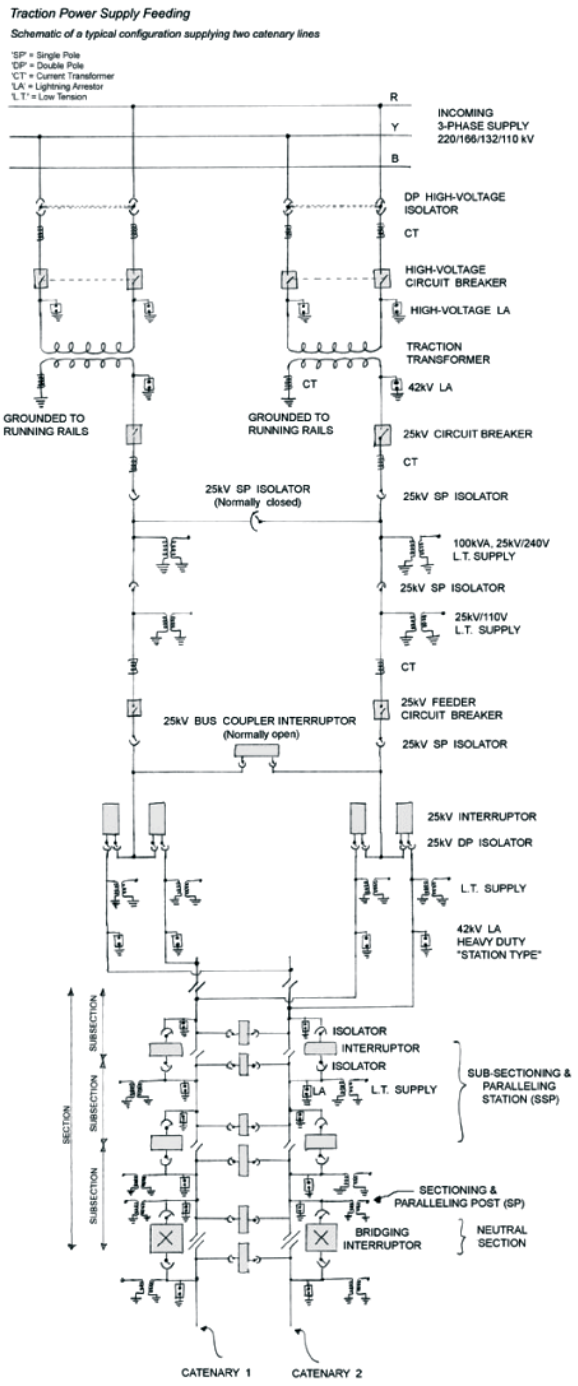

Figure 1.3: A typical traction power supply feeding system, Source: Indian Railways fan club, http://irfca.org

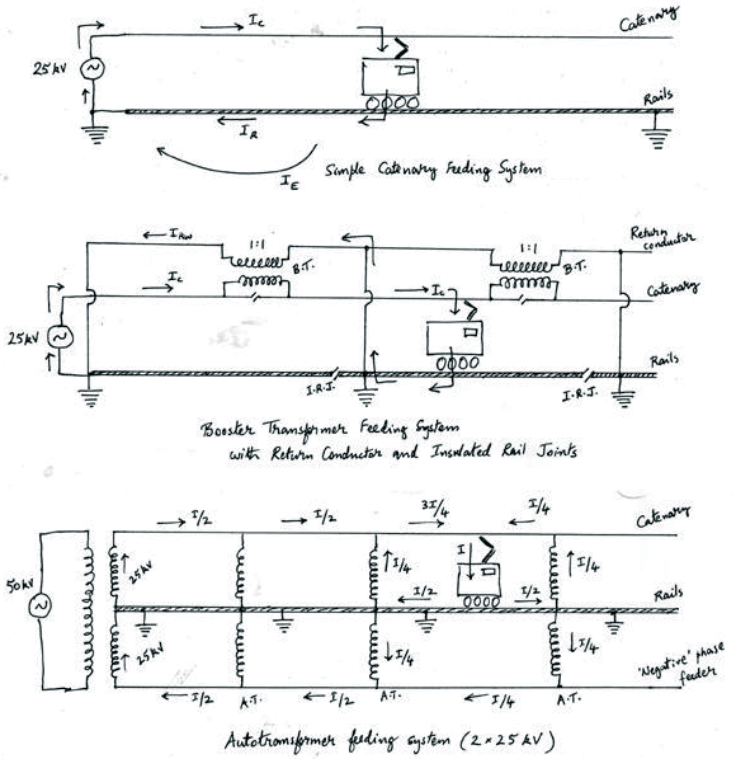

Figure 1.4: Different types of traction systems (Single Catenary (SC), Booster Transformer (BT) and Autotransformer (AT)) used in railways, Source: Indian Railways fan club, http://irfca.org

applied the integral equations of *Carson's* theory[1] [5] to their track models for the estimation of the track series impedance, thus, for the first time extending their study to a frequency of a few kHz. Another interesting part of their study was that experimental investigations were also carried out to support their models [6]. *Hill et al.* [7] have also provided some electrical material data for railway track transmission line parameter studies. It is to be noted that all these studies were carried out in the modeling of the tracks alone and that too for low frequency studies.

Some very limited study, carried out in modeling the overhead catenary system and tracks, is available only for low frequency up to $5kHz$ [8]. Most of the EMC studies nowadays are concentrated on low frequency traction noise due to switching and arcing phenomena at the pantograph [9, 10]. From all

[1]Carson John Renshaw in 1926 was first to derive ground impedance expression for overhead wires (discussed in Chapter-4), which was a revolution in the electrical power industry. He was also the first to theoretically study the induction from alternating current electrified railways, between track/overhead wire to very nearby telephone line for a frequency of $25Hz$ [5].

these studies it can be inferred that low frequency EMC problems were given more importance and that these EMC problems don't pose any direct threat or serious damage at equipment level, i.e. equipments like signal systems, transformers, communication systems, railway power systems etc. are not damaged by the above said EMC problems. **There is yet an important/a crucial problem in the railway systems that has either been neglected or not received much attention: i.e. EMC problems caused by lightning strikes. This thesis marks the beginning of the studies on the lightning interaction with railway systems.**

Modern developments in the railway systems have made the system more vulnerable to lightning transients, because the overall network is not designed to reduce the lightning surges to the low levels tolerable to the electronic systems widely being introduced in the railway system. Railway networks are extensive and modernization of signal/control/communication systems is carried out only in stages at different times, it is not unusual to find transient related problems in a section of the network on account of inadequate lightning protection design (or EMC design) of the existing network in which a new module (equipment or system) is introduced. One wonders if these problems act as a brake on the upgradation plans of the Railways. Even the new railway systems which incorporate advanced signal/control/communication systems sometimes suffers from the effects of lightning transients because many of the standards and guidelines used in the design dates back to the age of electromechanical devices and hence do not include robust transient protection design. There were many attempts to address EMC issues in railways, but usually these attempts were confined to solving immediate problems of EMI due to introduction of new locomotive drives and EMI due to sparks at the pantograph. **A comprehensive review of railway system from the angle of lightning protection and EMC is not yet carried out.**

This work is focused on the electromagnetic compatibility problems of large distributed systems, with special application to the interaction of lightning with the Swedish rail network. Statistics from Banverket show that the delay caused in the regular running of trains during thunderstorms is several hundreds of hours. The delay was about 1000*hours* and 900*hours* in the year 2002 and 2001 respectively [11]. The equipments that were damaged in the railway network were track circuit systems that include rectifier and relays, wayside telephone systems and cables, booster transformers, communication equipments, signal circuits, etc. Uppsala University and the Swedish National Rail Administration (Banverket) have agreed upon to work together in an effort to come up with efficient schemes of lightning protection to minimize delays and to ensure normal operations of trains. Most organizations dealing with railway transportation technology has practical experience with lightning protection and EMC. They try to consolidate this experience and share it with

others in the organization in the form of internal standards and guidelines. Often these documents are designed for very specific systems and not well suited when there are system changes. If there is a simulation software that simulate the important parts of the railway system from the lightning protection and EMC point of view, and if the internal standards and guidelines are coupled to this software, then such a software can cope up with the changes in the system more effectively. Well, then the heart of such software would be a set of simulation programs that use various electromagnetic techniques, which would be capable of simulating the effects of the interference sources on different parts of the railway network. The aim of this thesis is to develop such simulation programs based on theoretical studies, giving importance is also given for experimental investigations, so as to support/validate the simulation programs in the future and also to determine the vulnerability of various systems as discussed above.

1.2 How to begin this study?

There are many ways on could carry out this study. From a system protection perspective, an engineering approach would be to immediately act, i.e. replace the damaged part of system (damaged due to lightning) with a new part or device and add some additional protections based on the available standards or based on experience or trial and error if the damage is not serious or expensive. Such an approach is indeed beneficial, because the normal operation is restored quickly, and the delay is only limited to time taken in the restoration. This approach has some serious drawbacks. To elucidate few of them,

- It is not made sure whether the installed protective device is at sufficient level of protection, mainly because the voltage appearing at the terminal where the protection is installed is not known a priori and might be too statistical or stochastic. Further the breakdown level of the device itself is not known.
- It is not ascertained whether the installed protection will hamper the normal operation of the other interconnected systems, perhaps due to different ground potentials and possible low impedance paths in the event of lightning transient diversions.
- It is not clear also whether the protection should be given from power side or track side, since it true that in the event of lightning strikes both the tracks and overhead traction and auxiliary power wires (if present) will be raised to considerable over voltages, whose magnitudes depends on the ground material property, grounding system, induced/coupled lightning electromagnetic fields, non-linear phenomena like insulator flashover and soil ionization, etc.

So the striking question that comes to mind is: what are the realistic voltages or currents in the event of lightning strikes within the different parts of the railway systems? This is a difficult question to answer for a large distributed system like the railway system. This thesis attempts to partly answer the question. **Another interesting question would be, what are the breakdown voltage levels of the different equipments used in the railways so as to design suitable protection?** This perhaps can only be answered if impulse withstand experiments are conducted on those devices. This thesis attempts to study some of those aspects as well.

Bearing in mind that the first step in any lightning protection study is to identify the way in which the lightning transients enter into different parts of the systems. The devices mentioned in earlier paragraphs that get damaged during the thunderstorms are associated with the tracks and overhead conductor systems. Both the tracks and overhead conductors can be thought of as Multi-conductor Transmission Lines (MTLs) [12] above ground. All the transmission lines are taken to be infinite in either direction. This confines our problem to be a two-dimensional one. Our first task is to find out how a lightning stroke interacts with this overhead system. A photograph of the railway line near Gistad (Sweden) is shown in Fig. 1.5. This shows the complexity of the MTLs. To start with only a single-track system is considered here. However, an analysis with the double track system would be similar as described here but with more conductors.

1.3 Single track overhead traction system of the Swedish railways and the associated components

Before discussing a lightning interaction with the system, let us discuss the system and its associated parameters necessary for the simulations later. The MTLs model for single-track electrified railway system commonly found in Sweden is as shown in the Fig. 1.6, and the associated conductor systems are described in Table. 1.1. The different mediums that would be of interest for the wave propagation studies (discussed later) is shown in Table. 1.2. The values shown are typical and are taken from *Hill et al.* [7]. But these are nominal values and do not correspond to some extreme conditions of climate or temperature. The sleepers between the rail and ballast are neglected. The two conductors numbered R3 in Fig. 1.6 are interconnected or shorted to each other at every $7-10m$. They are considered here as a single conductor using the principle of bundled conductors [13]. Thus in the system analysis there are 9 conductors instead of 10. It is first necessary to find out on which conductor lightning can strike, for the location of the lightning current source, an impor-

Figure 1.5: Railway lines near Gistad, which shows the complexity of MTLs

tant input for the lightning attachment studies and is discussed in Chapter-2.

Conductors R1 and R2 are the rails. R1 is called the S-rail and is continuous and forms one of the reference/return conductors. R2 is the I-rail, which is broken every 1.02km and is used for the signaling purpose. The track circuits are connected across the S-rail and I-rail and across which a constant potential of few volts exists. This voltage collapses to zero once the locomotive is on this section of the rails. The relay units are also connected across the tracks (see Fig. 1.2). These serve the purpose of train positioning and signaling. R3 is the contact wire, which feed the locomotives through the pantograph. The

Table 1.1: *Conductor nomenclatures*

Conductor Name	*Conductor with Bundle*
S-rail	R1
I-rail	R2
Contact and Messenger	R3
Reinforcement	R4
Return	R5, R6
Help	R7, R8, R9

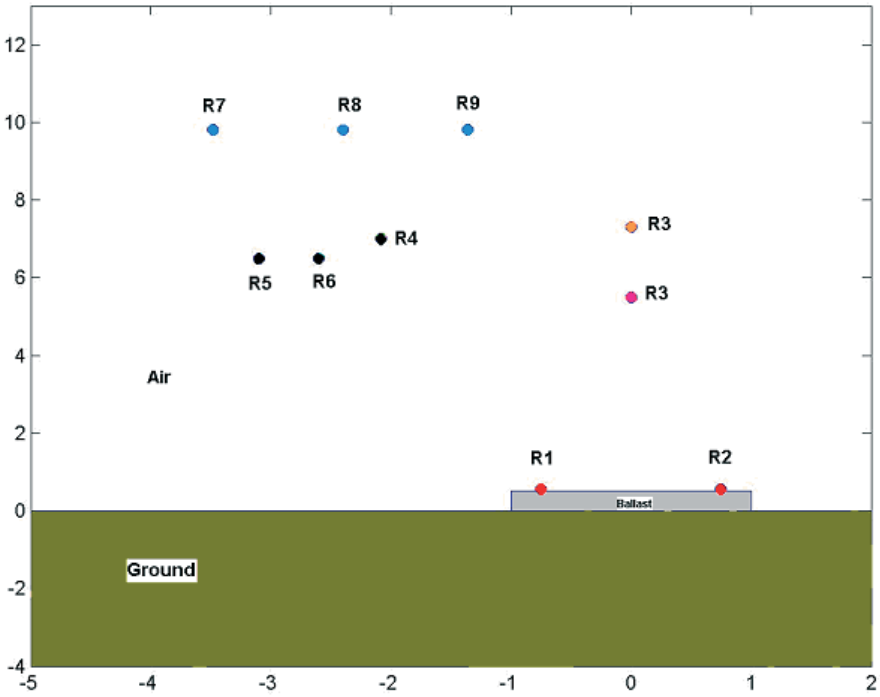

Figure 1.6: Geometry of the single-track Swedish railway system (axes in meters)

Swedish railway system works at $15kV$ and $16.67Hz$. R4 is a mechanical reinforcement wire used to provide mechanical tensions between the wires and the poles. R5 and R6 are the return conductors for both the traction currents and booster transformer currents. R7, R8 and R9 are the auxiliary help wires of $22kV$, $50Hz$ that run along the tracks. They give power supply to different equipments along the tracks after being stepped down to $400/230V$.

There is yet another conductor, in addition to the ones shown in Fig. 1.6, it is the telecommunication cable. Banverket uses different types of telecommunication cables in their systems. Further, they are either laid in cable trenches or buried in the ground at a depth of 0.5m to 0.75m and about 1m to 2m away from the tracks. The new cables that are used are $BV-ECLALPLE1S1.2+28P0.9$ from Ericsson [14] as shown in Fig. 1.7. The cable is double shielded, the outer shield is a steel armor and inner shield is a cage type construction made of aluminum. Further, the cable has complex multi-conductor configuration, with total sixty conductors many are twisted pairs and some are independent conductors that are not twisted and arranged in different layers. It has been observed that there are damages in the form of breakdown between the inner shield and conductor pairs. There seems to be also an ambiguity whether the damage is really caused by lightning or due to the traction currents getting

Table 1.2: *Material properties*

$Mediums$	ε_r	μ_r	$\sigma(S/m)$
Air	1.0	1.0	1.0×10^{-11}
$Ballast$	10.0	1.0	1.0×10^{-5}
$Ground$	10.0	1.0	4.0×10^{-4}
$R1, R2$	1.0	20.0	4.4×10^{-6}
$R3$	1.0	1.0	5.8×10^{7}
$R4 to R9$	1.0	1.0	3.5×10^{7}

into the shield during normal operation of traction system itself [15].

One of the important devices that are connected between the traction conductor and the return conductors is the booster transformer. In some places of Banverket systems they are now being replaced by the autotransformers [16]. A typical old type booster transformer with nameplate details **ASEA TRAFO, AMP 140/140, VOLT 16000, TILLVERK NR 526140**. is shown in Fig. 1.8. It is a 1 : 1 current transformer. The primary and secondary terminals are marked in the Fig. 1.8, which means that the primary terminals are connected to the traction catenary conductor and the secondary terminal to the return conductor.

Let us now look at the track circuits. The track circuit system consists of two sections that are connected in parallel. One is the power supply rectifier unit and the other is the relay unit. The rectifier unit takes the power from the auxiliary power at $50Hz$, $230V$. This is then rectified to $7V$ DC that is maintained across the rails. A typical rectifier unit **BML 301053 Nr. 56654** from Adtranz, Telekraft Industries and DiamlerChrysler Rail Systems used by Banverket is shown in Fig. 1.9, where the diodes and smoothing capacitor is shown. Track circuits works on the following principle: on an empty section of track, a potential difference is maintained between the two rails. When a vehicle reaches the section, a current is conducted through the wheels and axle, which effectively short circuits the two tracks. This fall in voltage and consequent increase in current activates a relay, which is also connected across the tracks as shown in Fig. 1.2. A typical relay unit **JRK 10470 nr. D. 156369** from Ericsson used by Banverket is shown in Fig. 1.10, which is a mechanical relay with many contacts and a core coil.

1.4 Skeleton of the thesis

Chapter-2 reviews the parameters of lightning that are important in the interaction of lightning with the railway systems. A necessary step in any study of direct lightning strike to a conductor system would be to determine to which

Figure 1.7: Telecommunication cable used in Banverket systems

conductor or group of conductors the lightning would attach. Some discussions on electromagnetic fields from lightning are also made for studying the indirect effects of lightning.

Chapter-3 is a detailed study on the wave propagation aspects in wires above the ground using the transmission line theory. This Chapter forms a foundation for other chapters as far as the simulations and modeling are concerned.

Chapter-4 is a detailed study on the MTLs theory as applied to one conductor being finitely conducting lossy half space. Discussion is made on differences between lossless and lossy transmission lines. The concept of internal impedance for internal loss and ground impedance for external loss are also discussed. Solution of telegrapher's equations for MTLs systems in frequency and time domain is discussed and compared. Importance of transmission line parameters for above ground conductors is also discussed. The FDTD method accounting for internal and external losses is presented.

Chapter-5 deals with the lightning induced voltage calculations for

Figure 1.8: Typical booster transformer used in the Banverket systems

the above ground wires. Factors that influence the induced voltage pulse propagation are discussed. Simulations and modeling for direct and indirect strikes are discussed. A transmission line model for return strokes is proposed. Modeling non-linear phenomena like insulator flashover, soil ionization at the pole footing and incorporation of interconnections between multi-conductor lines are discussed.

Chapter-6 presents some experiences with the measurements of transients entering a Swedish railway facility. The measurement setup and some measured transients and their correlation with the lightning location systems are presented.

Chapter-7 discusses the subject of pulse propagation in buried wires. A new expression for the ground impedance for buried wires is proposed. Importance of ground impedance and admittance parameters is discussed. Pulse propagation aspects of bare and insulated wires are presented.

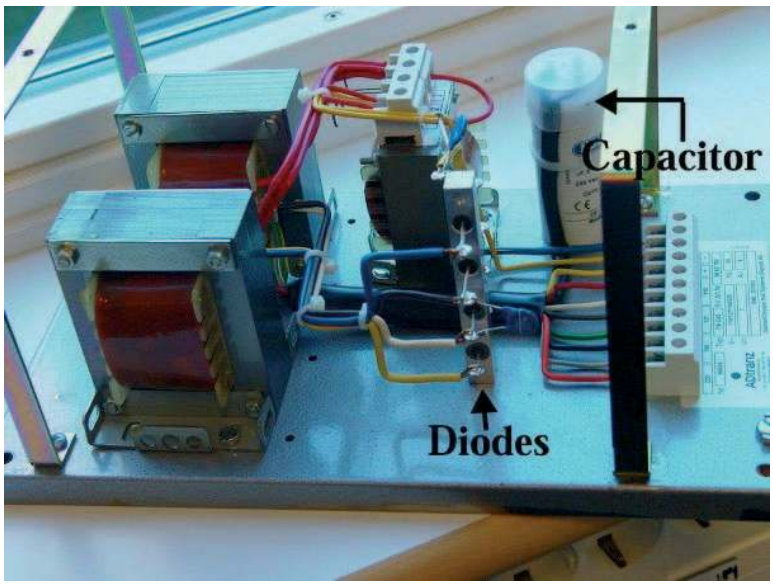

Figure 1.9: Typical rectifier unit used in the track circuits

Figure 1.10: Typical relay unit used in the track circuits

Chapter-8 details on the phenomena of coupling through cable shields. Concept of tube impedances for shields of the cables is discussed. A transmission line model for multi-core cables including shields is presented and also compared with experiments. A method for reducing the induced voltage in the core conductors of the cable using a bare follow on grounding conductor along with the cable is demonstrated. A method for determining capacitance matrix for complex twisted pair cables is also discussed for a possible future application of multi-conductor transmission line model for the buried telecommunication cables.

Chapter-9 discusses the modeling of the booster transformer. A simple circuit model is developed from the short circuit experiments. Some discussions on the failure modes of track circuit namely the relay and the rectifier units are discussed.

Chapter-10 shows one of the applications of the present thesis, wherein the computer simulation software for studying the transient phenomena in railway systems is described. Some of the aspects for future research are outlined.

2. Direct and Indirect Lightning Strikes to Outdoor Conductor System of Swedish Railways

A cloud-to-ground (CG) lightning can cause damage to an object on earth by directly attaching to it or by induction effects while striking somewhere near the object. Sometimes lightning may strike far from the object, but the surge is conducted to the object via power lines or other conducting systems causing damage. The extent and nature of damage depend both on the characteristics of the lightning and the characteristics of the object. The physical properties of lightning that are important in causing damage are the currents and electromagnetic fields. In this Chapter characteristics of lightning current and electromagnetic fields, important in producing damage to earth bound systems, are first considered and then the phenomenon of direct and indirect lightning attachments/strikes to conductors above and on the ground and buried conductor systems is presented. For engineering applications the information on lightning characteristics presented in this Chapter is taken from *Thottappillil* [17 - 19] and classical books namely Lightning Flash by *Cooray* [20] and Lightning Physics and Effects by *Rakov and Uman* [21], which give advanced, exhaustive and detailed information on the phenomena of lightning flash.

2.1 Lightning current and electromagnetic field parameters

The most important properties of lightning current that cause damage is peak current, maximum rate of change of current, the integral of the current over time (charge), and the integral of the square of current over time (action integral).

In a CG lightning the largest currents are produced by the return strokes. Peak return stroke currents are important in cases where the struck object essentially presents a resistive load, for example the surge impedance of a long power line, a tree, ground rods driven into earth etc. As an example, when a lightning return stroke with a peak current of $30kA$ strikes a power line with a surge impedance of 400Ω, it can produce a prospective over voltage of $1200kV$. This large voltage can cause flashover across insulators, from line

to ground, to adjacent lines and to other objects nearby. The magnetic forces produced by the peak current can cause wires to be pulled out of the walls and electrical machines, and the metal tubes to be crushed. A $30kA$ current entering earth through a grounding impedance of 10Ω causes a potential rise of $300kV$ and also cause surface arcing. Available evidence indicate that the average value of peak lightning current is unaffected by the conductivity of the soil. However, the same peak value of the current will have more adverse effects in low conductivity soil compared to high conductivity soil. Soil conductivity in most part of Sweden is poor in the range of $0.2-1mS/m$ and hence more surface arcing can be expected. However, in east Småland and in the middle region of the upper Nörrland the soil conductivity is in the range of $0.1-0.2mS/m$. Only in Skåne and around the big lakes is soil conductivity is above $1mS/m$. In Sweden there is photographic evidence to show that lightning striking bare ground can arc along the surface as much as $200m$.

In objects that present essentially inductive impedance such as wires in electronic systems, earth leads etc. the maximum over voltage produced is proportional to the maximum rate of change of current. Maximum di/dt occurs at the return stroke current wave front. Assume that 10% of the $30kA$ peak current (i.e. $3000A$) with front time $0.3\mu s$ finds its way to the wiring of an electronic apparatus. For an inductance of $1mH$ per meter, the inductive voltage produced in a $10cm$ long wire is $1000V$, enough to destroy most electronics unless there is adequate protection. In negative return strokes the average value of di/dt is $110kA/\mu s$. In positive return strokes these values are much smaller [20, 21].

As a first approximation the heating and burn through of metal sheets (e.g., metal roofs, airplane wings) is proportional to the amount of charge transferred, and depend also on the current at which this charge is delivered. Charge is the integral of the current over time. The power delivered to the lightning attachment point is the product of the current and the voltage drop ($5to10V$) at the arc-metal interface. Most of the charge in a lightning is due to the long continuing current that follows some of the return strokes. Even a severe return stroke that lasts perhaps a few tens of a microsecond may not transfer as much charge as a low-level ($100A-1000A$) continuing current that lasts a few hundred milliseconds. Charge lowered by a typical stroke followed by a continuing current is $11C$ to $15C$ in a negative flash and $80C$ in a positive flash.

Action integral is a measure of the ability of lightning current to generate heat in the resistive impedance of the struck object. This represents the prospective energy that would have been dissipated in a 1Ω resistor due to joule heating if the entire current of the return stroke flows through it and is represented as the time integral of the square of the current. The rapid heating of materials and the resulting explosion of nonconducting materials are, to a

first approximation, due to the value of the action integral. A doubling of the return stroke current tends to quadruple the action integral, for similar wave shape and duration of the return stroke. An action integral of $2.0 \times 10^6 A^2 s$ would create a temperature rise in excess of 200° centigrade in a copper strap of $10mm^2$ in cross sectional area, creating an explosion hazard where flammable materials or vapors may exist. Much thinner wires or straps may melt and vaporize when subjected to the above value of action integral. Action integral is an important parameter that has to be considered in the dimensioning of conductors, directly subjected to lightning strikes. Typical values of action integral are $5.5 \times 10^4 A^2 s$ and $6.5 \times 10^5 A^2 s$ for negative first return stroke and for positive return stroke, respectively. The lightning return stroke current wave shape is highly variable even within the same flash. The rise time can vary from $0.1 \mu s$ to several microseconds and the half-peak width can vary from a few microseconds to a few hundreds of microseconds [20, 21]. Current wave shape very rarely follow exactly the $1.2/50 \mu s$ or the $8/20 \mu s$ or the $10/350 \mu s$ wave shape or any other specified wave shape. These are test wave shapes adopted by various standards for simulating the effects of lightning in the laboratory.

The most important among the field parameters are the peak electric field and the maximum time rate of change of electric or magnetic field. Peak voltages on exposed metallic surfaces in lightning field are proportional to peak electric field and peak voltages produced in a loop of wire is proportional to the rate of change of magnetic field. For example, a typical return stroke striking $100m$ away may induce an over voltage in excess of $200V/m^2$ of loop area formed by the equipment and its cables, for certain orientation of the loop. The degree of penetration of fields inside shielded enclosures through apertures is largely proportional to the rate of change of magnetic and electric fields. The magnitude of peak fields and rate of change of fields are important parameters in over voltages caused in above ground wires and underground cables.

The finite conductivity of ground creates a horizontal component of electric field (or horizontal component of magnetic field) on the surface of the earth. This component of the field is large if soil conductivity is low. Typically, peak value of horizontal component of the field can be $10-20\%$ of the peak vertical component of the field at ground if the ground conductivity is of the order of $1mS/m$ [22]. This field is oriented radially from the lightning channel and induces over voltages in overhead lines and cables on the ground. A peak vertical electric field of $2kV/m$ at a distance of 1 km from the lightning channel may be accompanied with a horizontal field component of $200-400V/m$. Effect of this horizontal field may be seen as a series voltage sources distributed along the conductors, each source turned on in sequence as the field sweeps along the conductor. These series voltage sources will drive a common-mode current in the conductors. The typical values for the elec-

Table 2.1: *Electric and Magnetic fields associated with lightning [17 - 19]*

$Distance(m)$	$E_{typical}(kV/m)$	$E_{max}(kV/m)$	$dE/dt_{typical}(kV/m/\mu s)$	$dE/dt_{max}(kV/m/\mu s)$	$H_{typical}(A/m)$	$H_{max}(A/m)$	$dH/dt_{typical}(A/m/\mu s)$	$dH/dt_{typical}(A/m/\mu s)$
10	300	650	600	1500	500	1300	1800	6500
50	60	130	120	300	100	250	350	1300
100	30	65	60	150	50	130	180	650
500	6	13	12	30	10	25	35	130

tric and magnetic fields related to lightning are shown in Table. 2.1, [17 - 19]. Now it is to determine whether the stroke is going to terminate on the structure above the ground or on to a flat ground. Some times these studies are termed as the lightning interception studies and are discussed next.

2.2 Direct strikes on the railway systems

A CG flash always starts with a stepped leader, which is initiated after a preliminary discharge between the charges in the middle and bottom regions of the cloud. It is highly branched due to randomly distributed space charge between the cloud and the earth. Thus the path traced by it is highly tortuous. A stepped leader has the following properties: a). Step length: $3-200m$, b). Time interval between steps: $30-125\mu s$, c). Velocity of propagation: $1.0\times10^7-2.5\times10^6 m/s$, c). Charge deposited on the channel: $3-20C$ and d). Charge per unit length (average): $1C/km$. These are the parameters usually considered in the lightning interception studies. When the stepped leader propagates towards the ground, the field at the ground/grounded objects gradually increases. When the field reaches a critical value, upward streamers originate and propagate towards the tip of the stepped leader. There is a transition of these upward streamers into upward leaders. However, in the lightning literature the terms 'streamer' and 'leader' are often used interchangeably. A strike is established when one of the upward streamers/leaders succeeds in establishing a contact with a descending stepped leader.

A leader mechanism of breakdown has been observed in the breakdown of long air gaps stressed with impulse voltages [23, 24]. This motivated researchers to extrapolate the data from long air gap experiments to the lightning protection [24]. Their aim was to arrive at a suitable model that relates

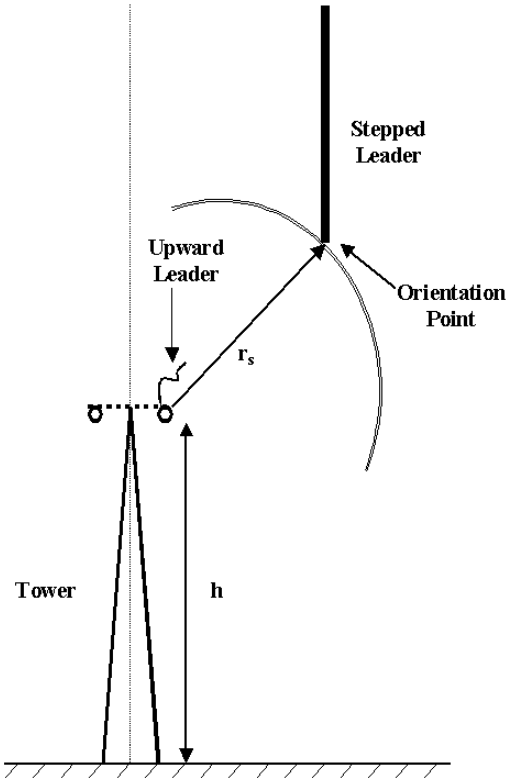

Figure 2.1: Striking distance for a given conductor held by tower of given height

charge on the stepped leader and the attractive effect of the grounded structure. Efforts in this direction have led to the so-called Electro-geometric model (EGM) [23, 25]. EGM is based on the principle that the point of strike of lightning is determined only during the final jump (at the striking distance) [25]. The electric field produced by the charge of the leader channel initiates connecting leader (upward leader) as shown in Fig. 2.1. The final path is thus dependent upon this moment. The position where the lower end of the downward leader is at this moment is called the orientation point because the path of the lightning is believed to turn towards the point of strike. The gap between the orientation point and the earth/earthed structures is called the orientation distance or the striking distance and it is determined by the field strength at the earth. The striking distance r_s is shown in Fig. 2.1.

The orientation distance is related to the charge on the leader channel and hence to the prospective stroke current. *Armstrong and Whitehead* have developed an analytical expression for the striking distance (r_s in meter) in terms of the amplitude of the prospective return stroke current (I_S in kilo Amps) [23,

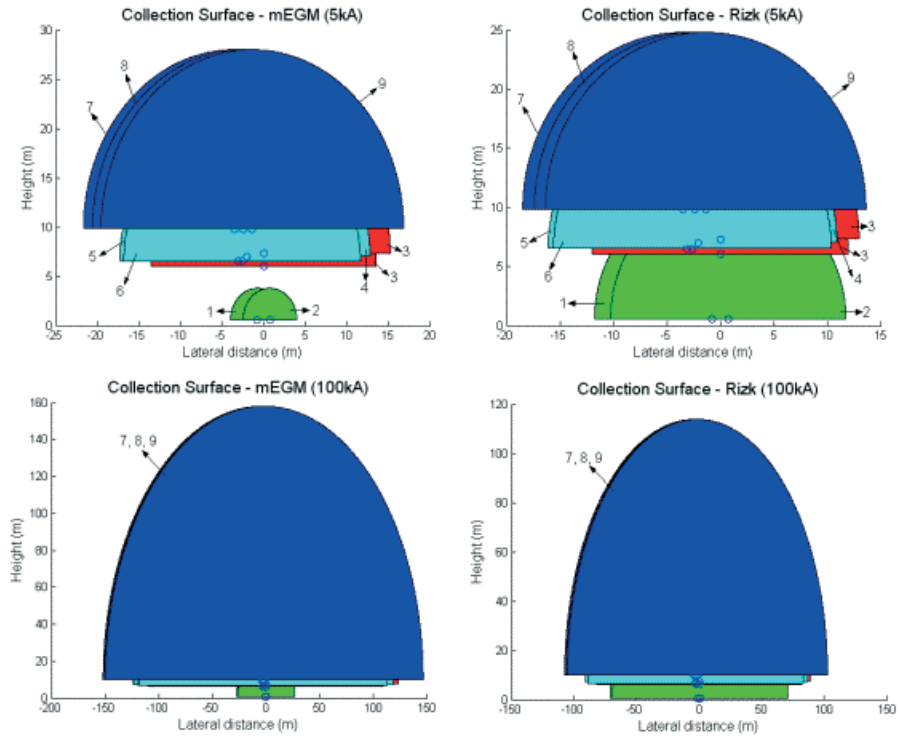

Figure 2.2: Collection surface offered by a single-track railway system to a descending stepped leader with prospective return stroke amplitude of 5*kA* and 100*kA*

25].

$$r_s = a_{s1} \cdot I_S^{c_{s1}} \tag{2.1}$$

Where a_{s1} and c_{s1} are constants. Many other researchers have also arrived at the same equation but with different values of a_{s1} and c_{s1}. The lightning task force of *IEEE* has compiled them [26] and the range of variation of a_{s1} was reported to be $6-10$, and that for c_{s1} is $0.6-0.8$. Some of the researchers have modified EGM expression for striking distance (2.1) and included also the height of the structure into the expression (2.1) to account for the possible field intensification due to the structure height, thus the expression for modified EGM is [25],

$$r_s = a_{s2} \cdot I_S^{c_{s2}} \cdot h^{b_{s2}} \tag{2.2}$$

Where, h is the height of the structure/conductor with $a_{s2} = 1-1.5$, $b_{s2} = 0.5-0.7$ and c_{s2} is same as c_{s1}.

Imagine now that a sphere of radius equal to the striking distance is rolled in the outward directions and around the conductor surfaces of the system

shown in Fig. 1.6 of the single-track system. Then the exposure surface or the collection surface through which the descending stepped leader can attach to the overhead conductor system [25] is obtained. Fig. 2.2 shows the possible collection surface offered by the conductors for two different values of the prospective return stroke currents $5kA$ and $100kA$ respectively using modified EGM. It can be seen that the strokes can only attach to the conductors R7, R8 and R9 of the system and that conductors R7, R8 and R9 shelter all the other conductors acting as some sort of shield wires. Any stroke descending outside this region of the collection surface of R7, R8 and R9 will terminate on the ground and will result in an indirect strike more of which will be discussed later. Note that the striking distance and the lateral distance are the same in case of modified EGM. However they have different definitions [27]. Lateral or attractive distance is the maximum horizontal distance from the structure location at which an incepted upward leader from the tip of the structure is capable of intercepting the stroke of a given prospective current [27]. *Rizk* [27] mentions that it's not necessary that all the incepted upward leaders for a given prospective current will intercept the stroke. As an additional information for the readers, the author would like to inform/caution that there are some devices/products available in the market known as early streamer emission (ESE) terminals/rods for protecting buildings, houses, etc. An interesting theoretical discussion on whether an ESE terminal really works or not can be found in **Paper-M**.

To verify whether the above statement that R7, R8 and R9 are the only possible candidates that can be struck by lightning, simulations were also carried out using the recent models for lightning attachment proposed by *Rizk* [27]. *Rizk's* model is based on three important criteria namely upward leader inception criterion, upward leader propagation criterion and final jump criterion [27], which were considered in the simulations. Upward leader inception criterion of *Rizk's* model considers both the height and the radius of the conductors, derivation of which can be found in [27]. The lateral distances and collection surface for all the conductors based on *Rizk's* method is shown in Fig. 2.2. Still it can be seen that the strokes mainly attach to the conductors R7, R8 and R9 of the system. A detailed discussion about direct lightning strikes on the above ground structures was carried out here, because it is the experience of power engineers that lightning stroke currents are conducted to sensitive equipments through overhead power wires [26], which is very relevant with railway systems too. Some recent developments in determining more accurate relationship between the leader charge and the return stroke current can be found in **Paper-N**.

In some railway systems like that in Holland, cables are laid on the surface of the ground [28] at about $1m$ to $2m$ away from the tracks. There could be direct strikes to such cable systems. It has been observed that the lightning strike

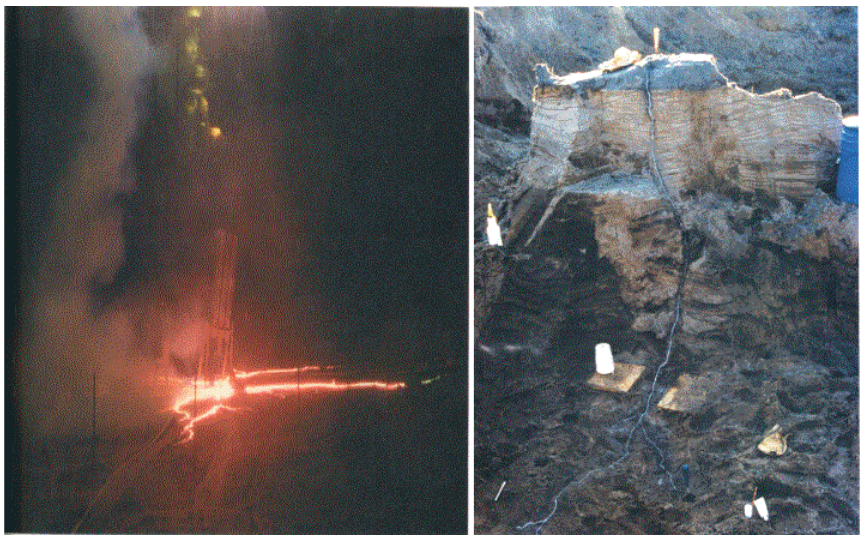

Figure 2.3: Surface arcs (left panel) and penetration of stroke (right panel) into the ground (adapted from [21])

at the ground can create long surface arcs as shown in Fig. 2.3 (left figure). In [21] it is mentioned that visually observable surface arcs had lengths of the order of $10m$. Such an arcing phenomena can easily couple to the cables on the ground. In the Banverket systems mostly the cables are buried [29]. In Fig. 2.3 (right figure), it is seen that a stroke has penetrated into the soil, the length of the arc that penetrated being about $5m$. From this it can be concluded that the direct strike to buried cables are indeed possible.

2.3 Indirect strikes to railway systems

Indirect strikes are not severe when compared to direct strikes. However the severity depends on the stroke currents that are involved in the return stroke phase of lightning flash [20, 21]. The electric and magnetic fields from the return strokes are discussed section 2.1 and their typical values are shown in Table 2.1.

In lightning, the first return strokes and the subsequent return strokes that follow the first have different properties. First return strokes are slow and have frequencies in the range of few tens of kHz to few hundreds of kHz. Subsequent strokes are faster with frequencies could be up to few MHz [20, 21]. A typical example of return stroke current waveforms measured by *Eriksson*[2]

[2]Eriksson Andrew John was a pioneer in the field of transmission line lightning interaction. His equations and experimental data are used worldwide by the electric power industry.

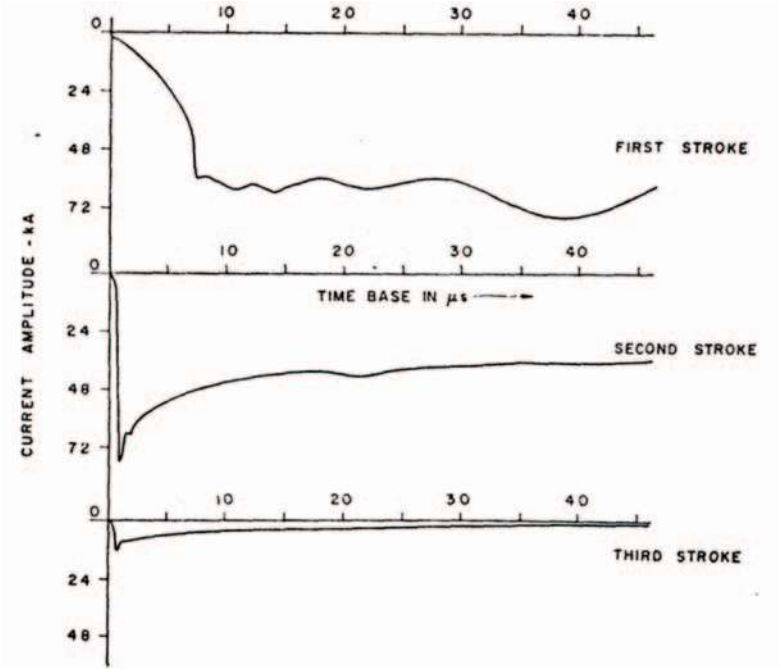

Figure 2.4: Current waveforms measured at tower bottom for a flash with two subsequent strokes by Eriksson

for a flash is shown in Fig. 2.4 [30]. During the return stroke phase the electromagnetic fields from it, illuminates structures and conductor systems whether it is above the ground or on the ground or under the ground. With regard to present discussion, consider a return stroke channel illuminating a system of three conductors at location (P1, P2 and P3) as shown in Fig. 2.5 (upper sketch), for the sake of explanation of the phenomena only. Depending upon the distance of the stroke from the object and magnitude of the return stroke, there are two components of exciting electric fields (horizontal and vertical) that contribute to what are known as fictitious sources[3] on the wires as shown in Fig. 2.5 (lower sketch). The vertical component of electric field will create distributed voltage sources appearing all along between the line and reference, which is proportional to the height or depth of the conductor. If the conductor is on the ground there is no contribution from this component. Vertical component of electric field has negligible effects from finitely conducting ground medium. The vertical component only contributes to the total voltage on the line at a given point. The most important distributed voltage sources that will always exist are from the horizontal component of electric field. The distrib-

[3]Distributed sources appear along the length of the conductor as long as the fields are illuminating it. This is a classical way of imagining and realizing field to wire coupling phenomena.

uted voltage sources from horizontal field are also proportional to height or depth of the conductor and also on the finite ground medium (ground conductivity and ground permittivity).

Note the mention about horizontal and vertical components of exciting electric fields and the corresponding distributed voltage source representation. It doesn't mean that the exciting magnetic fields are not important or doesn't contribute. It has been shown by *Rachidi* [31] and *Nucci and Rachidi* [32], that above representation also partly known as the *Agrawal et al.* model (contributions from only horizontal electric fields) [33] is equivalent to various other representations, like *Taylor et al.* model [34] in terms of transversal component of exciting magnetic fields and vertical component of exciting electric fields and *Rachidi* model [31, 32] in terms of the transversal and longitudinal components of exciting magnetic field (a_x and a_y directions). All these can be later transformed into either distributed voltage or current sources. Researchers and engineers prefer the *Agrawal et al.* model due to its computational simplicity while considering dissipative ground in wave propagation along transmission lines (details in Chapter-5).

All these distributed sources will start to launch voltage and current waves in either direction along the line leading to the well-known phenomena of induced over voltages [32]. Those induced voltages depending upon their magnitudes could pose threat to other interconnected systems and devices connected to the line.

2.4 Conclusions

In this Chapter it is shown that the return stroke phase of the lightning flash decides the extent of damage to the systems, while the stepped leader phase of lightning flash decides whether the stroke will terminate on to the system to be protected, known as direct strikes, or to the flat ground, known as indirect strikes. The magnitudes of the currents and their corresponding wave shapes decide the severity of the damage, and hence they should be effectively taken care in the lightning protection study. The number of outages occurring in a region depends on the annual ground flash density of the region [26], which is further dependant on the thunderstorm days [26] of that region. Standard insulation coordination practices [26, 35] consider these factors while designing protection schemes for power lines from lightning.

In Swedish railway systems most of the transients enters through the conductors above the ground, either due to direct strikes to R7 - R9 auxiliary power conductors or indirect strikes to all the exposed conductors of R1 - R9. Interesting measurements of induced voltages due to indirect lightning strikes in the Swedish railway systems conducted by Uppsala University in coop-

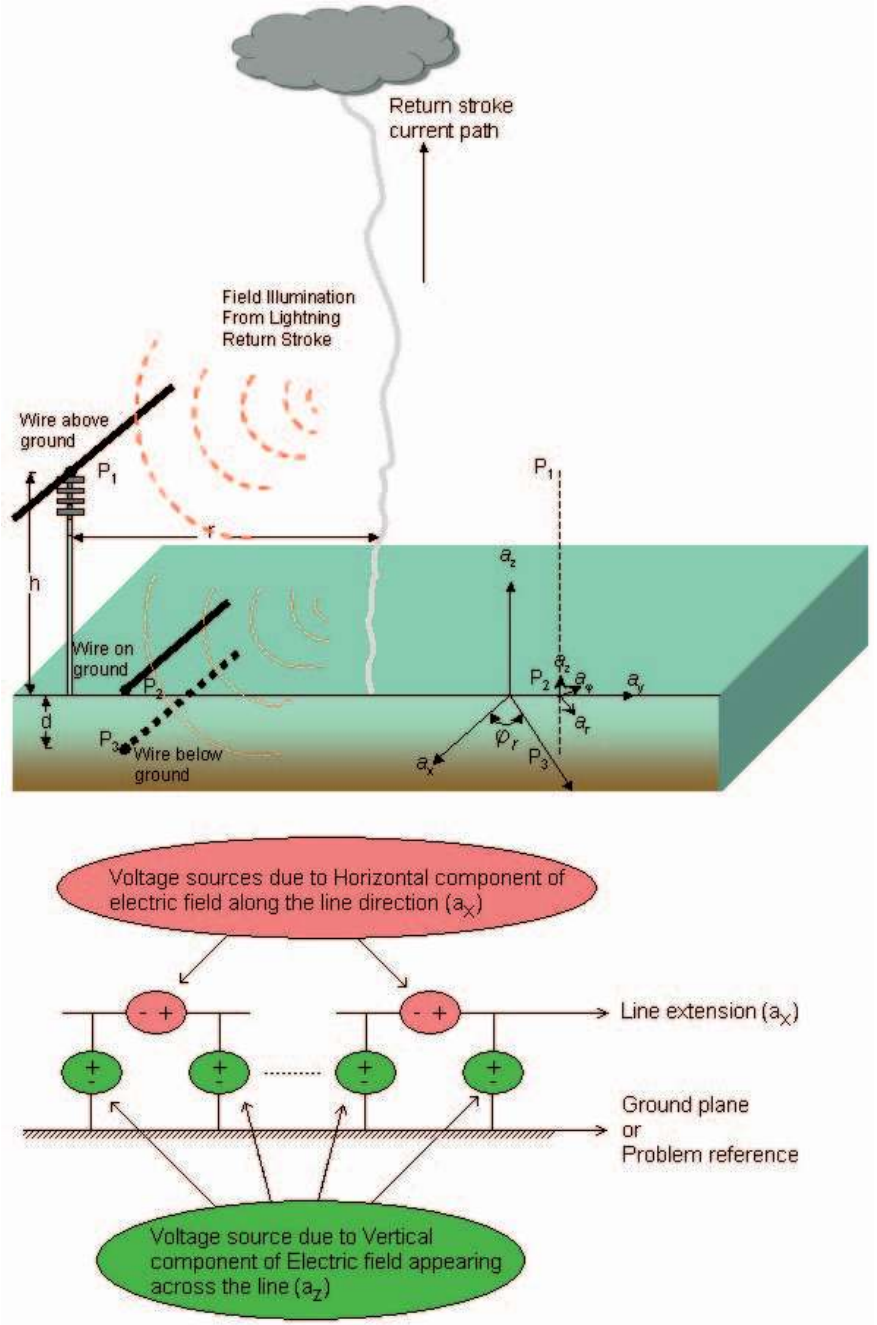

Figure 2.5: Sketch showing field illumination phenomena due to return strokes and the consequent representation of field to wire coupling phenomena by means of distributed voltage sources

eration with Banverket will be discussed in Chapter-6. Whether it is direct or indirect strikes, once there is a strike to any of conductor systems (above ground or on ground or under the ground), the subject of wave propagation needs to be understood for knowing the possible realistic voltage or current transients appearing across the terminals of the equipment that are to be protected. The next Chapter discusses in detail wave propagation in above ground wires, starting from the of transmission line theory. The primary focus will be the influence of ground return parameters in the wave propagation.

3. Genesis of Transmission Line Theory

The electromagnetic fields from the lightning channel, when they couple to the railway conductor system, for example as shown in Fig. 1.6, will cause lightning induced voltages on the conductor system and propagate along the conductor system of the MTLs. Similarly, a direct strike to one of the conductors as mentioned in the Chapter-2 will also cause the induced voltages in other neighboring conductors and they propagate along the MTLs and that this situation would be more severe than the case of indirect strikes. These induced voltages could damage the devices and sub systems connected to the MTLs. This happens if those voltages appearing across the devices are above their protective levels. Then the question is what are those voltages on the MTLs in the event of lightning strikes? The main focus of this thesis is to search clearly for the factors that influence the realistic voltage/current (through simulations) surge propagation and hence determine whether those surges appearing at different positions along the conductors of MTLs are above the threshold destruction value of the connected devices and subsystems. Bearing the above goal in mind the immediate subject that might help studying the problem is the wave propagation in wires or parallel wires or transmission lines. An effort in this direction has helped the author in either judging, and, wherever necessary, developing suitable models for pulse propagation studies based on transmission line theory.

3.1 What our good old masters did?

In the year 1864, *Maxwell*[4] proposed his **Dynamical Theory of the Electromagnetic field** [36 - 38], wherein he observed theoretically that and electromagnetic disturbance travels in free space with the velocity of light, further concluding that light is a transverse electromagnetic wave. In 1873 *Maxwell* published **A Treatise on Electricity and Magnetism**, ending a decade long effort to unify the two phenomena, thereby gifting us with a beautiful sub-

[4]Maxwell James Clarke (1831 - 1879), renowned physist and mathematician, whose contributions form one of the most important intellectual achievements of the 19^{th} century, beyond doubt, he is the father of modern electromagnetism.

ject of electromagnetic fields, which, has become the foundation of electrical engineering. *Maxwell* died in the year 1879, and in his commemoration, *Helmohltz* sponsored a prize for the first experimental confirmation of *Maxwell's* theory [38]. Two parallel contenders for this prize were *Hertz*[5] and *Lodge*[6]. *Hertz* in 1888 [36, 38], through his groundbreaking experiments discovered electromagnetic waves, thus confirming that *Maxwell* theory and equations were perfectly correct! *Lodge* published his own confirmation one month after *Hertz*. Just missed winning the competition! The cause of the delay was that Lodge took a vacation [38]. If *Hertz* hadn't won the race, today we would have had lodgian waves with frequencies of kilolodges, megalodges etc.

Maxwell's original equations were 20 equations in component form with 20 variables, which incidentally were a blend of all that was then known about electricity and magnetism, from the works of *Oersted*[7], *Gauss*[8] , *Ampere*[9], *Faraday*[10], *Henry*[11], *Biot*[12], *Savart*[13] and others including *Maxwell* himself who introduced the very essential concept of displacement current. The actual symbols used by *Maxwell* are shown in the second column of Table 3.1 and their corresponding modern vector and scalar notation is also given. More details about the original equations can be found in [36].

The main problem with *Maxwell's* original equations was that he used

[5]Hertz Rudolf Heinrich (1857 - 1894) was a professor and former student of Herman von Helmholtz at the Technische Hochschule in Karlsruhe. He tested Maxwell's hypothesis with loops fitted to brass doorknobs - basis of the Hertzian dipole. He worked on electromagnetic phenomena, discovered radio waves and the photoelectric effect.

[6]Lodge Oliver (1851 - 1940) was a physics professor at University College in Liverpool. He was known as one of the Maxwellians. Lodge developed the famous 'recoil kick' experiment, which showed that a strong spark could be produced at the far end of a transmission line only when the line was resonant.

[7]Oersted Hans Christian (1777 - 1851) in 1820 discovered that a current carrying wire produces magnetic fields.

[8]Gauss Johann Carl Friedrich (1777 - 1855) was both mathematician and physist, who formulated separate electrostatic and electrodynamical laws, including 'Gauss law'; contributed to development of number theory, differential geometry, potential theory, theory of terrestrial magnetism.

[9]Ampere Andre Marie (1775 - 1836) is the father of electrodynamics, who in 1821 put Oersted's observations into mathematical form.

[10]Faraday Michael (1791 - 1867) is the father of electricity, who discovered electromagnetic induction and devised the first electrical transformer.

[11]Henry Joseph (1797 - 1878) performed extensive fundamental studies of electromagnetic phenomena, devised first practical electric motor. He demonstrated long distance communication by sending an electric current over one mile of wire to activate an electromagnet striking a bell.

[12]Biot Jean-Babtiste (1774 - 1862) co-discovered that intensity of magnetic field set up by a current flowing through a wire varies inversely with the distance from the wire.

[13]Savart Felix (1791 - 1841) co-discovered that intensity of magnetic field set up by a current flowing through a wire varies inversely with the distance from the wire.

Table 3.1: *Twenty variables originally used by Maxwell in his dynamical theory of the electromagnetic field adapted from [36]*

Maxwell's variables (Equivalent)	Maxwell's symbols (Equivalent)
Electromagnetic momentum	F,G,H
(Magnetic vector potential)	$(\vec{A})$
Magnetic force	α,β,γ
(Magnetic field intensity)	$(\vec{H})$
Electromotive force	P,Q,R
(Electric field intensity)	$(\vec{E})$
Conduction current	p,q,r
(Conduction current density)	$(\vec{J})$
Electric displacement	f,g,h
(Electric flux density)	$(\vec{D})$
Total current	$(p,q,r)^1 = (p,q,r) + \frac{d(f,g,h)}{dt}$
(Cond. and Disp. current density)	$(\vec{J_T})$
Quantity of electricity	e
(Volume charge density)	(ρ)
Electric potential	φ
(Electric scalar potential)	(φ)

quaternion[14] principally for the field quantities [36, 37]. *Gibbs*[15] developed

[14]Hamilton William Rowan (1805 - 1865) developed the quaternion theory in 1843, while searching for general properties of complex numbers. If we have three numbers that are all square roots of -1, denoted by i, j and k, then the quaternion is q = w + xi + yj + zk, where w is a real number, and x, y and z are complex numbers. Another common representation is q=[w,v], where v = (x, y, z) is called a *vector* and w is called a *scalar*. Although the v is called a vector, don't think of it as a typical 3 dimensional vector. It is a vector in 4D space, which is totally unintuitive to visualize. Hamilton's quaternions paved the way for the study of new algebraic

the vector algebra and *Heaviside*[16] started to apply the vector analysis exclusively on *Maxwell's* original equations. *Heaviside* gave detailed account of the vector representation of *Maxwell's* original equations (what we know today as *Maxwell's* equations) in a series of publications from 1881 to 1884 well before the experimental confirmation by *Hertz*. *Heaviside*, in his 1881 paper **on induction between parallel wires**, demonstrated mathematically the clear differentiation between static and electromagnetic induction and more importantly proved the existence of traveling wave phenomena (discussed later), when both types of induction take part simultaneously in parallel wires [37], which, undoubtedly, was landmark achievement. The vector representation of *Maxwell's* equations is given by (3.1) in differential form and (3.2) in integral form[17],[18] [39 - 43],

$$\nabla \bullet \vec{E} = \frac{\rho}{\varepsilon_0} \tag{3.1a}$$

$$\nabla \times \vec{E} = -\frac{\partial \vec{B}}{\partial t} \tag{3.1b}$$

$$\nabla \bullet \vec{B} = 0 \tag{3.1c}$$

$$\nabla \times \vec{B} = \mu_0 \cdot J + \varepsilon_0 \cdot \mu_0 \cdot \frac{\partial \vec{E}}{\partial t} \tag{3.1d}$$

$$\int_v \nabla \bullet \vec{E} \cdot dv = \oint_s \vec{E} \bullet \vec{ds} = \frac{1}{\varepsilon_0} \cdot \int \rho \cdot dv \tag{3.2a}$$

$$\int_s (\nabla \times \vec{E}) \bullet \vec{ds} = \oint_c \vec{E} \bullet \vec{dl} = -\frac{\partial}{\partial t} \oint_s \vec{B} \bullet \vec{ds} \tag{3.2b}$$

$$\int_v \nabla \bullet \vec{B} \cdot dv = \oint_s \vec{B} \bullet \vec{ds} = 0 \tag{3.2c}$$

---

systems.

[15]Gibbs Josiah Willard (1839 - 1903) was a professor of mathematics who independently developed three-dimensional vector analysis that could be applied to physics and engineering. He published his Elements of Vector Analysis in three parts from 1881 to 1884.

[16]Heaviside Oliver (1850 - 1925) contributed to the development of electromagnetism, introduced operational calculus and invented the modern notation for vector calculus. He predicted existence of the Heaviside layer (a layer of the Earth's ionosphere)

[17]Among the Maxwell's equations the first is Gauss law for electric fields, the second is the Faraday's law, the third is the Gauss law for magnetic fields and the last is the Ampere's law with a correction to it by Maxwell himself for displacement currents.

[18]Majority of researchers and engineers owing to the complexity of integral equations adopt the corresponding differential form, which is easier to understand.

$$\int_s (\nabla \times \vec{B}) \bullet \vec{ds} = \oint_c \vec{B} \bullet \vec{dl} = \mu_0 \cdot \int_s \vec{J} \bullet \vec{ds} + \mu_0 \cdot \varepsilon_0 \cdot \frac{\partial}{\partial t} \oint_s \vec{E} \bullet \vec{ds} \qquad (3.2d)$$

In some representations use of electric and magnetic field intensities is common, which can be obtained using (3.3) for any medium.

$$\vec{B} = \mu_0 \cdot \vec{H} \qquad (3.3a)$$

$$\vec{D} = \varepsilon \cdot \vec{E} \qquad (3.3b)$$

$$\vec{J} = \sigma \cdot \vec{E} \qquad (3.3c)$$

There are two potentials in the above system of equations, one is electric scalar potential and the other is magnetic vector potential[19]. Some salient relations between those potentials and electric and magnetic field vectors are shown in (3.4).

$$\vec{B} = \nabla \times \vec{A} \qquad (3.4a)$$

$$\nabla \times \vec{E} = -\frac{\partial}{\partial t}(\nabla \times \vec{A}) = -\nabla \times \frac{\partial \vec{A}}{\partial t} \qquad (3.4b)$$

$$\vec{E} = -\nabla \varphi - \frac{\partial \vec{A}}{\partial t} \qquad (3.4c)$$

How to obtain transmission line equations from the above *Maxwell's* equations, so as to solve our actual problem of MTLs systems? For this, there is a need to see some of the wave propagation aspects [39 - 44] associated with wires or transmission lines, which will be discussed next.

3.2 Wave propagation aspects

First let's begin with the definition of uniform plane waves, because this is the simplest type of wave propagation one can imagine. *Paul* [41] mentions that wave propagation on transmission lines, waveguides and antennas are very similar to uniform plane waves. The term uniform plane waves means that at any point in space the electric and magnetic field intensity vectors lie in a plane, and the planes at any two different points are parallel. Further, the electric and magnetic field vectors are independent of position in each plane.

For discussion of plane waves, assume the magnetic and electric field vec-

[19] Some researchers use the vector potential and scalar potential methods to start their numerical or theoretical investigations - Hertz potential theory.

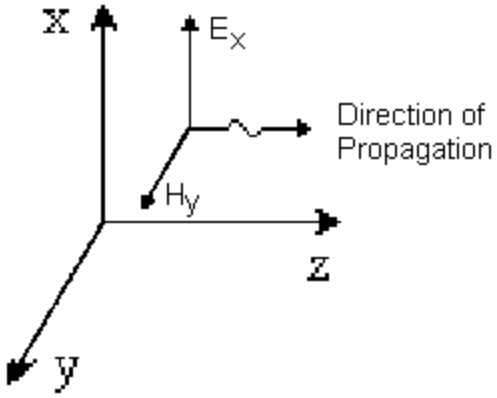

Figure 3.1: Uniform plane wave: propagation direction and direction of magnetic and electric fields

tors to lie the *xy* plane as shown in the Fig. 3.1. Let the electric field be directed along *x* axis which is given by (3.5).

$$\vec{E} = E_x(z,t) \cdot \vec{a}_x \tag{3.5a}$$

$$\frac{\partial E_x}{\partial x} = \frac{\partial E_x}{\partial y} = 0 \tag{3.5b}$$

The above equation necessitates that magnetic field is given by (3.6)

$$\vec{H} = H_y(z,t) \cdot \vec{a}_y \tag{3.6a}$$

$$\frac{\partial H_y}{\partial x} = \frac{\partial H_y}{\partial y} = 0 \tag{3.6b}$$

Equations (3.5) and (3.6) are hence orthogonal and the uniformity of plane wave is accounted. Using *Faraday's* and *Ampere's* law, which for this situation is,

$$\frac{\partial E_x(z,t)}{\partial z} = -\mu \cdot \frac{\partial H_y(z,t)}{\partial t} \tag{3.7a}$$

$$\frac{\partial H_y(z,t)}{\partial z} = -\sigma \cdot E_x(z,t) - \varepsilon \cdot \frac{\partial E_x(z,t)}{\partial t} \tag{3.7b}$$

For the sake of better understanding of the propagation aspects, let's take the discussions entirely in frequency domain. It is well known that the transformation back to time domain can be discussed later through the inverse *Fourier* or *Laplace* transforms. Hence for sinusoidal variation replacing in the above

equations time to frequency i.e. for a given frequency,

$$\frac{dE_x(z,j\omega)}{dz} = -j\omega\cdot\mu\cdot H_y(z,j\omega) \tag{3.8a}$$

$$\frac{dH_y(z,j\omega)}{dz} = -(\sigma + j\omega\cdot\varepsilon)\cdot E_x(z,j\omega) \tag{3.8b}$$

If (3.8a) is differentiated with respect to z and then put into (3.8b) the wave equations in one dimension are obtained, which are uncoupled second order differential equations as shown in (3.9).

$$\frac{d^2E_x(z,j\omega)}{dz^2} = \gamma^2\cdot E_x(z,j\omega) \tag{3.9a}$$

$$\frac{d^2H_y(z,j\omega)}{dz^2} = \gamma^2\cdot H_y(z,j\omega) \tag{3.9b}$$

The above equations have the solution as shown in (3.10), in terms of forward $(+)$ and backward $(-)$ waves.

$$E_x(z,j\omega) = E_m^+\cdot e^{-\gamma\cdot z} + E_m^-\cdot e^{\gamma\cdot z} \tag{3.10a}$$

$$H_y(z,j\omega) = \frac{E_m^+}{\eta}\cdot e^{-\gamma\cdot z} + \frac{E_m^-}{\eta}\cdot e^{\gamma\cdot z} \tag{3.10b}$$

In the above equations the parameters in front of the exponents are the complex undetermined coefficients and has to be determined from the boundary conditions. The two important coefficients are propagation constant (3.11a) and intrinsic impedance (3.11b), from them it can be concluded that when a plane wave propagates in a uniform medium the factors effecting the propagation is the medium and more importantly the frequency of the wave itself.

$$\gamma = \sqrt{j\omega\cdot\mu\cdot(\sigma + j\omega\cdot\varepsilon)} = \alpha + j\beta \tag{3.11a}$$

$$\eta = \sqrt{\frac{j\omega\cdot\mu}{\sigma + j\omega\cdot\varepsilon}} \tag{3.11b}$$

In any media the wave's propagation characters like the attenuation constant, velocity and the wave length of the wave are determined as in (3.12a), (3.12b) and (3.12c) respectively.

$$\alpha = \omega\sqrt{\frac{\varepsilon\cdot\mu}{2}\cdot\left(\sqrt{1+\frac{\sigma^2}{(\omega\cdot\varepsilon)^2}} - 1\right)} \tag{3.12a}$$

$$v = \frac{\omega}{\beta} = \frac{1}{\sqrt{\frac{\varepsilon \cdot \mu}{2} \cdot \left(\sqrt{1 + \frac{\sigma^2}{(\omega \cdot \varepsilon)^2}} + 1\right)}} \tag{3.12b}$$

$$\lambda = \frac{2\pi}{\beta} \tag{3.12c}$$

If the wave is propagating in a lossless media the conductivity term in the above equations is zero, due to which the attenuation becomes zero and wave velocity would be the famous equation what we know as $\frac{1}{\sqrt{\mu \cdot \varepsilon}}$,which for air is speed of light.

3.3 Transmission Line equations (Telegrapher's equations)

Before applying the above plane wave theory on the transmission lines to get the transmission line equations, it would be necessary to demonstrate the fundamental difference between transmission lines and waveguides. Any structure that guides electromagnetic waves can be considered as a waveguide [44]. It is more applicable to closed hollow metal cylinders that have same cross sectional dimensions over long distances. When such cylinders (waveguides) are filled with low loss dielectric (e.g. air), then they exhibit lower losses (skin effect and dielectric loss: discussed later) than conventional transmission lines. Thus their major application is in transporting radio frequency (1 to 200 GHz) energy to very long distances. Waveguides are practical only for waves of extremely high frequency. Waveguides being single-conductor elements, the mechanism of propagation of electrical energy through it is very different compared to two-conductor transmission line. The subject of two-conductor transmission line is used as the basis for the derivation of transmission line equations.

Along the length of a normal transmission line, both electric and magnetic fields are perpendicular (transverse) to the direction of wave travel [12, 41]. This is known as the principal mode, or TEM (transverse electric and magnetic) mode. *This mode of wave propagation can exist only when there are at least two conductors or more out of which one is a return conductor and will be a dominant propagation mode for all frequencies if the cross-sectional dimensions of the transmission line are small compared to the wavelength of the propagating electromagnetic pulse.* At microwave frequencies between 100 - 300 GHz, two-conductor transmission lines of any length operating in standard TEM mode become impractical. Lines with smaller cross-sectional dimension to maintain TEM mode of signal propagation for microwave signals

exhibit low voltage ratings and suffer from huge power loss [12, 41 - 43]. Still, at these short wavelengths there exist other modes of propagation[20] that are not lossy as discussed in the beginning of this section, if conductive tube was used rather than two parallel conductors [44]. It is now known when a TEM field structure is violated. Only the TEM field structure is considered as it is applicable to our present study. Further, it is well within the bandwidth of lightning transients.

It is to be noted that when a plane wave propagating in one medium encounters another medium at the interface two important conditions must be satisfied. The tangential components of both electric field and magnetic field intensity vectors must be continuous. In addition to this at the interface the normal components of the electric and magnetic flux density vector must be continuous. These two conditions are mathematically described as shown in (3.13) if the mediums are represented as 1 and 2 [41].

$$\vec{E_{t1}} = \vec{E_{t2}} \tag{3.13a}$$

$$\vec{H_{t1}} = \vec{H_{t2}} \tag{3.13b}$$

$$\vec{D_{n1}} = \vec{D_{n2}} \tag{3.13c}$$

$$\vec{B_{n1}} = \vec{B_{n2}} \tag{3.13d}$$

Consider a two conductor transmission line with the following conditions, a). the conductors are parallel to each other and also to the x-axis, b). the conductors are perfect and c). the conductors have uniform cross section. For the time being consider the medium surrounding the lines are homogeneous with some finite conductivity, permittivity and permeability. When an incident electromagnetic field illuminates a perfectly conducting body, a scattered electric field is created such that sum of the tangential components of both incident and scattered electric fields is zero at the surface of the conductor. The scattered component of the field is maintained/caused by the current density and surface charge density, which exist on the surface of the scatterer [42]. The transmission line equations will be derived from a field illumination perspective so as to cover both direct and indirect effects of lightning. As mentioned earlier consider a two conductor transmission line. The representation is as shown in Fig. 3.2a. Consider the *Faraday's* law in frequency domain integral

[20]For electromagnetic wave propagating in a hollow tube, only one of the fields, either electric or magnetic, will be transverse to the wave's direction of travel. The other field will *loop* longitudinally to the direction of travel still maintaining perpendicularity to the other field. Whichever field remains transverse to the direction of travel determines whether the wave propagates in TE mode (transverse electric) or TM (transverse magnetic) mode.

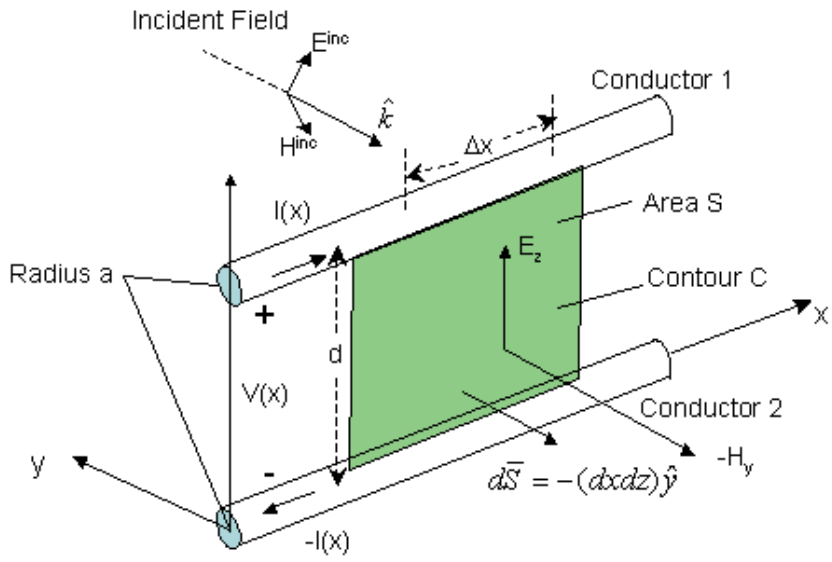

(a) Application of Faraday's law for derivation of first telegrapher's equation

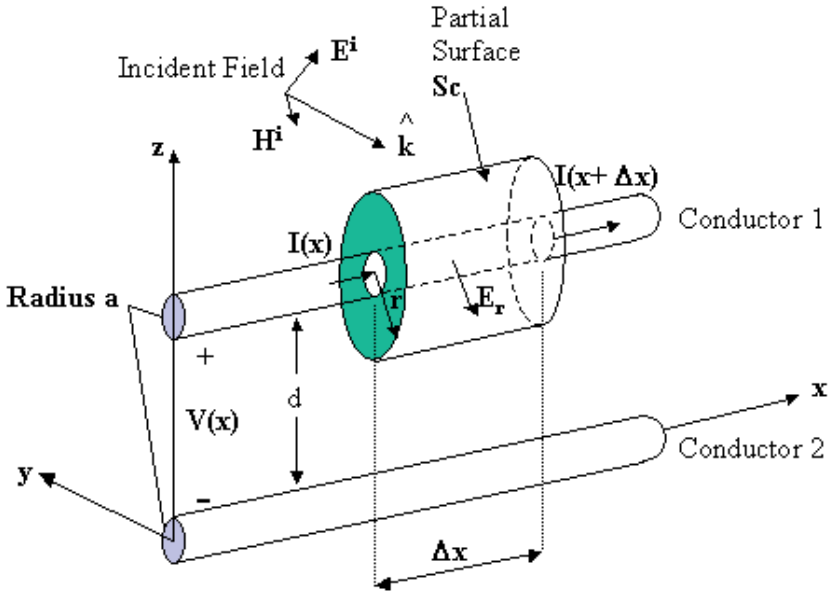

(b) Application of complete Ampere's law for second telegrapher's equation

Figure 3.2: Application of Maxwell's curl equations for derivation of telegrapher's equation (adapted from [42])

form,

$$\int_c \vec{E} \bullet \vec{dl} = -j\omega \cdot \mu \cdot \iint_s \vec{H} \bullet \vec{ds} \tag{3.14}$$

Integrating in the contour marked C in the *anticlockwise* direction and the area marked S, using (3.14), (3.15) is obtained.

$$\begin{aligned} &\int_0^d [E_z(x+\Delta x, z) - E_z(x,z)] \cdot dz - \int_x^{x+\Delta x} [E_x(x,d) - E_x(x,0)] \cdot dx \\ &= -j\omega \cdot \mu \cdot \int_0^d \int_x^{x+\Delta x} -H_y \cdot dx \cdot dz \end{aligned} \tag{3.15}$$

In the quasi-static sense the line-to-line voltage can be defined as (3.16) with a sign convention such that the voltage on the conductor at level d is positive with respect to the other reference conductor,

$$V(x) = -\int_0^d E_z(x,z) \cdot dz \tag{3.16}$$

Note that the tangential components of electric fields along the conductor are zero for perfect conductors. Dividing (3.15) by Δx on both sides and taking the limits $\Delta x \to 0$,

$$\frac{dV(x)}{dx} = -j\omega \cdot \mu \cdot \int_0^d H_y(x,z) \cdot dz \tag{3.17a}$$

$$\begin{aligned} -j\omega \cdot \mu \cdot \int_0^d H_y(x,z) \cdot dz \quad &= \quad -j\omega \cdot \mu \cdot \int_0^d H_y^{inc}(x,z) \cdot dz \\ &\quad -j\omega \cdot \mu \cdot \int_0^d H_y^{sca}(x,z) \cdot dz \end{aligned} \tag{3.17b}$$

The scattered part of the magnetic flux term is due to a current $I(x)$ flowing in the conductors with an assumption of uniform current distribution and also $d >> a$ and $d << \lambda$. The incident part of the magnetic field will appear as distributed source on the line. Hence,

$$j\omega \cdot \mu \cdot \int_0^d H_y^{sca}(x,z) \cdot dz = j\omega \cdot L \cdot I(x) \tag{3.18a}$$

$$j\omega \cdot \mu \cdot \int_0^d H_y^{inc}(x,z) \cdot dz = -V_{S1}(x) \tag{3.18b}$$

Thus the first telegrapher's or transmission line equations is obtained as shown (3.19). The right hand term is zero in (3.19) if there is no incident

source excitation.

$$\frac{dV(x)}{dx} + j\omega \cdot L \cdot I(x) = V_{S1}(x) \tag{3.19}$$

Consider Ampere's law in frequency domain differential form,

$$\nabla \times \vec{H} = j\omega \cdot \varepsilon \cdot \vec{E} + \vec{J} \tag{3.20}$$

Applying *Stoke's* theorem, to (3.20), for a closed surface S surrounding one of the conductors as shown in Fig. 3.2b,

$$\oint_S (\nabla_s \times \vec{H}) \bullet \vec{ds} = I(x+\Delta x) - I(x) + j\omega \cdot \varepsilon \cdot \iint_{S_c} E_r \cdot r \cdot d\phi \cdot dx \tag{3.21}$$

The radial electric field in the vicinity of the wire is considered, which will be used for integration in the partial surface S_c. The total electric field is a combination of incident and scattered field. Dividing (3.21) with Δx and then with limits $r \to a$ and $\Delta x \to 0$,

$$\frac{dI(x)}{dx} + j\omega \cdot \varepsilon \cdot \int_0^{2\pi} E_r^{sca}(x) \cdot a \cdot d\phi + j\omega \cdot \varepsilon \cdot \int_0^{2\pi} E_r^{inc}(x) \cdot a \cdot d\phi = 0 \tag{3.22}$$

The electric field in the vicinity of the wire is independent of ϕ, and since $a << d$,

$$j\omega \cdot \varepsilon \cdot \int_0^{2\pi} E_r^{sca}(x) \cdot a \cdot d\phi = j\omega \cdot q(x) \tag{3.23}$$

The charge $q(x)$ is related to the scattered voltage through the capacitance as, and the total line voltage is a sum of incident and scattered voltage. The contribution of the incident field is in the form of distributed current sources.

$$q(x) = C \cdot V^{sca}(x) \tag{3.24a}$$

$$V^{inc}(x) = -\int_0^d E_z^{inc}(x,z) \cdot dz \tag{3.24b}$$

$$V(x) = V^{inc}(x) + V^{sca}(x) \tag{3.24c}$$

$$I_{S1}(x) = -j\omega \cdot \varepsilon \cdot \int_0^d E_z^{inc}(x,z) \cdot dz \tag{3.24d}$$

Thus rearranging the above equations the second telegrapher's equation is obtained,

$$\frac{dI(x)}{dx} + j\omega \cdot C \cdot V(x) = I_{S1}(x) \tag{3.25}$$

The right hand term is zero in (3.25), if there is no incident source excitation.

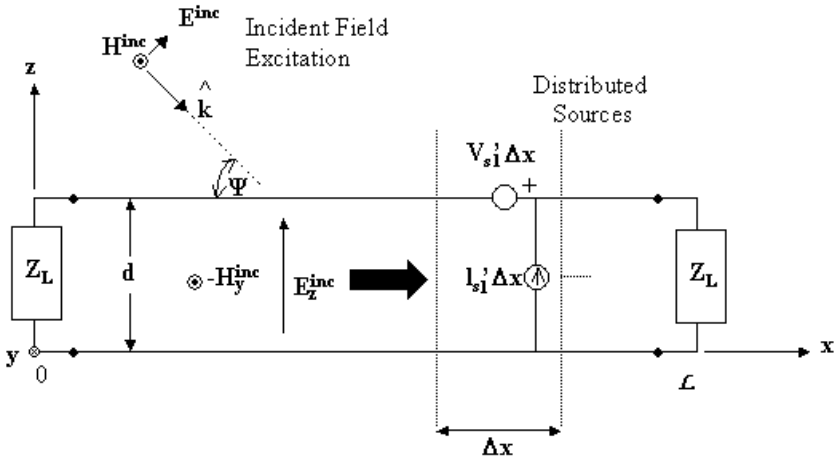

Figure 3.3: Distributed source locations on the line for incident field excitation (adapted from [42])

The distributed source representation of the above two-wire transmission line system is shown in Fig. 3.3 [42]. Transmission line equations now known as telegrapher's equations (3.19) and (3.25), had been derived by *Heaviside* long back in 1887, where he mathematically proved the traveling wave phenomena for two parallel wires[21][37].

It was interesting that *Heaviside* even gave account for the losses in the medium in his derivation of the telegrapher's equations. When the losses are discussed, one talks about the conductivity of the medium in which the wires exist and also the conductivity of the wires themselves. Those two conductivities bring about an additional term in each of the telegrapher's equations, which are the wire resistance and conductance between the wires respectively. The wire resistance is due to the integrals of the electric field along the conductor. It is already mentioned that there isn't any field along the conductors, which is a violation to the TEM definition. Still one can assume that TEM field structure is not fully violated for the wires with small losses. Hence it is appropriate to include the resistance of the wire in the first telegrapher's equation. If the wires are placed in a medium that has finite conductivity, then there exists conduction currents in addition to displacement currents. Then using again the *Maxwell's* curl equation for the magnetic field that includes medium

[21] It has been a long standing request at the IEEE, whether the transmission line equations now commonly known telegrapher's equations are renamed as Heaviside equations in recognition of his remarkable scientific contributions to transmission line theory and electromagnetic field theory [37]. The name telegrapher's equations came into existence because these equations where developed for the pulse propagation studies in the well known Trans Atlantic cable problem.

conductivity an additional term in telegrapher's second equation appears,

$$\sigma \cdot \int_0^{2\pi} E_r^{sca} \cdot a \cdot d\phi = I_c(x) = G \cdot V^{sca}(x) \tag{3.26}$$

Thus the complete telegrapher's equations are given by (3.27a) and (3.27b) respectively.

$$\frac{dV(x)}{dx} + (R + j\omega \cdot L) \cdot I(x) = V_{S1}(x) \tag{3.27a}$$

$$\frac{dI(x)}{dx} + (G + j\omega \cdot C) \cdot V(x) = I_{S1}(x) \tag{3.27b}$$

It should be reminded here that later, in the next Chapter, two other losses known as internal loss and external loss will be discussed in detail.

3.4 Circuit representation of transmission lines

Can the above system of equations (3.27) be realized in the circuit form? How does a two-conductor transmission line behave at low and high frequencies? It is true that since there are inductance, capacitance and distributed current and voltage sources it is possible to form a circuit out of these. For convenience let's discuss without the distributed sources so as to look at it from a circuit perspective and again derive the source free telegrapher's equations. At low frequencies the transmission line is considered to be a short piece of wire with a negligibly small, distributed resistance (if in air) that can be considered as lumped for the purpose of analysis. At higher frequencies, however, the resistive, conductive, capacitive and inductive properties can't be separated and that each infinitesimal length Δx of the transmission line exhibits these properties, as shown in Fig. 3.4. This equivalent circuit is referred to as a distributed circuit model of a two-conductor transmission line and will be used to derive the governing differential equations for propagating voltage and current waves along a transmission line.

Writing down the *Kirchhoff*[22] laws (KVL and KCL) for the Δx transmission line segment in Fig. 3.4,

$$-\frac{V(x+\Delta x,t) - V(x,t)}{\Delta x} = R \cdot I(x,t) + L \cdot \frac{\partial I(x,t)}{\partial t} \tag{3.28}$$

[22] Kirchhoff Gustav Robert (1824 - 1887) developed the famous rules of electric circuit analysis and is the basis of many electromagnetic field problems solved using circuit approach.

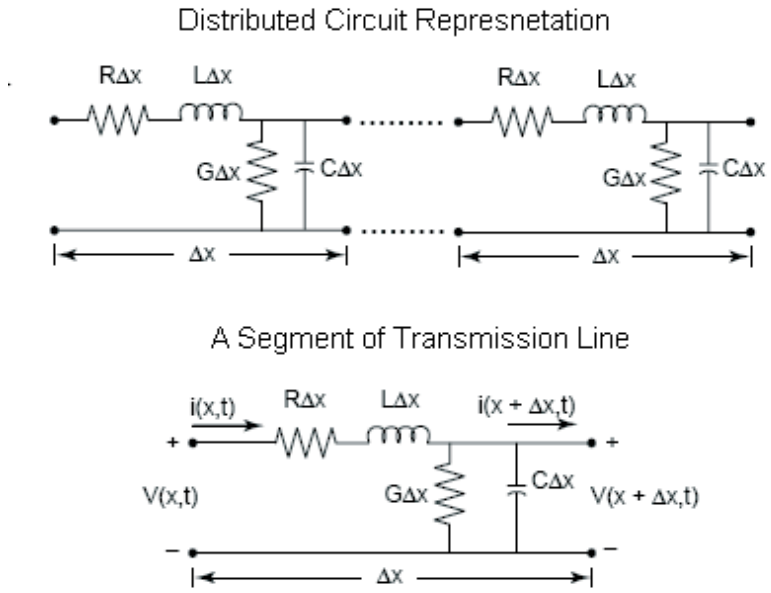

Figure 3.4: Circuit representation of a two-wire transmission line

Limit as $\Delta x \rightarrow 0$ (3.28) becomes,

$$-\frac{\partial V(x,t)}{\partial x} = R \cdot I(x,t) + L \cdot \frac{\partial I(x,t)}{\partial t} \tag{3.29}$$

Similarly,

$$-\frac{I(x+\Delta x,t) - I(x,t)}{\Delta x} = G \cdot V(x,t) + C \cdot \frac{\partial V(x,t)}{\partial t} \tag{3.30}$$

Limit as $\Delta x \rightarrow 0$ (3.30) becomes,

$$-\frac{\partial I(x,t)}{\partial x} = G \cdot V(x,t) + C \cdot \frac{\partial V(x,t)}{\partial t} \tag{3.31}$$

Equations (3.29) and (3.31) are coupled, one can decouple them for the final solutions by differentiating the above equations (3.29) and (3.31), to have second order differential equations as,

$$\begin{aligned} \frac{\partial^2 V(x,t)}{\partial x^2} &= L \cdot C \cdot \frac{\partial^2 V(x,t)}{\partial t^2} + (R \cdot C + L \cdot G) \cdot \frac{\partial V(x,t)}{\partial t} \\ &\quad + R \cdot G \cdot V(x,t) \end{aligned} \tag{3.32a}$$

$$\frac{\partial^2 I(x,t)}{\partial x^2} = L \cdot C \cdot \frac{\partial^2 I(x,t)}{\partial t^2} + (R \cdot C + L \cdot G) \cdot \frac{\partial I(x,t)}{\partial t} + R \cdot G \cdot I(x,t) \tag{3.32b}$$

The solution to the above equations can be obtained using differential operators and the time frequency transformations leading to voltages and currents in their phasor form in space and time for sinusoidal variation of the sources with lines in steady state conditions,

$$V(x,t) = \Re(V(x, j\omega) \cdot e^{j\omega \cdot t}) \tag{3.33a}$$

$$I(x,t) = \Re(I(x, j\omega) \cdot e^{j\omega \cdot t}) \tag{3.33b}$$

To discuss some of the aspects of line propagation parameters, let's take the discussion to frequency domain in Laplace or s domain with $s \Leftrightarrow j\omega$.

$$\frac{d^2 V(x,s)}{dx^2} - \gamma^2 \cdot V(x,s) = 0 \tag{3.34a}$$

$$\frac{d^2 I(x,s)}{dx^2} - \gamma^2 \cdot I(x,s) = 0 \tag{3.34b}$$

Solution of second order differential equations gives us,

$$V(x,s) = V^+(s) \cdot e^{-\gamma x} + V^-(s) \cdot e^{\gamma x} \tag{3.35}$$

The current can be obtained from voltage,

$$I(x,s) = \frac{-1}{R + s \cdot L} \cdot \frac{dV(x,s)}{dx} = \frac{V^+(s) \cdot e^{-\gamma x} - V^-(s) \cdot e^{\gamma x}}{Z_0} \tag{3.36}$$

In (3.36) Z_0 is referred to as characteristic impedance of the line, which will be discussed soon. At this juncture it is interesting to define the well-known A, B, C and D constants of the transmission line. Let the impedance and admittance of the line be given as (3.37a) and (3.37b) respectively which are uniformly distributed along the line,

$$Z(s) = R + s \cdot L \tag{3.37a}$$

$$Y(s) = G + s \cdot C \tag{3.37b}$$

Let $V_s(x = 0)$ be the voltage at the sending end and $V_r(x = l)$ be the voltage at some receiving end on the line. At $x = 0$

$$V_s(s) = V^+(s) + V^-(s) \tag{3.38a}$$

$$I_s(s) = \frac{V^+(s) - V^-(s)}{Z_0} \tag{3.38b}$$

From which the undetermined constants are,

$$V^+(s) = \frac{V_s(s) + Z_0 \cdot I_s(s)}{2} \tag{3.39a}$$

$$V^-(s) = \frac{V_s(s) - Z_0 \cdot I_s(s)}{2} \tag{3.39b}$$

Substituting (3.39) in (3.35) and (3.36), and rearranging, for any point on the line,

$$V(x,s) = V_s(s) \cdot \cosh(\gamma x) + I_s(s) \cdot Z_0 \sinh(\gamma x) \tag{3.40a}$$

$$I(x,s) = I_s(s) \cdot \cosh(\gamma x) + \frac{V_s(s)}{Z_0} \cdot \sinh(\gamma x) \tag{3.40b}$$

$$A_t = D_t = \cosh(\gamma x) \tag{3.41a}$$

$$B_t = Z_0 \cdot \sinh(\gamma x) \tag{3.41b}$$

$$C_t = \frac{1}{Z_0} \cdot \sinh(\gamma x) \tag{3.41c}$$

Usually the voltage and current at the sending end is known, from which using the transformation matrix the voltage at receiving end at $x = l$, can be obtained as,

$$\begin{pmatrix} V_r(s) \\ I_r(s) \end{pmatrix} = \begin{pmatrix} A_t & B_t \\ C_t & D_t \end{pmatrix} \cdot \begin{pmatrix} V_s(s) \\ I_s(s) \end{pmatrix} \tag{3.42}$$

Transmission line can be realized in a 'T' network arrangement as shown in Fig. 3.5. It can be used to derive the characteristic impedance. By definition, it is the input impedance of an infinite transmission line. Consider a line of length Δx with its line impedance and line admittance forming the elements of 'T' network. Let us view the input impedance from port 1-1 and to demonstrate the infinite line terminate port 2-2 with impedance Z_0. The equivalent input impedance from Fig. 3.5 is,

$$Z_0 = \frac{Z}{2} \cdot \Delta x + \frac{\left(\frac{Z}{2} \cdot \Delta x + Z_0\right)}{Y \cdot \Delta x} \cdot \left(\frac{Z}{2} \cdot \Delta x + Z_0 + \frac{1}{Y \cdot \Delta x}\right)^{-1} \tag{3.43}$$

$$\lim_{\Delta x \to 0} Z_0 = \sqrt{\frac{Z}{Y}} \tag{3.44}$$

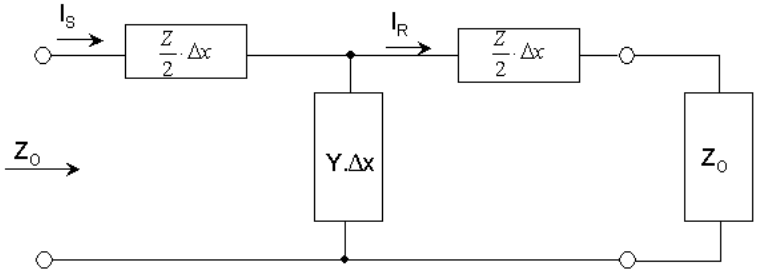

Figure 3.5: T model representation of the transmission line

A pulse launched on the transmission line from the sending end will reach the receiving end after some time delay, to demonstrate this let's relax the system to lossless case meaning one has just the inductance and capacitance of the line. For this case using the relation $\gamma = j\beta$, $\beta = \frac{\omega}{v}$, ABCD constants of the line, with $T = \frac{1}{v}$,

$$\begin{pmatrix} V_r(s) \\ I_r(s) \end{pmatrix} = \begin{pmatrix} \left(\frac{e^{sT}+e^{-sT}}{2}\right) & -Z_0 \cdot \left(\frac{e^{sT}-e^{-sT}}{2}\right) \\ -\frac{1}{Z_0} \cdot \left(\frac{e^{sT}-e^{-sT}}{2}\right) & \left(\frac{e^{sT}+e^{-sT}}{2}\right) \end{pmatrix} \cdot \begin{pmatrix} V_s(s) \\ I_s(s) \end{pmatrix} \quad (3.45)$$

The shifting theorem in Laplace transforms, is defined by, $F(s) \cdot e^{\pm a \cdot s} = f(t \pm a)$, which in the present context means, wave traveling in MTLs systems reaches at different points with specific time delays.

3.5 Solutions to Two Conductor Transmission Line equations

Tesche [42] has derived the general solution for a transmission line. The expressions for the voltage and currents along the transmission line in terms of propagation constant and reflection coefficients at the line terminals are shown in equation (3.46). The simplicity of equation (3.46) are that the voltages and currents can be obtained for each frequency sweeps and the corresponding time domain signal can be obtained from the frequency response by a direct inverse Fourier transform operation. In the present work the inverse discrete Fourier transform is carried out in *Matlab 6.5.1* [45], for faster computation. The current distribution in the wire was calculated first in frequency domain using vectorised coding and then an *ifft* operation in *Matlab* was carried out. Consider a wire of length L, with the line having voltage source V_0 or current source I_0 at any point along the wire say at x_s as shown in Fig. 3.6, then the solution for transmission line equations is [42],

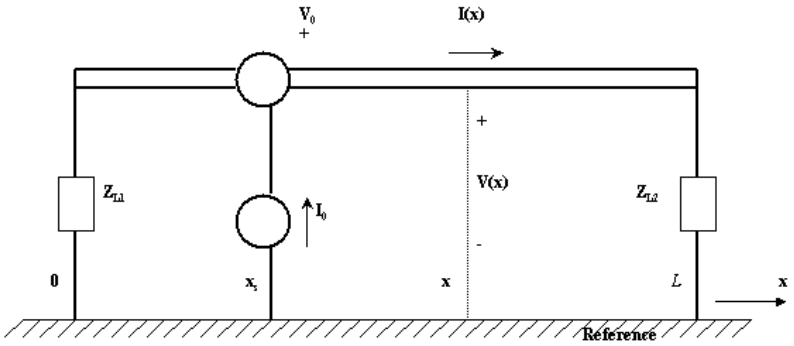

Figure 3.6: Schematic of the transmission line under analysis for equation (3.42)

for $x > x_s$

$$V(x) = \frac{e^{-\gamma x} + \rho_2 \cdot e^{\gamma \cdot (x-2L)}}{2(1-\rho_1\rho_2 e^{-2\gamma L})} \cdot \left[\left(e^{\gamma x_s} - \rho_1 \cdot e^{-\gamma x_s}\right) \cdot V_0 + \left(e^{\gamma x_s} + \rho_1 \cdot e^{-\gamma x_s}\right) \cdot Z_0 \cdot I_0\right] \tag{3.46a}$$

$$I(x) = \frac{e^{-\gamma x} - \rho_2 \cdot e^{\gamma \cdot (x-2L)}}{2Z_0 \cdot (1-\rho_1\rho_2 e^{-2\gamma L})} \cdot \left[\left(e^{\gamma x_s} - \rho_1 \cdot e^{-\gamma x_s}\right) \cdot V_0 + \left(e^{\gamma x_s} + \rho_1 \cdot e^{-\gamma x_s}\right) \cdot Z_0 \cdot I_0\right] \tag{3.46b}$$

for $x < x_s$

$$V(x) = \frac{e^{\gamma(x-L)} + \rho_1 \cdot e^{-\gamma(x+L)}}{2 \cdot (1-\rho_1\rho_2 e^{-2\gamma L})} \cdot \left[-\left(e^{\gamma(L-x_s)} - \rho_2 \cdot e^{-\gamma(L-x_s)}\right) \cdot V_0 + \left(e^{\gamma(L-x_s)} + \rho_2 \cdot e^{-\gamma(L-x_s)}\right) \cdot Z_0 \cdot I_0\right] \tag{3.46c}$$

$$I(x) = \frac{e^{\gamma(x-L)} - \rho_1 \cdot e^{-\gamma(x+L)}}{2Z_0 \cdot (1-\rho_1\rho_2 e^{-2\gamma L})} \cdot \left[-\left(e^{\gamma(L-x_s)} - \rho_2 \cdot e^{-\gamma(L-x_s)}\right) \cdot V_0 + \left(e^{\gamma(L-x_s)} + \rho_2 \cdot e^{-\gamma(L-x_s)}\right) \cdot Z_0 \cdot I_0\right] \tag{3.46d}$$

In the above

$$\rho_{Li} = \frac{Z_{Li} - Z_0}{Z_{Li} + Z_0}; i = 1, 2, ... \tag{3.46e}$$

The above set of transmission line solutions will be used in a number of occasions in the later chapters. Also there will be a discussion later, on how to solve telegrapher's equations numerically in time domain.

3.6 Conclusions

In this Chapter it is shown in detail the definition of a transmission line, its governing equations for voltages and currents. The telegrapher's equations, which will be used widely in the later chapters, are derived here from both field theory and circuit theory approaches. Some of the definitions with regard to propagation aspects like attenuation, phase constant, characteristic impedance and velocity of propagation is also discussed. It is true that if in the transmission line equations resistance and conductance terms are present then it is a lossy line. But those losses may not be constant when the frequencies are changing, in literature they are referred to as frequency dependant losses and will be discussed in detail in the next Chapter. The next Chapter will also deal with multi-conductor lines above ground. *One important message delivered from this Chapter is that the discussions made are always in the limits of transmission line approximation, that is, the distances between the wires carrying currents and voltages are much smaller than the wavelengths of the propagating voltage and current waves. If the frequencies of the propagating waves do not satisfy this important condition, then clearly transmission line approximation is questionable!*

4. Wave Propagation in Multiconductor Transmission Lines above Ground

In two-conductor transmission line theory as discussed in the earlier Chapter one of the wires was carrying the currents in the opposite direction with respect to the other because of which there was a sign convention adopted for the voltages of the conductor, i.e. the conductor carrying current in the positive direction of x had a positive voltage and the conductor carrying the current in the negative x direction had a negative voltage. The wire that was carrying current in the negative x direction is referred to as return conductor (refer Fig. 3.2a and 3.2b). Thus in the case of MTLs systems above ground the reference conductor is the ground that carries or returns currents in the negative x direction. Thus all philosophizes and theories discussed in the previous Chapter apply here as well. The problems here one could face are of two types. What would happen to the voltages and currents propagating on the MTLs system if, 1.) reference ground is not perfect and it is a real earth and 2.) wires of MTLs system are not perfect? In the previous Chapter uniform homogeneous medium was considered. This Chapter will seek to find some answer to those above questions. More emphasis is given for direct numerical time domain solutions of the telegrapher's equations. This is necessary because later while calculating the induced voltages, continuous monitoring of the voltages and currents on the MTLs system of the Swedish railway system is needed, for modeling the non-linear phenomena like insulator flashover and soil ionization at the pole footing. These non-linear phenomena will be used with computationally efficient schemes of numerical calculations.

4.1 Telegrapher's equations for MTLs

Voltage and current wave propagation in MTLs is well represented by the two set of equations, described for perfectly conducting ground and non dissipative line (lossless/ideal) case as shown in (4.1) and for imperfect/dissipative lines and ground (lossy and frequency independent) case as shown in (4.2), respectively in frequency domain. *Note that in the Laplace domain frequency is represented by s, while in Fourier domain it is* $j\omega$. Those equations (4.1)

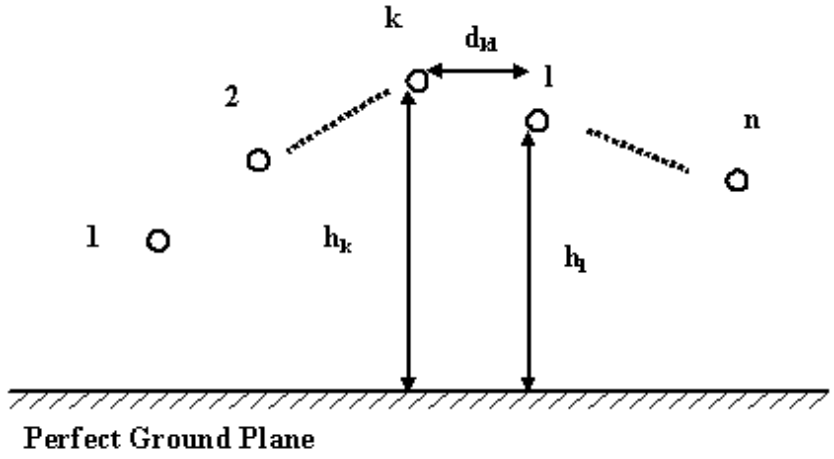

Figure 4.1: System of MTLs above a perfect ground plane

and (4.2) are popularly known as telegrapher's equations as discussed in previous Chapter. Equations (4.1a) and (4.2a) are the voltage wave equations and (4.1b) and (4.2b) are the current wave equations. For a system of n conductors as shown in Fig. 4.1, the terms $\overline{V}(x, j\omega)$ and $\overline{I}(x, j\omega)$ in (4.1) and (4.2), are the voltage and current vectors having size n. Further, L_i, L_e, C_e, R and G are the per unit length series inductance (internal and external), shunt capacitance, series resistance and shunt conductance matrices of size n respectively. Note, that for convenience, discussions below are for no external field conditions.

Under ideal or lossless conditions,

$$\frac{dV(x, j\omega)}{dx} + L_e \cdot j\omega \cdot I(x, j\omega) = 0 \tag{4.1a}$$

$$\frac{dI(x, j\omega)}{dx} + C_e \cdot j\omega \cdot V(x, j\omega) = 0 \tag{4.1b}$$

Under lossy conditions,

$$\frac{dV(x, j\omega)}{dx} + R \cdot I(x, j\omega) + (L_i + L_e) \cdot j\omega \cdot I(x, j\omega) = 0 \tag{4.2a}$$

$$\frac{dI(x, j\omega)}{dx} + G \cdot V(x, j\omega) + C_e \cdot j\omega \cdot V(x, j\omega) = 0 \tag{4.2b}$$

When the conductors are in air the G matrix is negligible since the conductivity of air is negligible. Further, the R matrix is also negligible as it represents the internal resistance of the conductors, hence is usually neglected. In the previous Chapter it was mentioned that it is a parameter due to the longi-

tudinal component of the electric field along the line. While dealing with high frequencies the R matrix cannot be neglected due to skin effect, a frequency dependant internal loss in the conductors, that will be discussed later. The resistance matrix R is diagonal as it deals with the internal resistance of each of the conductors. The internal inductance L_i matrix is also diagonal whose value is approximately $\frac{\mu_0}{8\pi}$. The internal inductance and internal resistance are not constant and are functions of frequency, which will be discussed while dealing with skin effect phenomenon of the conductors.

Now let's consider the per unit length parameter L_e and C_e matrix calculations. Consider in Fig. 4.1 with conductors k and l that has heights h_k and h_l, radii r_k and r_l and horizontal separation of d_{kl}. Then for external inductance matrix the k_{th} diagonal element and the kl_{th} mutual element are given by (4.3) [12, 41 - 43].

$$L_{ekk} = \frac{\mu_0}{2\pi} \cdot \ln\left(\frac{2h_k}{r_k}\right) \tag{4.3a}$$

$$L_{ekl} = \frac{\mu_0}{2\pi} \cdot \ln\left(\frac{\sqrt{(h_k+h_l)^2+d_{kl}^2}}{\sqrt{(h_k-h_l)^2+d_{kl}^2}}\right) \tag{4.3b}$$

To get the capacitance matrix, one has to first obtain the potential coefficient matrix in the same way as the inductance coefficients as in (4.3) and it is given by (4.4). Finally, the capacitance matrix is obtained by the inversion of the potential coefficient matrix (4.5) [46]. Note that all the expressions for inductance and capacitance matrices are calculated using the image theory [12, 42, 46] first developed by *Lord Kelvin*[23].

$$P_{ekk} = \frac{1}{2\pi\varepsilon_0} \cdot \ln\left(\frac{2h_k}{r_k}\right) \tag{4.4a}$$

$$P_{ekl} = \frac{1}{2\pi\varepsilon_0} \cdot \ln\left(\frac{\sqrt{(h_k+h_l)^2+d_{kl}^2}}{\sqrt{(h_k-h_l)^2+d_{kl}^2}}\right) \tag{4.4b}$$

[23]Lord Kelvin (William Thomson - 1824 - 1907) was a professor at Glasgow University where he was studying the pulse propagation in Trans Atlantic cable (1855) a landline connecting North America and Europe via Alaska and Siberia. On 17th August 1858, the first messages were exchanged, among them one between Queen Victoria and President Buchanan. The cable failed due to an erroneous theory making it unusable after exchange of about few hundreds of messages. Lord Kelvin assumed that magnetic effects are negligible for transmission line theory and considered only the capacitance and resistance per unit length of the cable, which when used in the present telegrapher's equations one ends up in diffusion equation. Kirchoff proposed the long line theory to include self-induction effects in 1857. It was Heaviside who later formulated all the parameters required for complete transmission line theory [37].

$$C_e = [P_e]^{-1} \tag{4.5}$$

Next let us discuss how to include frequency dependant losses in the system. They are referred to as internal and external loss and let's take them one by one.

4.2 Internal losses in telegrapher's equations - conductor skin effect

While dealing with high frequencies the R matrix is frequency dependant and cannot be neglected. The same applies for internal inductance as well. These are due to the phenomena of skin effect, a frequency dependant internal loss in the conductors [12, 41 - 43]. Let us rewrite (4.2a), considering only the internal parameters/impedance and rewrite the voltage wave equations (4.2a), dropping the external inductance term as in (4.6).

$$\frac{dV_i(x, j\omega)}{dx} + Z_{iint}(j\omega) \cdot I(x, j\omega) = 0 \tag{4.6a}$$

$$Z_{iint}(j\omega) = R_i(j\omega) + j\omega \cdot L_i(j\omega) \tag{4.6b}$$

4.2.1 Skin effect phenomena

Skin effect is mostly due to high frequency current flow in the conductor, wherein it is seen that the currents tend to be concentrated in a thin layer or skin near the surface of the conductor, which are nearest to the field sources producing them [47]. A good conductor is one in which the conduction current exceeds largely the displacement current, due to which,

$$\nabla \times \vec{H} = \vec{J} = \sigma \cdot \vec{E} \tag{4.7a}$$

Taking curl of Faraday's law

$$\nabla \times \nabla \times \vec{E} = -j\omega\mu \cdot \nabla \times \vec{H} \tag{4.7b}$$

Since $\nabla \bullet \vec{E} = 0$,

$$\nabla^2 \vec{J} = -j\omega\mu \cdot \sigma \cdot \vec{J} \tag{4.8}$$

Equation (4.8) is known as the well known diffusion equation and for any given cross section is some times known as the *Ohm's*[24] law. The interesting feature of the above diffusion equation is that the $\vec{J}$ can be replaced with

[24] Ohm Georg Simon (1789 - 1854) in 1826 discovered that current flow is proportional to potential difference and inversely proportional to resistance. Ohm's law!

$\vec{E}$ or $\vec{H}$, which will give the relation between the space and time derivatives of magnetic or electric fields or current densities at any point in a conductor. Consider a plane conductor of infinite depth as shown in Fig. 4.2, with no field variations along the width or the length dimensions, thus one has a semi-infinite solid in the $x < 0$ direction, with yz plane coinciding the surface. Let the current flow be in z direction and x is normal to the surface with no variations in y and z direction.

$$J_z = \int_0^\infty I_z \cdot dx \tag{4.9}$$

$$\frac{d^2 I_z}{dx^2} = j\omega\mu \cdot \sigma \cdot I_z = \tau_d^2 \cdot I_z \tag{4.10a}$$

The complete solution will be in terms of exponentials by using the boundary conditions i.e. $I_z = i_0$ at $x = 0$,

$$\tau_d = \frac{1+j}{\delta_i} \tag{4.10b}$$

$$\delta_i = \frac{2}{\sqrt{\omega \cdot \mu \cdot \sigma}} \tag{4.10c}$$

$$I_z = i_0 \cdot e^{-\frac{x}{\delta_i}} \cdot e^{-j\frac{x}{\delta_i}} \tag{4.10d}$$

The implication of the equation (4.10d) is that magnitude of the current decreases exponentially with penetration into the conductor and δ_i has the significance at the depth at which the current density has decreased to $\frac{1}{e}$ of its value at the surface. δ_i is widely referred to as the skin depth of the conductors. The internal intrinsic impedance for this case for unit length and width, with surface field as $E_{z0} = \frac{i_0}{\sigma}$ is,

$$Z_s = \frac{E_{z0}}{J_z} = \frac{1+j}{\sigma \cdot \delta_i} \tag{4.11}$$

4.2.2 Internal impedance for circular wires ¶

Shelkunoff [48, 49] gave the exact expression for internal impedance for round wires of radiu r_w as shown in (4.12), which was in terms of modified *Bessel's* functions of the first kind of order zero and one.

$$Z_{iint}(j\omega) = \frac{\sqrt{j\omega \cdot \mu \cdot \sigma}}{2\pi \cdot \sigma \cdot r_w} \cdot \frac{I_0(\sqrt{j\omega \cdot \mu \cdot \sigma} \cdot r_w)}{I_1(\sqrt{j\omega \cdot \mu \cdot \sigma} \cdot r_w)} \tag{4.12}$$

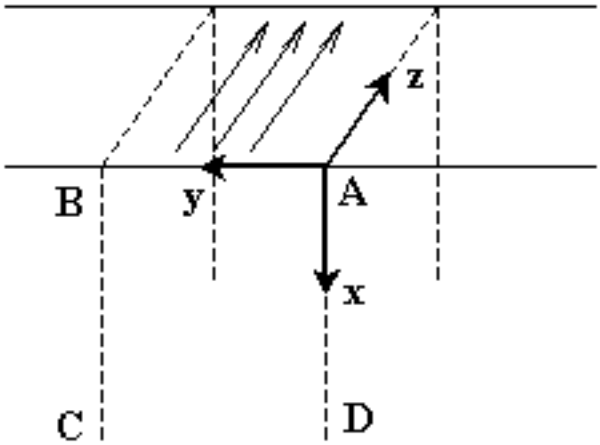

Figure 4.2: Plane solid conductor for demonstrating skin effect phenomena (adapted from [47])

Nahman and Holt [50] propose approximate formula for wide range of frequencies as given by (4.13).

$$Z_{iint}(j\omega) \approx A + B\sqrt{j\omega} \tag{4.13a}$$

$$A = R_{DC} = \frac{1}{\pi \cdot \sigma \cdot r_w^2} \tag{4.13b}$$

$$B = \frac{1}{2\pi \cdot r_w} \cdot \sqrt{\frac{\mu}{\sigma}} \tag{4.13c}$$

Wedepohl and Wilcox [51] gave another approximate formula as given by (4.14).

$$Z_{iint}(j\omega) = \frac{\sqrt{j\omega \cdot \mu \cdot \sigma}}{2\pi \cdot \sigma \cdot r_w} \cdot \coth(0.777 \cdot r_w \cdot \sqrt{j\omega \cdot \mu \cdot \sigma}) + \frac{0.356}{\pi \cdot \sigma \cdot r_w^2} \tag{4.14}$$

Let's compare the above equations for internal impedance for wide range of frequencies and judge their efficacy for our later applications. Fig. 4.3a and Fig. 4.3b shows the internal impedance for rails ($R1$ or $R2$ in Fig. 1.6) with radius $0.0495m$ and an overhead wire e.g. $R7$ in Fig. 1.6, with radius $0.0056m$ respectively. Their material properties can be found in Table 1.2. From Figs. 4.3a and b it is clear that all the three expressions for the internal impedances (4.12, 4.13 and 4.14) are valid. The magnitudes of all the internal impedance are identical whether it is a rail or an overhead conductor. What seems to be

in error is the phase, equation (4.13) shows very large differences in phase compared to equations (4.12) or (4.13). The best choice therefore is either (4.12) or (4.14), but (4.13) has an added advantage when the time domain simulations are to be carried out.

To investigate the errors involved in the application of equation (4.13) for future simulations, let's simulate two pulse propagation problems corresponding to the lightning frequency. Consider two current impulses one that has a rise time of $0.1\mu s$ (fast) and the other with a rise time of $10\mu s$ (slow). The 50% tail time is around $70\mu s$ in both the cases. The former pulse corresponds to subsequent type strokes and the later to first type return strokes. The simulations were carried out with simple and/or more valid expression (4.14) and (4.13) with pulse injected from one end of the line with the other end of the line open. The simulations were performed for a rail and an overhead wire separately with the same material data as was used for Fig. 4.3. Note, the simulations were carried out in frequency domain and then transformed to time domain as discussed in Chapter-3 using equations (3.46). The rail is at a height of $0.55m$, while the overhead wire is at height of $10m$. The length of the line was $1km$. The simulation results with current waveforms at three distances injection point, $400m$ and $800m$ from the injection point are shown in Fig. 4.4a and 4.4b for fast and slow impulses respectively. It can be seen that even though there is an error in the phase of equation (4.13), simulations show that whether ones uses exact (4.12) or approximate expressions (4.13 or 4.14) the errors are nominal. It was decided to use equation (4.13) for later direct time domain simulations without going to frequency domain solutions, because of the need to do so as discussed in the beginning of this Chapter.

4.2.3 Internal impedance in time domain ¶

In time domain simulations telegrapher's equations involving any frequency dependant loss in frequency domain, leads to convolution integrals in time domain. Internal loss in time domain is expressed by *Laplace* Transform, as shown in (4.15a and b) for the voltage due to internal loss be $V_i(x,s)$, then,

$$\frac{dV_i(x,s)}{dx} = -(Z_{iint}(s)) \cdot I(x,s) \tag{4.15a}$$

$$\frac{dV_i(x,s)}{dx} = -(A + B\sqrt{s}) \cdot I(x,s) \tag{4.15b}$$

Equation (4.15a) when transformed to time domain leads to a convolution as shown in (4.15d).

$$\frac{\partial V_i(x,t)}{\partial x} = -[Z_{iint}(t)] * I(x,t) \tag{4.15c}$$

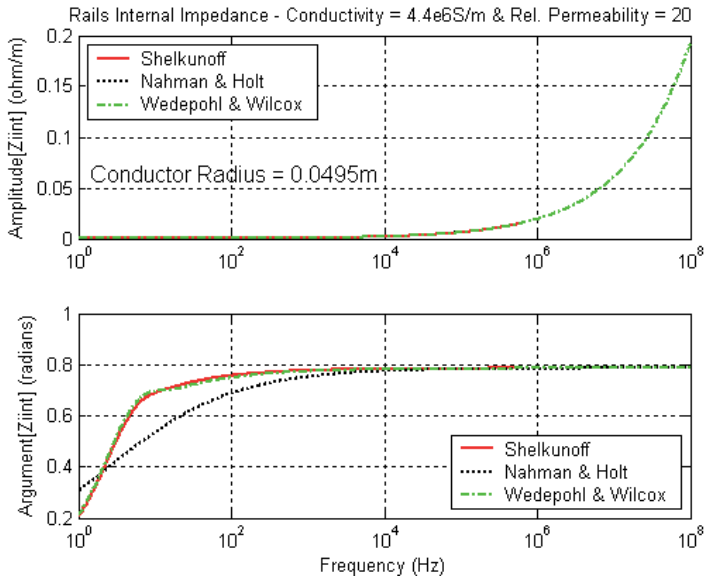

(a) Rails

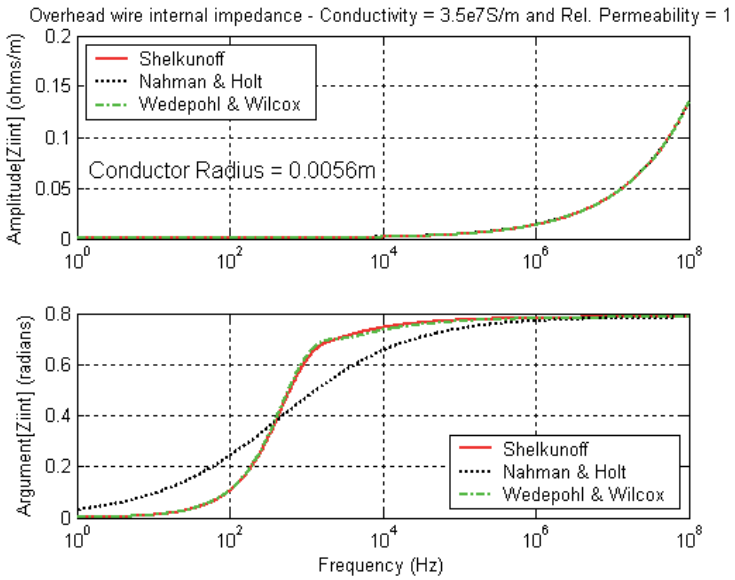

(b) Overhead wire

Figure 4.3: Internal impedance for rails and overhead wire using exact and approximate expression

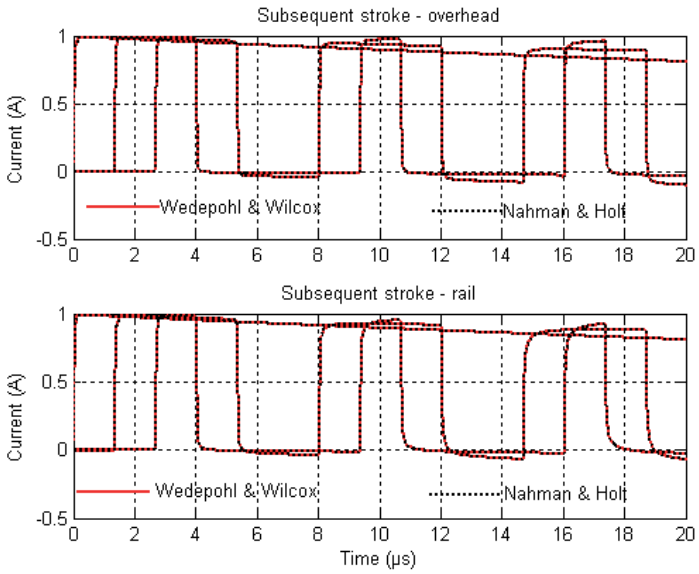

(a) Fast impulse

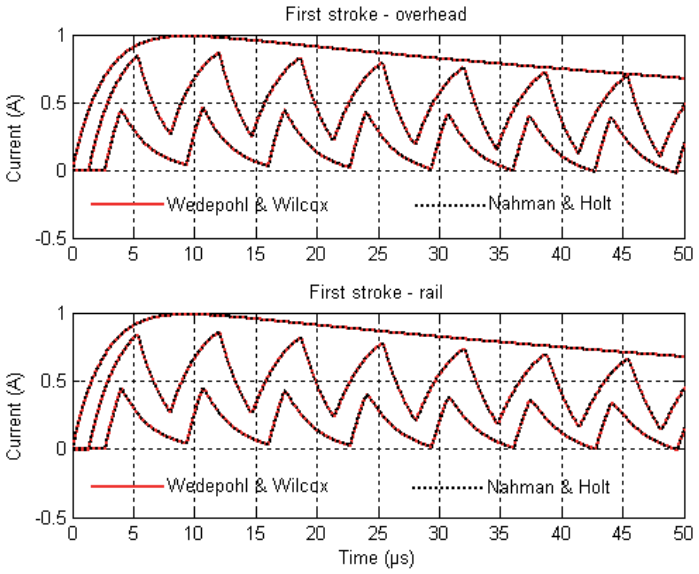

(b) Slow impulse

Figure 4.4: Current responses at injection point, 400m and 800m using Wedepohl and Wilcox (solid red) and Nahman and Holt (dotted black) expressions for internal impedance for fast and slow impulse current injections

$$\frac{\partial V_i(x,t)}{\partial x} = -A \cdot I(x,t) - \frac{1}{\sqrt{\pi}} \cdot B \cdot \left(\int_0^t \frac{1}{\sqrt{\tau}} \cdot \frac{\partial I(x,t-\tau)}{\partial (t-\tau)} \cdot d\tau \right) \qquad (4.15d)$$

Time domain expression (4.15d) is later used in the study. It is very interesting to note that for using (4.15d) later one needs to know only the values of A and B as given by (4.13), which is very computationally efficient when used for time domain simulations using recursive convolutions [12]. This is discussed later while dealing with numerical time domain simulations of telegrapher's equations.

4.3 External loss in telegrapher's equations - dissipative or lossy ground

Now, let us introduce yet another and most important frequency dependant loss, a loss due to the imperfect or lossy or dissipative ground. Usually, for typical overhead wires this ground loss is more important when compared to the skin effect of the conductors discussed in the previous section [20, 52, 53]. Let us see what this loss is and how it can be incorporated into the telegrapher's equations. In the earlier discussion of skin effect phenomena it was seen that magnitude of the current decreases with depth in the semi-infinite metallic medium. A somewhat similar phenomenon rather more complex happens, if instead of a perfectly conducting plane or a semi-infinite metallic medium the multi conductor transmission lines are located above a real soil or ground medium. The complexity is in identifying the proper meaning to the line voltage. As was discussed in the previous Chapter the line voltage is defined as the line integral of electric field from the reference conductor to the location of the other conductor. Thus in wire above perfect ground the voltage is the line integral from the surface of the ground to the height of the conductor. For real ground or soil, the electric field in the earth is non-zero and the zero/reference level is only at a certain depth. Well, the question is at what depth one can find this?

4.3.1 Ground impedance and its role in telegrapher's equations

Tesche [42], mentions that in order to get the total voltage of the line or wire, the line integral is to be split into two parts. One integral is between the surface of the ground to the wire location in air and the other integral is from the $-\infty$ in the earth to the surface of the earth. For discussions below, let's drop the incident fields and consider only the wire above the ground and assume that some incident field caused the induced current in the wire and neglect the

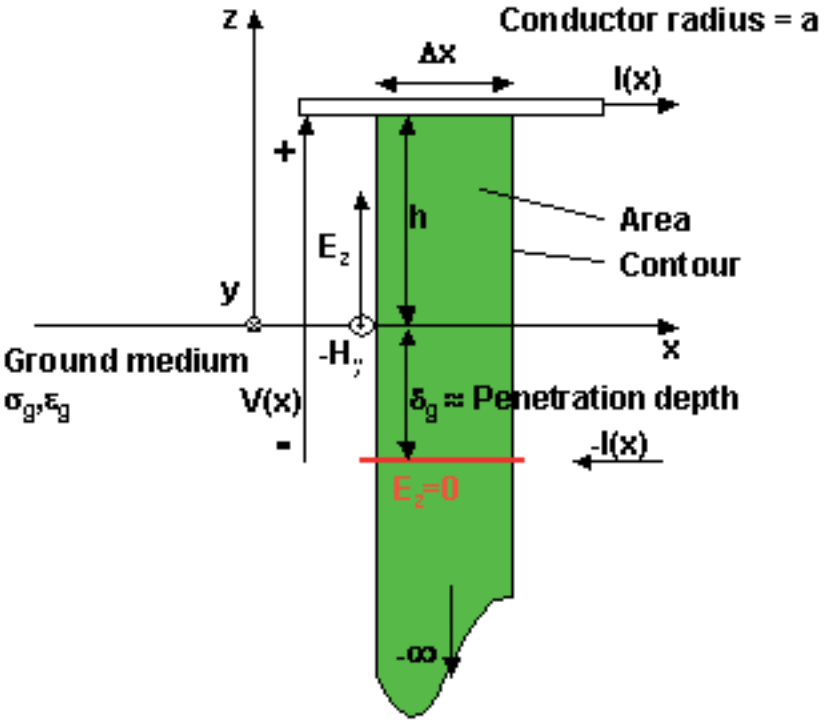

Figure 4.5: Single conductor above a dissipative semi-infinite earth (adapted from [42] and modified)

distributed sources due to the reflected and transmitted fields. Let's start with the equation (3.14) and referring to the Fig.4.5, taking the integration from $-\infty$ (assuming the zero reference point) to h (conductor height), one has,

$$\int_{-\infty}^{h} [E_z(x+\Delta x,z) - E_z(x,z)] \cdot dz - \int_{x}^{x+\Delta x} [E_x(x,d) - E_x(x,0)] \cdot dx$$
$$= -j\omega \cdot \mu_0 \cdot \int_{-\infty}^{h} \int_{x}^{x+\Delta x} -H_y \cdot dx \cdot dz \tag{4.16}$$

The first integral in the left hand side is the required voltage at two points on the line and the second integral corresponds to the internal loss, which for perfect conductor is zero. Under the limits $\Delta x \rightarrow 0$, the left hand side of the equation (4.16) gives the derivative of the voltage drop and also the drop due to skin effect (internal impedance) of the conductor. Similarly the right hand side of equation (4.16) for no incident or transmitted fields and with only scattered

field gives,

$$-j\omega\cdot\mu_0\cdot\int_{-\infty}^{h}H_y^{sca}(x,z)\cdot dz=-(j\omega\cdot L_e+Z_g(j\omega))\cdot I(x,j\omega) \tag{4.17}$$

Equation (4.17) is the flux due to the wire current and the return current in the ground.

$$-\frac{dV(x,j\omega)}{dx}=(Z_{iint}(j\omega)+j\omega\cdot L_e+Z_g(j\omega))\cdot I(x,j\omega) \tag{4.18}$$

Note, there exists only external inductance term for wire above a perfect ground. From (4.17) and (4.18) it is seen that the total external impedance is a series combination of impedance due to external impedance due to inductance of wire with perfect ground and the ground impedance Z_g. The ground impedance is the subject of study in this section. Many researchers have contributed to its development. Only the most important ones with regard to the present study are considered. Also corresponding time domain expressions, needed for direct time domain solutions of telegrapher's equations are discussed.

Similar to ground impedance one might expect ground admittance term. In the previous Chapter equation (3.23) gives the linear charge density along the conductor, which is completely related to the capacitance of the system and the associated scattered voltage, since $V_{sca}(x,j\omega)=V(x,j\omega)$ for the problem one has,

$$j\omega\cdot q(x,j\omega)=j\omega\cdot C_{system}\cdot V(x,j\omega)=Y(j\omega)\cdot V(x,j\omega) \tag{4.19}$$

$$\frac{j\omega\cdot q(x,j\omega)}{Y(j\omega)}=\int_0^h E_z\cdot dz+\int_{-\infty}^0 E_z\cdot dz \tag{4.20}$$

$$\frac{1}{Y(j\omega)}=\frac{1}{j\omega\cdot C_e}+\frac{1}{Y_g(j\omega)} \tag{4.21}$$

$$-\frac{dI(x,j\omega)}{dx}=Y(j\omega)\cdot V(x,j\omega) \tag{4.22}$$

$$Y=\frac{j\omega\cdot C_e\cdot Y_g(j\omega)}{j\omega\cdot C_e+Y_g(j\omega)} \tag{4.23}$$

Thus it is seen that the total admittance is a series combination of external admittance due to capacitance of the wire to ground with perfect ground and the ground admittance.

4.3.2 Earth's behavior to incident electromagnetic fields and the transmission line limit for wires above ground

The critical frequency for the soil is the instant when the displacement currents become equal to the conduction currents. For a given soil if the critical frequency is $\omega_c = \frac{\sigma_g}{\varepsilon_g}$ and if the impinging electromagnetic wave to the soil has a frequency ω, then the behavior of the earth to those incident waves is shown in Table. 4.1 [54 **Paper-A**, 55] . The last column in the Table. 4.1, gives the different types of electromagnetic pulses that are encountered in different practical EMC problems, valid approximations for transmission line analysis are also given [54 **Paper-A**].

Table 4.1: *Earth's behavior to incident electromagnetic waves corresponding to critical frequency* ω_c

Approx.	Condition	Earth property	Region	Pulse type
Low	$\omega < 0.1\omega_c$	σ_g	Carson	Power/ Switching/ Typical first stroke
High	$0.1\omega_c < \omega < 2\omega_c$	σ_g & ε_g	Transition	First and Subsequent strokes
Very High	$2\omega_c < \omega$	ε_g	Seymlen/ Asymptotic	NEMP/ HEMP

Since transmission line type analysis is being dealt, it is necessary to note that there is a restriction on the height of the conductor such that (4.24) is satisfied [42, 52, 53].

$$\frac{2\pi \cdot h}{\lambda_{pulse}} << 1 \tag{4.24}$$

With increase in the frequency the wavelength decreases and there would be an instant when the wavelength is comparable to the heights of the conductor. Therefore the discussions below are valid only under the so-called limits of transmission line approximations [42, 52, 53]. For the lightning type of transients the frequencies are of the order few MHz. Hence the transmission line approximation is valid as the wave lengths are either less than or close to the

limits as discussed above. Table. 4.1, is needed before one starts the transient analysis and uses the different approximations that are required for ground losses.

Note that the telegrapher's equation is valid for any type of pulse input/incidence, but if the frequency dependant losses from the ground are to be included, no complete and simple closed form expressions exists and efforts in this direction have led to a number of approximations, which are valid for different frequencies of interest. Usually, in the telegrapher's equations the loss due to ground as explained above is incorporated in the form of a correction term, observe the last term in (4.18) for the case of total wire impedance. Let's devote the next section in a search for various ground impedance expression. Simplified and more valid ground impedance expressions that are computationally efficient are also one of our targets.

4.3.3 Ground impedance expression for above ground wires - A comparative overview ¶

In the discussions to follow let's first deal with ground impedance in frequency domain and later discuss the concept of time domain transient ground impedance/resistance using telegrapher's equations. Similar to external mutual inductances (4.3b) for wires above ground, one has mutual ground impedance too.

Carson [5, 56] was the first to investigate the concept of ground impedance (also called as earth return impedance). He first derived the general solution of axial electric field in the ground and related this axial electric field to the magnetic field components using the *Maxwell's* curl equation. He then splits the magnetic field components to two parts i.e. one part of the field coming from the current in the wire and the other part due to the current in the ground. The axial displacement currents in the ground were neglected and it is assumed that the wire is of sufficiently small radius so that the distribution of current over its cross section is symmetrical for electric field. The axial electric field was further related to the scalar and vector potentials and he derives the final ground impedance expressions as an improper integral shown in (4.25a) and (4.25b) for self and mutual values respectively. The infinite integral terms in (4.25) have certain solutions in terms of *Bessel's* functions of first and second kind. Those functions can be expanded in terms of infinite series. For simpler computations *Carson* further expanded the integrals to infinite series as shown in (4.26) [5, 56, 57], which is widely used by power engineers. Kindly refer to the Fig. 4.6 for the details of the terms used in (4.26). *Carson's* infinite series converge very quickly at low frequencies and convergence decrease as

the frequencies are increased.

$$Z_{gkk}^{Carson} = \frac{j\omega\mu_0}{\pi} \cdot \int_0^{\infty} \frac{e^{-2h_k u}}{\sqrt{u^2 + j\omega\mu_0\sigma_g} + u} \cdot du \tag{4.25a}$$

$$Z_{gkl}^{Carson} = \frac{j\omega\mu_0}{\pi} \cdot \int_0^{\infty} \frac{e^{-2(h_k+h_l)u} \cdot \cos(d_{kl}u)}{\sqrt{u^2 + j\omega\mu_0\sigma_g} + u} \cdot du \tag{4.25b}$$

$$Z_{gkk}^{Carson} = R_g + jX_g \tag{4.26a}$$

$$Z_{gkl}^{Carson} = R_{gm} + jX_{gm} \tag{4.26b}$$

$$R_g = 4\omega \times 10^{-7}(\frac{\pi}{8} - b_1 k + b_2[(C_2 - \ln k)k^2] + b_3 k^3 - d_4 k^4 - \cdots) \tag{4.26c}$$

$$X_g = 4\omega \times 10^{-7} \begin{pmatrix} \frac{1}{2}(0.62 - \ln k) + b_1 k - d_2 k^2 + \\ b_3 k^3 - b_4[(C_4 - \ln k)k^4] + \cdots \end{pmatrix} \tag{4.26d}$$

$$R_{gm} = 4\omega \times 10^{-7} \begin{pmatrix} \frac{\pi}{8} - b_1 k_m \cos\theta + \\ b_2[(C_2 - \ln k_m)k_m^2 \cos 2\theta + \theta k_m^2 \sin 2\theta] + \\ b_3 k_m^3 \cos 3\theta - d_4 k_m^4 \cos 4\theta - \cdots \end{pmatrix} \tag{4.26e}$$

$$X_g = 4\omega \times 10^{-7} \begin{pmatrix} \frac{1}{2}(0.62 - \ln k_m) + b_1 k_m \cos\theta - \\ d_2 k_m^2 \cos 2\theta + b_3 k_m^3 \cos 3\theta - \\ b_4[(C_4 - \ln k_m)k_m^4 \cos 4\theta + \theta k_m^4 \sin 4\theta] + \cdots \end{pmatrix} \tag{4.26f}$$

$$b_1 = \frac{\sqrt{2}}{6}; b_2 = \frac{1}{16}; b_i = b_{i-2}\frac{sign}{i(i-2)} \tag{4.26g}$$

sign of the coefficient changes every four terms i.e. sign=+1 when i=1,2,3,4; sign=-1 when i =5,6,7,8 and so on.

$$C_i = C_{i-2} + \frac{1}{i} + \frac{1}{i+2}; C_2 = 1.37 \tag{4.26h}$$

$$d_i = \frac{\pi}{4} b_i \tag{4.26i}$$

$$k = 4\pi\sqrt{5} \times 10^{-4}(2h_k)\sqrt{\frac{\omega\sigma_g}{\omega}} \tag{4.26j}$$

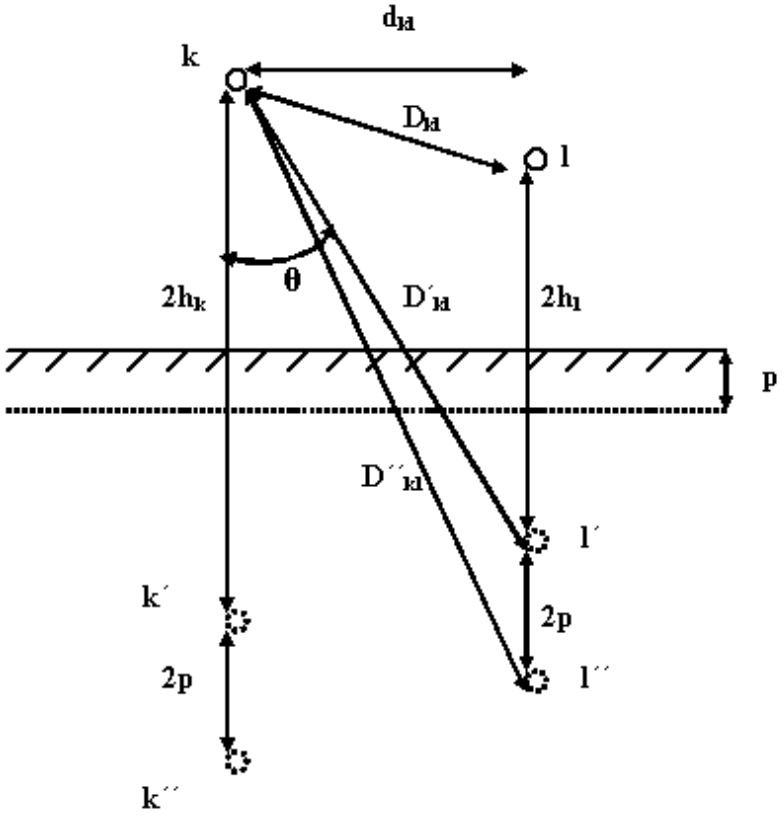

Figure 4.6: Allocation of conductors' k and l and their images k´ and l´ with a skin depth of p [57]

$$k_m = 4\pi\sqrt{5} \times 10^{-4} D'_{kl} \sqrt{\frac{\omega\sigma_g}{\omega}} \tag{4.26k}$$

$$\theta = \arcsin\left(\frac{d_{kl}}{D'_{kl}}\right) \tag{4.26l}$$

On careful observation of equation (4.25) it is seen that the low frequency approximation is used (see the denominator terms, wherein ε_g is missing). Further, under the limits frequency tending to infinity, *Carson's* expression poses singularity, i.e. ground impedance tends to infinity. In reality, as frequency tends to infinity the ground impedance tends to be finite, which will be discussed later.

The next important person to contribute to the development of ground impedance and perhaps for many other cases with regard to the location of wire above and below ground, for wide frequency range, with specific attention to

propagation characteristics was by *Sunde* [58] in his classic text on *Earth conduction effects on transmission systems*. In author's opinion, he was the first to bring the concept of transmission line modeling with earth conduction effects, judging from all his interesting works and publications during the early 1940's. During his time the lightning induced voltage and may be power system transient estimations was of at most significance. This perhaps might have led him to investigate the wave propagation in buried cables, overhead wires, grounding rods and wires etc. *Sunde* [58] derived his expression by assuming a dipole in air above the earth surface, with earth assumed to consist of two layers. He then used the wave functions or the *Hertz* potentials [58 - 60] in the three media and derives the result by satisfying the boundary conditions corresponding to the continuity of the tangential components of the electric and magnetic fields at the interfaces. His expressions are shown in (4.27).

$$Z_{gkk}^{Sunde} = \frac{j\omega\mu_0}{\pi} \cdot \int_0^{\infty} \frac{e^{-2h_k u}}{\sqrt{u^2+\gamma_g^2}+u} \cdot du \tag{4.27a}$$

$$Z_{gkl}^{Sunde} = \frac{j\omega\mu_0}{\pi} \cdot \int_0^{\infty} \frac{e^{-2(h_k+h_l)u} \cdot \cos(d_{kl} \cdot u)}{\sqrt{u^2+\gamma_g^2}+u} \cdot du \tag{4.27b}$$

The only difference between *Carson's* (4.25) and *Sunde's* (4.27) expression is that full propagation constant in the ground, $\gamma_g = \sqrt{j\omega \cdot \mu_0 \cdot \sigma_g - \omega^2 \cdot \mu_0 \cdot \varepsilon_g}$ was used by *Sunde* in his expression, the justification being that at higher frequencies the displacement currents in the soil could not be neglected. *Sunde* for the self-ground impedance (4.27a) gave a logarithmic approximation as shown in (4.28),

$$Z_{gkk}^{Sunde-log} = \frac{j\omega \cdot \mu_0}{2\pi} \cdot \ln\left(\frac{1+h_k \cdot \gamma_g}{h_k \cdot \gamma_g}\right) \tag{4.28}$$

In the recent studies on the field wire coupling problems in overhead power lines for wide range of frequencies the *Sunde's* logarithmic approximation is used [53] based on the recommendation from *Chen and Damrau* [61]. It is said in [61, 62], that for overhead power lines (4.28) is a very good approximation of (4.27a) and the logarithmic formula are valid for a wide frequency range [61, 62].

To overcome the difficulty of convergences of Carson's equations and may be perhaps to study some of the then power system transients, *Gary* proposed the complex depth earth return method in 1976 but without any analytical proof of his proposition [56, 57]. In 1981, *Deri et al* [57] theoretically proved the relationship between the *Carson's* method and the complex depth ground return method, thereby proving *Gary's* proposition of complex depth ground

return method [56, 57]. This method is somewhat a closed form approximation to *Carson's* integral equation (4.22). *Deri et al* [57], method assumes that the current in conductor k returns through an imagined earth path located directly under the original conductor at a depth of $(h_k + 2p)$ as shown in Fig.4.6, in which $k^{''}$ refers to the imagined earth return conductor of conductor k and p to the skin depth of the ground. In other words the earth can be replaced by a set of earth return conductors. The distance between a conductor and its imagined earth return conductor equals twice its height above ground plus the skin depth of the ground (i.e. $2(h_k + p)$). It must be emphasized that the skin depth p is a complex number. The relevant ground impedance equations are shown in (4.29) which has terms corresponding to Fig.4.6. The equations (4.25) and (4.29) are referred to as low frequency approximations and it is only applicable in the *Carson's* region of Table 4.1. The drawbacks of *Carson's* integral equations with regard to high frequency also apply to *Deri et al.* expressions as the frequency is increased. Observe that under low frequency approximations $p = \frac{1}{\gamma_g}$ with displacement currents neglected.

$$Z_{gkk}^{Deri-etal} = \frac{j\omega \cdot \mu_0}{2\pi} \cdot \ln\left(\frac{h_k + p}{h_k}\right) \tag{4.29a}$$

$$Z_{gkl}^{Deri-etal} = \frac{j\omega \cdot \mu_0}{2\pi} \cdot \ln\left(\frac{D_{kl}^{''}}{D_{kl}^{'}}\right) \tag{4.29b}$$

$$p = \frac{1}{\sqrt{j\omega\mu_0\sigma_g}} \tag{4.29c}$$

Now, having known the drawback of low frequency approximations, the immediate question is, does *Sunde's* logarithmic or integral expression suffer the same drawbacks? No! As the frequency tends to infinity *Sunde's* expression specifically logarithmic expression is finite and never pose any singularity. The integral expression (4.27a) have convergence problems, hence the author has not investigated its behavior for higher frequency. *Rachidi et al.* [62] have mentioned that the integral expression (4.27a) do not pose any singularity. Let's discuss in a little while about this finite value. Hence *Sunde's* expression is more valid compared to other low frequency approximations.

Equation (4.28) has been extended by *Rachidi et al.* [62], for the mutual impedance as given below in (4.30) and it is also claimed that (4.30) is a very good approximation of (4.27b). It can be shown that (4.30) and (4.29b) are similar, excepting that the low frequency approximation of ground propaga-

tion constant was used in (4.29b).

$$Z_{gkl}^{Sunde-log} = \frac{j\omega \cdot \mu_0}{4\pi} \cdot \ln\left(\frac{\left[1+0.5\cdot\gamma_g\cdot(h_k+h_l)\right]^2+\left(0.5\cdot\gamma_g\cdot d_{kl}\right)^2}{\left[0.5\cdot\gamma_g\cdot(h_k+h_l)\right]^2+\left(0.5\cdot\gamma_g\cdot d_{kl}\right)^2}\right) \quad (4.30)$$

Considering ground as a cylindrical conductor surrounding the wire *Vance* [63] derived the expression for ground impedance. His approximation is quite similar in behavior to that of *Sunde's* for wide frequency range. But it uses the *Hankel* functions [63] as shown in (4.31). Hence for the discussions to follow only *Sunde's* approximation is used.

$$Z_{gkk}^{Vance} = \frac{-j\gamma_g}{2\pi\cdot h_k\cdot\sigma_g}\cdot\frac{H_0^1(j\gamma_g\cdot h_k)}{H_1^1(j\gamma_g\cdot h_k)} \quad (4.31)$$

Semlyen's analysis is more suitable for frequencies that are above the critical frequency only [55], hence it is termed as an asymptotic model. The reason being that the earth behaves either both as an insulator and conductor or only as an insulator beyond the critical frequencies. He calculates the impedances by neglecting the space harmonics under the wires. He uses the expressions for the complex power related to the ground return for a pair of unit length of the conductors above the ground and derives the ground impedance by integrating the powers penetrating the earth over its surface [55]. He found that the obtained ground impedances as shown in (4.32) are all proportional to the intrinsic impedance of the ground (discussed later). This ground intrinsic impedance [55, 63] will be used as tool for a comparative study later. *Semlyen's* expressions for ground impedance are more suitable when the earth's dielectric behavior is dominant over the conductive behavior [55]. It may be specifically applied to both the very high and partly to the high frequency regions shown in Table. 4.1.

$$Z_{gkk}^{Semlyen} = \frac{1}{2\pi h_k}\cdot\sqrt{\frac{j\omega\mu_0}{\sigma_g+j\omega\varepsilon_g}} \quad (4.32a)$$

$$Z_{gkl}^{Semlyen} = \frac{h_k+h_l}{\pi\cdot\left[(h_k+h_l)^2+d_{kl}^2\right]}\cdot\sqrt{\frac{j\omega\mu_0}{\sigma_g+j\omega\varepsilon_g}} \quad (4.32b)$$

Yet another reason why some times (4.32) is referred to as the asymptotic expressions, is because those expressions can be used for the analysis under the limits of frequency tending to infinity, due to which it can be seen that (4.32) approaches (4.33). In fact transient ground impedances must have an asymptotic value as the frequency tends to infinity [52, 55, 62], because the penetration depth (skin depth) in the soil as frequency tends to infinity, tends to a constant asymptotic value (shown later) [55, 63]. This will be discussed

next.

$$\lim_{\omega\to\infty} Z_{gkk}^{Semlyen} = \frac{1}{2\pi h_k}\cdot\sqrt{\frac{\mu_0}{\varepsilon_g}} = \lim_{\omega\to\infty} Z_{gkk}^{Sunde/Vance} \tag{4.33a}$$

$$\lim_{\omega\to\infty} Z_{gkl}^{Semlyen} = \frac{h_k+h_l}{\pi\cdot\left[(h_k+h_l)^2+d_{kl}^2\right]}\cdot\sqrt{\frac{\mu_0}{\varepsilon_g}} = \lim_{\omega\to\infty} Z_{gkl}^{Sunde/Vance} \tag{4.33b}$$

Equation (4.33), doesn't mean that *Sunde's* or *Vance's* expressions is identical to *Semlyen's* expressions. What matters is how these expressions reach the asymptotic value as the frequency is increased. An asymptotic value of ground impedance is needed for later time domain analysis of ground impedance so as to use it in the time domain telegrapher's equations.

Consider the ground impedances for a conductor of $0.5m$ height above a ground with $500\Omega.m$ ground resistivity as shown in Fig. 4.7a and for another conductor of $10m$ height above a ground with $10000\Omega.m$ ground resistivity as shown in Fig. 4.7b. In both the cases the relative permittivity of the earth was 10. The ground impedances are shown for *Carson* (4.29a), *Sunde* (4.28) and *Semlyen* (4.32a). The asymptotic limit of the ground impedance and another line representing the ratio $\frac{\sigma_g}{\omega\varepsilon_g}$ are also shown in Fig. 4.7a and b.

From Table 4.1, the earth behaves like a conductor for all frequencies where the ratio is greater than 10 and *Carson's* or *Sunde's* approximation seems to be in perfect agreement as can be seen in Fig. 4.7a and 4.7b. In addition for all the frequencies where the ratio is less than 0.5, it is *Semlyen's* ground impedance expressions that are valid, because it was derived for the case when the earth's dielectric behaviour dominates more than the conductive behaviour of the earth. The region where the ratio is between 10 and 0.5 is the transition region where the earth behaves as both conductor and dielectric. It is not clear which expression is valid in this region. What ever be the case, some approximation has to be made in this region. Moreover one can see that both *Semlyen's* and *Sunde's* expression have asymptotic values as frequency tends to infinity. Those values are $37.9\Omega/m$ and $1.9\Omega/m$ for $0.5m$ and $10m$ conductor heights respectively. The only difference is in the frequency instants at which they attain asymptotic values. It was observed that for low ground resistivities, both *Sunde's* and *Semlyen's* expressions attain asymptotic values at nearly same frequency instants. The deviation happens as the ground resistivity is increased. It can be observed that ground impedance due to *Carson* in Fig. 4.7, monotonically increases reaching to infinity/singularity at infinite frequency. It is surprising that though *Carson's* equation is a low frequency approximation whose validity is strictly in the conductive region of earth's behaviour, it appears from Fig. 4.7a and 4.7b that both *Sunde's* and *Carson's* expression are in agreement up to twice the critical frequency. It should be understood that comparison based only on amplitude in frequency domain solu-

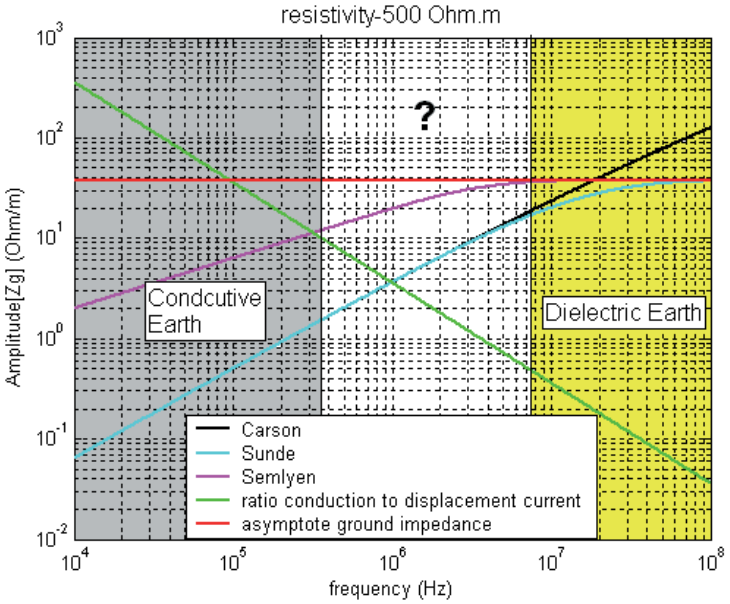

(a) 0.5m height, $\sigma_g = 2mS/m$ and $\varepsilon_{rg} = 10$

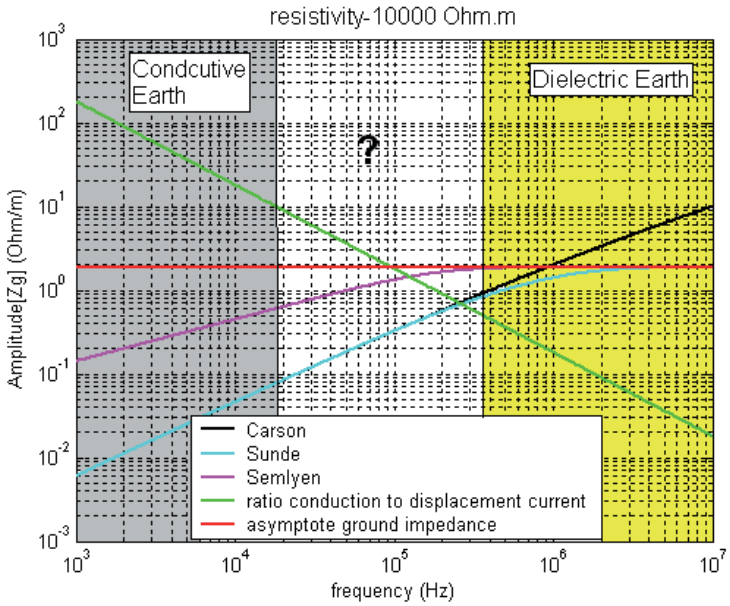

(b) 10m height, $\sigma_g = 0.1mS/m$ and $\varepsilon_{rg} = 10$

Figure 4.7: Ground impedance amplitude curves for a conductor at different heights and with different ground resistivity

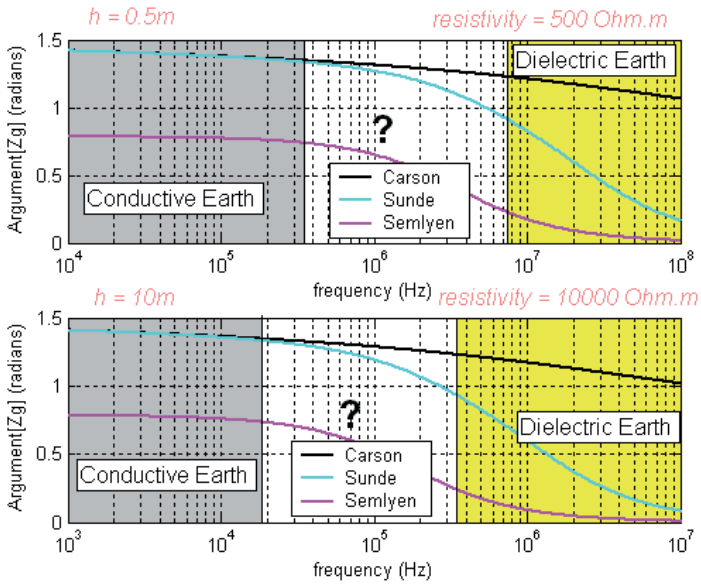

Figure 4.8: Ground impedance argument response corresponding to conductor at (top) 0.5m height, $\sigma_g = 2mS/m$ and (below) 10m height, $\sigma_g = 0.1mS/m$

tions are invalid. One has to compare the phase responses as well to make sure that their comparisons are valid for the phase values. The differences between *Sunde's* and *Carson's* expressions are clearly seen in the phase responses as shown in Fig. 4.8. Observe the *Sunde's* and *Carson's* curves deviates exactly at the beginning of the transition region. From this one can also say that the critical frequency that separates earth's conductive and transition behaviour is around $\frac{f_c}{10}$. The reasons to why the magnitude responses do not show this difference are beyond the scope of this thesis. The implication of the phase response is that in frequency domain solutions both the real and imaginary part magnitudes are affected due to the phase differences.

If one observes the manner in which the ground impedance curves of *Semlyen*, decay from the start of the asymptotic point in Figs. 4.7a and 4.7b and compare it with the decay of ground intrinsic impedances given by (4.34a) for various ground conductivities from the start of the asymptotic point as in Fig. 4.9, it is clear that expressions (4.32) are valid. This argument can be also explained on the basis of ground penetration depth (4.35a). The transient ground impedance is dependent on the depth up to which, where the electromagnetic fields penetrate. In general as the frequency is increased the depth starts decreasing and finally tends to an asymptotic value as given by (4.35b). Moreover for the soils with different conductivities the frequency at which the asymptotic value of the ground penetration depth is attained are also varying. Poorer the ground conductivity larger is the ground penetration depth as

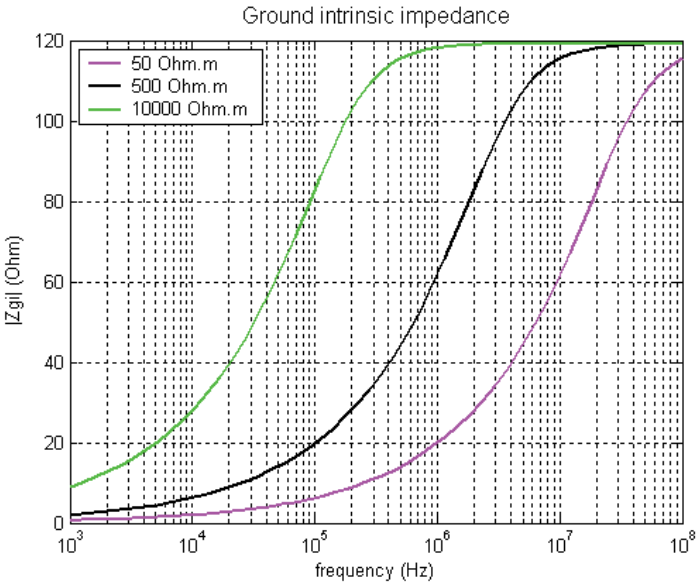

Figure 4.9: Intrinsic impedance for various ground conductivities

shown in Fig. 4.10. It can be observed from Fig. 4.10 that when the ground conductivity is lower much earlier is the frequency at which the asymptotic ground penetration depth is attained.

$$\eta_g = \sqrt{\frac{\mu_0}{\varepsilon_g \cdot (1 + \frac{\sigma_g}{j\omega \cdot \varepsilon_g})}} \tag{4.34a}$$

$$\lim_{\omega \to \infty} \eta_g = \frac{120\pi}{\sqrt{\varepsilon_{rg}}} \tag{4.34b}$$

$$\delta_g = \frac{1}{\omega \sqrt{\frac{\varepsilon_g \cdot \mu_0}{2} \cdot \left(\sqrt{1 + \frac{\sigma_g^2}{(\omega \cdot \varepsilon_g)^2}} - 1 \right)}} \tag{4.35a}$$

$$\lim_{\omega \to \infty} \delta_g = \frac{2}{\sigma_g} \cdot \sqrt{\frac{\varepsilon_g}{\mu_0}} \tag{4.35b}$$

Semlyen's expression seems to be very consistent with the intrinsic impedance curves at all the heights, specifically the frequency point at which the asymptote is reached. From these analyses it can be concluded that while dealing with poor conductivity grounds only *Semlyen's* equations can be used

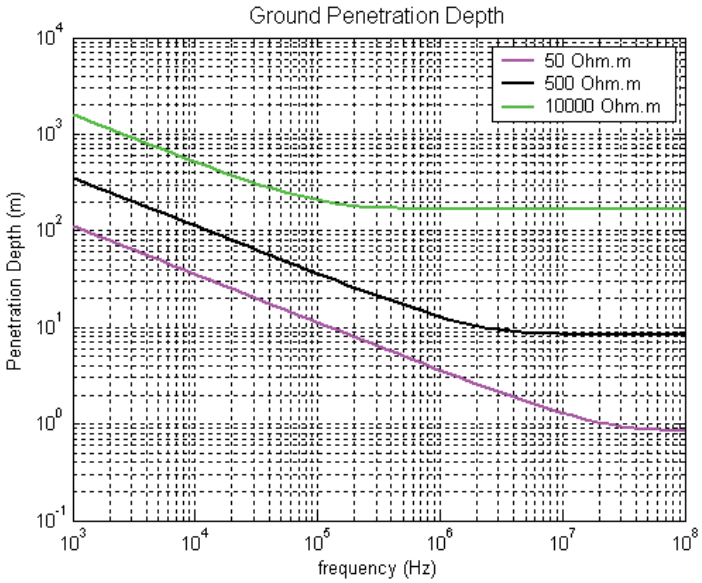

Figure 4.10: Penetration depth of electromagnetic fields in the ground for various ground conductivities

as it is valid for most frequencies above twice the critical frequency limit and for all ground conductivities. On the contrary, the author is doubtful whether *Sunde's* approximation is valid because it does not exhibit the associated features of either the intrinsic impedance or ground penetration depth. To conclude it is right to say that to get the complete spectrum of ground impedance all the behaviour i.e. conductive, transition and dielectric (insulator) behaviour of the earth have to be considered. Thus the limits are for, all frequencies less than $\frac{f_{cr}}{10}$ one uses *Carson's* expression and for all frequencies greater than $2 \cdot f_{cr}$ one uses *Semlyen's* expression and in the intermediate or transition region (which is between the upper two limits) one uses a combination of the two ground impedance expression as discussed next in the transient ground impedance in time domain.

4.3.4 Ground impedance in time domain - transient ground impedance ¶

To begin with let's get to the telegrapher's equations i.e. voltage wave equation (4.18) and the current wave equation (4.22). Both of these equations are referred to as modified telegrapher's equations. The modified telegrapher's equations in time domain will look like as shown in (4.36) which marks the beginning of all our lossy MTLs problems. In equation (4.36a) $\zeta(t) =$

$F^{-1}(\frac{Z_g(j\omega)}{j\omega})$ is known as the transient ground impedance in time domain.

$$\frac{\partial V(x,t)}{\partial x} + A \cdot I(x,t) + \frac{1}{\sqrt{\pi}} \cdot B \cdot \left(\int_0^t \frac{1}{\sqrt{\tau}} \cdot \frac{\partial I(x,t-\tau)}{\partial (t-\tau)} \cdot d\tau \right)$$
$$+ L_e \cdot \frac{\partial I(x,t)}{\partial t} + \int_0^t \zeta(t-\tau) \frac{\partial I(x,\tau)}{\partial \tau} d\tau = 0 \tag{4.36a}$$

$$\frac{\partial I(x,t)}{\partial x} + C_e \cdot \frac{\partial V(x,t)}{\partial t} = 0 \tag{4.36b}$$

One may wonder why there isn't any ground admittance or transient ground admittance in the discussion or in the above equations. The transient ground admittance term in the current wave equation (4.36b) is not used because of the fact that among the fields that penetrate the lossy ground magnetic field penetrates more compared to electric field. Thus the contribution of ground admittance to the overall shunt admittance for the overhead or above ground lines is negligible, further in [61] it is mentioned that the ground admittance becomes important only when the wires are touching the ground. It has been shown by *Rachidi et al.* [52, 62] that for wires above the ground the over all admittance in equation (4.23) is approximately equal to the shunt admittance due to external line capacitance, i.e. $Y \approx j\omega C_e$. Since the magnetic field penetrates the earth more than the electric field, ground impedance becomes very important and cannot be neglected. Soon it will be demonstrated with an example to see the error one would expect by neglecting the ground admittance.

Let's study what are the available approximate expressions for the time domain transient ground impedance. As mentioned earlier, one needs ground impedance from both *Carson's* expressions and *Semlyen's* expressions, which will be combined to use in the transition region. As *Carson's* expressions are low frequency approximations in time domain its contribution will be in late time (LT), while as *Semlyen's* approximation is a very high frequency approximation its contribution will be in early time (ET). Researchers have contributed to the development of late time and early time transient ground impedance expressions.

Timotin [64] first developed the time domain transient ground impedance expression by performing inverse *Fourier* transforms of *Carson's* expression. Later *Orzan* [65] extended *Timotin's* expressions for the mutual transient ground impedance, as shown in (4.37).

$$\begin{aligned} \zeta_{kl}^{LT}(t) &= \frac{\mu_0}{2\pi\tau_{kl}^*} \left[\frac{1}{2\pi} \frac{\tau_{kl}^*}{t} + \frac{e^{\frac{\tau_{kl}^*}{t}}}{4} erfc\left(\sqrt{\frac{\tau_{kl}^*}{t}} \right) - \frac{1}{4} \right] \\ &\quad + \frac{\mu_0}{2\pi\tau_{kl}} \left[\frac{1}{2\pi} \frac{\tau_{kl}}{t} + \frac{e^{\frac{\tau_{kl}}{t}}}{4} erfc\left(\sqrt{\frac{\tau_{kl}}{t}} \right) - \frac{1}{4} \right] \end{aligned} \tag{4.37a}$$

$$\tau_{kl} = \mu_0 \sigma_g \cdot \left[\left(\frac{h_k + h_l}{2} \right) + j \frac{d_{kl}}{2} \right]^2 \tag{4.37b}$$

$$\tau_{kl}^* = conj(\tau_{kl}) \tag{4.37c}$$

The low frequency approximation limit is known, hence the above expressions are not valid for time less than $t \leq \frac{20\pi\varepsilon_g}{\sigma_g}$, based on the arguments in the previous section. Moreover, it was seen that there is a singularity at time zero in (4.37). It also predicts very large values if one substitutes in (4.37) times corresponding to a ten times critical frequency.

Sunde's expression does not have a closed form inverse *Fourier* or *Laplace* transform. But *Semlyen's* expression has an exact inverse *Laplace* transform as shown in (4.38), which is referred to as early time expression obtained by *Araneo and Celozzi* [66].

$$\zeta_{kl}^{ET}(t) = \frac{h_k + h_l}{\pi \cdot \left[(h_k + h_l)^2 + d_{kl}^2 \right]} \cdot \sqrt{\frac{\mu_0}{\varepsilon_g}} \cdot e^{-\upsilon \cdot t} \cdot I_0(\upsilon \cdot t) \tag{4.38a}$$

$$\upsilon = \frac{\sigma_g}{2\varepsilon_g} \tag{4.38b}$$

Note that in (4.37) and (4.38) the self-transient ground impedance can be obtained by putting $h_k = h_l$ and $d_{kl} = 0$. Now to combine the early time and late time approximations two recent models are taken up for discussions they are *Araneo and Celozzi* approximation [66] and *Rachidi et al.* approximation [67]. *Semlyen* [55] points out that there is a region, where both the early time and the late time contribute together to the transient ground impedance known as the transition region, which appears only after the early time region. The region after the transition region is only due to the late time contribution of the transient ground impedance (*Carson's* region). The possible demarcation of the above three regions is difficult, that's the reason why it is attempted to combine early time and late time approximations.

Araneo and Cellozzi [66] have given the general expressions for transient ground impedances (4.39). It was derived based on the knowledge from Table. 4.1. The maximum frequency at which *Carson's* equation is still valid is evaluated as a minimum criterion $f_{cr}^{LF} = min[\frac{0.1 \cdot \sigma_g}{2\pi \cdot \varepsilon_g}; \frac{0.1 \cdot (3 \times 10^8)}{2\pi \cdot h}]$ [55, 59, 66]. Hence in time domain the corresponding late time approximation (4.37) can be used at a time $t \geq \frac{1}{f_{cr}^{LF}}$ [66]. Since, *Semlyen's* expression (4.32) can be used for frequency, $f_{cr}^{HF} \geq \frac{\sigma_g}{\pi\varepsilon_g}$ [55, 66], in time domain the early time transient ground impedance (4.38) can be used for times $t \leq \frac{1}{f_{cr}^{HF}}$[66]. It is said that (4.39) is a reasonable approximation for wide range of frequencies and can be thought

of as the best approximation that is available.

$$\zeta_{kl}^{Araneo-Cellozi}(t) = e^{-\frac{5t}{\tau_L}} \cdot \zeta_{kl}^{ET}(t) + (1 - e^{-\frac{5t}{\tau_L}}) \cdot \zeta_{kl}^{LT}(t) \tag{4.39a}$$

$$\tau_L = \left[min\left(\frac{0.1\sigma_g}{2\pi\varepsilon_g}; \frac{0.1 \cdot 3 \times 10^8 \cdot (h_k + hl)}{\pi\left[(h_k + h_l)^2 + d_{kl}^2\right]} \right) \right]^{-1} \tag{4.39b}$$

In principle for times close to $t = 0$ (i.e. early time), only early time approximation (4.38) is valid and there is no contribution from either the late time (4.37) or combination of late time and early time (4.39). It was observed that (4.39) predicts values that are slightly higher than (4.38) in the possible early time region, even though the difference is negligible in the case treated in all this work. In the transition region (4.39) can be conveniently used because it uses effectively both the early time and late time approximations. Because of the nature of the equation (4.39) only the late time term is most dominant at late times. The crucial parameter in (4.39) is the condition on τ_l, which uses a minimum condition for the low frequency limit based on *Wait* [59].

Another time domain ground impedance expression proposed by *Rachidi et al.* (4.40) [67], is also a good approximation to obtain the transient ground impedance as a function of time, as it uses the minimum of asymptotic value of the transient impedance and the late time approximation. This is valid in the sense that the transient ground impedance can have only a maximum value corresponding to (4.33), the asymptotic values.

$$\zeta_{kl}^{Rachidi-etal}(t) = min\left(\sqrt{\frac{\mu_0}{\varepsilon_g}} \cdot \frac{(h_k + hl)}{\pi\left[(h_k + h_l)^2 + d_{kl}^2\right]}; \zeta_{kl}^{LT}(t) \right) \tag{4.40}$$

One of the main concerns with (4.40) is that it uses the asymptotic value of the transient ground impedance in the entire early time region rather than using equation (4.38), and in the possible transition region it uses the late time approximation. It is true that the transient ground impedance at any time can be either equal to or less than the early time transient ground impedance (4.38) depending upon the time under consideration.

It was decided to calculate the transient ground impedances using a minimum criterion based on the *Rachidi et al.* approximation, i.e. the transient ground impedance at any time is equal to a minimum of the early time approximation (4.38) and *Araneo and Cellozzi* approximation (4.39), as shown below in (4.41) [72, 73 **Paper-B**].

$$\zeta_{kl}^{Modified}(t) = min\left(\zeta_{kl}^{ET}(t); e^{-\frac{5t}{\tau_L}} \cdot \zeta_{kl}^{ET}(t) + (1 - e^{-\frac{5t}{\tau_L}}) \cdot \zeta_{kl}^{LT}(t) \right) \tag{4.41}$$

It should be mentioned here that whether one uses equation (4.39) or (4.41), the choice do not have any significant influence on the transient ground im-

pedance. The differences were very nominal. This allows us to use shifting theorem on (4.39) to obtain the ground impedance in frequency domain by *Laplace* transforming (4.39) leading to (4.42),

$$L[\zeta(t)] = \frac{Z_g(s)}{s} \tag{4.42a}$$

$$M = s + \frac{5}{\tau_L} \tag{4.42b}$$

$$\gamma_g{}' = \sqrt{M\mu_0 \cdot (\sigma_g + M\varepsilon_g)} \tag{4.42c}$$

$$\begin{aligned} \frac{Z_g(s)}{s} &= \frac{\mu_0}{4\pi} \cdot \ln\left[\left(\frac{\gamma_g{}'}{\gamma_g}\right)^2 \frac{\left[1+0.5\cdot\gamma_g\cdot(h_k+h_l)\right]^2 + \left(0.5\cdot\gamma_g\cdot d_{kl}\right)^2}{\left[1+0.5\cdot\gamma_g'\cdot(h_k+h_l)\right]^2 + \left(0.5\cdot\gamma_g'\cdot d_{kl}\right)^2}\right] \\ &\quad + \frac{h_k+hl}{\pi M\cdot\left[(h_k+h_l)^2+d_{kl}^2\right]} \cdot \sqrt{\frac{M\mu_0}{\sigma_g+M\varepsilon_g}} \end{aligned} \tag{4.42d}$$

This expression can be used in the frequency domain solution of the telegrapher's equations.

Before proceeding further let's clear the doubt on the importance of ground admittance. *Vance* [42, 53, 63], says that the ground admittance is related to ground impedance through the ground propagation constant as shown in (4.43).

$$Y_g(j\omega) \approx \frac{\gamma_g^2}{Z_g(j\omega)} \tag{4.43}$$

Let's perform two simulations for the worst-case scenario i.e. with ground conductivity of $0.1mS/m$ and ground relative permittivity of 10. The conductor is at a height of $0.5m$ above the ground with a radius of $0.0495m$ and $1km$ long. Let's inject the same current pulses representing subsequent and first return strokes as discussed in section 4.2.2 at one of the ends of the line and the line is terminated with their characteristic impedance 180Ω at both the ends. The currents are measured at the injection point, $400m$ and $800m$ from the injection point and are shown in Fig. 4.11 for both the current impulses. It is very clear that whether one uses the ground admittance in the simulations or not the differences are negligible. For the simulations the ground impedance expression (4.42) was used and simulation in frequency domain was carried out using (3.46). Next let's move on the solution of MTLs systems in frequency domain and time domain. Which will be used in the future for various calculations.

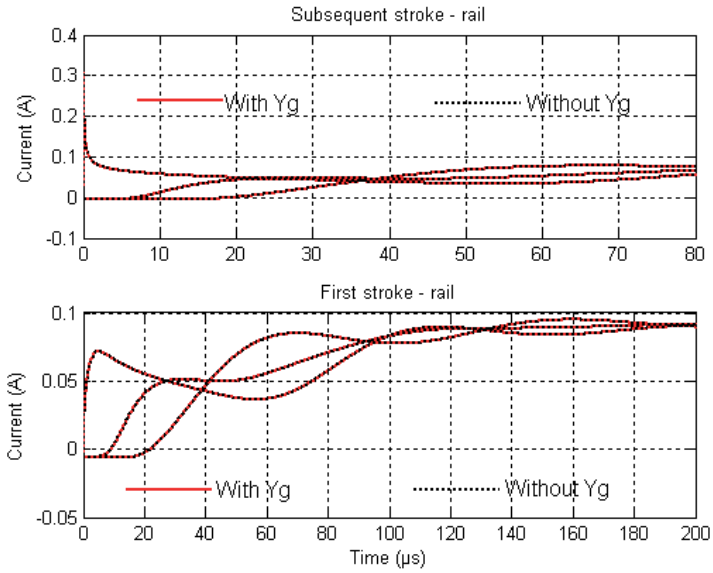

Figure 4.11: Simulations for demonstrating the lack of importance of ground admittance for rail conductors above ground for fast (top) and slow (bottom) impulses, no change in rail current whether one uses ground admittance or not

4.4 Solutions of telegrapher's equations in frequency and time domain

4.4.1 Frequency domain solution for MTLs

Telegrapher's equations can be solved in both frequency and time domain. In frequency domain the MTLs system has to be uncoupled and then the system of uncoupled equations have to be solved. There are numerical complexities involved in frequency domain, while solving for eigenvalue problem. The *Matlab* functions for eigenvalue calculations can be used [45]. It was seen that some errors propagate at this stage. Another aspect of error is while performing the inverse *Fourier* transforms to the frequency response of voltages or current. This however could be minimized by playing around with sampling frequency and number of points in the 2^N values. The frequency domain solution is referred to as modal solutions or analysis.

Let us begin with uncoupled second order MTL equations. Note that the impedance matrix has inductance, internal impedance and ground impedance matrix and the admittance matrix has the external capacitance matrix.

$$\frac{d^2V(x)}{dx^2} = Z \cdot Y \cdot V(x) \tag{4.44a}$$

$$\frac{d^2I(x)}{dx^2} = Z \cdot Y \cdot I(x) \tag{4.44b}$$

If one can find two $n \times n$ matrices T_V and T_I which can diagonalize simultaneously both the per-unit length impedance and admittance matrices, then the solution reduces to the solution of n uncoupled first order differential equations [12, 42]. Thus when the matrices are diagonalized, the system of equations are known as modal telegrapher's equations, which can be easily solved since they are in uncoupled form as,

$$\frac{dV_m(x)}{dx} = -z \cdot I_m(x) \tag{4.45a}$$

$$\frac{dI_m(x)}{dx} = y \cdot V_m(x) \tag{4.45b}$$

In (4.45) z and y are the modal impedance matrices (diagonal) and they are connected to the actual line impedance and admittance matrix through the transformation matrix, obtained as,

$$z = T_V^{-1} \cdot Z \cdot T_I \tag{4.46a}$$

$$y = T_I^{-1} \cdot Y \cdot T_V \tag{4.46b}$$

The second order modal MTLs equations in uncoupled form is given by,

$$\frac{d^2V_m(x)}{dx^2} = z \cdot y \cdot V_m(x) \tag{4.47a}$$

$$\frac{d^2I_m(x)}{dx^2} = z \cdot y \cdot I_m(x) \tag{4.47b}$$

An important observation is that the product of diagonal modal impedance and admittance matrix is commutative because of which it can shown that $T_I^t = T_V^{-1}$ [12, 42]. Consider the second order modal MTLs equation corresponding to the current,

$$\frac{d^2I_m(x)}{dx^2} = T_I^{-1} \cdot Y \cdot Z \cdot T_I \cdot I_m(x) = \gamma^2 \cdot I_m(x) \tag{4.48}$$

In (4.48) γ^2 is a diagonal matrix. The solution to the modal currents are given by,

$$I_m(x) = e^{-\gamma x} \cdot I_m^+ - e^{\gamma x} \cdot I_m^- \tag{4.49}$$

The exponential terms in (4.49) are diagonal matrices and the other terms are

vectors. The final solution for the current is (4.50).

$$I(x) = T_I \cdot I_m(x) = T_I \cdot (e^{-\gamma x} \cdot I_m^+ - e^{\gamma x} \cdot I_m^-) \tag{4.50}$$

The solution to the modal voltages are given by,

$$V_m(x) = e^{-\gamma x} \cdot V_m^+ + e^{\gamma x} \cdot V_m^- \tag{4.51}$$

The final solution for the voltage is (4.52).

$$V(x) = \left(T_I^{-1}\right)^t \cdot V_m(x) = \left(T_I^{-1}\right)^t \cdot (e^{-\gamma x} \cdot V_m^+ + e^{\gamma x} \cdot V_m^-) \tag{4.52a}$$

$$V(x) = Z_0 \cdot T_I \cdot (e^{-\gamma x} \cdot I_m^+ + e^{\gamma x} \cdot I_m^-) \tag{4.52b}$$

$$Z_0 = Z \cdot T_I \cdot \gamma^{-1} \cdot T_I^{-1} = Y^{-1} \cdot T_I \cdot \gamma \cdot T_I^{-1} \tag{4.52c}$$

Now the solutions of voltages and currents at any point on the line is obtained. The unknown parameters can be obtained by solving the boundary or terminal conditions along the line either using *Thevenin*[25] or *Norton*[26] equivalents. An example for resistive loads with voltage sources at either ends of the line, the following equations are applicable considering the near end and far end boundary conditions.

$$V(0) = V_S - Z_S \cdot I(0) \tag{4.53a}$$

$$V(\ell) = V_L - Z_L \cdot I(\ell) \tag{4.53b}$$

$$\begin{pmatrix} (Z_0 + Z_S) \cdot T_I & (Z_0 - Z_S) \cdot T_I \\ (Z_0 - Z_L) \cdot T_I \cdot e^{-\gamma \ell} & (Z_0 + Z_L) \cdot T_I \cdot e^{\gamma \ell} \end{pmatrix} \cdot \begin{pmatrix} I_m^+ \\ I_m^- \end{pmatrix} = \begin{pmatrix} V_S \\ V_L \end{pmatrix} \tag{4.54}$$

Let's use the above to demonstrate an example for comparing the frequency

[25]Thevenin Leon Charles (1857 - 1926) was an engineer at France's Postes et Telegraphes who published a network theorem in 1893, which states: 'A current flowing through a load impedance Z_L connected across any two terminals ap and bp of a linear, active bilateral network is given by $\frac{V_{oc}}{Z_i + Z_L}$, where V_{oc} is the open circuit voltage (with load across two terminals removed) and Z_i is the internal impedance of the network as viewed back into the open circuited network from terminals ap and bp with all voltage sources replaced by their internal impedances (if any) and current sources by infinite impedance'

[26]Norton Edward Lawry (1898 - 1983) was an engineer at the USA's Bell Telephone Laboratory who published a network theorem alternative to Thevenin's theorem, which states: 'Any two terminal active network containing voltage sources and impedances when viewed from its output terminals is equivalent to a constant current source and a parallel impedance. The constant current source is equal to the current which would flow in a short circuit placed across the terminals and parallel impedance is the impedance of the network when viewed from these open circuited terminals after all the voltage and current sources have been removed and replaced by their internal impedances'

domain and time domain solutions later.

4.4.2 Time domain solutions for MTLs - FDTD method

The best available and simple method to solve the telegrapher's equations is to use the finite difference time domain technique. It is well known as FDTD method. It was first used to solve the *Maxwell* equations using the *Yee* cell approach [68]. Later several researchers developed it to solve the transmission line type problems, the simplicity being that the problem has one dimensional propagation and all the main parameters with regard to field coupling between wires is inherent in the inductance, capacitance and ground impedance and admittance matrix. Thus the space and time variables are connected to voltages and currents along the line in the differential equations (4.36). The FDTD method splits (4.36) by central difference approximations. The solution to the problem is achieved by means of leap-frog scheme [12, 42]. In the FDTD method there are $NDX+1$ voltage nodes and NDX current nodes on the line separated by a length of dx [12, 42]. The ends of the line are essentially voltage nodes and every current node is at the midpoint between two voltage nodes. The voltage nodes are solved first and then the current nodes, the recursive equations for the voltage nodes are given below. The stability of FDTD method depends on the time and space discritisations and it must satisfy the *Courant* conditions $\frac{\Delta x}{\Delta t} \geq v_p$ [12, 42], where v_p is the maximum phase velocity of the system.

For the first node,

$$\begin{aligned} V_1^{n+1} &= \Big(\frac{Z_S^{-1}}{2}+\frac{G\Delta x}{4}+\frac{C_e\Delta x}{2\Delta t}\Big)^{-1} \\ &\quad \Big[\Big(-\frac{Z_S^{-1}}{2}-\frac{G\Delta x}{4}+\frac{C_e\Delta x}{2\Delta t}\Big)V_1^n+\frac{Z_S^{-1}}{2}\Big(V_S^{n+1}+V_S^n\Big)-I_1^{n+\frac{1}{2}}\Big] \end{aligned} \tag{4.55}$$

For any node in between the line,

$$V_k^{n+1} = \Big(\frac{G}{2}+\frac{C_e}{\Delta t}\Big)^{-1}\Big[\Big(-\frac{G}{2}+\frac{C_e}{\Delta t}\Big)V_k^n-\frac{I_k^{n+\frac{1}{2}}+I_{k-1}^{n+\frac{1}{2}}}{\Delta t}\Big] \tag{4.56}$$

For the last node,

$$\begin{aligned} V_{NDX+1}^{n+1} &= \Big(\frac{Z_L^{-1}}{2}+\frac{G\Delta x}{4}+\frac{C_e\Delta x}{2\Delta t}\Big)^{-1} \\ &\quad \Big[\Big(-\frac{Z_L^{-1}}{2}-\frac{G\Delta x}{4}+\frac{C_e\Delta x}{2\Delta t}\Big)V_{NDX+1}^n+\frac{Z_L^{-1}}{2}\Big(V_L^{n+1}+V_L^n\Big)+I_{NDX}^{n+\frac{1}{2}}\Big] \end{aligned} \tag{4.57}$$

Next let us consider the current equations. In (4.36) there are two integrals corresponding to the frequency dependant losses in the form of convolution integrals, which has to be computed at each current node and at every time step. Solving the convolution numerically by some integration schemes would require the storage of the complete time history of current vectors at each node and requires the calculation of the sums at every time step. This causes considerable burden on the memory requirements in the computer. In addition to that if there are many conductors in the MTLs systems, similar to the overhead traction systems, such an approach is computationally very inefficient. For efficient computational solutions it is thus advantageous to use the recursive convolution technique [12, 66]. For this the transient impedances due to the internal loss and the ground loss have to be fitted as sums of exponentials.

$$\vartheta(m) = \int_m^{m+1} \frac{d\rho}{\sqrt{\rho}} = \sum_{i=1}^{10} a_i \cdot e^{-\alpha_i m} \tag{4.58a}$$

$$\zeta(t) = AA_1 \cdot e^{-\chi_1 t} + AA_2 \cdot e^{-\chi_2 t} + \ldots \tag{4.58b}$$

For the internal impedances the sums of exponentials are simple and they are constant for all the conductors, the function to be approximated is shown in (4.58a) and it's only the constants A and B for the skin effect that changes for different conductors. *Paul* [12] has adopted a ten-term *Prony* approximation for the internal impedance, the constants and exponential parameters can be found in [12]. Hence for internal loss only A and B constants with the ten constant exponential terms need to be saved. In the recursive equations for the current (4.59), Ψ is the recursive convolution term for the internal impedance of the conductors.

$$\begin{aligned} I_k^{n+\frac{1}{2}} \quad = \quad & \Big(\frac{L_e}{\Delta t} + \frac{A}{2} + \frac{2 \cdot B\rho(0)}{\sqrt{\pi \Delta t}} + \frac{\zeta(0)}{2}\Big)^{-1} \\ & \Big[\Big(\frac{L_e}{\Delta t} - \frac{A}{2} + \frac{2 \cdot B\rho(0)}{\sqrt{\pi \Delta t}} + \frac{\zeta(0)}{2} - \frac{\zeta(1)}{2}\Big) I_k^{n-\frac{1}{2}} \\ & - \frac{B}{\sqrt{\pi \Delta t}} \sum_{i=1}^{10} \Psi_i^n + \frac{\zeta(1)}{2} \cdot I_k^{n-\frac{3}{2}} - \frac{V_{k+1}^n + V_k^n}{\Delta x} - C I_k^n\Big] \end{aligned} \tag{4.59}$$

For the ground impedances one can use any number of exponential terms. One can adopt the fitting of the transient ground impedances in time domain using (4.41) by any standard curve fitting package like in *Matlab* [45] or the best way of fitting is to fit in frequency domain using very accurate vector fitting method [69]. But if the vector-fitting method is used then the function to be fitted is $(equation 4.42d) \div s$ in *Laplace* domain. Since the transient ground

impedance for each conductor is unique one needs to save constants and exponential parameters corresponding to a number given by twice the product of number of conductors and the exponential terms. In the recursive equations for the current CI is the recursive convolution term for the transient ground impedance of the conductors.

For internal impedance approximated with ten *Prony* terms as a_i and α_i for the constants and exponential terms,

$$\Psi_i^n = a_i \cdot e^{\alpha_i} \cdot \left[I_k^{n+\frac{1}{2}} - I_k^{n-\frac{1}{2}} \right] + e^{\alpha_i} \cdot \Psi_i^{n-1} \tag{4.60}$$

With N_e number of sums of exponential terms as AA_i and χ_i for the transient ground impedance with N_c number of conductors each entry of CI_m of the vector CI_k^n is obtained as [66],

$$CI_m = \sum_{j=1}^{N_c} CI_{mj} \tag{4.61a}$$

Each convolution integral in (4.61a) can again be expressed as,

$$CI_{mj} = \sum_{r=1}^{N} CI_{mj,r} \tag{4.61b}$$

Recursive expression for each term in (4.61b) is given by,

$$\begin{aligned} CI_{mj,r_k^{n+1}} &= e^{\chi_{mj,r} \cdot \Delta t} \cdot \left(CI_{mj,r_k^n} + \frac{1}{2} AA_{mj,r} \cdot \left[I_k^{n+\frac{1}{2}} - I_k^{n-\frac{1}{2}} \right] \right. \\ &\quad \left. + \frac{1}{2} AA_{mj,r} \cdot e^{\chi_{mj,r} \cdot \Delta t} \cdot \left[I_k^{n-\frac{1}{2}} - I_k^{n-\frac{3}{2}} \right] \right) \end{aligned} \tag{4.61c}$$

What is the number of exponential terms that are required for fitting the transient ground impedances? The choice of number of exponentials to be used depends on the user who decides the accuracy required in the final result. In order to demonstrate this let's take a system of two conductors as shown in Fig. 4.12 that has an emitter and receptor MTLs system.

The receptor is either at a height of $10m$ or $0.5m$ as the case may be. But the emitter was always at $10m$ above the ground. The radius of the conductor was $5.6mm$ and the length of the line was $1km$. At the near end of the emitter a unit step current with an initial ramp of slope $1A/\mu s$ was injected. The responses at the receptor loads for different number of exponential terms for two different cases, namely $Case-R-UP$ (when the receptor is at $10m$ hight) and $Case-R-DOWN$ (when the receptor is at $0.5m$ hight) are estimated. The emitter in both the cases is terminated with 50Ω loads at its ends. Similarly the receptor has 50Ω loads at its ends for both cases. Fig. 4.13 and Fig. 4.14 show the current responses at the near and far ends of the receptor with three different

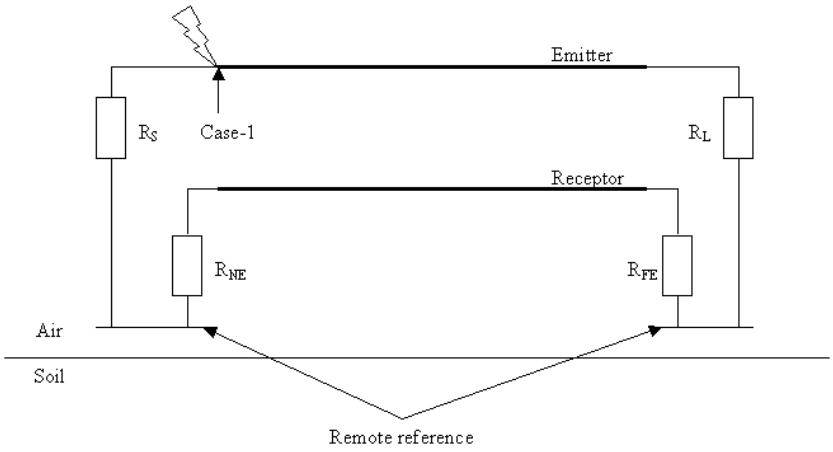

Figure 4.12: Emitter and receptor setup for studying the induced voltage on the receptor for a current injection at the near end of the emitter

numbers of exponential terms, namely 3 terms, 5 terms and 10 terms. The exponential terms were estimated using either *Levenberg-Marquardt* method [45, 70] or vector-fitting (frequency domain) method [69] for $Case-R-UP$ and $Case-R-DOWN$ respectively. The ground conductivity was $0.01 S/m$ and ground relative permittivity was 10.

It is seen for both the cases as to what should be the judicious choice of number of exponentials. Note that lesser the number of exponential terms greater is the possible error in the late time. However the early time peaks are comparatively less dependent on the number of exponential terms as can be seen in the Figs. 4.13, 4.14. Usually number of trials is needed to decide the optimum of exponential terms. Based on [66], care has to be taken to have minimum error at the time $t = 0$ and at first time step. The decaying nature of the transient impedance decides the peaks and rise times of the final wave shapes. When the number of conductors is more, as in the example of railway overhead system, it is not computationally efficient to use more exponential terms for highest possible accuracy. The aim should be to use minimum number of exponential terms so that lightning interaction with such an overhead system as in Swedish railways can be analyzed. Hence an exponential approximation that fits the transient ground impedance to a reasonable accuracy is needed. For the problem under study three to four exponentials as the case may be using the *Levenberg-Marquardt* method [45, 70] was found appropriate. Simulations with more number of exponentials were also carried out, but the differences were negligible for the simulation time considered [73 **Paper-B**].

Before completing this Chapter it is good to demonstrate a problem that

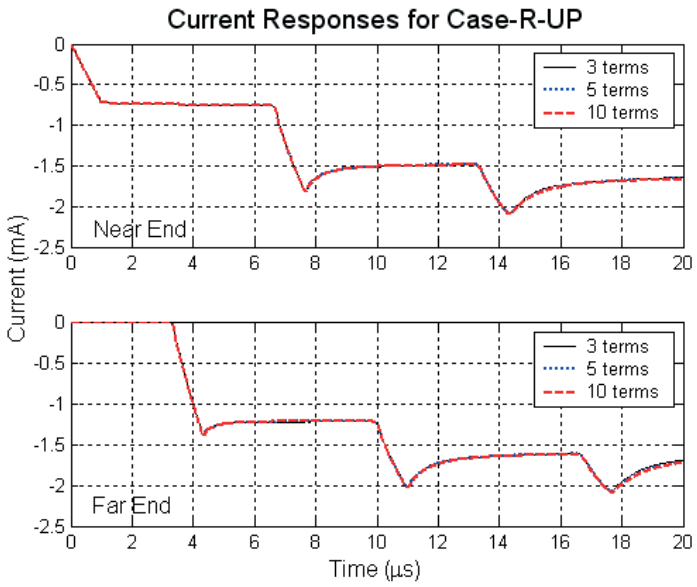

Figure 4.13: Simulations for the Case-R-UP (receptor height is 10m), with different number of exponential terms for transient ground impedance

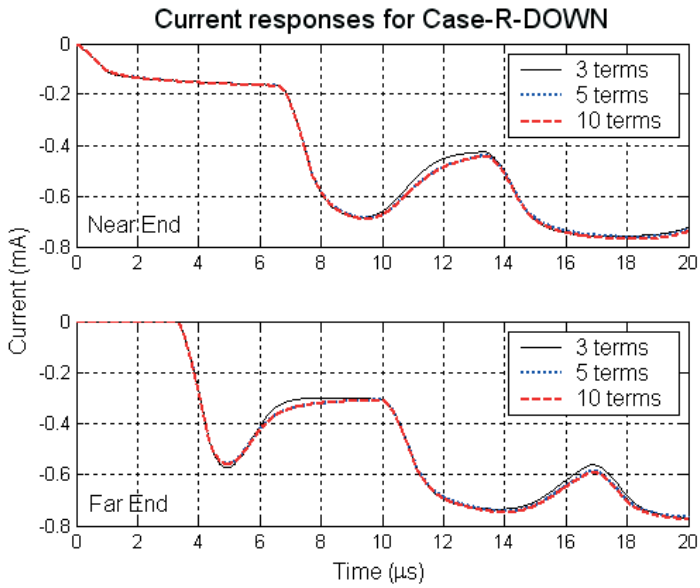

Figure 4.14: Simulations for the Case-R-DOWN (receptor height is 0.5m), with different number of exponential terms for transient ground impedance

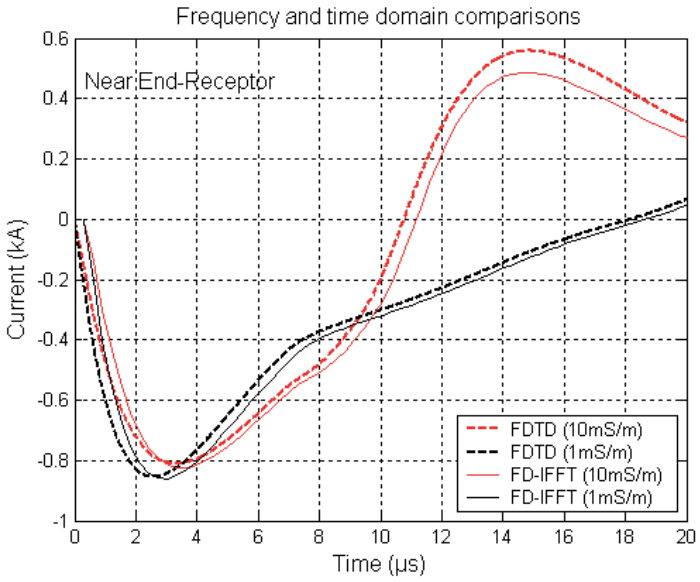

(a) Near end response

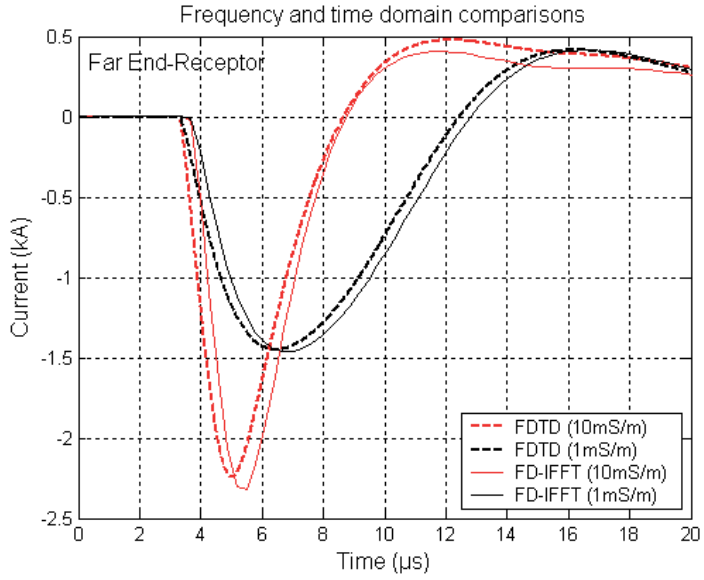

(b) Far end response

Figure 4.15: Responses at the near and far end loads of the receptor (0.5m height) - based on FD-IFFT and FDTD methods

was solved using both frequency domain and FDTD methods. The problem is solved in frequency domain using (4.54) and was later transformed to time domain using inverse *Fourier* transform (FD-IFFT). The same system as in Fig. 4.12 was chosen. The emitter was at $10m$ height and receptor was at $0.5m$ height and the conductor dimensions were the same as before. The loads were the same at both the ends of the line $Z_S = Z_L = [491,0;0,311]$. The injected current at the near end of the emitter was a double exponential impulse that has a shape given by $1.3 \times 10^5 (e^{-3\times10^5 \cdot t} - e^{-5.8\times10^5 \cdot t})$[73 **Paper-B**].

Fig. 4.15a shows the simulations for the currents at the near end of the receptor for two ground conductivities $10mS/m$ and $1mS/m$. Fig. 4.15b shows the similar simulations at the far end. It is seen that the errors are nominal and any differences that is seen is due to numerical errors both in frequency and time domain methods which are slightly difficult to control. Several cases were compared by this procedure the errors were nominal. Hence for the future simulations it is decided to adopt the FDTD method for the solutions of the MTLs above ground problems. In many cases this FDTD method has some advantages because as the voltages and currents are obtained at every time instant it is easier to model non-linear phenomena and also to connect non-linear loads, that primarily depends on the voltages and currents.

4.5 Conclusions

In this Chapter it is seen in detail what the internal and external losses are in the MTLs system and how they can be included into the telegrapher's systems. For lightning transient studies *Rachidi et al.* [52, 62] have shown that internal losses are negligible compared to the external losses they were however included in the simulations for completeness. Among the external losses it is shown that ground impedance is more dominant compared to the ground admittance. Also for lightning transients it is shown and concluded that the ground admittance can be neglected for above ground wires this will save enormous computation time. Having understood the essence of FDTD equations, let's move on to the next Chapter where some applications of FDTD method for lightning interaction studies are discussed.

5. Calculations of Lightning Induced Surges in Swedish Railway Overhead System

In this Chapter let's consider some of the important aspects of lightning induced over voltages, specifically with regard to what are the parameters that mainly affect the voltage or current distribution and propagation on the lines. In the previous Chapter it was shown, how the losses can be effectively included in the telegrapher's equations and how it can be solved using the FDTD method. Here let's apply some sensitivity analysis on the pulse propagation in the above ground wires. Calculations will be made with both types of excitation, namely direct and indirect lightning which will be also applied to the system shown in Fig. 1.6. It is however known that direct strikes are more severe than the indirect ones. The focus is mainly on determining, through simulations, as to how the lightning transients propagate within the system. Further the behavior of the various devices to be protected (relays, track circuits, transformers etc.) and protective devices (if installed like surge arresters, circuit breakers, switchgear, etc.) depends on the voltages across it or the currents entering into it via the overhead lines and tracks. Most of such devices have typical and a unique transfer function that can be determined only through experiments and later transformed into networks/circuits type of models, an example for the booster transformer will be studied later in Chapter-9.

5.1 How are the Swedish railway traction and power line systems different from the conventional overhead power lines?

Most of the studies in the recent past were focused on the power line lightning interaction [32, 52, 62, 71] and the configurations of the MTLs were such that conductors were located at similar heights (typically at $10m$ above the ground) and with symmetrical spacing between them. The Swedish railway traction system has MTLs that are spread out from heights of $10m$ to as low as $0.5m$ above the ground and has many conductors located in an unsymmetrical manner as in Fig. 1.6. In a multi track system as in Fig. 1.5, the number of

Table 5.1: *Impulse withstand voltages of the insulators for the single-track MTLs system*

Conductor Name	*Ceramic Insulator*	*Impulse withstand voltage (kV)*
R3	Rod/composit	225
R4	Lie post	170
R5 and R6	Spool	60
R7, R8 and R9	Pin	140

conductors is higher and level of unsymmetrical spacing is bit complex.

The lightning interaction to the railway system studied here is different compared to power line conductor system owing to many reasons, but the following are the main reasons based on *Theethayi et al.* [74 **Paper-C**],

- There are nine conductors in the system (Fig. 1.6), which are located at different heights. Hence their ground impedances as discussed in the previous Chapter, required for the wave propagation analysis are unique and have to be determined independently. Whereas in power line conductors located at a heights of 10m and close to each other the self and mutual ground impedances are comparable. More details on the magnitudes and shapes of ground impedance curves for various conductor heights can be found in *Theethayi et al.* [54 **Paper-A**].
- Insulators on the pole (supporting the conductors) are of different types and in particular have different impulse withstand levels as shown in Table 5.1, because each conductor has different operating voltages. The location of insulators on the pole is shown in Fig. 5.1. This causes flashover behavior to be more unique at every pole locations. However, in the case of power lines as they have common operating voltages, similar kind of insulators are used.
- The pole footing at every pole suffers soil ionization phenomenon [35] and hence they additionally modify the pole footing resistance. This poses an additional termination on one of the tracks at every pole (one of the tracks is grounded at every pole) location. While the other track is floating without any termination. The connection between the pole and the track is shown in Fig. 5.1.

Several interconnections between the traction conductors exist. An important interconnection between the overhead line conductors and tracks is shown in Fig. 5.2, which is rather unusual in power lines, where the lines are interconnected through a load like transformer, generator, etc. and is located usually at the sending or receiving end.

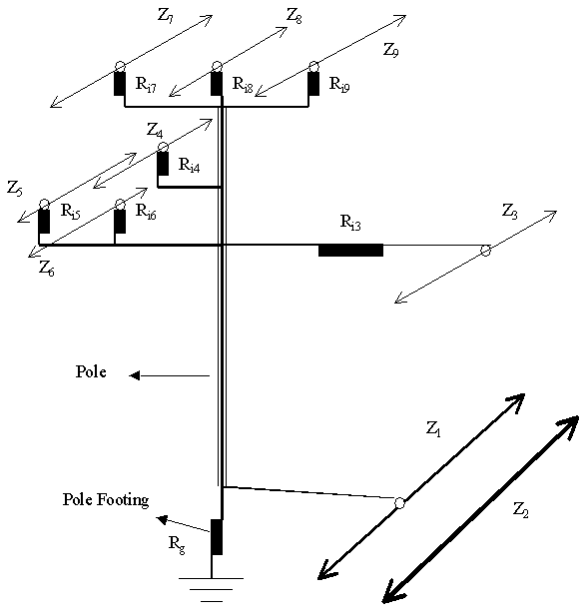

Figure 5.1: Schematic diagram of insulators and the connection of the track to the pole footing [74]

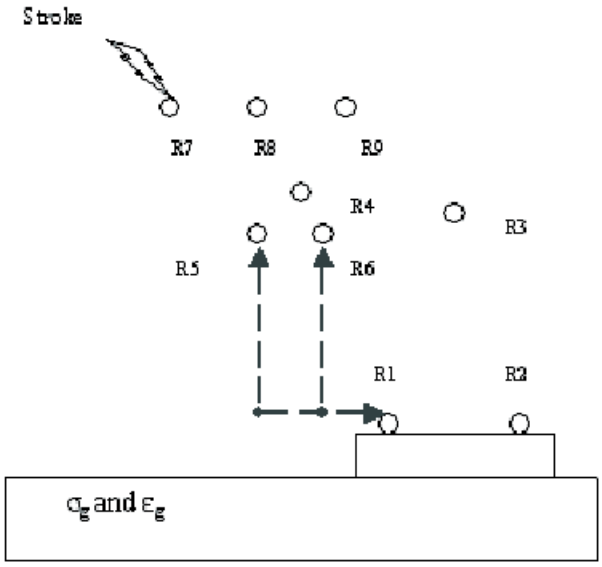

Figure 5.2: Interconnection between conductors R5, R6, R1

5.2 Parameters that influence lightning induced over voltage (LIOV) phenomena in MTLs

When the distance between source (emitter wire: say wire struck by lightning) of disturbance and the system suffering interference (receptor: other adjacent conductors) is very small, the victim system (receptor) is in the near field region of the source system. The coupling path between the source and victim is commonly referred to as crosstalk [12]. It mainly happens through EM coupling in the near field and occurs primarily due to inductive or capacitive coupling. To understand the EM coupling due to direct or indirect lightning strike it is first necessary to study a three-conductor system with two conductors forming the MTLs and the third conductor as ground return for direct strike and then a two-conductor system with a single conductor and second conductor as ground return for indirect strike. These studies are needed to see how the loads, conductor heights and ground conductivity influence the surge propagation along the conductors. Let's use the three-conductor system for direct strikes to be consistent with the earlier discussion in Chapter-2, where it was mentioned that conductors at larger heights are more prone to receive direct strikes. In indirect strike the ground additionally modify the fields illuminating the wire. Such influences are also included in the study.

5.2.1 Current waveform used for the present study in the thesis for the sake of discussions

For all the study presented here the source is a lighting current impulse that has a wave shape and time derivative as shown in Fig. 5.3. It represents a typical subsequent return stroke [75]. This current waveform has a high current derivative of about $110kA/\mu s$ typical of subsequent return strokes. It has a rise time of about $0.15\mu s$ corresponding to an upper frequency of $2MHz$. The wavelength corresponding to $2MHz$ is $150m$ and line length in this study is about $1km$. Various researchers use different waveforms for lightning for the first and subsequent strokes [20, 21]. It is believed that the conclusion presented in the discussion here might not change much within the range of lightning return stroke current wave shapes as far as the crosstalk phenomenon is concerned. More discussions on the behavior of crosstalk phenomenon can be found in [54 **Paper-A**, 72, 73 **Paper-B**] with a slower rise time pulse, having $1-2\mu s$ rise time corresponding to upper frequency of a few hundreds of kHz.

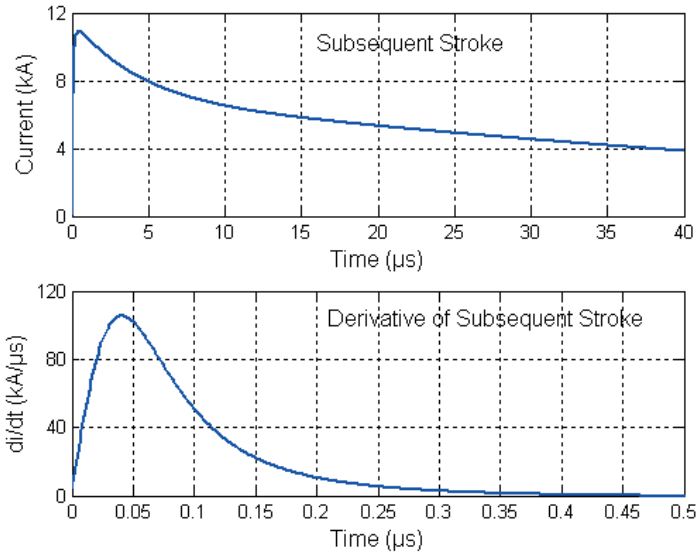

Figure 5.3: A typical subsequent stroke current waveform and its derivative

5.2.2 Direct strike pulse propagations on MTLs ¶

For direct strike, an emitter-receptor configuration as shown in the Fig. 5.4 was taken and the current was injected into the middle of the emitter line. The lengths of the lines were $1km$. The ground conductivity was varied between $10mS/m$ to $0.1mS/m$ and the voltages were measured on the receptor at three different points as shown in Fig. 5.4. The receptor height was either at $10m$ for the case close to the emitter line resembling the auxiliary power lines in Fig. 1.6 or it could be a track close to the ground at $0.5m$ above ground to see the coupling between the auxiliary wire and the track in the event of a strike to auxiliary wire. Note that whatever the height of the receptor, the height of the emitter was fixed at $10m$. The three points marked on the receptor are **S** *(close to strike point)*, **L** *(load point)* and **M** *(mid point between L and S)*. These points are chosen because the pulse propagation behavior/aspects can be clearly noticed as a function of the distance along the line. All the voltages are specified with a common unknown remote reference at zero potential. In all the cases the lines were terminated in their characteristic impedance, i.e. $Z_S = Z_L = [522,0;0,522]$ for receptor at $10m$ height and $Z_S = Z_L = [491,0;0,311]$ for receptor at $0.5m$ height above ground. These values are based on perfect ground conditions and it is kept the same even when the ground conductivity is varied.

The simulation results, when the receptor was at $10m$ height, are shown in Fig. 5.5a. From Fig. 5.5a the following observations can be made:

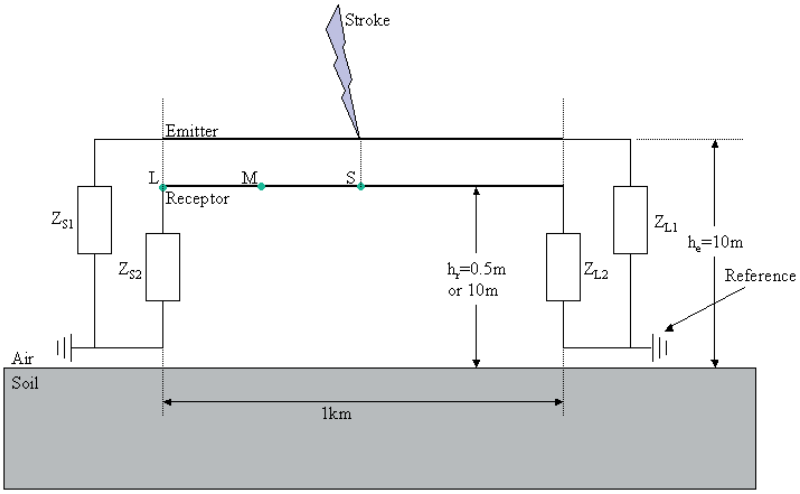

Figure 5.4: Direct stroke to the midpoint of the emitter line

- At the strike point (first window of Fig. 5.5a), poorer the ground conductivity, higher the induced voltage before the first reflection. The voltage after the reflection is decreasing but observe the time instants at which it crosses zero. It is seen that poorer the ground conductivity, larger the time delay at which voltage crosses zero level.
- At the mid point of the line (second window of Fig. 5.5a), again, it is seen that poorer the ground conductivity, higher the induced voltage. Here the influence of multiple reflections can be seen. However the conclusion that poorer the ground conductivity larger the time delay at which voltage crosses zero level applies here as well.
- At the load point (third window of Fig. 5.5a), always a kind of bipolar nature of the voltage is seen. Observe that for all the cases the voltage has a small or large negative going pulse and then it goes to the positive direction before the first reflection comes. Now it all depends on what one compares. If one compares the first negative going pulse then the proposition that poorer the ground conductivity, higher the induced voltage holds. But if one compares the positive part of the pulse, it seems that this proposition does not hold good. It is felt that the load in conjunction with the ground conductivity has influenced the wave shape and magnitude of the voltages. Well, the instant at which the voltage crosses zero level is again in agreement with the observation made in earlier two points. It is also interesting to note that though the lines are terminated with the characteristic impedance calculated under ideal conditions of perfect ground, there are reflections which clearly indicates that with ground loss characteristic impedances are frequency dependant. *Theethayi et al.* [54 **Paper-A**] have

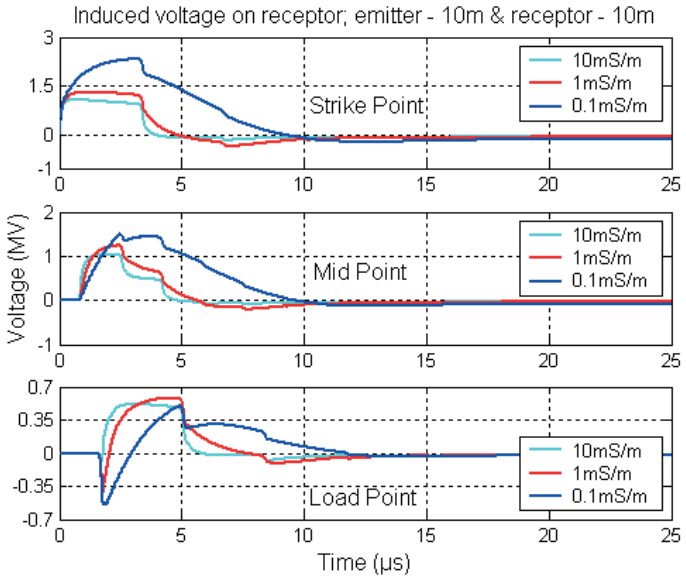

(a) 10m receptor height

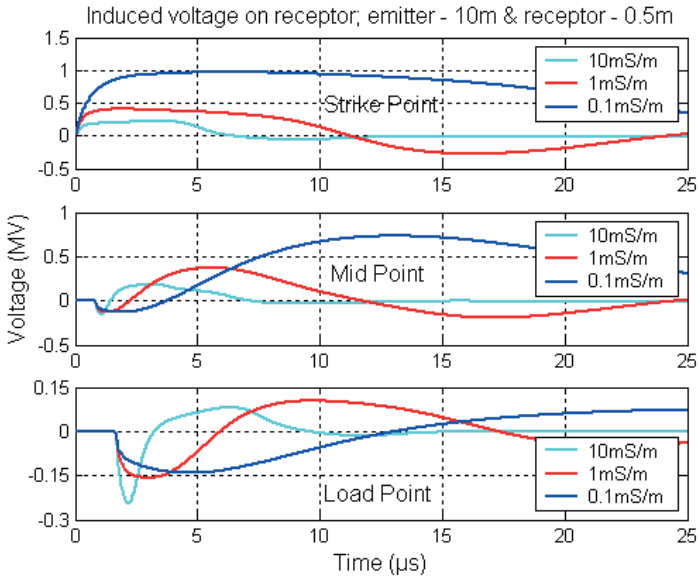

(b) 0.5m receptor height

Figure 5.5: Induced voltage at the points S, M, L corresponding to direct strike at middle of emitter for various ground conductivities, for receptor height 10m and 0.5m

also seen reflections when the lines were matched at both the ends and for simulations with perfect ground. This forces us to make another conclusion that in MTLs the concept of matching the loads with the characteristic impedance is not applicable.

The simulation results, when the receptor was at $0.5m$ height are shown in Fig. 5.5b. From Fig. 5.5b the following observations can be made:

- At the strike point (first window of Fig. 5.5b), poorer the ground conductivity, higher the induced voltage before the first reflection. The voltages are less compared with the case when receptor was at 10m height. It is seen that poorer the ground conductivity, larger the time delay at which voltage crosses zero level. Comparing with the case when the receptor was at $10m$, there seems to be larger dispersions. Compare Fig. 5.5b first window with corresponding window of Fig. 5.5a. It is seen that if the conductors are close to the ground, poorer the ground conductivity, longer the time delay for voltage zero crossing.
- At the mid point of the line (second window of Fig. 5.5b) the initial voltage wave shape has gone negative and then it goes up to the positive direction. It is interesting to see an opposite phenomenon, i.e. for the negative part of the voltage, poorer the ground conductivity, less the induced voltage. But in positive part of the voltage wave shape, poorer the ground conductivity, larger the induced voltage. On comparison with the corresponding case in Fig. 5.5a, when the receptor was at $10m$, negative going part of the voltage wave is not seen. It is felt that some different reflection coefficients exist in this case as clear signatures of multiple reflections similar to corresponding case of Fig. 5.5a is not seen.
- At the load (third window of Fig. 5.5b), all the features of the negative part observed at the mid point have become prominent, where it is seen that poorer the ground conductivity, less the induced voltage and finally it seems to saturate. Moreover, the positive part of the voltage is more or less similar in magnitude but with large dispersion.

From the simulations and observations of Fig. 5.5a and 5.5b, it is concluded that the in a typical crosstalk problem all the factors, like ground conductivity, heights of the conductors and loads at the terminals of the conductor participate together in the crosstalk phenomena and it is very difficult to isolate the influences one by one. Note that with ground losses included the lines have complex surge impedances changing with frequency, unlike perfect ground case where the surge impedances of the lines are more or less constant. The simulations above are influenced by the type of load connected at the ends of the lines, which when combined with ground losses gives complex valued reflection coefficients at the line terminations.

5.2.3 Indirect strikes pulse propagation on MTLs

The subject of indirect lightning strikes has been of interest to many researchers and engineers across the world. This is mainly attributed to the fact that in the event of indirect strikes the coupling to the electrical systems is through fields, and in majority of the cases it is the indirect strikes that decide the number of outages occurring within the various systems in a given area or region. Several cases have been reported in the recent past where even grid blackouts[27] occur due to lightning strikes. Power line lightning interaction has gained importance in the recent past. Several researchers, to name a few of them, *Rubinstein et al.* [76, 77], *Nucci et al.* [78], *Rachidi et al.* [71], *Jankov* [79], etc., were concentrating more on modeling the power line lightning coupling mechanism and developing the relevant models for studying the phenomena. *Borgheti et al.* [80] and *Paolone et al.* [81], etc., have applied those models to a real power grid network and studied the associated mitigation and outages using statistical approaches. Such studies have a practical advantage to predict the threat levels involved and assist in power system protection practices. Let's see the modeling of indirect strikes to the railway systems. To begin with let's start with return stroke electromagnetic fields.

Return stroke electromagnetic fields

The vertical electric fields and the horizontal magnetic fields from the return strokes have unique features at various distances. *Lin et al.* [82] have measured the remote electromagnetic fields from the return strokes at different distances. From those data the features of electric and magnetic fields at $5km$ and $100km$ are discussed.

At $100km$ the electromagnetic fields from the lightning have the characteristics of radiation fields. Fig. 5.6 provides examples of the radiation fields generated by subsequent return strokes [83]. Very far from the return stroke channel both electric and magnetic fields from the return strokes have the same shape and will be shown later. The radiation field begins with an initial slow ramp followed by a fast transition, which will culminate in an initial peak. After the initial peak the radiation field shows one or two subsidiary peaks located within a few microseconds from the beginning of the waveform. Subsequently, the waveform decays more or less monotonically and crosses the zero line around $30-100\mu s$.

A typical example of the measured electric and magnetic fields at $5km$ for subsequent return strokes is shown in dotted line in Fig. 5.7. The electric fields at $5km$ have one or two subsidiary peaks and finally it monotonically increases

[27] On a hot, mid-July evening in 1977, series of lightning struck two high-voltage power lines just north of New York City. Eight million people in New York metropolitan area were in total darkness without power for twenty-five hours.

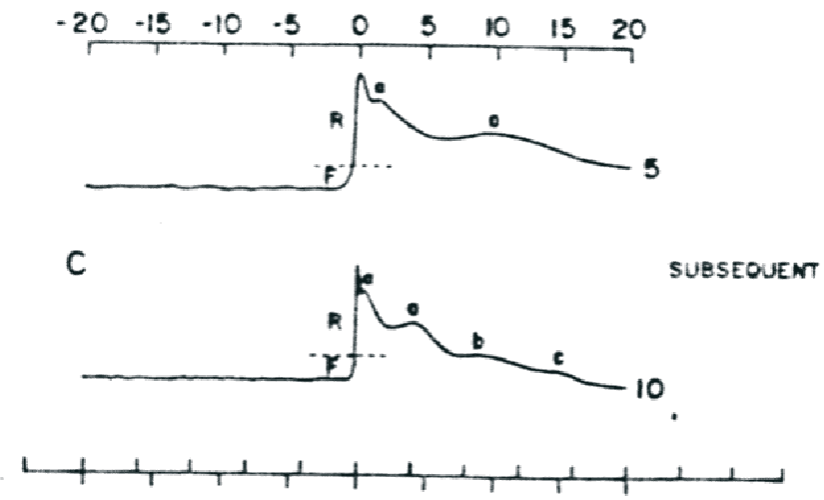

Figure 5.6: Vertical electric fields at ground level from subsequent strokes at 100km (adapted from [83])

(increasing ramp). The magnetic fields, unlike the electric fields, have one subsidiary peak a kind of hump after which the field decreases.

No information is available today on the electric fields at $50m$ generated by natural subsequent return strokes. However, experimental data are available for subsequent return strokes from rocket-triggered lightning. This experimental data show that the electric field at $50m$ rises to its peak value in a few microseconds and then remains more or less constant with increasing time. A typical example is shown in Fig. 5.8 [84].

Consider Fig. 5.9, where a return stroke segment is propagating up the channel. The expressions for electric and magnetic fields from this current element for vertical component of electric field, horizontal component electric fields, horizontal component of magnetic fields are shown in equations (5.1), (5.2) and (5.3) respectively for a return stroke speed of v at any point $p(r,z,\phi)$ above ground in cylindrical coordinates [52]. Note that equations (5.1), (5.2) and (5.3) do not include the influence of the ground. Equations similar to (5.1), (5.2) and (5.3) can be written for the image dipole (see Fig. 5.9) and added to corresponding equations (5.1), (5.2) and (5.3) to the get the total field from the dipole in presence of an infinitely conducting ground. In the above equations (5.1), (5.2) and (5.3) it is assumed that the stroke is propagating above a perfect ground.

When the field is calculated at the ground level, and including the contribution of the image channel to the fields the horizontal component of electric

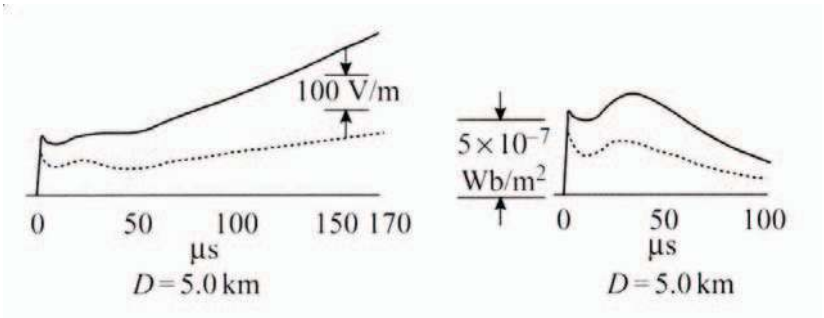

Figure 5.7: A typical example of vertical electric field at ground level (left) and the corresponding magnetic field (right) at 5km from the stoke (adapted from [82]), with return stroke field starting at t=0

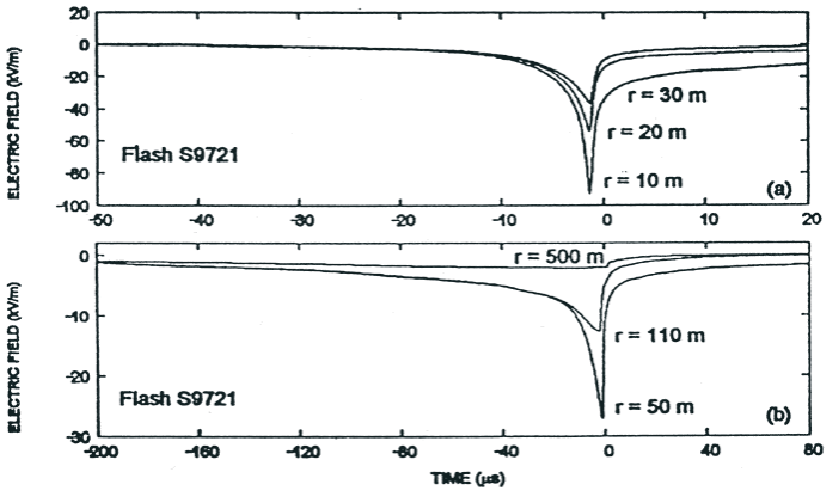

Figure 5.8: A typical example of vertical electric field at ground level, at 50m distance from the stroke, with return stroke field starting at t=0, (triggered lightning experiment [84])

field disappears. It is mentioned by *Nucci et al.* [85], that the variation of the vertical component of electric field with height above the ground is negligible, because of which the incident voltage at any height of the conductor above ground is simply the product of vertical component of electric field at ground level and the height of conductor.

$$dE_z(r,z,t) = \frac{dz^{'}}{4\pi\cdot\varepsilon_0}\left[\begin{array}{l}\dfrac{2(z-z^{'})^2-r^2}{R^5}\cdot\displaystyle\int_0^t i\Big(0,\tau-\frac{z^{'}}{v}-\frac{R}{3\times10^8}\Big)d\tau \\ +\dfrac{2(z-z^{'})^2-r^2}{(3\times10^8)\cdot R^4}\cdot i\Big(0,\tau-\dfrac{z^{'}}{v}-\dfrac{R}{3\times10^8}\Big) \\ -\dfrac{r^2}{(3\times10^8)^2\cdot R^3}\cdot\dfrac{di\Big(0,\tau-\frac{z^{'}}{v}-\frac{R}{3\times10^8}\Big)}{dt}\end{array}\right] \quad (5.1)$$

$$dE_r(r,z,t) = \frac{dz^{'}}{4\pi\cdot\varepsilon_0}\left[\begin{array}{l}\dfrac{3\cdot r\cdot(z-z^{'})}{R^5}\cdot\displaystyle\int_0^t i\Big(0,\tau-\frac{z^{'}}{v}-\frac{R}{3\times10^8}\Big)d\tau \\ +\dfrac{3\cdot r\cdot(z-z^{'})}{(3\times10^8)\cdot R^4}\cdot i\Big(0,\tau-\dfrac{z^{'}}{v}-\dfrac{R}{3\times10^8}\Big) \\ +\dfrac{r\cdot(z-z^{'})}{(3\times10^8)^2\cdot R^3}\cdot\dfrac{di\Big(0,\tau-\frac{z^{'}}{v}-\frac{R}{3\times10^8}\Big)}{dt}\end{array}\right] \quad (5.2)$$

$$dH_\phi(r,z,t) = \frac{dz^{'}}{4\pi}\left[\begin{array}{l}\dfrac{r}{R^3}\cdot i\Big(0,\tau-\dfrac{z^{'}}{v}-\dfrac{R}{3\times10^8}\Big) \\ +\dfrac{r}{(3\times10^8)\cdot R^2}\cdot\dfrac{di\Big(0,\tau-\frac{z^{'}}{v}-\frac{R}{3\times10^8}\Big)}{dt}\end{array}\right] \quad (5.3)$$

As mentioned earlier, that the finite ground conductivity and the relative permittivity additionally modify the above fields. *Rachidi et al.* [52] mentions clearly that it is the horizontal component of electric field that is affected/modified largely by the finite ground return parameters. On the contrary the vertical component of electric field is least affected by lossy ground. This led to the development of well-known *Cooray-Rubinstien* formula by *Rachidi et al.* [52], which is a correction to horizontal field accounting for the propagation loss of lightning electromagnetic fields over a dissipative ground. *Rachidi et al.* [52] and *Cooray* [86] also confirms that *Cooray-Rubinstien* formula can predict fields accurately for nearby or close lightning strokes. It is therefore decided to use the *Cooray-Rubinstien* formula in the present investigations too. The horizontal component of electric field at a given height above the

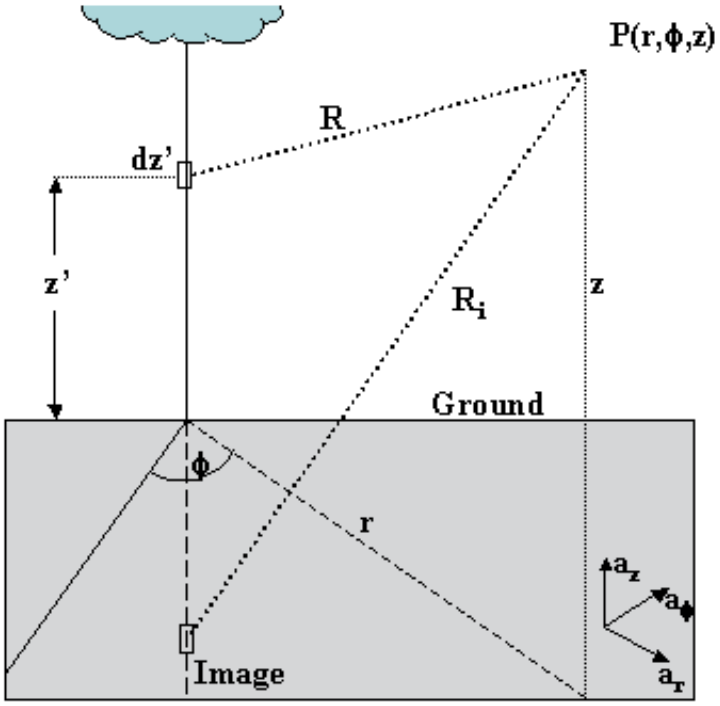

Figure 5.9: A return stroke current segment in air and its image for the field calculations at any point in air medium

lossy ground is,

$$E_{rg}(z=h,r,s) = E_r(z=h,r,s) - H_\phi(z=0,r,s)\cdot\sqrt{\frac{s\cdot\mu_0}{\sigma_g + s\cdot\varepsilon_g}} \tag{5.4a}$$

In (5.4a) E_{rg} is the horizontal electric field including the effect of finite ground conductivity. E_r and H_ϕ are the horizontal electric and horizontal magnetic field components respectively with infinitely conducting ground. The time domain expression of the correction factor i.e. for the surface impedance of the ground is given by,

$$\begin{aligned} Z_{si} &= L^{-1}\left(\sqrt{\frac{s\cdot\mu_0}{\sigma_g + s\cdot\varepsilon_g}}\right) \\ &= \sqrt{\frac{\mu_0}{\varepsilon_g}}\cdot\left(I_0\left(\frac{\sigma_g\cdot t}{2\varepsilon_g}\right) + I_1\left(\frac{\sigma_g\cdot t}{2\varepsilon_g}\right)\right)\cdot e^{-\frac{\sigma_g\cdot t}{2\varepsilon_g}} \end{aligned} \tag{5.4b}$$

The time domain expression for the horizontal electric field with finite ground conductivity is given by,

$$E_{rg}(z=h,r,t) = E_r(z=h,r,t) - H_\phi(z=0,r,t) * Z_{si}(t) \tag{5.4c}$$

Usually the above convolution is tricky. Many researchers convolute the magnetic field and surface impedance terms in various ways using step function [86] or ramp function [87] technique. The ramp function technique is adopted here, wherein the magnetic field is broken to piecewise linear sloped delayed ramps in between each time steps of the time axis and the convolution is simply the product of slope of the magnetic field multiplied by the surface impedance in time as (5.4d), if M_{Hi} represents the slope at i^{th} time instant and if t_i represents the time delay.

$$E_{rg}(t) = E_r(t) - M_{Hi}(t - t_i) \cdot Z_{si}(t - t_i) \tag{5.4d}$$

Before moving on to the induced voltage calculations it is interesting to take up a small investigation into the return stroke models.

Models for return stroke

There are a number of return stroke models available in the literature. With regard to the present work, they are transmission line *TL* model by *Uman and McLain* [88], modified transmission line *MTL* model [89], modified transmission line with exponential decay *MTLE* model [89], modified transmission line with linear decay *MTLL* model [90], etc. All these models, excepting the first use mathematical techniques (adjustments, perhaps, in author's opinion) to reproduce the remote experimentally observed electromagnetic fields, as seen in the previous section. The first *TL* model [88], is based on the assumption, that the return stroke is a pulse propagating on a vertical transmission line without any attenuation or dispersion. The later *TL* models (modified) assume pulse propagation with certain current attenuation as a function of channel height. All the above *TL* models assume pulse propagation with speeds less than speed of light (one thirds or two thirds speed of light to have some agreement with measured return stroke speeds). Indeed the stroke is propagating up in a channel, which could be thought of as a transmission line. A theoretically proven fact, as seen before is that a pulse propagating in air has speed of light. It has been shown by *Thottappillil et al.* [91, 92 **Paper-E**] that a semi-infinite vertical thin wire of vanishing radius above ground excited by a point source at the bottom and all conductors being perfect, supports a TEM field structure. In that case the pulse travels along the wire at speed of light without attenuation and distortion, as in a lossless transmission line. Developers of various modified transmission line models still assume that stroke is propagating in a lossless ideal transmission line but with different speeds; different from speed of light (author question's: **how some pulse propagating in air have different speeds?**) and different current attenuation along the channel. However the author agrees, that they are models to reproduce remote electromagnetic fields in some way or the other. But the word transmission line keeps bugging. Let's look at what *Theethayi and Cooray* [93 **Paper-D**, 94 **Paper-F**] argued

about the representation of return stroke as a current pulse propagating along a transmission line.

It is assumed that lightning return stroke can be represented as a pulse propagating along a transmission line. What now really matters is the different transmission line parameters that will control the pulse propagation aspects, which will further effect the attenuation and dispersion of the propagating pulse. The return stroke propagates only in a thin channel of about $1-10cm$ radius and that this thin channel can be considered as a vertical transmission line above the perfect ground. Since each segment of this transmission line experiences different heights from the ground, it is very clear that the channel inductance and capacitance is height dependant. The capacitance and inductance of the channel as a function of height has been computed separately with the same radius using charge simulations and it was found that the distribution of the inductances and capacitances are such that the factor $\frac{1}{\sqrt{L(z)\cdot C(z)}}$ gives velocity distribution as a function of height equal to speed of light. In order to get a reduced return stroke velocity, some researchers obtain the inductance of the line using the radius of the thin channel through which the longitudinal current is propagating and the capacitance of the line is calculated by using the radius of the corona sheath (which was formed during the stepped leader phase of lightning discharge). This approach is not correct because $C(z)$ and $L(z)$ in the transmission line model formulation correspond to the inductance and capacitance of the line through which the longitudinal current is propagating. No longitudinal current propagates through the corona sheath and its radius is thus irrelevant in the calculation of the channel capacitance that is needed in the evaluation of the speed of propagation of currents along the transmission line. In reality, neither the leader nor the return stroke channel is a perfect conductor and, therefore, one has to take into account the channel resistance in the transmission line equations. Since the return stroke current is propagating along the leader channel, the resistance experienced by the front of the return stroke is equal to the resistance of the leader channel. However, as the return stroke current increases in a given channel segment, one would expect the channel resistance to decrease. Thus, one has to treat the channel resistance as a time dependent parameter with decay time constants for the channel resistance at each channel segment varying between a few hundreds of nanoseconds to a few tens of microseconds. These observations are valid from the experimental data corresponding to long sparks. It is well established that if the amplitude of the current wave propagating along a conductor is such that the electric field at the surface of the conductor exceeds the corona threshold field then corona will set in leading to the leakage of the current out of the conductor. This obviously is the case with the return strokes, since a large current exceeding several kilo-amperes is confined to a channel thickness of about a few centimeters. Moreover, in reality, there is a corona sheath, which

is generated by the leader, surrounding the return stroke channel. This will also enhance the electric field on the surface of the central channel. Indeed, the available experimental data show that as the return stroke current propagates upwards along the leader channel, luminous discharges propagate out from the central current carrying region. In a real representation of the return stroke as a current wave propagating along a transmission line, one has to take into account the leakage of current out of the conductor. This can be easily accomplished by introducing a finite conductance in the transmission line equations. It is essential to point out an important difference between this representation and the reality. In the real situation the corona discharges will change the conductance of the medium only in the vicinity of the central conductor i.e. in the volume of the corona sheath. The charge leaking out of the conductor will be deposited on the corona sheath thus neutralizing it. Here the conductance is assumed to be uniform across the two conductors of the transmission line, which indeed is an approximation. This makes it necessary to consider the magnitude of the conductance that is introduced in the calculation as an effective value that represents the leakage of current out of the central conductor. *Theethayi and Cooray* [94 **Paper-F**] attempted to model the neutralization of corona sheath by means of a time dependant conductance term in telegrapher's equations. All the modeling strategy associated with return stroke current propagation in transmission line was simulated using the FDTD method. The advantage is in having control of varying transmission line parameters at each point on the line and their corresponding variation as a function of time too. Some of the simulations for the vertical electric and horizontal magnetic fields from [93 **Paper-D**, 94 **Paper-F**] at distances $50m$ (Fig. 5.10 upper window), $5km$ (Fig. 5.10 middle window) and $100km$ (Fig. 5.10 lower window) are shown. It can be seen that the calculated fields in Fig. 5.10 are comparable with experimentally observed remote electromagnetic fields as discussed in previous section. For the discussions on induced voltage the simple *TL* return stroke model with subsequent strokes is used. Though a better and reasonably physical *TL* type return stroke model was discussed above, the author would like to use it only after the model gains credibility in the lightning community. Further, more investigations on the physical phenomena associated with the return strokes are needed. *Thottappillil and Uman* [95], recommend that if one is only interested in the magnitude of the fields and not very particular about the exact shape of the experimentally observed fields, the simple *TL* model [88] can be used.

Induced voltage on the conductors above ground due to indirect strikes ¶

As mentioned in Chapter-2, there are many models available in the literature for field to wire coupling type problems. The most popular and simplest model

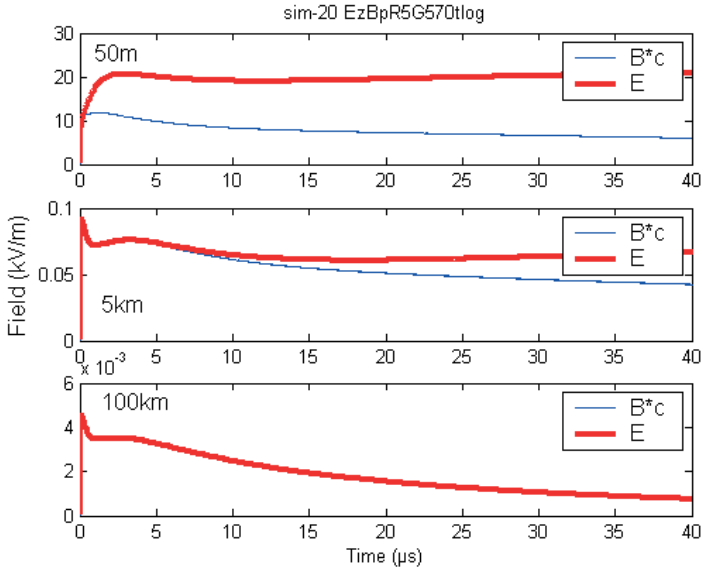

Figure 5.10: Electromagnetic fields from the return stroke transmission line model proposed by Theethayi and Cooray in [93]

is the *Agrawal et al.* [33] model. *Nucci et al.* [32, 78] have compared the various coupling models, namely *Taylor et al.* model [34] and the *Rachidi* model [31], through simulations for the induced voltage on a single power line from a nearby return stroke and concluded that all the models agree very well. Let's use the *Agrawal et al.* [33] model for the discussions here. Neglecting the internal loss we have the transmission line representation of the coupling phenomena as shown in Fig. 5.11. *Rubinstien et al.* [76] have applied the *Agrawal model* on a typical power line configuration and validates with real measurements from lightning.

$$\frac{dV^S(x,t)}{dx} + L_e\frac{dI(x,t)}{dt} + \int_0^t (\zeta(t-\tau))\cdot\frac{\partial I(x,\tau)}{\partial\tau}d\tau = E_x^i(x,h,t) \tag{5.5a}$$

$$\frac{dI(x,t)}{dx} + C_e\frac{dV^S(x,t)}{dt} = 0 \tag{5.5b}$$

Note that from the above telegrapher's equations one has only the scattered voltage, the total voltage on the line at any point is the sum of the voltage induced due to vertical component and the scattered voltage at the point under consideration.

$$V^i(x,t) \approx -E_z^i(x,0,t)\cdot h \tag{5.6a}$$

$$V(x,t) = V^S(x,t) + V^i(x,t) \tag{5.6b}$$

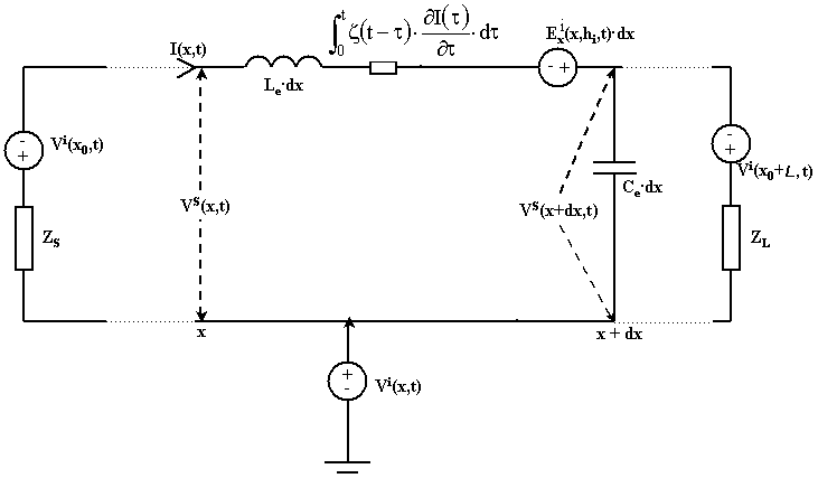

Figure 5.11: Equivalent transmission line representation for lightning induced voltage calculation: Agrawal et al. [33] coupling model used for horizontal field contribution

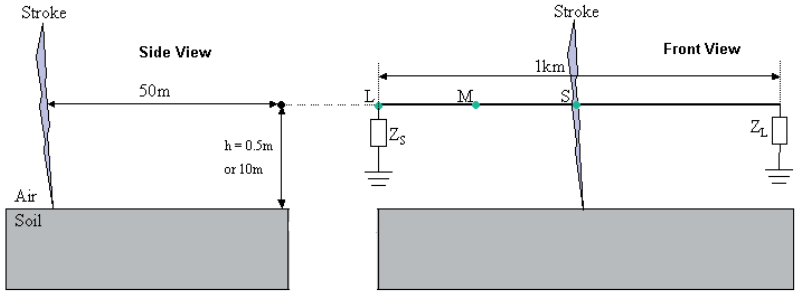

Figure 5.12: Schematic showing an indirect lightning stroke at a horizontal distance of 50m from the point S on the line for induced voltage calculations

$$V^S(0,t) = -Z_S \cdot I(0,t) - V^i(0,t) \tag{5.6c}$$

$$V^S(L,t) = Z_L \cdot I(L,t) - V^i(L,t) \tag{5.6d}$$

Note that the voltage sources due to the horizontal field E_x is along the line and they have to obtained from the E_r components. In the simulations to follow the induced voltages are calculated at three points on the line as shown in Fig. 5.12. The stroke was located at a distance of $50m$ from the center of the line marked **S**. The length of the line is $1km$ and the voltages are measured at $250m$ (marked **M**) from point **S**and $500m$ (at the load marked **L**) from point **S**.

Before proceeding to the simulations it would be meaningful to see the levels of horizontal electric field at $10m$ and $0.5m$ height due to a stroke located

at $50m$ from the line center as shown in Fig. 5.12. Note that simple *TL model* with stroke propagating without any attenuation, dispersion and with a stroke velocity equal to speed of light is used in all the simulations below.

The vertical component of electric field and the horizontal component of magnetic field at the ground level are shown in Fig. 5.13a, note that it will have the same shape of the injected channel base current as shown in Fig. 5.3, these curves can be obtained by the exact simple formula proposed by *Thottappillil et al.* [91, 92 **Paper-E**]. The vertical component of electric field has negligible height dependence.

The horizontal component for electric field is shown in Fig. 5.13b for $10m$ height point of observation and Fig. 5.13c for $0.5m$ height location. At $10m$ height the horizontal component of electric field as shown in Fig. 5.13b for perfect ground has the highest peak and is not bipolar in nature. The moment the ground conductivity is included the bipolar nature dominates and it is seen that the initial peak increases with decreasing ground conductivity. It seems that the horizontal component of electric fields at $10m$ height follows the field due to the perfect ground case during the late times even though the magnitude of fields with finite ground conductivity are slightly higher than the perfect ground case in the late times.

At $0.5m$ height the horizontal component of electric field are negligible for perfect ground, hence not shown in Fig. 5.13c. It can be seen that the only contribution of horizontal electric field at $0.5m$ is due to the product of horizontal component of magnetic field at ground level multiplied by the surface impedance (convolution in (5.4c)). Compare the top and bottom windows in Fig. 5.13c, from which it can be seen that the magnitude of horizontal component of electric field at $0.5m$ height and at the ground level are comparable. Interestingly the horizontal component of electric field at ground level decays rapidly with in $10-20\mu s$, even though the actual horizontal component of magnetic field at the ground level follows the shape of the channel base current. The immediate decay is a result of the convolution in (5.4c). There are some numerical oscillations in the top window of Fig. 5.13c, which has appeared due to the adopted simulation methodology; the author has confirmed that these oscillations are only for the case when the observation point is close to the ground and have not caused any difference in the simulation results to follow.

Based on the analysis and discussion made in the previous sections let's simulate a special case for a conductor above perfect ground. The conductor is located at a height of $10m$ above ground with $Z_S = Z_L = 491\Omega$. The simulation results are shown in Fig. 5.14.

In each of the windows of Fig. 5.14 one can see the curves corresponding to the following cases,

- E_x contribution: in these simulations the voltage sources due to horizontal

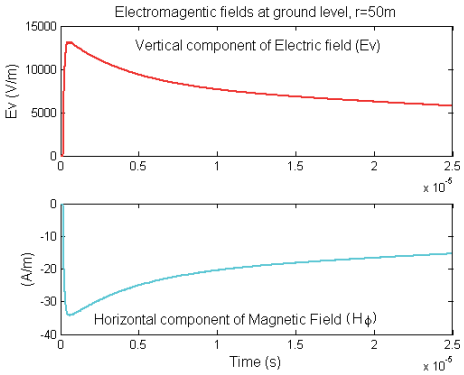

(a) E_z and H_ϕ at z=0

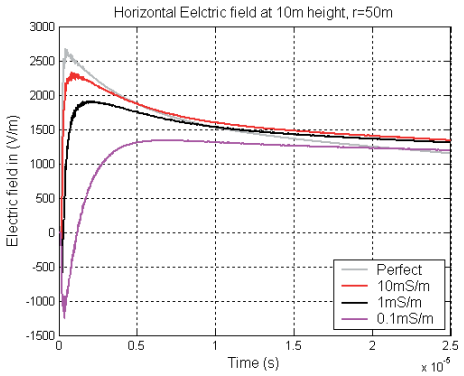

(b) E_{rg} at z= 10m

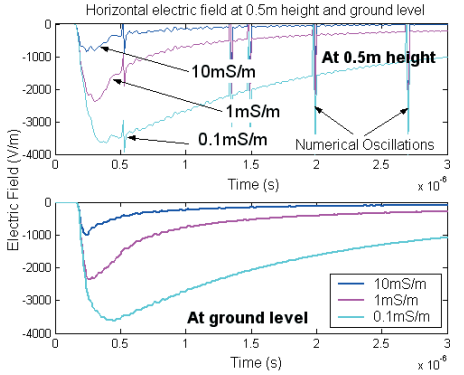

(c) E_{rg} at z=0.5m

Figure 5.13: Vertical and Horizontal electromagnetic fields: stroke at r=50m and for different ground conductivities

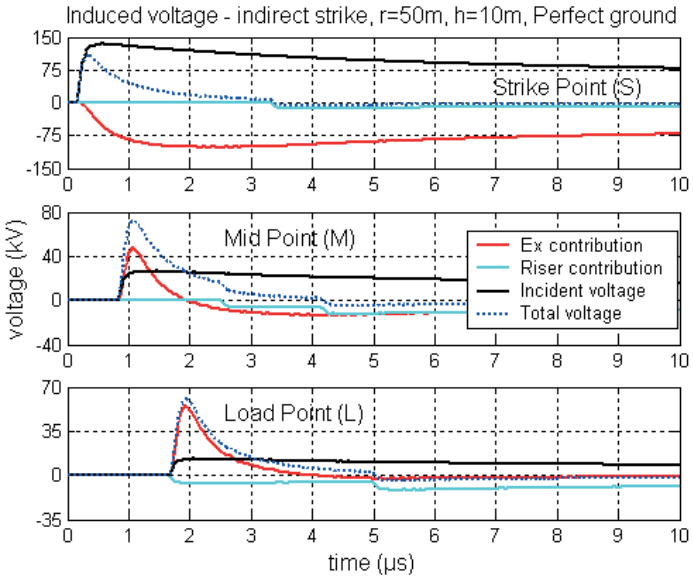

Figure 5.14: Induced voltages due to indirect strike at the points S, M, L on the line, which is at a height of 10m above a perfect ground

component of electric field are considered with all the other sources killed.

- Riser contribution: in these simulations the voltage sources at the loads are considered with all the other sources killed.
- Incident voltage: in these simulations it is the voltage source at the point on the line due to the vertical component of the electric field is only considered with all the other sources killed.
- Total voltage: in these simulations the entire sources are on the line and the total voltage on the line is calculated based on equation (5.6b).

From Fig. 5.14 it is clear always the contribution for horizontal field is considerable.

- At the strike point the E_x contribution of the voltage is negative and at the mid point and the load point its contribution is positive. As one moves to the mid point from the strike point, the voltage peak due to E_x contribution increases form negative to positive and at the load point it is fully positive. The magnitude is higher at the strike point compared to the load point.
- When only the riser contribution is considered, the voltages are negligible at all points on the line.
- When only the incident voltage is considered, the voltage at the strike point is the highest and decreases towards the load point.
- As for the total voltage is concerned, at the strike point it is the highest and it decreases towards the load. This is also observed in the calculations by *Nucci et al.* in [85] and *Rachidi et al.* in [62] for the same example. It is

interesting to note that the present simple *TL* model with velocity speed of light with perfect ground gives identical result for the total induced voltage on the line when compared with simulations by *Nucci et al.* in [85] and *Rachidi et al.* in [62] based on *MTL* model with return stroke speed one thirds the speed of light, channel base current derivative of $40kA/\mu s$ and with similar current peak as shown in Fig. 5.3. This is a validation of the present simulations.

Let's now consider the case when a lossy ground is included in the simulations. In all the lossy ground simulations the ground conductivity was varied between $10mS/m$ to $0.1mS/m$ and the ground relative permittivity was 10.

The first simulation is similar to the case above with a conductor at height $10m$. The simulation results are shown in Fig. 5.15a ($10mS/m$), Fig. 5.15b ($1mS/m$), Fig. 5.15c ($0.1mS/m$).

- When the ground conductivity is $10mS/m$ the total induced voltages are similar to perfect ground case at the strike point. But as the ground conductivity is reduced the total voltage at the strike point due to horizontal field contributions are increasing from negative to positive values. When the ground conductivity is $0.1mS/m$ the total voltage has increased to large value. The contribution for riser voltage is negligible. The variation in the horizontal field has caused an increase in the total voltage as the ground conductivity is decreased at the strike point.
- At the mid point, one can see a bipolar nature of the total voltage due to horizontal field, the total voltage going negative first and then positive. This is very typical induced voltage characteristic when the ground loss is considered as shown by *Rachidi et al.* [62]. The negative peak is increasing with decreasing ground conductivity. The positive peak first decreases and then increases with decreasing ground conductivity. The riser contribution is almost same in all the cases. The total voltage at the mid point has somewhat similar behavior/shape as the E_x contribution. When the ground conductivity is $10mS/m$, only a positive peak is seen; but as the ground conductivity is decreased the bipolar nature is seen.
- At the load point the bipolar nature is more prominent than the mid point case such that the total negative voltage peaks are increasing with decreasing ground conductivity. It is mainly due to the horizontal field contribution.

The second simulation is for the case when the conductor is at the height $0.5m$ above the ground with $Z_S = Z_L = 311\Omega$. The simulation results are shown in Fig. 5.16a ($10mS/m$), Fig. 5.16b ($1mS/m$), Fig. 5.16c ($0.1mS/m$). There are some numerical oscillations in the simulations at the strike point, which were difficult to eliminate. One has to remember for the conductors close to the ground the voltage source due to vertical component of electric fields are relatively small (can some times be neglected). Thereby the total in-

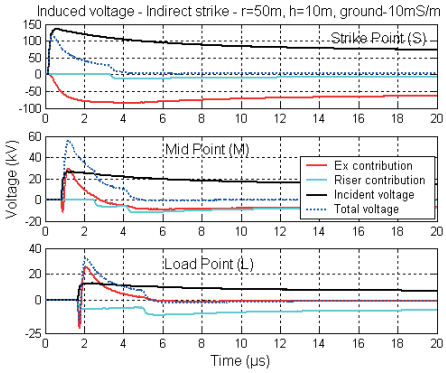

(a) $\sigma_g = 10mS/m$ and $\varepsilon_{rg} = 10$

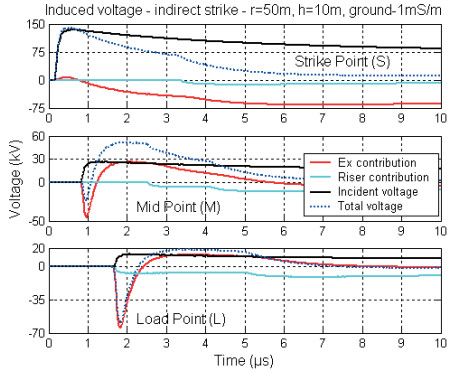

(b) $\sigma_g = 1mS/m$ and $\varepsilon_{rg} = 10$

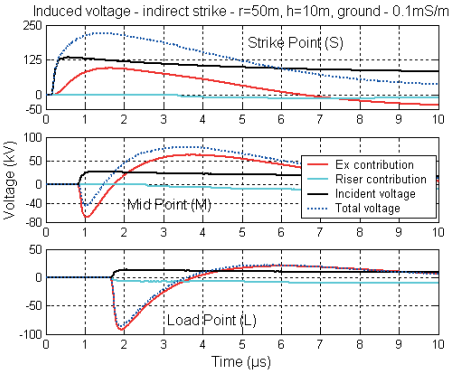

(c) $\sigma_g = 0.1mS/m$ and $\varepsilon_{rg} = 10$

Figure 5.15: Induced voltages due to indirect strike: line height h=10m, for various ground conductivities

Table 5.2: *Geometrical details of the conductors used in single-track railway systems in Sweden*

Conductor No.	*Conductor height(m)*	*Conductor radius (m)*
R1,R2	0.55	0.0495
R3	6.32	0.05
R4	7.0	0.082
R5,R6	6.5	0.082
R7, R8, R9	9.8	0.0056

duced voltage will be due to the distributed voltage source contribution from horizontal electric fields calculated from the convolution (5.4c).

The following main observations can be made in the case of conductor at height $0.5m$ above the ground,

- At the strike point, the E_x contribution and the total voltage increase as the ground conductivity decreases, and the magnitude of the induced voltage is less compared with the $10m$ height case.
- At the mid point the bipolar nature is seen, but the dispersion is larger compared with the $10m$ height case. Again the total induced voltage is less compared with the $10m$ height case. The total induced voltage seems to be less dependant on the ground conductivity in terms of magnitude.
- The voltage at the load point decreases with the decrease in ground conductivity. This is similar to the conclusion made in the three-conductor simulations presented in Fig. 5.5b, perhaps due to complex reflection coefficients as mentioned earlier.
- It is very clear that all the conductors close to the ground whether it is rail or cable or Balise will experience larger induced voltage due to the horizontal component of electric field. This could be a possible reason why the track circuits and Balise are damaged during thunderstorms.

5.2.4 Application of the above modeling concepts to single-track railway system

Before proceeding to the other non-linear mechanisms that would happen on the MTLs system during the pulse propagation it is good to apply the above models on the Swedish single-track railway system as shown in Fig. 1.6. For this let's take the same current source as in Fig. 5.3 and simulate two cases of lightning strikes, only for the sake of demonstration. The first case is a direct strike, where the stroke attaches to conductor R7 and the second case is an indirect strike at a horizontal distance of $50m$ from the middle of conductor R7. The voltages on all the conductors at the points **S**, **M**, **L** are shown in Fig. 5.17 and Fig. 5.18 for the direct and indirect

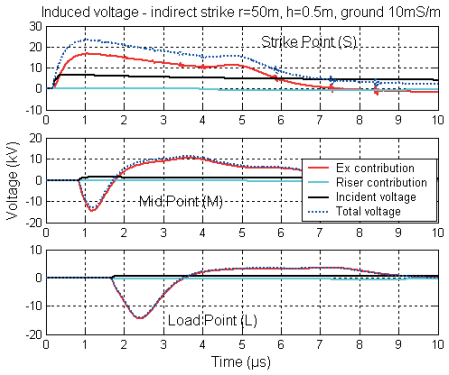

(a) $\sigma_g = 10mS/m$ and $\varepsilon_{rg} = 10$

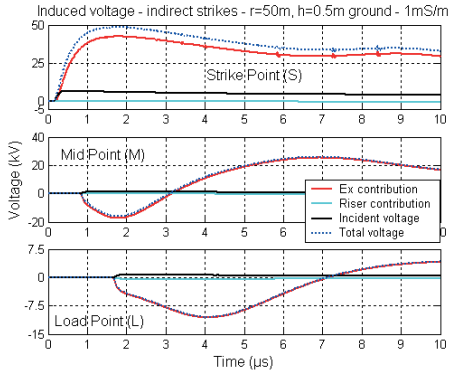

(b) $\sigma_g = 1mS/m$ and $\varepsilon_{rg} = 10$

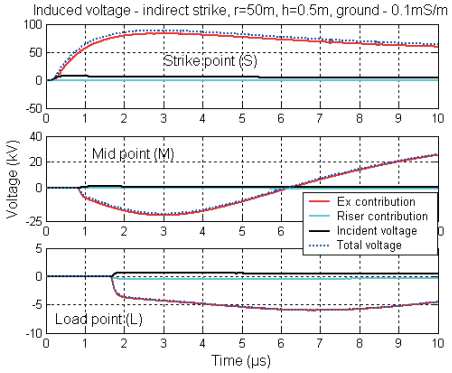

(c) $\sigma_g = 0.1mS/m$ and $\varepsilon_{rg} = 10$

Figure 5.16: Induced voltages due to indirect strike: line height h=0.5m, for various ground conductivities

strike cases respectively. The simulations are corresponding to data shown in Table 1.2 with regard to medium properties and the actual conductor dimensions shown in Table 5.2. The termination impedances were $Z_S = Z_L = diag[95, 95, 301, 381, 375, 366, 433, 421, 431]$ and the length of the line was $1km$. The capacitance and conductance matrices were determined using FEMLAB with Matlab [45], using the principle of stored and dissipated energies [96]. This was needed for taking into account the ballast between the track and the earth. The geometry is first set in the graphical user interface as shown in Fig. 1.6, with perfect ground but with ballast medium as in Table 1.2.

5.3 Lightning strike to Swedish railway MTLs system: Incorporating non-linear phenomena and interconnection between the line conductors

Theethayi et al. [74 **Paper-C**] has simulated a direct lightning strike to a single-track electrified railway system of Banverket, where the focus was towards modeling interconnections between the conductors as shown in Fig. 5.2 and the non-linear phenomena of insulator flashover and soil at the pole footing which leads to termination matrix at each pole and on the line based on Fig. 5.1. Here let's discuss only the modeling concepts and some important conclusions made by *Theethayi et al.* in [74 **Paper-C**] for a direct strike to conductor R7 in the middle of the line for the same material mediums as shown in Table 1.2. The current waveform that was used there was corresponding to standard $1.2/50\mu s$ with $31kA$ peak.

5.3.1 Modeling interconnection

An interconnection will lead to an additional termination matrix, which enters as conductance matrix (admittance in general) in the FDTD equations at the point of interconnection. It is good to explain this concept by an example. Consider four MTLs at any point on the line, let the voltage at the nodes be as shown in Fig. 5.19, and let the sum of currents entering or leaving a node, which is already taken care by the FDTD equations, be as shown in Fig. 5.19. Then at that node of interest let us write the *Kirchoff's* current law, by which one has,

$$I_{enter} = G \cdot V_{node} \tag{5.7a}$$

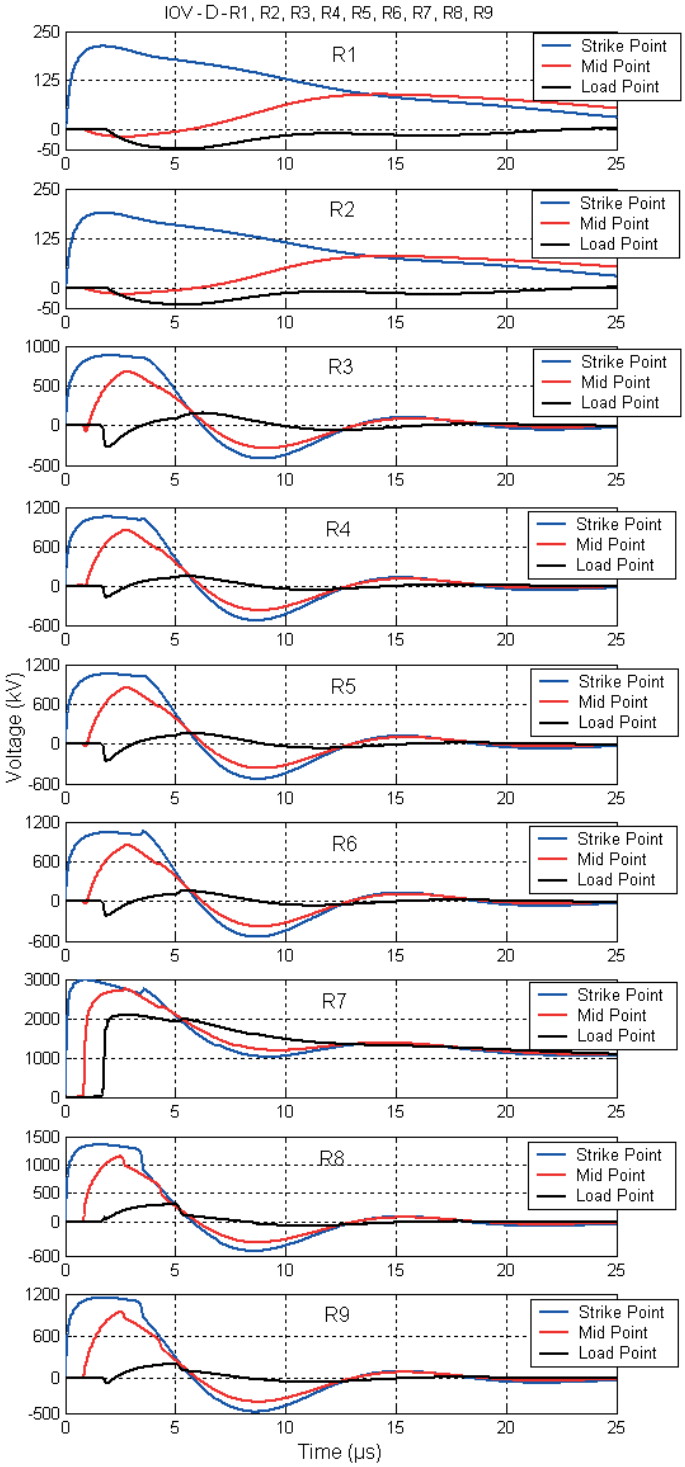

Figure 5.17: Induced voltage on all the conductors of Fig. 1.6 at points S, M and L due to a direct strike on conductor R7

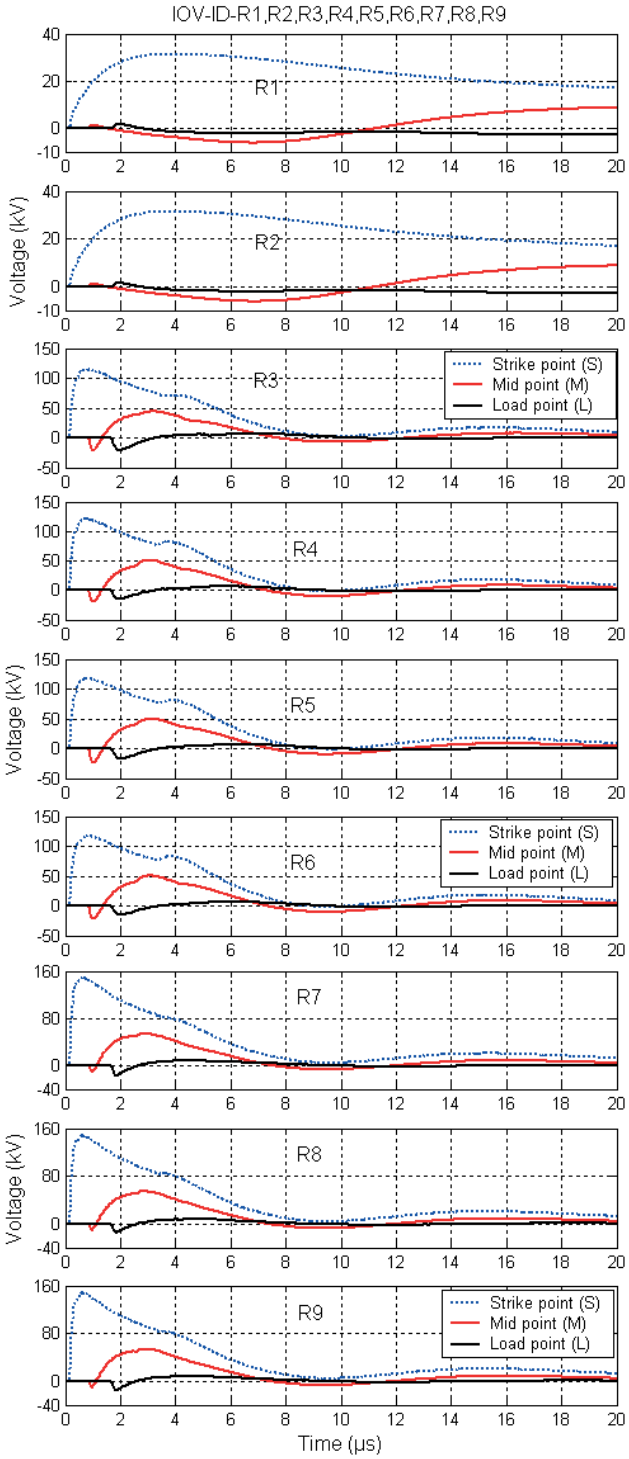

Figure 5.18: Induced voltage on all the conductors of Fig. 1.6 at points S, M and L due to an indirect strike at 50m horizontal distance from the line center of R7

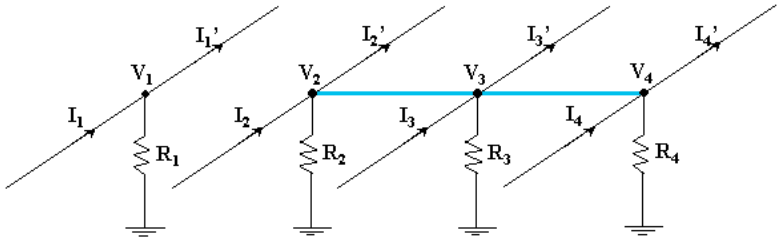

Figure 5.19: Schematic shown an interconnection in MTLs system

$$G_{jun} = \begin{pmatrix} \frac{1}{R_1} & 0 & 0 & 0 \\ 0 & \frac{1}{R_2} + \frac{1}{R_{short}} & -\frac{1}{R_{short}} & 0 \\ 0 & -\frac{1}{R_{short}} & \frac{1}{R_3} + \frac{1}{R_{short}} + \frac{1}{R_{short}} & -\frac{1}{R_{short}} \\ 0 & 0 & -\frac{1}{R_{short}} & \frac{1}{R_4} + \frac{1}{R_{short}} \end{pmatrix} \tag{5.7b}$$

If it is assumed that $R_{short} = 1\mu\Omega$, then the above matrix no matter whatever be the values of R_2, R_3, R_4, the shorts dominate because of which one has,

$$G_{jun} = \begin{pmatrix} \frac{1}{R_1} & 0 & 0 & 0 \\ 0 & 10^6 & -10^6 & 0 \\ 0 & -10^6 & 2\times 10^6 & -10^6 \\ 0 & 0 & -10^6 & 10^6 \end{pmatrix} \tag{5.8}$$

The above principle is used for simulating the interconnection between the return conductors $R5$ and $R6$ and $R1$ as shown in Fig. 5.2.

5.3.2 Modeling insulator flashover and soil ionization phenomena

From Table. 5.1 and Fig .5.1, it can be seen that other than tracks, all the conductors are held by the insulators that are on the poles. These form the other terminations on the line, which are due to the insulators own resistance and pole footing ionization/static resistance as the case may be. The equivalent termination resistance for the same is complex and depends on the soil ionization characteristics at the pole footing and insulator flashover behavior. Note that when the flashover takes place the resistance changes from high value $100M\Omega$ to some low value depending on the adopted arc model. A simple empirical arc model proposed by *Toepler* [97] where the arc resistance is function of the current (5.11) is used. The constant $k_{Toepler}$ was taken as 0.00454 and d is the

arcing distance, which is approximately taken as the insulator length [97].

$$R_{arc}(t) = \frac{k_{Toepler} \cdot d}{\int_0^t I(t) \cdot dt} \tag{5.9}$$

Since $R1$ is connected to the pole directly, the pole is always held at the potential of $R1$ an important boundary condition. The resistance R_g due to soil ionization (5.12) at the pole footing is calculated using the model proposed by the IEEE standard [35],

$$R_g(t) = \frac{R_0}{\sqrt{1 + \frac{I_R}{Ig}}} \tag{5.10a}$$

$$I_g(t) = \frac{1}{2\pi} \cdot \frac{E_0}{\sigma_g \cdot R_0^2} \tag{5.10b}$$

In (5.12) R_0 is the footing resistance measured with low current, I_R is the lighting current through the footing resistance, I_g is the current required to produce a soil gradient, E_0, at which soil breakdown occurs, which is about $400kV/m$ [35]. The termination resistance at each pole is calculated based on the equivalent circuit shown in the schematic of Fig. 5.1. The schematic Fig 5.1 shows as to how many insulators/resistances come in the circuit at a pole. The $Z's$ are the surge impedances of the line as discussed in the previous section, on direct and indirect strike simulations. The $R_i's$ are the insulator resistance, which varies based on the arcing condition, and R_g is the variable ground resistance depending on the ionization levels. The termination resistance matrix R_t is assumed to be a diagonal matrix at each pole point. The flashover computation is done as follows, consider the insulators as shown in Fig. 5.1. Once the potential between the conductor holding the insulator V_i and that of the V_{R1} (potential of R1) exceeds or equals the insulator flashover voltage of Table. 5.1, then a flashover is assumed to take place across the insulator surface. At this instant the $R_i's$ change from the initial operating value (high) to some value as given by *Toepler's* law [97]. These resistances keep on changing until the current through them changes sign (+ to - or - to +), to ensure arc extinction. At this instant the initial operating values of the insulation resistance is assumed to be regained. Then the process is repeated for checking the flashover restrike conditions.

5.3.3 Some important conclusions for a direct strike of $31kA$ to the auxiliary conductors of the single-track railway system from *Theethayi et al.* [74 **Paper-C**]

Five kilometers from the lightning strike point on one of the help wires, common-mode surge voltages in excess of $500kV$ can be expected in

auxiliary power ($R7$, $R8$, $R9$), and return conductors ($R5$, $R6$). Very large differential mode voltages can be created between the lines of auxiliary power even beyond $5km$. Large surge voltages between line and neutral on the low voltage side of the transformer can also be expected. Therefore, critical low voltage equipments in the technical house of the railways require both common mode and differential surge protection. Common mode surge voltages in excess of $100kV$ can be expected on contact wires at a distance of $5km$ from lightning strike point. Similar voltages can also be expected between the contact wire and the rails. The differential mode voltage across the two rails at a distance of $5km$ from lightning strike is only a few kV. However, within one kilometer of the lightning strike the voltages can be in excess of $10kV$. These over voltages from trackside have to be taken into account while considering the vulnerability of circuits connected across the tracks.

5.4 Conclusions

In this Chapter it is seen in detail the various aspects that influence the pulse propagation phenomena in the MTLs above ground for lightning interaction studies. The models and methodologies discussed in this Chapter have also been applied to the Swedish single-track system and solved for induced voltage calculations using the FDTD method accounting for the ground losses, interconnections between conductors, non-linear behavior like insulation flashover and soil ionization in the system for the case of a direct lightning strike. It is shown that the contribution of the ground losses in the induced voltages/currents are predominant and cannot be neglected. Effects due to indirect strikes were not simulated using the non-linear phenomena, as it is less severe than a direct strike case. In the actual railway system there are several interconnections and terminations between the conductors, out of which some important ones have been considered. All these interconnections and terminations are important as it decides the voltage/current distributions in the various conductors. The simulations mark the beginning of an attempt to estimate the lightning surge voltages/currents that would appear at the equipment terminals connected to the railway conductor system. In the next Chapter let's discuss some real lightning induced voltage and current measurements carried out in a typical railway technical house of Sweden.

6. Measurements of lightning transients entering a Swedish railway facility

One of their main concerns of engineers for designing lightning protection is to find an answer to the question: how can lightning transients enter or couple into the system? The most efficient way is to find it out experimentally by making controlled measurements at the place of interest. As part of the study on the lightning interaction with the Swedish railway system, in the summer of 2003, Uppsala University in association with Banverket decided to investigate how lightning transients enter the railway systems and from, which direction transients find their port of entry. The measurement setup was made at the Division for Electricity and Lightning Research of Uppsala University. Such a measurement was carried out for the first time in a railway technical facility. The place chosen for the measurements was the technical house at Tierp station (about 60km from Uppsala). This place was chosen because it was easily accessible from Uppsala in case any intervention was necessary. Since computerized measurement was used using a data acquisition system, there could be situation when the data could fill up the disk, calling for freeing the disk space at least once a week; or when the system trigger settings needed change, etc. In this Chapter let's discuss the measurement set up, instruments/equipment used, discussions about the collected data and their correlation with lightning event. A discussion is also made on features/characteristics of a typical measured data. The information presented here is taken from the works of *Theethayi et al.* [98, 99 **Paper-G**].

6.1 Measurement setup

The measurement station is located at 17.51 degrees longitude and 60.3467 degrees latitude. Statistics available with Banverket shows that a large proportion of faults were caused by lightning transients associated with power lines. Therefore it was decided to measure lightning caused transients at the auxiliary power. The cable shown in Fig. 6.1, from the auxiliary power conductors/lines ($R7$, $R8$, $R9$ of Fig. 1.6), carry the $22kV/50Hz$ power to a distance of 500m where it enters the technical house as shown in the block diagram Fig.

Figure 6.1: Cable termination at the auxiliary power conductors

6.2.

In the technical house the cable enters the units as shown in Fig. 6.2. The auxiliary power supply cable enters first the switchgear unit and then the three-phase step down transformer and through the fuse unit reaches the Banverket local supply. Measurements were made at this point using the data acquisition system (DAQ) as shown in the Fig. 6.2. Four channel Data Acquisition (DAQ) system *NIPCI*6115 (programmable) was connected to four sensors measuring electric field near the track, phase voltage, phase current, and earth current respectively. These points are shown in the Fig. 6.2. All the analog inputs were sampled at $10MS/s/channel$ and with $12-bit$ resolution by the DAQ system. For later correlation with lightning location data system (LLP), vertical electric field from the lightning was measured using a flat plate antenna with a buffer amplifier as shown in Fig. 6.3.

The buffer amplifier is used for matching the impedance of the antenna with measurement cable system [20]. As mentioned in Chapter-1, conductor $R3$ carry $15kV$ at $16\frac{2}{3}Hz$ for the traction power and $R1$ (S-rail) acts as a return. The

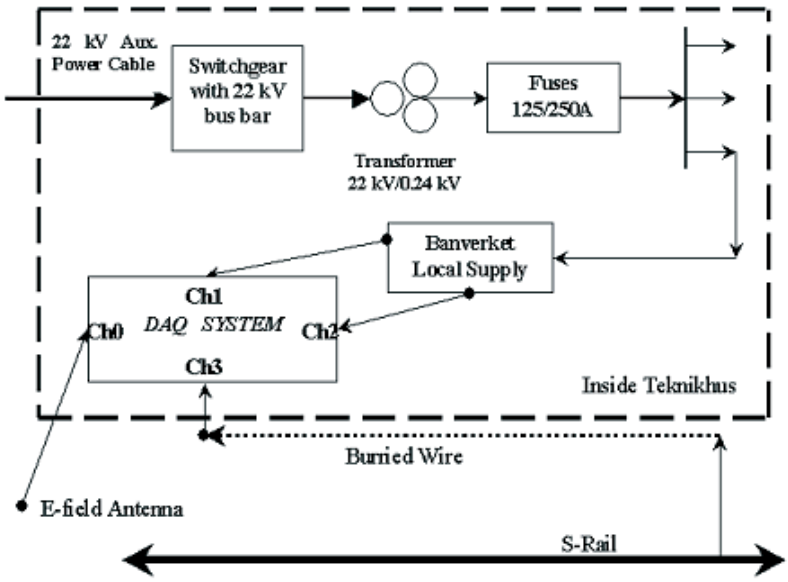

Figure 6.2: Inside technical house where the measurements are made, Ch0-Electric Field, Ch1-Voltage across Phase and neutral, Ch2-Phase Current and Ch3-local ground to S-rail current

Figure 6.3: Vertical electric field measuring system for lightning

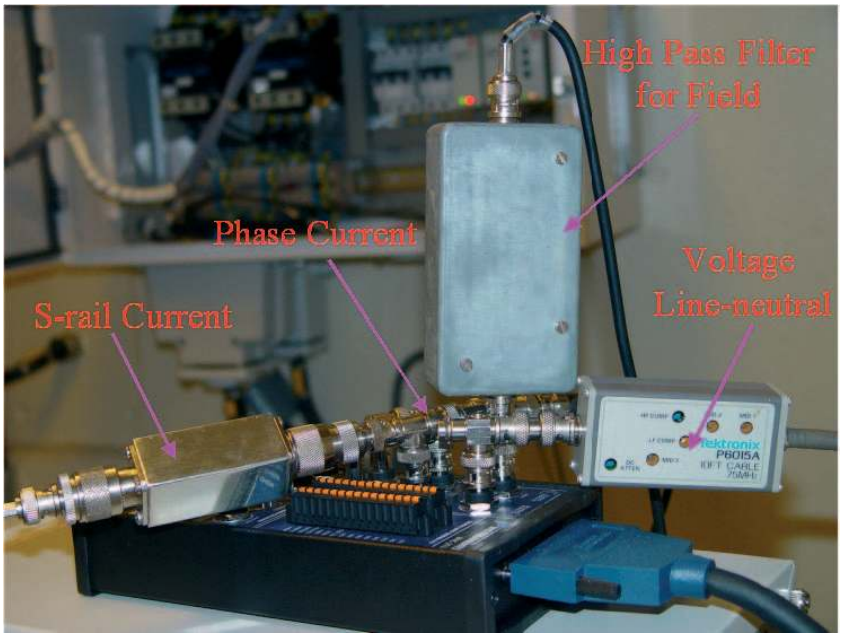

Figure 6.4: Terminations at the DAQ system

antenna was close to the track, about $10m$ away, and it was observed that the antenna was picking up the fields corresponding to $16\frac{2}{3}Hz$ and its associated harmonics. To get rid of those electric fields due to traction currents from the measurements, a high-pass filter (shown in Fig. 6.4) that has a lower cut off frequency of $20kHz$ was connected at the channel - 0 in the DAQ system. The transient voltage and current were measured at the Banverket local power supply as shown in Fig. 6.5. For the transient voltage measurement on channel - 1, a Tektronix voltage probe $P6015A$ that has a ratio of $1kV/1V$ was placed between the phase and neutral as shown in Fig. 6.5. For the transient current measurements in the phase, a Fischer current probe $F-33-1,SN403$ with ratio of $1A/5V$ was used, as shown in Fig. 6.5, with a series attenuator and 50Ω termination. All the equipment and the neutral of the three-phase system were grounded to a common grounding bar inside the technical house, which is further connected to the S-rail as shown in Fig. 6.6 and Fig. 6.2. It is possible that during a lightning event there will be a potential rise in the S-rail, because of which the grounding bar and the S-rail experience a potential difference. Hence there will be a current flow from the grounding bar to the S-rail or vice versa. It was decided to measure this current to clarify whether such a potential difference exists or not. The Fischer current probe $F-16-1,SN57$ with ratio of $2A/1V$ was used for the earth current measurements.

The DAQ card from National Instruments was programmed with Lab-View

software for operating it in continuous mode as explained by *Blomqvist et al* in [100]. It was programmed in such a way that once the system is triggered a binary data file will be created. The name of the data file would be of the form $day-month-year-hour-minute-second.millisecond$. The DAQ system was triggered by electric field (channel - 0) at $0.5V$. Each file contains one million samples at a sampling interval of $0.2\mu s$, giving the total time length of each record as $200ms$, the pretrigger delay was $20ms$. The antenna with the filter was not calibrated and hence the values of the fields that would be shown later correspond to arbitrary units. The measuring system was installed in Tierp on May 22, 2003 and operated until September 03, 2003. Even though the aim of the measurements was to record the transients caused by lightning, it was found that the system has recorded several transients apparently not caused by lightning, but caused by other events related to train movements. These events may be switching operations, arcing at pantograph, etc. Such data were ignored after confirming and correlating the data with Swedish lightning location system/network (LLP) system and the train timetables. Attempts were made to change the trigger settings on other channels too, i.e. on voltage and currents. Under such circumstances the number of data collected was either too large or too small and most of the data obtained could not be correlated with lightning. Hence only the cases where the trigger was kept on electric field (channel - 0) are considered.

6.2 Lightning induced events recorded by the measurement system ¶

The data from LLP for the year 2003 indicates that within a radius of $50km$ around the measurement station 7757 strokes were recorded. The measurement system has recorded in total of 4885 data files, and from which 174 data files had exact/perfect time correlation with the location network corresponding to the lightning events. Majority of the lightning activity took place on the 30^{th} and 31^{st} of July and the correlation of the collected data with that of lightning location system was above 99% accuracy. Almost all the data had one to one correspondence with the lightning events recorded in the lightning location system. Interesting discussions on the shapes of the induced voltage/current waveforms and its relation to stroke location can be found in *Theethayi et al.* [98, 99 **Paper-G**]. To explain the induced phenomena an example of a flash (FLASH - 30) that occurred on 30^{th} July is considered.

The position of the strokes associated with FLASH - 30 is shown in Fig. 6.7, a map that also indicates the measurement station location. Below Fig. 6.7 one can see a table that indicates date, time, location and amplitude of each of the strokes. There are four strokes corresponding to FLASH - 30.

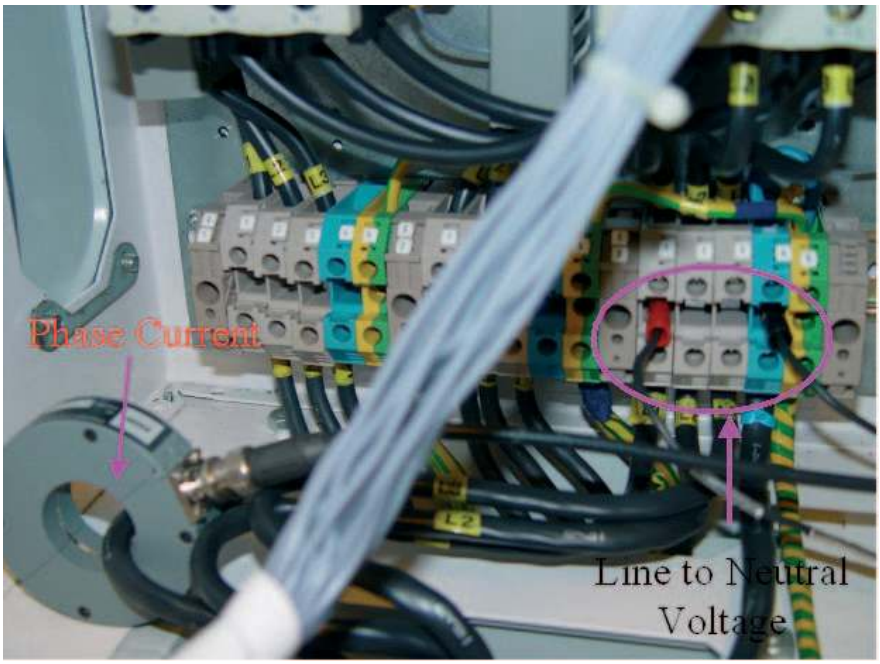

Figure 6.5: Line to neutral voltage and line current measurement point

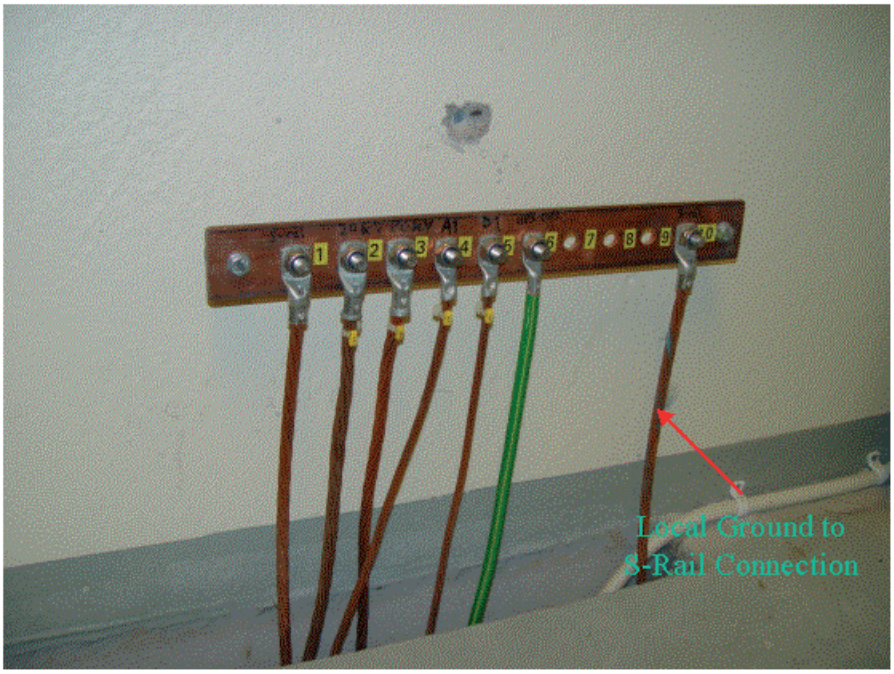

Figure 6.6: Local ground to S-rail connection

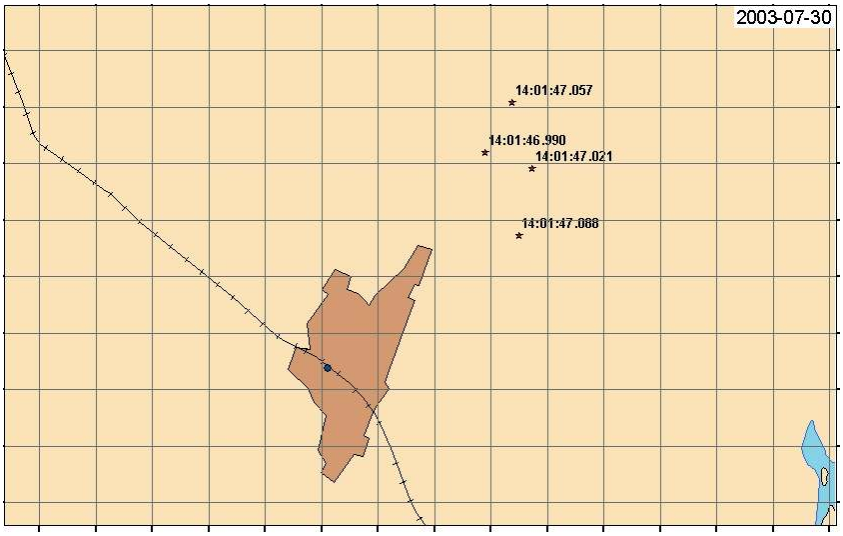

FID	Shape	DAG	TID	LAT	LON	AMP	Actual current
191857	Point	20030730	14:01:46.990	60,3803	17,5627	-170,4	-31,5
191858	Point	20030730	14:01:47.021	60,3775	17,5776	-104,5	-19,3
191859	Point	20030730	14:01:47.057	60,3881	17,5718	-57	-10,5
191860	Point	20030730	14:01:47.088	60,367	17,5726	-57,3	-10,6

Figure 6.7: Location of the strokes corresponding to FLASH - 30 (each square has a size of 1sq.km) as per the Swedish lightning location network

Each square in the map corresponds to $1Sq.km$. This flash occurred on 30^{th} of July at $14:01(GMT)$ i.e. at $16:01 local time$. All the strokes in FLASH - 30 were within a distance of $4.13km$ (nearest stroke) and $5.73km$ (farthest stroke).

Fig. 6.8 shows the corresponding electric field and Fig. 6.9 shows the corresponding phase to neutral voltage and local ground to S-rail current wave shapes respectively. The waveform corresponding to the phase currents are not shown as its signal was close to the noise floor. The electric field begins with a preliminary cloud discharge followed by all the four strokes. The duration of preliminary discharge is $11.3ms$. The preliminary discharge perhaps owing to its low magnitude is not reflected prominently [101] either in the phase to neutral voltage or the local ground to S-rail currents. One can see that for each stroke there is a corresponding induced phenomenon (compare each peak of phase to neutral voltage and local ground to S-rail current of Fig. 6.9 to corresponding electric field peaks in Fig. 6.8). It seems that the first stroke caused a larger induced voltage and a corresponding larger local ground to S-rail current. This could be due to large magnitude of associated stroke current. It can be seen from the table below the map (see last two columns in Fig. 6.7 for sign and magnitude) that the first stroke had amplitude of $31.5kA$, the second $19.3kA$ and the other two were about $10.5kA$. The first stroke caused an induced phase voltage of $5.3kV$ peak to peak and earth current of $7.6A$ peak to

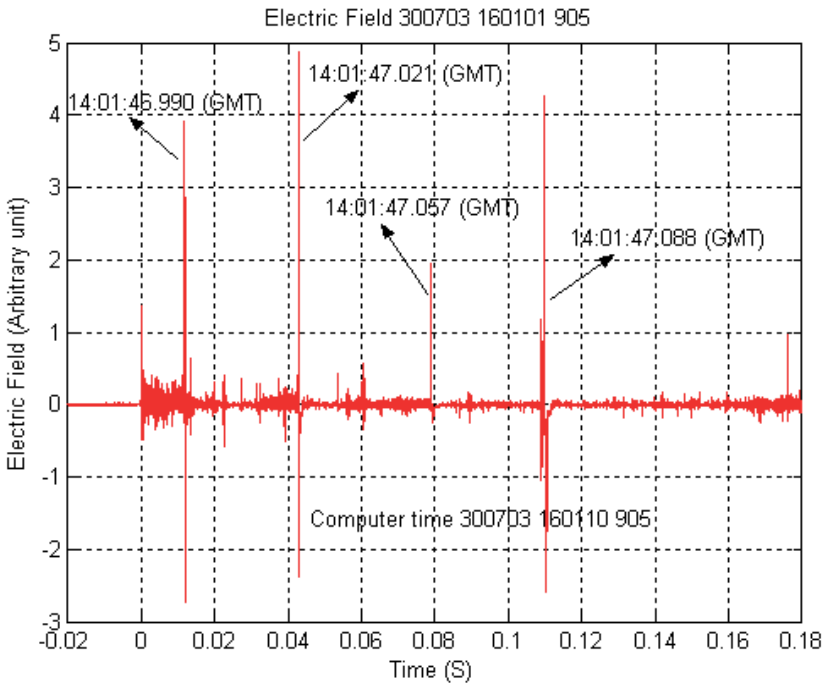

Figure 6.8: Electric field waveform due to FLASH - 30 (magnitude in arbitrary units)

peak. The induced phenomena corresponding to the other subsequent strokes are lesser than the first. But this does not affirm that the subsequent strokes are of lesser amplitudes, there are instances and data that show subsequent stroke amplitudes higher than the first. It can be also seen that the time difference between each stroke occurrences has perfect correlation with the lightning location system data as shown in table below the map in Fig. 6.7, even though lightning location system is based on GMT time and measuring system based on local computer time.

The computer time was corrected to the GMT time every week when the data from the computer was collected thus making the hard disk free for new data storage. Every week it was observed that the computer had drifted by several seconds from the GMT time. In order to make the analysis as accurate as possible, the following technique was adopted to account for this time drift. This was necessary to accurately identify which flash or strokes had caused the induced phenomenon. The time difference between the Swedish local time and the GMT time is exactly two hours. Due to this, it was made sure that all the times recorded by the computer and that of lightning location system should have a difference of perfect $1 : 59 : 14 : 866 hours$.

To obtain this, first it was observed that the measuring computer did not record any data before the time $05 : 59 : 11 : 375$ (local time) corresponding

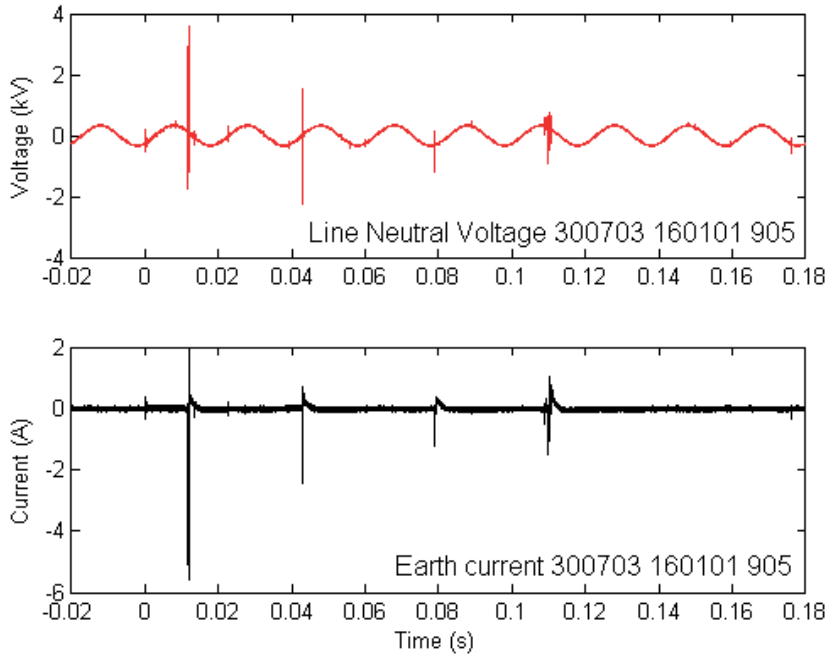

Figure 6.9: Line to neutral voltage and local ground to S-rail current waveforms for FLASH - 30

to, say, a flash referred to as FLASH - 30 - 1 and also there was no data recorded after the time 17 : 39 : 29 : 186 (local time) corresponding to FLASH - 30 - 2 on the 30^{th} of July 2003. The time difference between the above two flashes is 11 : 39 : 31.675*hours*. The FLASH - 30 - 1 had all the strokes comparable with the lightning location system. Further, the time interval between the strokes for this flash were also comparable. The calculated time difference between the lightning location system and the measuring computer recordings for FLASH - 30 - 1 as 01 : 59 : 13 : 764*hours*. Similarly, for FLASH - 30 - 2, the difference between the lightning location system time and the measuring computer time was 01 : 59 : 15 : 103*hours*. Time lag between the FLASH - 30 - 1 and FLASH - 30 - 2 is about 1.339*seconds*, which gives us a drift of about $0.11494 seconds/hour$. This drift was identified for each data and corrected to correlate with the lightning location system. It has hence enabled us to identify to a greater accuracy as to which stroke has caused the induced voltage. From this a formula could be derived for the peak to peak induced line to neutral voltage in terms of stroke current and stroke locations, which is approximately given by (6.1). In deriving (6.1) peak to peak voltages of all the data corresponding to 30^{th} July were considered and the formula was derived using curve fitting and some trial/error methods. The approximate formula

that relates the induced line to neutral voltage (peak to peak) as a function of stroke current in kiloAmps and stroke location in kilometer is given by (6.1) [99 **Paper-G**].

$$V_{Line-Neutral} = \frac{0.288 \cdot I_{stroke-kA}}{D_{stroke-km}} \tag{6.1}$$

It was confirmed that there were no direct strikes in the auxiliary power lines in the radius of $50km$ around the station.

6.3 Conclusions

In these measurements it is seen how an indirect lightning strike causes induced activity inside a normally operating railway technical house in Sweden. It was seen that peak to peak voltages up to $6-7kV$ could appear at the secondary terminals of the three-phase transformer, a value that could depend upon the position and amplitude of the strokes. The voltages measured at the secondary of the transformer were found to be oscillatory, which is a common feature of the surges transferred through a transformer [102]. It was also seen that the induced voltages would have its first peak depending on the direction/position of the stroke. A stroke in the northern side of the tracks caused induced voltages and local ground to S-rail currents that have same polarity as that of the field. But for the strokes located in the southern side of the tracks had induced voltages and local ground to S-rail currents opposite to that of the field. The polarity of the field, however, depends on the polarity of the stroke current. It is seen in this Chapter that the tracks had different potentials during lightning activity because of which currents could enter or leave from technical house through buried wires and there are cases when telecommunication cables are affected in the event of lightning strikes as discussed in Chapter-1. To know how buried systems react to lightning transients, in the next Chapter let's study pulse propagation in buried wires.

7. Current Pulse Propagation in Underground Wires - A transmission line analysis ¶

Wave propagation in underground systems has been a subject of interest for many engineers. This is also true with our research partners like Banverket, Bombardier Transportation and FMV (Swedish material administration). In addition to the lightning interaction problems as discussed earlier with the Swedish railway systems, one could have lightning interaction with buried conductor systems in the power and communication systems. Every high voltage power transmission tower has a long running counterpoise wire [103] in the ground connected to the foot of the tower. The main purpose is to divert the stroke to tower directly to the counterpoise wire. How does the stroke diverted to the counterpoise wire propagate? This is particularly important when the potential at the tower top or at the footing is of interest [104, 105]. Moreover, in the substation, there are complex grounding systems, which include counterpoise wires, buried rods and buried grids/meshes. How to analyze those grounding systems (if at all transmission line models are applicable with reference to the present study) in the event lightning stroke currents are diverted to them? To get a broader insight into the problem, let's take an example of a communication system. Lightning strike to communication towers is a usual phenomenon [106, 107]. A schematic diagram showing most of buried conductor systems connected with the communication tower is shown in Fig. 7.1 [107, 108, 109 **Paper-K**].

In Fig. 7.1, the tower foundation and building foundation are connected to their respective ring conductors. The ring conductors are provided primarily to minimize the danger of step voltage [105]. Besides, the ring conductor relieves the electrical stress at the tower foundation reducing chances of damage to the foundation. The earth conductor between the tower and building ring conductors prevents ground surface arcs between tower and building and reduce lightning currents carried by cable shields by sharing part of it. The follow on earth conductor takes part of the lightning current away from the service cables. The radial conductors around the tower are for reducing the percentage of lightning current dispatched to the building via the tower cables and earth conductors. The radial conductors are beneficial only if it can substantially reduce the lightning currents dispatched to the building, espe-

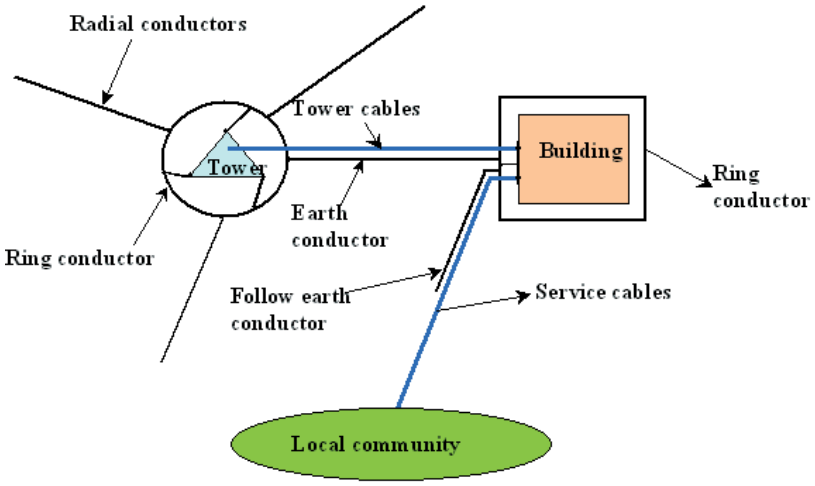

Figure 7.1: Schematic diagram of grounding conductors considering the tower and building as separate units (not to scale)

cially if the distance between the tower and building is long. The length and design of the radial conductors are to be governed by economy and its efficiency in dissipating lightning currents into the bulk earth. How to design a suitable lightning protection for the above system if one doesn't a priori know the possible realistic current or voltage distribution in the conductor systems of the ground? Even in the Swedish railway systems communication cables do get damaged in the event of lightning strikes: why? In an effort to find answers to the above questions, the author found it's obligatory to investigate into the interesting subject of wave propagation in underground wires. Interesting discussions about pulse propagation characteristics can be found in *Theethayi and Thottappillil* [110 - 112 **Paper-H, I, J**]. Some important observations/conclusions of the paper are presented here.

7.1 Telegrapher's equations for the buried wires with earth as return

Underground wires can be either bare (counterpoise - representative of grounding conductors) or insulated (representative of cable shields or unshielded cables). Hence one has two different systems for study as shown in Fig. 7.2. In addition to ground conductivity and ground permittivity, there is also insulation permittivity for the insulated cables [110 - 112 **Paper-H, I, J**]. The corresponding per unit length transmission line representation of the above system is shown in Fig. 7.3 [110 - 112 **Paper-H, I, J**]. In Fig. 7.3, V and I are the voltage and currents respectively. Z_{gb} and Y_{gb} are the ground

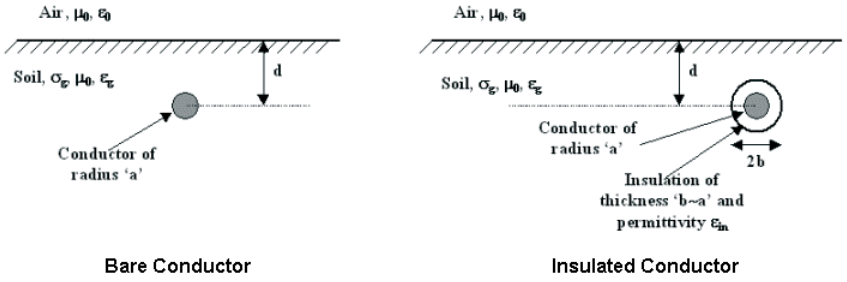

Figure 7.2: Bare and insulated conductor system in the soil under study

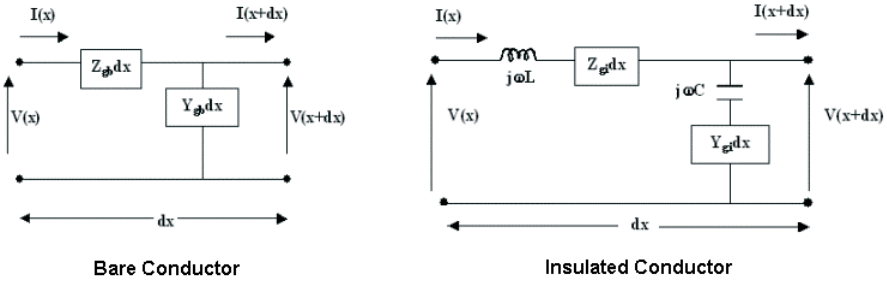

Figure 7.3: Per unit length transmission line representation for bare and insulated conductor system in the soil under study

impedance and ground admittance of the bare wire respectively and they are dependant on the radius of the wire and the depth. Z_{gi} and Y_{gi} are the ground impedance and admittance of the insulated wire with total radius of the wire (including insulation). L and C are the insulation inductance and capacitance respectively. In this Chapter let's discuss more about the ground impedance and ground admittance for buried wires. Some authors refer ground impedance and admittance as soil impedance and admittance [42, 113].

Next let's discuss various expressions for the ground impedance applicable up to lightning frequencies i.e. up to a few MHz. Beyond those frequencies, the transmission line approximation is questionable [42, 110 - 112 **Paper-H, I, J**, 113], which will be discussed later. Based on the above per-unit length transmission line representation, the governing telegrapher's equations for bare wires are,

$$\frac{dV(x,j\omega)}{dx} = -Z_{gb} \cdot I(x,j\omega) \tag{7.1a}$$

$$\frac{dI(x,j\omega)}{dx} = -Y_{gb} \cdot V(x,j\omega) \tag{7.1b}$$

Note that equation (7.1) is applicable only for pulse propagation studies with concentrated sources. For electromagnetic field interaction studies additional distributed source terms will be involved as discussed in Chapter-5 for the case of wires above the ground.

For insulated wires the voltage and current wave equations are given by (7.2a and b). The current wave equation for insulated wires in (7.2b) can be written in a convenient form as in (7.2c,d) so that the total shunt element, i.e., series combination of insulation capacitance $j\omega \cdot C$ and Y_{gi} as in Fig. 7.3, can be transformed to a parallel combination of insulation capacitance and modified/adjusted ground admittance, i.e., $j\omega \cdot C || Y_{gi}^{P}$. This seems to be more consistent in the sense that there is a similarity between the voltage and current wave equations for insulated cables and many researchers like [114] adopt such a representation. The per unit length insulation inductance and capacitance is calculated using (7.3) [42, 63, 113]. Let's next discuss what are the relevant expressions for the ground impedance for the transmission line analysis of the underground wires. For insulated wire

$$\frac{dV(x,j\omega)}{dx} = -(j\omega \cdot L + Z_{gi}) \cdot I(x,j\omega) \tag{7.2a}$$

$$\frac{dI(x,j\omega)}{dx} = -\frac{C \cdot Y_{gi}}{j\omega \cdot C + Y_{gi}} \cdot V(x,j\omega) \tag{7.2b}$$

$$\frac{dI(x,j\omega)}{dx} = -\left(j\omega \cdot C + Y_{gi}^{P}\right) \cdot V(x,j\omega) \tag{7.2c}$$

$$Y_{gi}^{P} = -\frac{(j\omega \cdot C)^2}{j\omega \cdot C + Y_{gi}} \tag{7.2d}$$

$$L = \frac{\mu_0}{2\pi} \cdot \ln\left(\frac{b}{a}\right) \tag{7.3a}$$

$$C = \frac{2\pi \cdot \varepsilon_{in}}{\ln\left(\frac{b}{a}\right)} \tag{7.3b}$$

7.2 Ground impedance and admittance for buried wires

Let us assume in the analysis below, that the radius of the wire is R_{ab}. If the bare wire is in analysis then $R_{ab} = a$ else $R_{ab} = b$ and the depth of the wire is d. Several researchers have contributed to the development of ground impedance expression for buried wires. The ground impedance expression for

buried wires was developed first by *Pollaczek* [115, 116] in 1926, as shown in (7.4), which is a low frequency approximation in the sense that it can be used when frequency of incident pulse satisfies $\omega << \frac{\sigma_g}{\varepsilon_g}$. Because of the low frequency approximation one can see that (7.4) does not include the permittivity of the ground. All complexities associated with *Carson's* ground impedance for above ground wires as discussed in Chapter-4, are also applicable to *Pollaczek's* ground impedance expression for buried wires. *Saad et al.* [117] have analytically proved that an excellent approximation for (7.4) is given by (7.5). Observe that if the infinite integral e.g. in equation (7.4) is eliminated, then those expressions without infinite integrals are referred to as closed form solutions e.g. (7.5). *Wedephol and Wilcox* [51], *Ametani* [118] and *Semlyen* [119] have proposed their own closed form ground impedance expressions and *Saad et al.* in [117] have shown that those expression are almost identical to (7.5), hence they are not discussed here.

$$\begin{aligned} Z_{gbbi}^{Pollaczek} &= \frac{j\omega\cdot\mu_0}{2\pi}\Bigg(K_0\big(R_{ab}\sqrt{j\omega\cdot\mu_0\cdot\sigma_g}\big) \\ &\quad -K_0\Big(\sqrt{j\omega\cdot\mu_0\cdot\sigma_g(R_{ab}^2+4d^2)}\Big) \\ &\quad +\int_{-\infty}^{+\infty}\frac{e^{-2d\sqrt{u^2+j\omega\cdot\mu_0\cdot\sigma_g}}}{|u|+\sqrt{u^2+j\omega\cdot\mu_0\cdot\sigma_g}}\cdot e^{ju\cdot R_{ab}}du\Bigg) \end{aligned} \tag{7.4}$$

$$Z_{gbbi}^{Saadet.al} = \frac{j\omega\cdot\mu_0}{2\pi}\left(K_0\big(R_{ab}\sqrt{j\omega\cdot\mu_0\cdot\sigma_g}\big)+\frac{2\cdot e^{-2d\sqrt{j\omega\cdot\mu_0\cdot\sigma_g}}}{4+R_{ab}^2\cdot j\omega\cdot\mu_0\cdot\sigma_g}\right) \tag{7.5}$$

For a wide range of frequencies so long as the transmission line approximation is valid, *Sunde* [58] has derived the ground impedance expression as given by (7.6). It is similar to that of (7.4), but the only difference is that full propagation constants of the soil was used in (7.6) instead of its corresponding low frequency approximation in (7.4) or (7.5).

$$\begin{aligned} Z_{gbbi}^{Sunde} &= \frac{j\omega\cdot\mu_0}{2\pi}\Bigg(K_0(R_{ab}\cdot\gamma_g)-K_0(\gamma_g\sqrt{R_{ab}^2+4d^2}) \\ &\quad +2\cdot\int_0^{\infty}\frac{e^{-2d\sqrt{u^2+\gamma_g^2}}}{u+\sqrt{u^2+\gamma_g^2}}\cdot\cos(u\cdot R_{ab})\cdot du\Bigg) \end{aligned} \tag{7.6}$$

The integral term in (7.6) converges slowly leading to longer computation times and possible truncation errors as the frequency is increased. Further, it was found that the first two *Bessel* terms in (7.6) are oscillatory when frequency is high. However, one can say *Sunde's* expression for ground impedance is more valid in the sense that it uses the full expressions for propa-

gation constant. Recently, *Bridges* [113], *Chen* [120] and *Wait* [121] have independently proposed more complex ground impedance expressions derived from rigorous electromagnetic theory and in [113] and [120] closed form logarithmic approximations for transmission line solution have been proposed. The author found that even those expressions, though simple, are oscillatory at high frequency hence not discussed here.

Bridges [113] mentions that his complete expression for ground impedance has two modes, namely transmission line modes and radiation/and surface wave modes. Moreover, the solution of his ground impedance expressions is based on complex integration theory and adds that pole term in his expression corresponds to transmission line mode and the branch cut corresponds to radiation/and surface wave modes [113]. Thus, under the transmission line modes as discussed by *Theethayi and Thottappillil* in [110 - 112 **Paper-H, I, J**], it can be shown that *Bridges's* expression is identical to *Sunde's* expression. Further, *Wait* [121] proposed a quasi-static approximation (under transmission line modes) of his complete ground impedance expression as given by (7.7). *Theethayi and Thottappillil* [110 - 112 **Paper-H, I, J**] have shown that even (7.7) is identical to (7.6). Can some simplified expressions, that do not involve *Bessel's* functions be obtained?

$$Z_{gbbi}^{Wait} = \frac{j\omega\cdot\mu_0}{2\pi}(1+\Theta)\cdot\ln\left(\frac{-j\cdot 1.12}{R_{ab}\sqrt{\varepsilon_g\cdot\mu_0\cdot\omega^2 - j\omega\cdot\mu_0\cdot\sigma_g}}\right) \tag{7.7a}$$

$$\xi = 2\cdot j\sqrt{\varepsilon_g\cdot\mu_0\cdot\omega^2 - j\omega\cdot\mu_0\cdot\sigma_g}\cdot d \tag{7.7b}$$

$$\Theta = \frac{K_0(\xi) + \frac{2}{\xi}\cdot K_1(\xi) - \frac{2}{\xi^2}\cdot(1+\xi)\cdot e^{-\xi}}{K_0\left(j\sqrt{\varepsilon_g\cdot\mu_0\cdot\omega^2 - j\omega\cdot\mu_0\cdot\sigma_g}\cdot R_{ab}\right)} \tag{7.7c}$$

Vance [63] proposed one of the simplest closed form approximations for (7.6) given (7.8), where *Henkel* functions are used instead of *Bessel's* functions.

$$Z_{gbbi}^{Vance} = \frac{\mu_0\cdot\omega}{2\pi\cdot R_{ab}\cdot\gamma_g}\cdot\frac{H_0^1\left(jR_{ab}\cdot\gamma_g\right)}{H_1^1\left(jR_{ab}\cdot\gamma_g\right)} \tag{7.8}$$

Recently, *Petrache* [114] has proposed a logarithmic approximation as shown in (7.9) for the ground impedance and also claims that it's the simplest expressions for the ground impedance that is available in the literature.

$$Z_{gbbi}^{Log} = \frac{j\omega\cdot\mu_0}{2\pi}\cdot\ln\left(\frac{1+\gamma_g\cdot R_{ab}}{\gamma_g\cdot R_{ab}}\right) \tag{7.9}$$

It can be seen in (7.8) and (7.9) that the depth of the wire is missing.

Models that neglect air-earth interface [63] are known as infinite earth models. *Wait* in [121] has shown that this condition exists if, $|2j \cdot d \cdot \sqrt{\varepsilon_g \cdot \mu_0 \cdot \omega^2 - j\omega \cdot \mu_0 \cdot \sigma_g} >> 1|$. From this condition, it was found that neglecting the wire depth might not be a good approximation for lightning frequencies. Moreover, it can be shown numerically that for any combination of ground material property, the logarithmic approximation and *Vance's* approximations for the ground impedance are identical, mathematical proof of which is beyond the scope of this thesis.

A modified formula is proposed to account for the depth term in expression (7.9) in the form of a correction term as shown in (7.10). (7.10) is called as the logarithmic-exponential formula. The significance of this correction formula will be discussed in following paragraphs and that this correction term was obtained after verifying many cases. Observe that in *Saad et al.* expression (7.5), second exponential term has the information about depth. By combining (7.9) and the depth term of (7.5) and after some sensitivity analyses the logarithmic-exponential formula (7.10) was obtained.

$$Z_{gbbi}^{Log-Exp} = \frac{j\omega \cdot \mu_0}{2\pi} \cdot \ln\left(\frac{1+\gamma_g \cdot R_{ab}}{\gamma_g \cdot R_{ab}}\right) + \frac{j\omega \cdot \mu_0}{2\pi} \cdot \frac{2e^{-2d\cdot|\gamma_g|}}{4+R_{ab}^2 \cdot \gamma_g^2} \tag{7.10}$$

Theethayi and Thottappillil [110 - 112 **Paper-H, I, J**] have compared all the above expressions and some observations are presented here. Fig. 7.4a and Fig. 7.4b show the comparison of various ground impedance expressions, and the deviations between expressions can be seen clearly both in amplitude and argument responses. The example is a wire of radius $2cm$ at a depth of $0.5m$. The radius of $2cm$ was selected with future applications of the theory of cable shields, which will be dealt in the next Chapter. The consequence of missing depth term in logarithmic expression is reflected in the amplitude and the consequence of low frequency approximation is reflected in argument response. It can be seen that logarithmic-exponential approximation is in good agreement with *Sunde's* or *Wait's* expression. It can be also shown that as $\omega \rightarrow \infty$ then $Z_{gbbi}^{Log-Exp} \rightarrow \frac{1}{2\pi \cdot R_{ab}} \sqrt{\frac{\mu_0}{\varepsilon_g}}$ [110 **Paper-H**], which is particularly useful for the researchers who work with time domain solutions.

Vance [63] mentions that ground impedance and ground admittance are related to each other approximately by the propagation constant as in (7.11).

$$Y_{gbbi} = \frac{\gamma_g^2}{Z_g} \tag{7.11}$$

Fig. 7.5 shows both ground impedance and admittance amplitudes for the same wire geometry as before for the example shown in Fig. 7.4. It can be clearly seen from Fig. 7.5, that the ground admittance seems to be more dom-

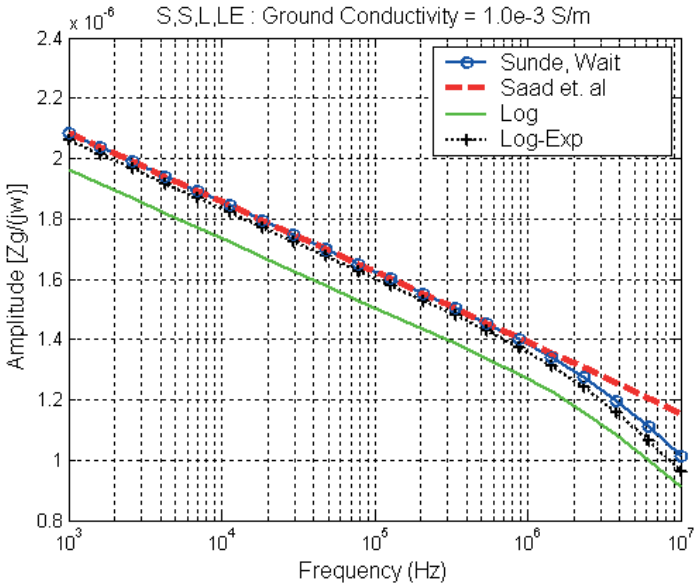

(a) Amplitude of $\frac{Z_g}{j\omega}$ with ground conductivity $1mS/m$

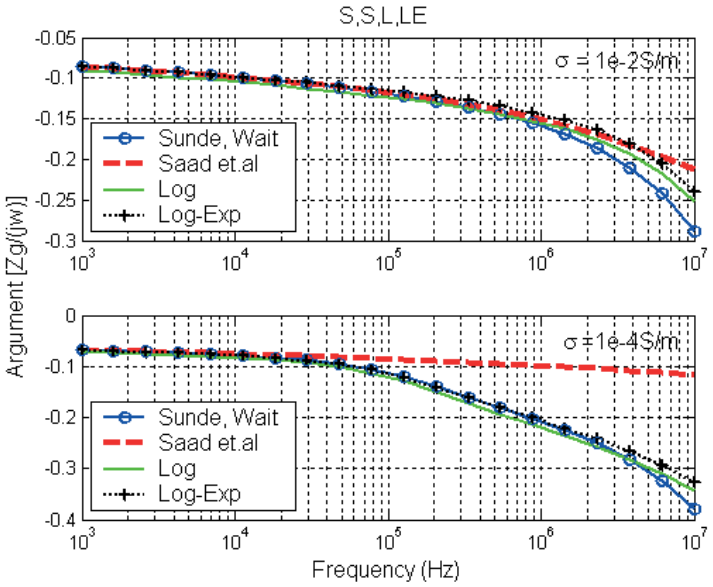

(b) Argument of $\frac{Z_g}{j\omega}$ with ground conductivity $10mS/m$ and $0.1mS/m$

Figure 7.4: Ground impedance comparisons between Sunde, Wait, Saad et al., Log and Log-Exp expressions: ground relative permittivity is 10 and wire buried at 0.5m depth

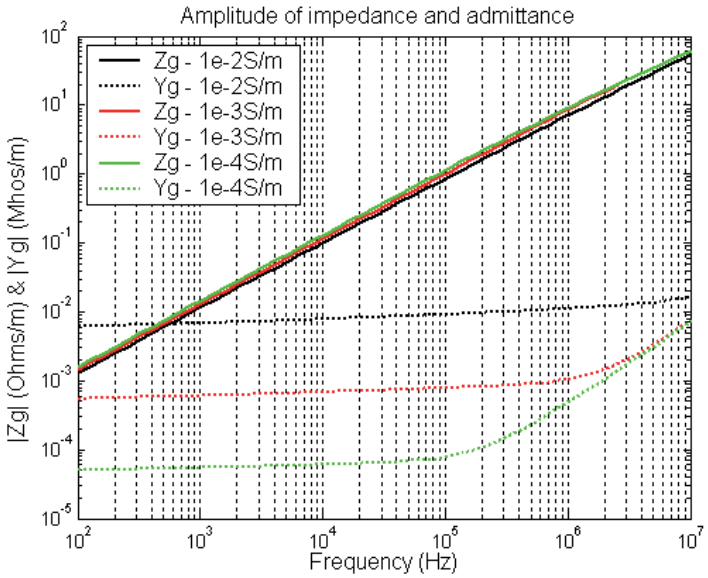

Figure 7.5: Ground impedance and admittance magnitude response for various ground conductivities for bare wire buried at 0.5m depth and ground relative permittivity is 10

inant than ground impedance as the former shows higher sensitivity to ground conductivity than the later. These observations are also applicable to the argument values.

Transient simulation packages like *EMTP* [121, 122] ignore ground admittance and uses low frequency approximation of ground impedance, i.e., it neglects ground permittivity for underground cables. For bare wires one cannot ignore ground admittance. Perhaps that's why there aren't any models for counterpoises etc. unlike line and cable models in *EMTP* [121, 122]. Let's take an example and demonstrate the consequence of neglecting the ground admittance for cables. Let's consider two cases. $Case-1$ is with ground admittance and $Case-2$ without ground admittance i.e. $Y_{gi} \rightarrow \infty$ for the system in Fig. 7.5. Mathematically the propagation constants for $Case-1$ and $Case-2$ are represented by (7.12) and (7.13) respectively in *Laplace* domian. Consider a double exponential current source $I(t) = k_0(e^{-at} - e^{-bt})$ that has a peak value of 1A. The exponential parameters are $a = 1 \times 10^4 s^{-1}$ and $b = 4 \times 10^5 s^{-1}$. This pulse has a rise time of $10\mu s$. Let us inject this pulse at one of the ends of an insulated cable $1km$ long, buried at a depth of $0.5m$, having a radius of $2cm$ and $2mm$ thickness of insulation and cable. The ground conductivity is $1mS/m$ and the ground relative permittivity is 10 and the insulation relative permittivity is either 2 or 5. Fig. 7.6 shows current responses at $0m$, $150m$ and $300m$ from the point of injection respectively. Simulations were carried out

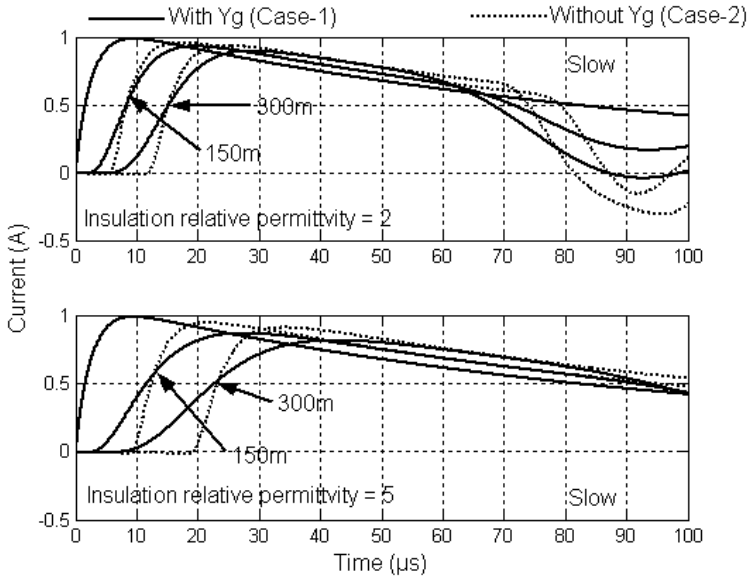

Figure 7.6: Simulations demonstrating the importance of ground admittance in pulse propagations with ground conductivity 1mS/m and ground relative permittivity of 10

using the expression (3.46).

$$\gamma_1^{Case:1}(s) = \sqrt{\left(s \cdot L + Z_{gi}\right) \cdot \left(\frac{s \cdot C \cdot Y_{gi}}{s \cdot C + Y_{gi}}\right)} \tag{7.12}$$

$$\gamma_2^{Case:2}(s) = \sqrt{\left(s \cdot L + Z_{gi}\right) \cdot s \cdot C} \tag{7.13}$$

It is seen that neglecting the ground admittance for underground cables can predict incorrect attenuation and velocity of propagation. Using (7.12) and (7.13), it can be shown that the velocity and attenuation are never the same for either of the cases, i.e. if $\gamma_{1,2} = \alpha_{1,2} + j\beta_{1,2}$ and $v_{1,2} = \frac{\omega}{\beta_{1,2}}$ then, $\frac{\alpha_1}{\alpha_2} \neq 1$ and $\frac{v_1}{v_2} \neq 1$. Interestingly the ratios for attenuation and velocity for $Case-1$ and $Case-2$ are approximately equal to unity below a frequency of $0.1kHz$ and $1kHz$ respectively for the assumed ground conductivity of $1mS/m$ and ground relative permittivity of 10. Which means that ground admittance is indeed essential for lightning transient studies for underground cables.

7.3 Limits of transmission line approximation

All the discussions until now are the analysis based on the transmission line theory. A critical reader may wonder as to what is the limit of transmission line

approximation for any system. In the case of above ground wires with ground as return, this limit has been well discussed in [42]. The critical frequency for the soil is discussed in Chapter-4, where the possible limit of low frequency approximation was also discussed. For transmission line type analysis to be valid for overhead conductors it is necessary to put a restriction on the height of the conductor such that $\frac{2\pi \cdot h}{\lambda_{apulse}} << 1$ is satisfied [42], where λ_{apulse} is the wavelength corresponding to the input pulse in air and h is the height of the conductor above the ground. As the frequency increases, the wavelength decreases and there would be an instant when the wavelength is comparable to the height of the conductor. Also note that the above wavelength is calculated based on the speed of light (maximum velocity in free space/air). That means if the wavelength is further decreased due to the increase in frequency; then the fundamental condition as discussed in Chapter-3, that **the distance between the wires' separation (current carrying wire and return wire/plane) should be much smaller than the wavelength** is violated based on the transmission line theory. This is mainly attributed to the fact that penetration depth (at which the return plane is located) as discussed in Chapter-4, attains an asymptotic value as frequency tends to infinity.

Now consider the case of underground wires, where the wires are buried at a depth of d meters. The penetration depth at which the currents return in the soil using (4.32a) are shown in Fig. 7.7a and Fig. 7.7b (solid lines) for ground relative permittivity of 10 and 40 respectively. It should be remembered that the discussion here is applicable for infinite earth model. So if one considers the infinite depth models then, the penetration depth is defined not from the surface of the ground but from the surface of the wire because of the axisymmetric nature of the problem, unlike overhead wires where the depth is measured from the surface of the ground.

For a wire located at a certain depth in the soil, the currents have a return path only in the soil, but at various depths calculated using (4.32) depending upon the frequency of the pulse propagating in the wire. Usually, simple underground wire type systems in the soil will not be at a depth more than one or two meters. The penetration depth attains asymptotic value when the frequency is sufficiently high, which is independent of frequency and is only dependant on the material properties of the soil (4.32). Further, the maximum velocity of the waves propagating in the soil is determined by its permittivity [63], i.e., $v_{gmax} = \frac{3\times10^8}{\sqrt{\varepsilon_{rg}}}$. The velocity of the wave propagating in the soil is a function of frequency as given by (7.14) and the wavelength in the soil at any frequency is given by, $\lambda_{gpulse} = \frac{2\pi v_g}{\omega}$.

$$v_g = \frac{1}{\sqrt{\frac{\varepsilon_g \cdot \mu_0}{2} \cdot \left(\sqrt{1 + \frac{\sigma_g^2}{\omega^2 \cdot \varepsilon_g^2}} + 1\right)}} \tag{7.14}$$

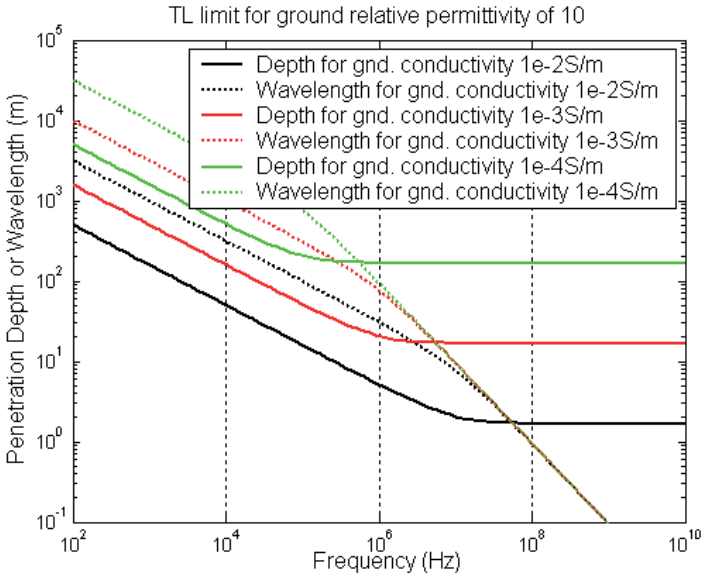

(a) Ground relative permittivity = 10

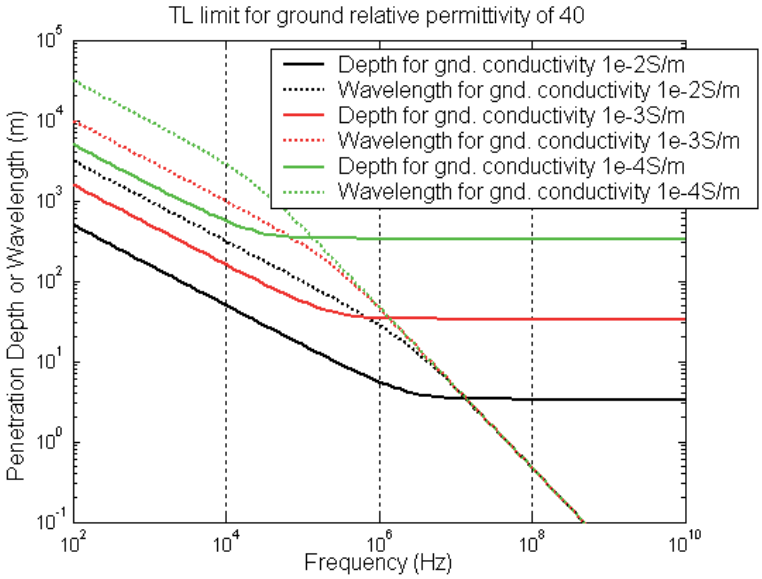

(b) Ground relative permittivity = 40

Figure 7.7: Penetration depth at which the currents return in the soil for underground wires and wavelength in the soil for ground relative permittivity of 10 and 40 for various ground conductivities

Similar to overhead wires for underground wires, one can impose a condition that the currents should return at a plane measured from the surface of the wire in the soil at depths smaller than the wavelength in soil, i.e., $\lambda_{gpulse} \geq \delta_g$. The condition $\geq$ is used instead of $>>$, because most of the return current is in the soil and the air earth interface is neglected due to the infinite earth model. Fig. 7.7a and Fig. 7.7b shows the cross-over points where the penetration depth (solid lines) equals the wavelength (dashed lines) in soil for ground relative permittivity of 10 and 40, respectively. Mathematically this limit (derived by the author) occurs at a frequency approximately given by (7.15).

$$f_{TL-limit} = \frac{\mu_0 \cdot \sigma_g \cdot \pi \cdot \left(3 \times 10^8\right)^2}{\sqrt{\varepsilon_{rg} \cdot \left[\varepsilon_{rg} + \mu_0 \cdot \varepsilon_g \cdot (2\pi \cdot 3 \times 10^8)^2\right]}} \tag{7.15}$$

While dealing with poor ground conductivity in conjunction with high soil permittivity, the currents return at depths much below the actual depth or location (return path is like a circular cylinder around the wire, with the wire as the axis) of the sourced wire. Under such circumstances, one can confidently say that transmission line model is very much questionable as the distance between the wire and its virtual return path in the soil is greater than the wavelength. In the present case, such a situation happens at about $200kHz$ as shown in Fig. 7.7b for a ground conductivity of $0.1mS/m$ and ground relative permittivity of 40. That is for this situation beyond a frequency of about $200kHz$ the transmission line approximation is questionable. When the ground conductivity is higher in conjunction with lower ground permittivity, the penetration depth is decreased and currents tend to crowd closer to the actual location of the underground wire, because of which the transmission line approximation becomes more valid. For a ground conductivity of $10mS/m$ and ground relative permittivity of 10 the limit is between $50-70MHz$ as shown in Fig. 7.7a. Hence, beyond the crossover points between the penetration depth and wavelength one can suspect the validity of transmission line approximation. For the case of lightning the author feels that the all the analysis is approximately within the limits of transmission line approximation. But it should be remembered that a pulse of certain frequency in air with wavelength corresponding to speed of light, would experience lesser wavelength in soil associated with slower speeds.

7.4 Validation of the proposed transmission line model

It is now necessary to justify whether the ground impedance model proposed in this Chapter, based on transmission line approximation, is comparable with other more accurate models. Even though the developed ground impedance and admittance expressions are for infinite bare/insulated wires, let us see if it can be extended to conductors of shorter length, i.e., whether it can predict reasonable voltage/current distribution at various points of finite length wires. To validate the present transmission line model, the best would be to simulate the horizontal wire type grounding conductors and compare it with other more accurate and approximate models in literature [123 - 125]. For this, some examples in the literature, which were simulated based electromagnetic field approach [123] for buried horizontal grounding wires of finite length, were compared.

It has been discussed widely by *Dawalibi* [126], *Grcev* [124] and *Visacro* [123], that for transient analysis of grounding systems, the electromagnetic models are more accurate, because of the very reason that the electromagnetic models adopt solution of *Maxwell's* equation [123, 124, 126]. Further, those electromagnetic models have good agreement with experiments [124]. Note that the electromagnetic models, though accurate, are difficult to implement from a computational point of view. The aim of this comparison, however, is to demonstrate that a simple transmission line model as presented here is also capable of predicting results close to the ones predicted by electromagnetic models. However, there exists some scope to extend the proposed transmission line approach to more complex grounding systems for lightning transient studies in the future.

Some examples comparing the transmission line model developed in this Chapter, i.e., using (7.10) and (7.11) with that of electromagnetic models in the literature are presented below. The first example is $Verification-1$, where a horizontal bare wire of length either $20m$ or $100m$ as the case may be, having a radius of $7.5mm$, buried at a depth of $0.5m$ in a homogeneous soil having ground conductivity of $10mS/m$ and ground relative permittivity of 50. Current injected at one of the ends of this grounding wire was given by $I(t) = 12935 \cdot (e^{-190099t} - e^{-2922879t})$, all these parameters are similar to that in [123]. The voltage at the injection point, at the middle of the wire and opposite end of the injection is shown in Fig. 7.8, and the simulation results are comparable with the corresponding simulation results in Fig. 7.9 (taken from [123]). The differences are nominal. Further, the propagation delays of the voltages are very similar to the simulation results in [123].

Another important question for verification is: can the model for grounding wire also predict the so-called effective length [125, 127]? The effective

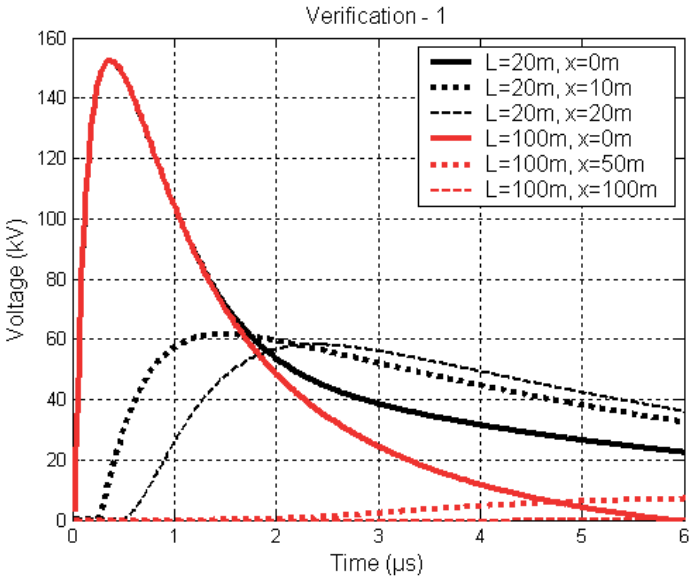

Figure 7.8: Verification - 1 simulated using the present transmission line model for buried bare wire

length of a single horizontal grounding wire is the length, above which the maximum transient voltage at injection point is length independent [127]. To investigate this let's perform $Verification-2$ and $Verification-3$, where the wire is buried at a depth of $0.75m$ and has a radius of $4mm$. The soil has ground conductivity of 1mS/m and ground relative permittivity of 4. In $Verification-2$ let's inject a current of wave shape $I(t)=(e^{-7924t}-e^{-400109t})$ [123], that has $10\mu s$ rise time and determine the transient voltage at injection point for various conductor lengths, in $Verification-3$ current of wave

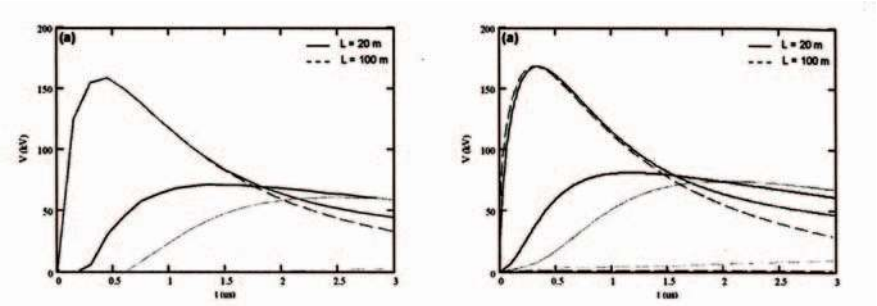

Figure 7.9: Verification - 1 simulated by the authors of [123] using complex electromagnetic field approach (left window) and complicated circuit approach (right window): figure is adapted from [123]

shape $I(t) = (e^{-27000t} - e^{-5600000t})$ [125], that has $0.36\mu s$ rise time was injected and an exercise similar to $Verification-2$ was carried out. In [125] a similar comparison was made using a complicated (in comparison with the one proposed here) non-uniform transmission line approach. The simulation results for $Verification-2$ and $Verification-3$ are shown in Fig. 7.10a and Fig. 7.10b, respectively. It can be seen that for faster rise times effective length is attained much earlier compared with that of slower rise times. This observation is also in line with the conclusions presented in [125, 127]. Hence it's clear that the present model is indeed capable of simulating buried wire of any length. It should be remembered that the present transmission line model is computationally very efficient and it's simpler to implement. While applying it on other complex grounding systems, it is important to investigate how to properly discritize the transmission lines and introduce the appropriate boundary conditions.

7.5 Ground impedance for wires on the surface of ground

Having known the expressions for ground impedance and admittance for wires above and below ground. It would be interesting to see what would be the expressions for the ground impedance for wires on the surface of the ground. This is needed because in the railway systems cables are some times laid on the ground beside the tracks or laid in cable trenches beside the tracks. Hence it is necessary to know the ground impedance expressions for wires on the ground. *Sunde* [58] has given the expression for ground impedance for the wires on the ground (7.16).

$$Z_{gsbi}^{Sunde} = \frac{j\omega \cdot \mu_0}{\pi \cdot \gamma_g^2 \cdot R_{ab}^2} \cdot [1 - \gamma_g \cdot R_{ab} \cdot K_1(\gamma_g \cdot R_{ab})] \tag{7.16}$$

Consider the Log-Exp expression (7.10), which is the ground impedance for wires below ground. If the depth term tends to zero, in this expression, one obtains the ground impedance expression for the wires on the surface of the ground and is given by (7.17).

$$Z_g^{Modified-log} = \frac{j\omega \cdot \mu_0}{2\pi} \cdot \ln\left(\frac{1+\gamma_g \cdot R_{ab}}{\gamma_g \cdot R_{ab}}\right) + \frac{j\omega \cdot \mu_0}{2\pi} \cdot \frac{2}{4+R_{ab}^2 \cdot \gamma_g^2} \tag{7.17}$$

What is interesting to note is that there isn't any exponential term in (7.17). It was seen that the logarithmic term corresponds to ground impedance of wires buried at infinite depth in the soil [63]. The second term in (7.17) modifies or corrects the infinite depth ground impedance model to obtain the ground

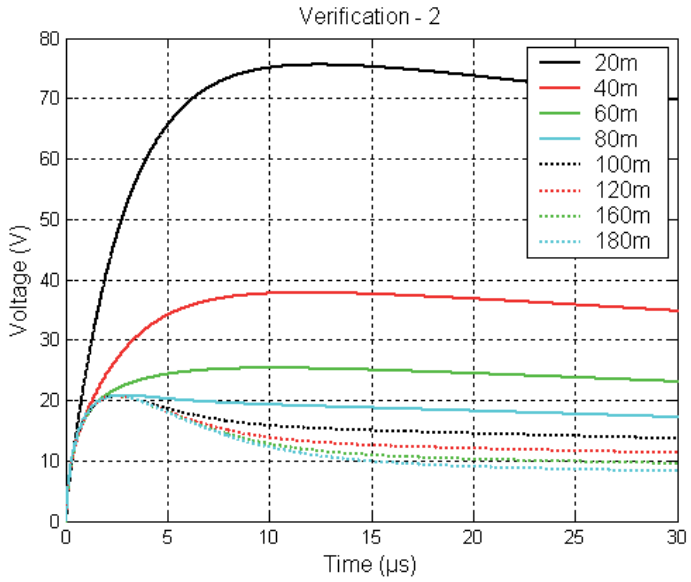

(a) Verification-2

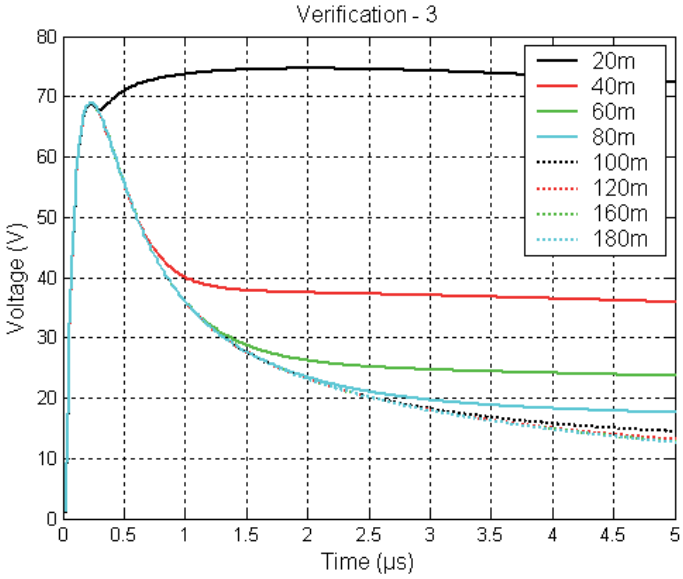

(b) Verification-3

Figure 7.10: Influence of current rise time on effective length Verification-2 and Verification-3

impedance expression for the wires on the surface of the earth. Therefore, the author refer's (7.17) as modified logarithmic formula. A comparison between the *Sunde's* more accurate formula (using *Bessel* function) and the modified logarithmic formula is demonstrated in Fig. 7.11. The example is a wire of radius $2cm$ and the ground conductivity is varied from $10mS/m$ to $0.1mS/m$ and the ground relative permittivity is 10. It is seen that (7.17) is a very good approximation for (7.16) and doesn't involve *Bessel* function.

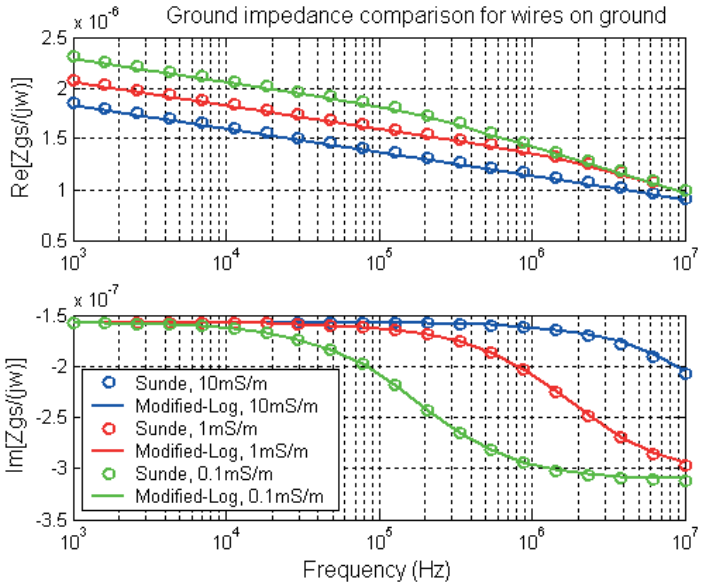

Figure 7.11: Comparison between Sunde (7.16) and Modified-logarithmic formula (7.17) for the ground impedance of the wires on the surface of the earth

It should be remembered that if there are many parallel wires, the mutual ground impedance expressions could be obtained by substituting in (7.17) the radius of the wire with horizontal distance between the wires. The same analogy is applicable with the wires below the ground for (7.10). The mutual ground impedance expressions between an overhead wire and buried wire can be derived from *Sunde's* method [58] but it involves infinite integrals as shown (7.18). In (7.18) d_{kl} is the horizontal distance between above ground and buried conductors. The height of the overhead wire is h and the wire depth is d. The author feels that simplified expression for (7.18) in terms of logarithms or exponentials should be derived to avoid infinite integrals. It is a subject for future study.

$$Z_{gabbi} = \frac{j\omega \cdot \mu_0}{2\pi} \cdot \int_0^{\infty} \frac{2 \cdot e^{-hu} \cdot e^{-d\sqrt{u^2+\gamma_g^2}}}{u+\sqrt{u^2+\gamma_g^2}} \cos(d_{kl} \cdot u) \cdot du \qquad (7.18)$$

7.6 Conclusions

A simple logarithmic-exponential approximation for the ground impedance of buried wires is proposed for frequencies up to $10MHz$, making it suitable for lightning current pulse propagation studies. The proposed expression is in good agreement with other valid/accurate expressions. It is shown that ground admittance cannot be neglected for buried insulated cables. It is seen that the proposed transmission line model based on simple logarithmic-exponential ground impedance expression can reasonably predict accurate current and voltage distributions along horizontal bare and insulated conductors in the ground. In addition, the model also predicts the effective length of horizontal grounding wires. An approximate formula for the frequency above which the transmission line approximation is questionable is proposed. A simple formula for the ground impedance of wires on the surface of the ground is proposed. The reason why one worries about proper current/voltage distribution on the insulated cable is that the coupling phenomena between cable shield and inner conductors/pairs of the cable depend mainly on the accuracy of current distribution on the cable shield as discussed in the next Chapter.

8. Coupling to cable core through cable shields ¶

In the previous Chapter it was shown how the current and voltage waves propagate in buried bare and insulated wires. In this Chapter it will be shown how the currents and voltages propagate in the internal conductors of shielded cables. For this one needs to know what characteristics of the shield influence the pulse propagation and which parameter of the shield contributes to the coupling phenomena between the shield and internal conductors. One could have multiple cable shields, some times the outer known as armor. Consider the typical telecommunication cable used by Banverket for their telecommunication and signaling applications as shown in Fig. 1.7. The outermost metallic tubular/cylindrical conductor is called the armor and the inner metallic tubular/cylindrical conductor is called the shield. EMC engineers interchange the words between armor and outermost shield. But power engineers' use the word armor widely for the outermost shield, perhaps for them armor serves as a mechanical protection for the cable as such. During thunderstorms Banverket has observed a breakdown between the shield and the inner conductors [15] of their communication cable as shown in Fig. 1.7. To investigate such a phenomena, one needs to first have a multi-conductor cable model. This Chapter discusses the associated transmission line parameters needed for the above said cable model.

To understand the coupling phenomenon between the tubular/cylindrical conductors and the internal conductors, let's start with the concept of transfer impedance [63] and later develop expressions for those phenomena in terms of what are known as tube impedances, first introduced by *Schelkunoff* [48] and later applied by *Wedepohl and Wilcox* [51]. The author has extended the analysis of single core cables proposed by *Wedepohl and Wilcox* [51] to multi core cables, for transient analysis of cables with complex internal conductor system. Let's discuss in this Chapter, the analysis based on tubular shields, because it is reasonable to represent the armor and shield of the telecommunication cable for lightning type of frequencies as a solid tube. The leakage effects, in the author's opinion, due to tube apertures and imperfections are predominant only at high frequencies beyond $1MHz$. Under such circumstances there exists no generalized expressions for tube impedances with imperfections and has to be determined either through experiments or extensive theory. A sim-

ple/approximate method for determining the capacitance matrix by bridge method is shown and is particularly useful for twisted pair cables, which is the case with cable shown in Fig. 1.7. A comparison of the proposed method with experiments is presented. Usually in communication system grounding arrangements, follow on bare earth conductors with the cable shields are used as in Fig. 7.1. Is it of any use to put such follow on earth conductors? An answer to this question is also given in this Chapter.

8.1 Generalized double shield three core cable

The discussion presented here is a generalization for a multi-conductor arrangement of the cable. By using the analogy presented here, one can apply the same to any practical arrangement of the cables. Let's take the following examples, a). Well-known RG-58 cable, that has single core and braided shield: A discussion on the concept of transfer impedance [63] and its experimental determination are presented, b). Three conductor power cable that has the same shield as that of RG-58 cable.

In the author's opinion, the analysis of coupling mechanism between the shield and inner conductor as proposed by *Vance* [63] is valid for a particular terminal condition only. In *Vance's* method when the inner conductor circuit does not carry any appreciable current, the coupling mechanism between the shield and the inner circuit, due to current in the shield, is represented by distributed series voltage sources in the transmission line formed by the inner circuit. This allows us to eliminate the shield circuit and simplifies the problem to a transmission line due to inner circuit only. This, in general, is not true for any arbitrary terminal conditions at the near and far ends of the shield and inner conductor/circuit. On the other hand, the analysis presented in the discussions to follow is valid for any arbitrary terminal conditions on either the shield or inner core conductors of the cable.

8.1.1 Telegrapher's equations for shielded cables

Consider a cable cut away view as shown in Fig. 8.1, which shows a three-core cable arrangement. It has two shields, solid tubular/cylindrical with annular cross-section. Let the core conductors carry currents I_1, I_2 and I_3 and the currents through the shield and the armor are marked as I_4 and I_5. In all the cases let us assume that the external inductance and capacitance matrices are known with the shield as the reference for the Fig. 8.1.

In equations (8.1) the voltages V_1, V_2, V_3, V_4, V_5 are written in differential form between inner conductors (cores) and the shield, between the shield and

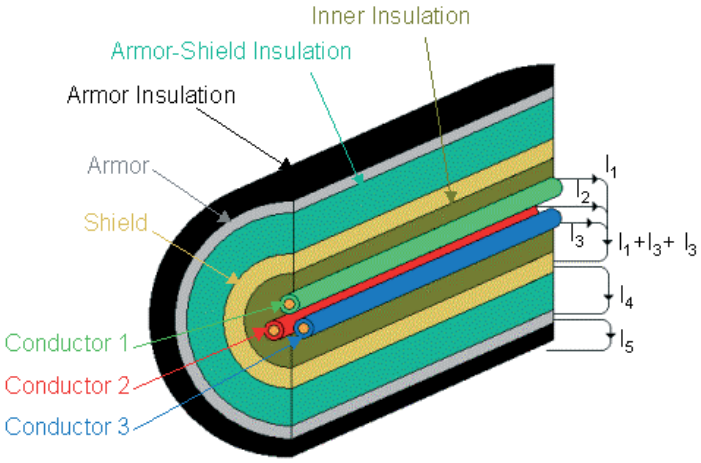

Figure 8.1: Generalized three-conductor cable arrangement for studying the coupling between the shields and internal conductors

the armor and the armor to remote reference, respectively. These voltages are also referred to as loop voltages [51]. The voltages like V_{1core}, V_{2core}, V_{3core}, V_{shield} and V_{armor} are that of the conductors with respect to remote reference [51]. These voltages are later useful for a transformation by which one can find voltages on any conductor with respect to any given/specified reference. The voltage wave equations based on the loop voltages are given by (8.2). Since loop voltages are adopted, the currents in (8.2) are referred to as loop currents I_1, I_2, I_3, I_4, I_5. These loop currents are related to the core currents I_{1core}, I_{2core}, I_{3core}, shield current I_{shield} and armor current I_{armor} as shown in (8.3). The relationship between the conductor currents and loop currents also helps in the transformation by which telegrapher's equations become in the form similar to MTLs systems as discussed in the earlier chapters. Now each parameter in the impedance matrix $[Z^{'}]$ in equation (8.2) is a combination of series impedance terms of internal and external impedances. Similarly, each admittance term in $[Y^{'}]$ is a combination of external and mutual admittance terms. These are discussed in the next section.

$$V_1 = V_{1core} - V_{shield} \tag{8.1a}$$

$$V_2 = V_{2core} - V_{shield} \tag{8.1b}$$

$$V_3 = V_{3core} - V_{shield} \tag{8.1c}$$

$$V_4 = V_{shield} - V_{armor} \tag{8.1d}$$

$$V_5 = V_{armor} \tag{8.1e}$$

$$-\frac{dV_1}{dx} = Z_{11}^{'} \cdot I_1 + Z_{12}^{'} \cdot I_2 + Z_{13}^{'} \cdot I_3 + Z_{14}^{'} \cdot I_4 + Z_{15}^{'} \cdot I_5 \tag{8.2a}$$

$$-\frac{dV_2}{dx} = Z_{21}^{'} \cdot I_1 + Z_{22}^{'} \cdot I_2 + Z_{23}^{'} \cdot I_3 + Z_{24}^{'} \cdot I_4 + Z_{25}^{'} \cdot I_5 \tag{8.2b}$$

$$-\frac{dV_3}{dx} = Z_{31}^{'} \cdot I_1 + Z_{32}^{'} \cdot I_2 + Z_{33}^{'} \cdot I_3 + Z_{34}^{'} \cdot I_4 + Z_{35}^{'} \cdot I_5 \tag{8.2c}$$

$$-\frac{dV_4}{dx} = Z_{41}^{'} \cdot I_1 + Z_{42}^{'} \cdot I_2 + Z_{43}^{'} \cdot I_3 + Z_{44}^{'} \cdot I_4 + Z_{45}^{'} \cdot I_5 \tag{8.2d}$$

$$-\frac{dV_5}{dx} = Z_{51}^{'} \cdot I_1 + Z_{52}^{'} \cdot I_2 + Z_{53}^{'} \cdot I_3 + Z_{54}^{'} \cdot I_4 + Z_{55}^{'} \cdot I_5 \tag{8.2e}$$

$$I_1 = I_{1core} \tag{8.3a}$$

$$I_2 = I_{2core} \tag{8.3b}$$

$$I_3 = I_{3core} \tag{8.3c}$$

$$I_4 = I_{shield} + I_{1core} + I_{2core} + I_{3core} \tag{8.3d}$$

$$I_5 = I_{armor} + I_{shield} + I_{1core} + I_{2core} + I_{3core} \tag{8.3e}$$

$$-\frac{dI_1}{dx} = Y_{11}^{'} \cdot V_1 + Y_{12}^{'} \cdot V_2 + Y_{13}^{'} \cdot V_3 + Y_{14}^{'} \cdot V_4 + Y_{15}^{'} \cdot V_5 \tag{8.4a}$$

$$-\frac{dI_2}{dx} = Y_{21}^{'} \cdot V_1 + Y_{22}^{'} \cdot V_2 + Y_{23}^{'} \cdot V_3 + Y_{24}^{'} \cdot V_4 + Y_{25}^{'} \cdot V_5 \tag{8.4b}$$

$$-\frac{dI_3}{dx} = Y_{31}^{'} \cdot V_1 + Y_{32}^{'} \cdot V_2 + Y_{33}^{'} \cdot V_3 + Y_{34}^{'} \cdot V_4 + Y_{35}^{'} \cdot V_5 \tag{8.4c}$$

$$-\frac{dI_4}{dx} = Y_{41}^{'} \cdot V_1 + Y_{42}^{'} \cdot V_2 + Y_{43}^{'} \cdot V_3 + Y_{44}^{'} \cdot V_4 + Y_{45}^{'} \cdot V_5 \tag{8.4d}$$

$$-\frac{dI_5}{dx} = Y_{51}^{'} \cdot V_1 + Y_{52}^{'} \cdot V_2 + Y_{53}^{'} \cdot V_3 + Y_{54}^{'} \cdot V_4 + Y_{55}^{'} \cdot V_5 \tag{8.4e}$$

8.1.2 Transmission line impedance and admittance parameters

Our aim is to arrive at the MTL equations of the form (8.5) after simplifying equations (8.2) and (8.4) using (8.1) and (8.3) respectively. The impedance parameters of (8.2) are defined in (8.6). In (8.6) there are some impedance terms in addition to external inductance (discussed later) of the internal conductors. Those impedances, excluding the internal impedances, are the ones that contribute to the coupling between the shield and inner conductors and the shield and the armor. Let's discuss them in some detail here.

Z_i is the internal impedance of the conductors, which is a consequence of skin effect phenomena of the core conductors as discussed in Chapter-4 and is obtained by equation (4.12 or 4.14).

$$-\begin{pmatrix} \frac{dV_{1core}}{dx} \\ \frac{dV_{2core}}{dx} \\ \frac{dV_{3core}}{dx} \\ \frac{dV_{shield}}{dx} \\ \frac{dV_{armor}}{dx} \end{pmatrix} = [Z] \cdot \begin{pmatrix} I_{1core} \\ I_{2core} \\ I_{3core} \\ I_{shield} \\ I_{armor} \end{pmatrix} \tag{8.5a}$$

$$-\begin{pmatrix} \frac{dI_{1core}}{dx} \\ \frac{dI_{2core}}{dx} \\ \frac{dI_{3core}}{dx} \\ \frac{dI_{shield}}{dx} \\ \frac{di_{armor}}{dx} \end{pmatrix} = [Y] \cdot \begin{pmatrix} V_{1core} \\ V_{2core} \\ V_{3core} \\ V_{shield} \\ V_{armor} \end{pmatrix} \tag{8.5b}$$

Schelkunoff in [48] gives a very good discussion on the surface impedances of hollow solid cylindrical shells. Discussions in this section are applicable only for imperfect conductors. Consider a hollow conductor whose inner and outer radii are a and b respectively. The return of the coaxial path could be partly inside and partly outside. Let Z_{aa} be the surface impedance with internal return and Z_{bb}, with that of external return. It seems with this situation one has in effect two transmission lines with distributed mutual impedance Z_{ab}. In *Schelkunoff's* language, Z_{ab} is due to the mingling of two currents in the hollow conductor common to both lines and since Z_{ab} is not the total mutual impedance between the two lines, Z_{ab} is called the transfer impedance from one surface of the conductor to the other [48]. Using magnetomotive intensities associated with the two currents, he derived the surface impedances as given by (8.7) and (8.8). The analysis presented here are for tubular shields only. If $[L]$ and $[C]$ are the inductance and the capacitance matrix of the core

conductors with respect to shield, then,

$$Z_{11}^{'} = Z_i + j\omega \cdot L_{11} + Z_{Shield-in} \tag{8.6aa}$$

$$Z_{12}^{'} = Z_{21}^{'} = j\omega \cdot L_{12} + Z_{Shield-in} \tag{8.6ab}$$

$$Z_{22}^{'} = Z_i + j\omega \cdot L_{22} + Z_{Shield-in} \tag{8.6ac}$$

$$Z_{13}^{'} = Z_{31}^{'} = j\omega \cdot L_{31} + Z_{Shield-in} \tag{8.6ad}$$

$$Z_{23}^{'} = Z_{32}^{'} = j\omega \cdot L_{23} + Z_{Shield-in} \tag{8.6ae}$$

$$Z_{33}^{'} = Z_i + j\omega \cdot L_{33} + Z_{Shield-in} \tag{8.6af}$$

$$Z_{14}^{'} = Z_{24}^{'} = Z_{34}^{'} = Z_{41}^{'} = Z_{42}^{'} = Z_{43}^{'} = -Z_{Shield-mutual} \tag{8.6b}$$

$$Z_{44}^{'} = Z_{Shield-out} + Z_{Shield-Armor-insulation} + Z_{Armor-in} \tag{8.6c}$$

$$Z_{15}^{'} = Z_{25}^{'} = Z_{35}^{'} = Z_{51}^{'} = Z_{52}^{'} = Z_{53}^{'} = 0 \tag{8.6d}$$

$$Z_{45}^{'} = Z_{54}^{'} = -Z_{Armor-mutual} \tag{8.6e}$$

$$Z_{55}^{'} = Z_{Armor-out} + Z_{Armor-Earth-insulation} + Z_{gbi} \tag{8.6f}$$

Note: the impedance due to the insulation between shields can be calculated using equation (7.3). Z_{aa}, Z_{bb} and Z_{ab} are the tube-in, tube-out and tube-mutual impedances, which can be used for the shield and the armor.

$$\begin{aligned} Z_{aa} &= \frac{\sqrt{j\omega \cdot \mu \cdot \sigma}}{2\pi \cdot \sigma \cdot a \cdot \Lambda}\Big(I_0\big(a \cdot \sqrt{j\omega \cdot \mu \cdot \sigma}\big) \cdot K_1\big(b \cdot \sqrt{j\omega \cdot \mu \cdot \sigma}\big) \\ &\quad + I_1\big(b \cdot \sqrt{j\omega \cdot \mu \cdot \sigma}\big) \cdot K_0\big(a \cdot \sqrt{j\omega \cdot \mu \cdot \sigma}\big)\Big) \end{aligned} \tag{8.7a}$$

$$\begin{aligned} Z_{bb} &= \frac{\sqrt{j\omega \cdot \mu \cdot \sigma}}{2\pi \cdot \sigma \cdot b \cdot \Lambda}\Big(I_0\big(b \cdot \sqrt{j\omega \cdot \mu \cdot \sigma}\big) \cdot K_1\big(a \cdot \sqrt{j\omega \cdot \mu \cdot \sigma}\big) \\ &\quad + I_1\big(a \cdot \sqrt{j\omega \cdot \mu \cdot \sigma}\big) \cdot K_0\big(b \cdot \sqrt{j\omega \cdot \mu \cdot \sigma}\big)\Big) \end{aligned} \tag{8.7b}$$

$$Z_{ab} = \frac{1}{2\pi \cdot \sigma \cdot a \cdot b \cdot \Lambda} \tag{8.7c}$$

$$\begin{aligned} \Lambda &= \Big(I_1\big(b \cdot \sqrt{j\omega \cdot \mu \cdot \sigma}\big) \cdot K_1\big(a \cdot \sqrt{j\omega \cdot \mu \cdot \sigma}\big) \\ &\quad - I_1\big(a \cdot \sqrt{j\omega \cdot \mu \cdot \sigma}\big) \cdot K_1\big(b \cdot \sqrt{j\omega \cdot \mu \cdot \sigma}\big)\Big) \end{aligned} \tag{8.7d}$$

There are two theorems proposed by *Schelkunoff* [48] with regard to tube impedances (author has simplified the second theorem for brevity).

Theorem - 1: If the return path is wholly external $(I_a = 0)$ **or wholly internal** $(I_b = 0)$**, the longitudinal electromotive force (voltage) on that surface which is the nearest to the return path equals the corresponding surface impedance (self) multiplied by the total current flowing in the conductor and the longitudinal electromotive force (voltage) on the other surface equals the transfer impedance (mutual) multiplied by the total current.**

Theorem - 2: If the return path is partly external and partly internal then the total longitudinal electromotive force (voltage) on either side of the surface can be obtained by applying Theorem - 1 with the principle of superposition.

Equations (8.7) gives the tube impedances. In comparison with (8.6), one can define (8.7a) as the tube-in impedance of either shield or the armor, (8.7b) as the tube-out impedance of either the shield or the armor and (8.7c) as the tube-mutual impedance of either the shield or the armor. The impedance due to the insulation is calculated from its thickness as discussed in Chapter-7 using (7.3). The ground impedance term appears in (8.6f), which has been discussed in detail in Chapter-7 and the logarithmic-exponential approximation (7.10) was used.

Wedepohl and Wilcox [51] have given a very simple approximation as shown in (8.8) for the tube impedances without any *Bessel* functions, and they are valid only if $\frac{b-a}{b+a} < \frac{1}{8}$. This has been validated for various practical tubular cable shields by the author and it was seen that approximations (8.8) are excellent ones to exact *Schelkunoff* [48] equations (8.7).

$$Z_{aa} \approx \frac{\sqrt{j\omega \cdot \mu \cdot \sigma}}{2\pi \cdot \sigma \cdot a} \cdot \coth\left((b-a) \cdot \sqrt{j\omega \cdot \mu \cdot \sigma}\right) - \frac{1}{2\pi \cdot \sigma \cdot a \cdot (a+b)} \quad (8.8a)$$

$$Z_{bb} \approx \frac{\sqrt{j\omega \cdot \mu \cdot \sigma}}{2\pi \cdot \sigma \cdot b} \cdot \coth\left((b-a) \cdot \sqrt{j\omega \cdot \mu \cdot \sigma}\right) - \frac{1}{2\pi \cdot \sigma \cdot b \cdot (a+b)} \quad (8.8b)$$

$$Z_{ab} \approx \frac{\sqrt{j\omega \cdot \mu \cdot \sigma}}{\pi \cdot \sigma \cdot (a+b)} \cdot \frac{1}{\sinh\left((b-a)\sqrt{j\omega\mu\sigma}\right)} \quad (8.8c)$$

It is shown how to obtain all the important impedance parameters that are needed to create equation (8.5a), the voltage wave equation. For the current wave equation (8.5b) the required admittance parameters are obtained as shown below.

The admittance matrix due to the external capacitance (discussed later) with

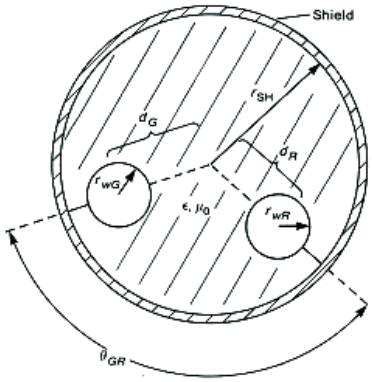

Figure 8.2: Non twisted parallel conductor arrangement in the shield for MTL parameter estimation for multi-conductor cable adapted from [12, 41]

shield as reference is given by (8.9).

$$\begin{pmatrix} Y'_{11} & Y'_{12} & Y'_{13} \\ Y'_{21} & Y'_{22} & Y'_{23} \\ Y'_{31} & Y'_{32} & Y'_{33} \end{pmatrix} = j\omega \cdot \begin{pmatrix} C_{11} & C_{12} & C_{13} \\ C_{21} & C_{22} & C_{23} \\ C_{31} & C_{32} & C_{33} \end{pmatrix} \tag{8.9}$$

Note that the following formulas for inductance and capacitance of the wires in a multi-conductor cable are not applicable if the cables have twisted pair arrangements (discussed in a later section).

The per meter inductance and capacitance parameters for a multi conductor cable that has homogeneous medium are given by *Paul* [12, 41] and are given by (8.10) and (8.11) respectively. For the capacitance matrix, let's first estimate the potential coefficient matrix and then invert the potential coefficient matrix similar to the above ground wires.

$$L_{GG,RR} = \frac{\mu_0}{2\pi} \ln\left(\frac{r_{SH}^2 - d_{G,R}^2}{r_{SH} \cdot r_{wG,R}}\right) \tag{8.10a}$$

$$L_{GR} = \frac{\mu_0}{2\pi} \ln\left(\frac{d_R}{r_{SH}} \cdot \sqrt{\frac{(d_G d_R)^2 + r_{SH}^4 - 2d_G d_R r_{SH}^2 \cos(\theta_{GR})}{(d_G d_R)^2 + d_R^4 - 2d_G d_R^3 \cos(\theta_{GR})}}\right) \tag{8.10b}$$

Equations (8.10) can be used to estimate the inductance parameters in equation (8.6a) if the core conductors are not twisted pair.

$$P_{GG,RR} = \frac{1}{2\pi\varepsilon_i} \ln\left(\frac{r_{SH}^2 - d_{G,R}^2}{r_{SH} \cdot r_{wG,R}}\right) \tag{8.11a}$$

$$P_{GR} = \frac{1}{2\pi\varepsilon_i} \ln\left(\frac{d_R}{r_{SH}} \cdot \sqrt{\frac{(d_G d_R)^2 + r_{SH}^4 - 2 d_G d_R r_{SH}^2 \cos(\theta_{GR})}{(d_G d_R)^2 + d_R^4 - 2 d_G d_R^3 \cos(\theta_{GR})}}\right) \tag{8.11b}$$

$$C = [P]^{-1} \tag{8.11c}$$

Equations (8.11) can be used to estimate the capacitance parameters in equation (8.9a) if the core conductors are not twisted pair.

Many of the mutual admittance terms are null for tubular shields and armor as shown in (8.12). The capacitances due to the insulation C_{44} and C_{55} are calculated by the same formula as discussed in Chapter-7 using (7.3). Y_{gbi} is the ground admittance as discussed in Chapter-7 and given by expression (7.11). The ground admittance in (8.14) is usually neglected in transient simulation packages like *EMTP* [119, 122], and which was shown to be not valid in the previous Chapter.

$$Y_{14}^{'} = Y_{15}^{'} = Y_{24}^{'} = Y_{25}^{'} = Y_{34}^{'} = Y_{35}^{'} = 0 \tag{8.12a}$$

$$Y_{41}^{'} = Y_{51}^{'} = Y_{42}^{'} = Y_{52}^{'} = Y_{43}^{'} = Y_{53}^{'} = 0 \tag{8.12b}$$

$$Y_{45}^{'} = Y_{54}^{'} = 0 \tag{8.12c}$$

Shield armor insulation capacitance is,

$$Y_{44}^{'} = j\omega \cdot C_{44} \tag{8.13}$$

Armor earth insulation capacitance and ground admittance are in series,

$$Y_{44}^{'} = j\omega \cdot C_{55} || Y_{gbi} \tag{8.14}$$

8.2 An example of RG-58 cable

This cable has a single core and a braided copper shield [63]. *ELFA* catalogue [128] specifies the capacitance of the core conductor with respect to the shield for the *RG-58* cable is $1.01 \times 10^{-10} F/m$. This can be obtained using the formula (8.11c). The inductance for this cable using the characteristic impedance of 50Ω [128] will be $2.55 \times 10^{7} H/m$. The shield is braided because of which the tube mutual impedance or the transfer impedance will not be the same as discussed above. Vance [63] mentions that there will be two components, which contribute to the net transfer impedance. One is due to the diffusion of electromagnetic energy and the other, due to the penetration of the magnetic field through apertures of the braid. The diffusion part is similar to the case as if the shield were like a tube, similar to the tube mutual impedance as shown

in the previous section. The penetration part is usually represented as a mutual inductance term as in (8.15).

$$Z_{Shield-mutual} = Z_T = Z_d + j\omega \cdot M_{12} \tag{8.15a}$$

$$Z_d = R_{dc} \cdot \frac{2r_{bw}\sqrt{j\omega\mu_0\sigma}}{\sinh(2r_{bw}\sqrt{j\omega\mu_0\sigma})} \tag{8.15b}$$

The values of Z_d and M_{12} are calculated from the shield geometries i.e., number of carrier wires on the braid and also on the weave angles. Associated formulas can be found in *Vance* [63]. For the moment let us assume that these are known for the $RG-58$ cable, and the values needed are picked up from *Vance* [63]. The typical values are $M_{12} = 1nH/m$, $R_{dc} = 14m\Omega/m$, $r_{bw} = 63.5\mu m$ and the copper conductivity and permeability was chosen.

Can transfer impedance be measured experimentally? Under weak coupling conditions, that is when the inner circuit does not carry any current and if the length of the cable is electrically small, it is possible to determine the transfer impedance exactly. Let us get back to our differential equations (8.5a). For the $RG-58$ the equations reduce to,

$$-\begin{pmatrix} \frac{dV_{core}}{dx} \\ \frac{dV_{shield}}{dx} \end{pmatrix} = \begin{pmatrix} Z_{11} & Z_{12} \\ Z_{21} & Z_{22} \end{pmatrix} \cdot \begin{pmatrix} I_{core} \\ I_{shield} \end{pmatrix} \tag{8.16}$$

$$Z_{11} = Z_{11}^{'} + Z_{12}^{'} + Z_{21}^{'} + Z_{22}^{'} \tag{8.17a}$$

$$Z_{12} = Z_{21} = Z_{12}^{'} + Z_{22}^{'} = Z_{21}^{'} + Z_{22}^{'} \tag{8.17b}$$

$$Z_{22} = Z_{22}^{'} \tag{8.17c}$$

Assume a $1m$ length of the RG-58 cable, which is electrically small, and at one end (near end marked as suffix N) let's short the inner conductor and shield and inject a current source with respect to reference plane. At the other end (far end marked as suffix F), let's open circuit the inner conductor and short the shield to the reference plane. Thus the voltage at the near and far ends with respect to core and shield currents can be written as,

$$-(V_{coreF} - V_{coreN}) = Z_{11} \cdot I_{core} + Z_{12} \cdot I_{shield} \tag{8.18a}$$

$$-(V_{shieldF} - V_{shieldN}) = Z_{21} \cdot I_{core} + Z_{22} \cdot I_{shield} \tag{8.18b}$$

The core current is zero, because of which,

$$-(V_{coreF} - V_{coreN}) = Z_{12} \cdot I_{shield} \tag{8.19a}$$

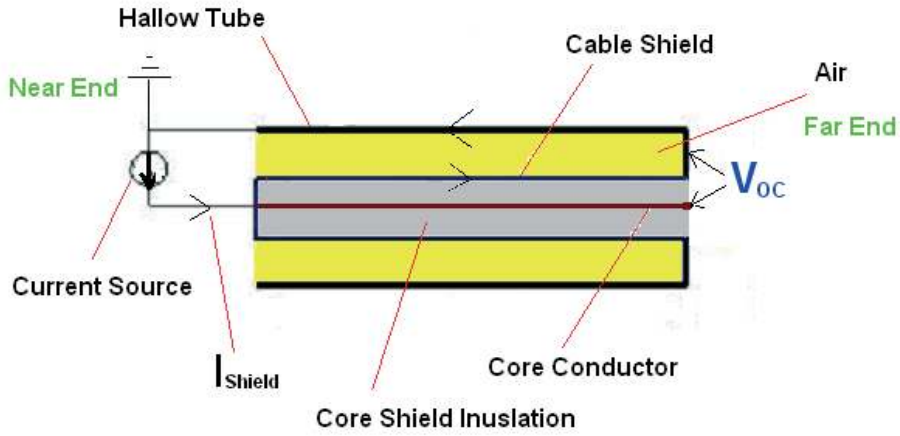

Figure 8.3: Triax setup for measuring the transfer impedance

$$-(V_{shieldF} - V_{shieldN}) = Z_{22} \cdot I_{shield} \tag{8.19b}$$

Also V_{coreN} and $V_{shieldN}$ are the same as they are shorted at the injection point, hence, by subtracting the two equations from each other in (8.19) one obtains,

$$(V_{coreF} - V_{shieldF}) = (-Z_{12} + Z_{22}) \cdot I_{shield} \tag{8.20a}$$

$$(-Z_{12} + Z_{22}) = Z_{12}^{'} \approx Z_T = \frac{V_{coreF} - V_{shieldF}}{I_{shield}} \approx \frac{V_{coreF}}{I_{shield}} \tag{8.20b}$$

This is the concept used in various transfer impedance measurement methods. Similar to transfer impedance one can also define the transfer admittance. Let's not discuss it here, as its influence is negligible compared to the transfer impedance. Let's now see if one can get the transfer impedance using the simulations. In all the simulations below, the leakage inductance part in (8.15a) is neglected, so as to be consistent with our tube impedance analogy.

Consider an $RG-58$ cable, from *ELFA* catalogue [128] or by physical measurement of the dimensions, one can arrive at the required values of tube impedances, insulation inductance and capacitance, etc. Let's take a $1m$ length of cable and make a simple *Triax* arrangement [43] as shown in the Fig. 8.3. Note that one can make the radius of the tube smaller so as to be in contact with the outer insulation (not shown in Fig. 8.3) so as to get rid of the external inductance and capacitance between the tube wall and insulation.

Let's inject a step pulse current at the near end with the connection as shown in Fig. 8.3 and measure the open circuit voltage at the far end between the inner core and the shield. The ratio of the open circuit voltage and the shield current should give us the required tube mutual impedance or the transfer im-

pedance based on (8.20). Fig. 8.4 shows this ratio in frequency and time domain for the $RG-58$ cable with actual $127\mu m$ shield thickness and if shield thickness were $254\mu m$. From Fig. 8.4a, it can be seen that at low frequency, the DC resistance of the shield predominates up to about $100kHz$, beyond which the transfer impedance decreases. The higher the thickness, the less the transfer impedance. If one uses braided shield (not discussed here) the transfer impedance increases after the corner frequency corresponding to (8.15a). The increment may be proportional to frequency or square root of frequency [42]. The ratio of open circuit voltage to the current in frequency domain was fitted using a ten poles vector fitting [69] and the time domain response is shown in Fig. 8.4b. Do not be surprised by the large value of transfer impedance in time domain. Transfer impedance features/characteristics cannot be discussed in time domain, simply because $\frac{V(j\omega)}{I(j\omega)} \neq \frac{V(t)}{I(t)}$. What is seen is a result of convolution.

An interpretation can be provided to time domain 'transfer impedance' presented in Fig. 8.4b. It takes some time for the shield current (magnetic field) to penetrate to the inside. The time, when the steady low value of transfer impedance is achieved in Fig. 8.4b is nearly the same as the time at which the steady value of the open circuit voltage is achieved in Fig. 8.5. *Stern* [129] has provided a time domain formula as a series expansion for *Schelkunoff's* expression (8.15b). The convergence of such a time domain formula depends on shield properties and shield dimensions. Another interesting feature of the transfer impedance is that it predicts the diffusion time [63] required for the development of the internal voltage. The diffusion time constant can be obtained from the shield thickness and shield material properties and is given by (8.21).

$$\tau_s = \mu\sigma \cdot (shield.thickness)^2 \tag{8.21}$$

To demonstrate this, let's take the same example of transfer impedance. The internal open circuit voltages for two thickness of the shield are shown in Fig. 8.5. It can be seen that the constant voltage is attained at about times corresponding to diffusion time of the shield and those times are marked in Fig. 8.5. The higher the thickness, the larger the diffusion time and the less the internal voltages due to low value of transfer impedance.

8.3 An example of ELEK 3G 1.5 - three-conductor power cable

Next let's take up a slightly complex multi-conductor cable. It is a power cable having three core conductors and a shield that is similar to the $RG-58$ cable in terms of the thickness of the shield. Let's now attempt to calculate

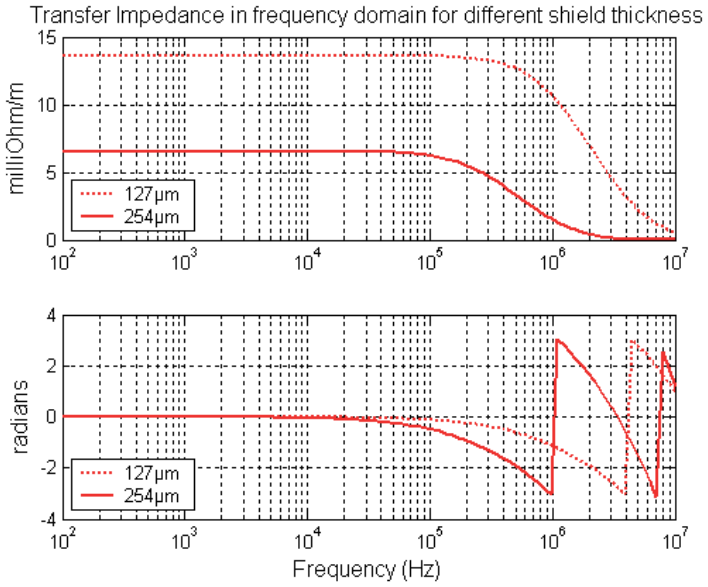

(a) $\frac{V_{oc}(j\omega)}{I_{shield}(j\omega)}$-Frequency domain response

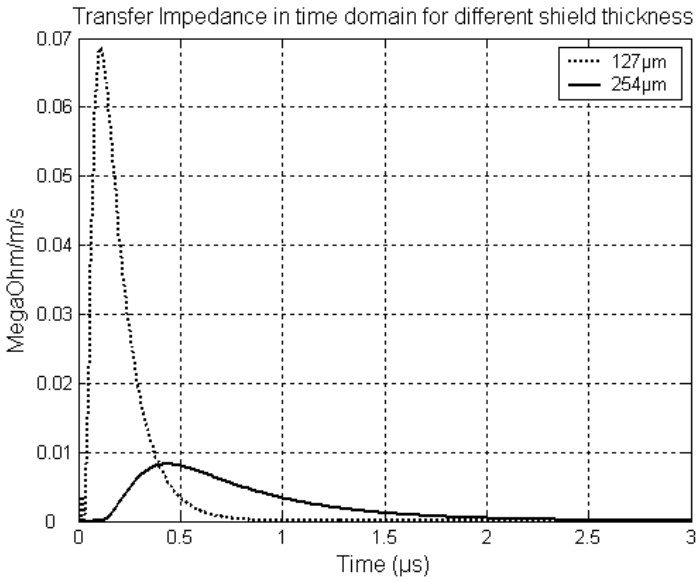

(b) $\frac{V_{oc}(t)}{I_{shield}(t)}$-After convolution

Figure 8.4: Frequency domain response of the ratio of open circuit voltage and shield current for two shield thicknesses, Time domain response of the transfer impedance obtained from fitting the frequency response of the ratio of open circuit voltage and shield current - equivalent to convolution in time domain

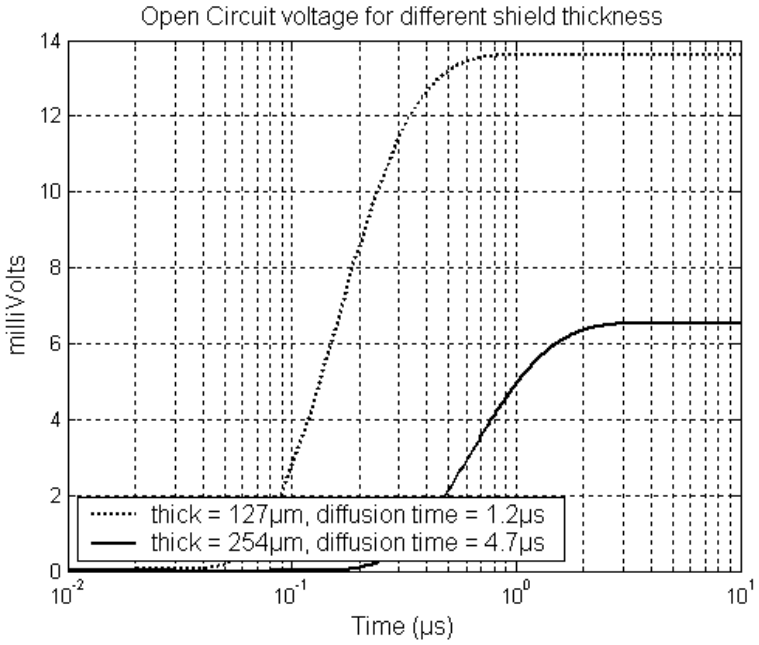

Figure 8.5: Time domain response of the internal open circuit voltages for two shield thicknesses

the transfer impedance for this multi-conductor cable. A 1*m* cable is inserted into the tube of the *Triax* setup as shown in Fig. 8.3 for experiments. So as to make a comparison with experiments and simulations, let's divide this section into four parts. Firstly, let's obtain the relevant capacitance matrix using the *Bridge* method, which could be generalized for any multi-conductor system. Secondly, let's obtain the expression for the current that was injected in the experiments. Thirdly, let's compare between the simulations and experiments for the various cases. Finally, let's investigate some cases as to how the induced voltages can be decreased in multi-conductor cable.

8.3.1 Line inductance and capacitance measurements

The capacitances of the cable were measured with a *General Radio 1658 RLC DigiBridge* [130]. In this multi-conductor cable there are three conductors, located as shown in Fig. 8.6 (left). Combinations of self and mutual capacitance distributions are shown in Fig. 8.6 (right).

Since there are six unknown quantities, six independent equations are needed. To get the first equation for any case, all the conductors are to be shorted, due to which, the system has all the self-capacitances in parallel, as shown in Fig. 8.7 (far left). The value given by the *Bridge* will be the sum of the self-capacitances in the cable. To obtain three other equations, one may

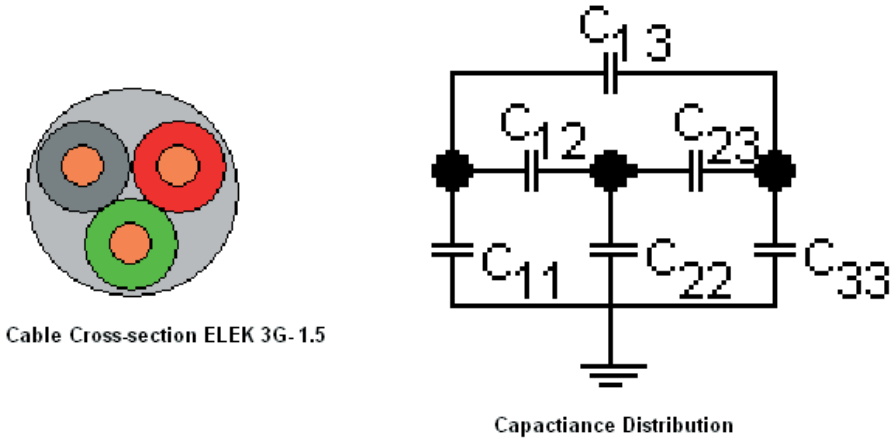

Figure 8.6: Capacitance distribution in three conductor ELEK 3G-1.5

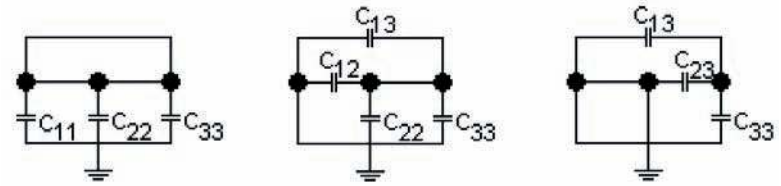

Figure 8.7: Various capacitance combinations for generalized independent equations (8.22)

ground a conductor and short the other two, e.g., grounding $conductor-1$ and shorting $conductors-2,3$, due to which the system looks like Fig. 8.7 (middle). Since the system has four capacitances in parallel, the measured value will be a sum of those capacitances. Until now, four independent equations have been obtained. To get the remaining two, let's ground two of the conductors and leave the other open, e.g., like in Fig. 8.7 (far right).

If the measurements are carried out in the same order as described above and the grounding procedure is made in numerical order of $conductor-number-1...3$, one has the following,

$$\begin{pmatrix} 1 & 1 & 1 & 0 & 0 & 0 \\ 0 & 1 & 1 & 1 & 1 & 0 \\ 1 & 0 & 1 & 1 & 0 & 1 \\ 1 & 1 & 0 & 0 & 1 & 1 \\ 0 & 0 & 1 & 0 & 1 & 1 \\ 0 & 1 & 0 & 1 & 0 & 1 \end{pmatrix} \cdot \begin{pmatrix} C_{11} \\ C_{22} \\ C_{33} \\ C_{12} \\ C_{13} \\ C_{23} \end{pmatrix} = \begin{pmatrix} ME_1 \\ ME_2 \\ ME_3 \\ ME_4 \\ ME_5 \\ ME_6 \end{pmatrix} \tag{8.22}$$

The unknown capacitances can be obtained by matrix inversion. Thus, for n conductor system the number of independent equations and its combinations are $\frac{n(n+1)}{2}$. The capacitance matrix for the ELEK 3G-1.5 the capacitance matrix is given by (8.23). With $\varepsilon_{rin} = 5$, obtained from Draka [131], was used to get the inductance matrix using $L_{cable} = \frac{\varepsilon_{rin}}{9\times10^{16}}[C_{cable}]^{-1}$, which gives (8.24).

$$[C]_{3\times3} = \begin{pmatrix} 2.02 & -0.168 & -0.168 \\ -0.168 & 2.02 & -0.168 \\ -0.168 & -0.168 & 2.02 \end{pmatrix} \times 10^{-10} \tag{8.23}$$

$$[L]_{3\times3} = \begin{pmatrix} 2.91 & 0.264 & 0.264 \\ 0.264 & 2.91 & 0.264 \\ 0.264 & 0.264 & 2.91 \end{pmatrix} 10^{-7} \tag{8.24}$$

The average error between the theory [12, 41] and measurements, for the individual elements in the capacitance matrix, is about 10%. The procedure described above is particularly useful, if the cable has complex twisted pair arrangement with different layers of conductors.

The communication cable of Banverket shown in Fig. 1.7, has a total of 60 conductors (some are twisted pairs), which gives us 1830 unknown capacitances, in which 60 are self-capacitances and 1770 are mutual capacitances between the conductors. In [132] this capacitance matrix was experimentally obtained using the same method as discussed above and the inductance matrix was obtained with an average insulation permittivity of 1.85. The procedure of determining capacitance matrix for twisted pair cables, based on *Bridge* methods, needs further extensive validation, based on more accurate and slightly difficult experimental methods as proposed by *Agrawal et al.* [133, 134], both in frequency domain and time domain. This is needed as there are no available expressions or formula for direct comparisons.

8.3.2 An experimental validation of the model

The cable (dimensions: outer radius with insulation $4mm$, outer insulation thickness $1mm$ with $\varepsilon_{rin} = 2.23$, shield is braided with $120\mu m$ thick) was inserted into the *Triax* tube that has a radius of $3.25cm$. The current was injected using a *Schaffner* generator *NSG 650* [135]. The measured current at the near end injected into the shield is shown in Fig. 8.7. The measured injected current was first taken to a direct *Fourier* transform and the response points are then taken for vector fitting [69] using a four pole fitting (complex poles) in frequency domain and, the fitted curve is shown in Fig. 8.8. The expression for the current is given by (8.25) and this was used in the simulations as well. The

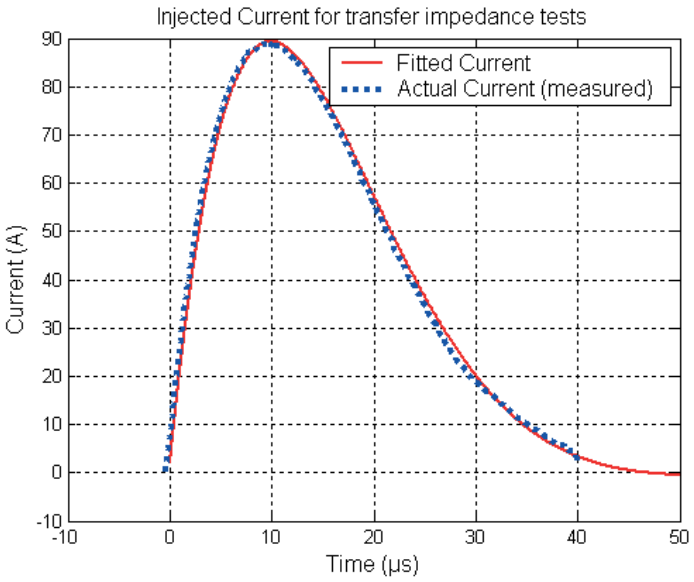

Figure 8.8: Injected current into the shield for experiment

fitted and measured curves agree quiet well. It is easier to write the injected current expression in time domain as sums of exponentials.

$$I_{injected}(s) = \frac{-0.01}{s+241.4} + \frac{84.1}{s+78230} - \frac{41.2+j115}{s+(90131-j88257.6)} - \frac{41.2-j115}{s+(90131+j88257.6)} \tag{8.25}$$

Three important conditions were simulated:

- Case-1: At the near end, all the conductors are shorted to the shield and current is injected with respect to tube. At the far end, all the core conductors are shorted to each other and left open and the shield was shorted to the tube.
- Case-2: At the near end, all the conductors are shorted to shield and current is injected with respect to tube. At the far end, out of three core conductors, two were shorted to each other and left open, while the other core conductor and the shield were shorted to the tube.
- Case-3: At the near end, all the conductors are shorted and current is injected with respect to tube. At the far end, out of three core conductors, one of them was left open and the other two core conductors and the shield were shorted to the tube.

In all the cases, the open circuit voltage was measured at the far end between the open conductors' and the shield and the simulations of each case

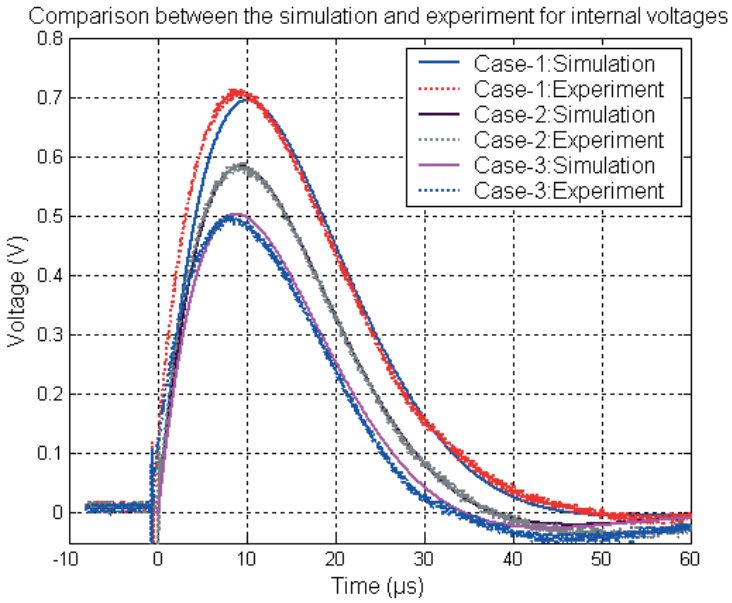

Figure 8.9: Comparison between experiment and simulation for three-conductor cable

with corresponding experimental results are shown in Fig. 8.9. It can be seen that the multi-conductor transmission line model with shield and armor as discussed in the previous sections are valid even though the theory was derived for tubular shields. It should be noted that the shield current had rise time of about $8\mu s$ and therefore, the magnetic field leakage through the holes of braid are negligible. For all the cases the simulations and experiments are in agreement.

The above phenomenon demonstrated in Fig. 8.9 could be beneficial from the perspective of lightning protection. Usually, in communication cable systems, several pairs are not connected to any load and is left open. Based on the simulation and experiment shown in Fig. 8.9, it is observed that if the unused pairs or conductors are shorted to the shield or grounded, there could be reduction in the induced effects. *According to the author the above phenomena needs further serious investigation and validation through experiments and theory.*

8.4 Can the transients entering to shield of the cable be diverted?

If one looks at Fig. 7.1, it can be seen that there are follow on earth conductor running parallel to the cable. The shield of the cable is connected to

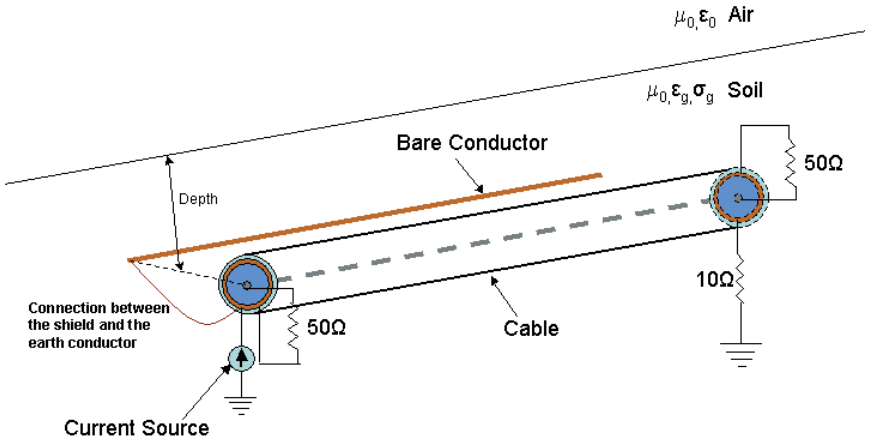

Figure 8.10: Arrangement of cable and follow on earth wire

the follow on earth conductor at the point of entry (beginning of the cable). Let's take an example with the length of the cable as $500m$ and the arrangement is shown in Fig. 8.10. In Fig. 8.10 the cable and bare wire are at a depth of $0.75m$ and the distance between the bare wire and the cable is $10cm$. The cable core inductance and capacitance are $0.255\mu H/m$ and $0.102nF/m$ respectively. The outermost radius of the cable is $1.2cm$ and has an insulation thickness of $2mm$ with insulation permittivity of 2.26. The shield thickness is $127\mu m$ and is made of copper. Consider this to be a hypothetical cable as it's only an example for demonstration.

Let us simulate two cases. One is a situation when the bare wire is not present and the other with a follow on earth wire present beside the cable with the cable shield connected to the earth wire at the injection point. The far end of the earth wire is open and in both the cases the inner core conductor is terminated with 50Ω load at both the ends connected to the shield. The shield at the far end is terminated in 10Ω load, representing the impedance of a grounding network.

The currents injected into the shield in both cases were double exponential impulse given by $I(t) = k_0(e^{-at} - e^{-bt})$. For the slow impulse the values are $k_0 = 1.1274$, $a = 10^4$ and $b = 4.0 \times 10^5$. For the fast impulse, the values are $k_0 = 1.0019$, $a = 10^4$ and $b = 1.5 \times 10^7$. The slow impulse has a rise time of $10\mu s$ while the fast impulse has a rise time of $0.3\mu s$, and both currents have a peak of $1A$ and 50% tail time is about $60 - 70\mu s$. The simulation results are shown in Fig. 8.11 for a ground conductivity of $10mS/m$ (top figure) and $0.5mS/m$ (bottom figure). In both the cases, the ground relative permittivity is $\varepsilon_{rg} = 10$ and the potential difference between the shield and the inner conductor is calculated at $50m$ from the injection point. The simulations indeed show

that connecting the bare wire to the shield at the point of entry largely diverts the currents and thereby reduce the internal voltages to a minimum. *Thottappillil and Theethayi* in [109 **Paper-K**] came up with a similar conclusion.

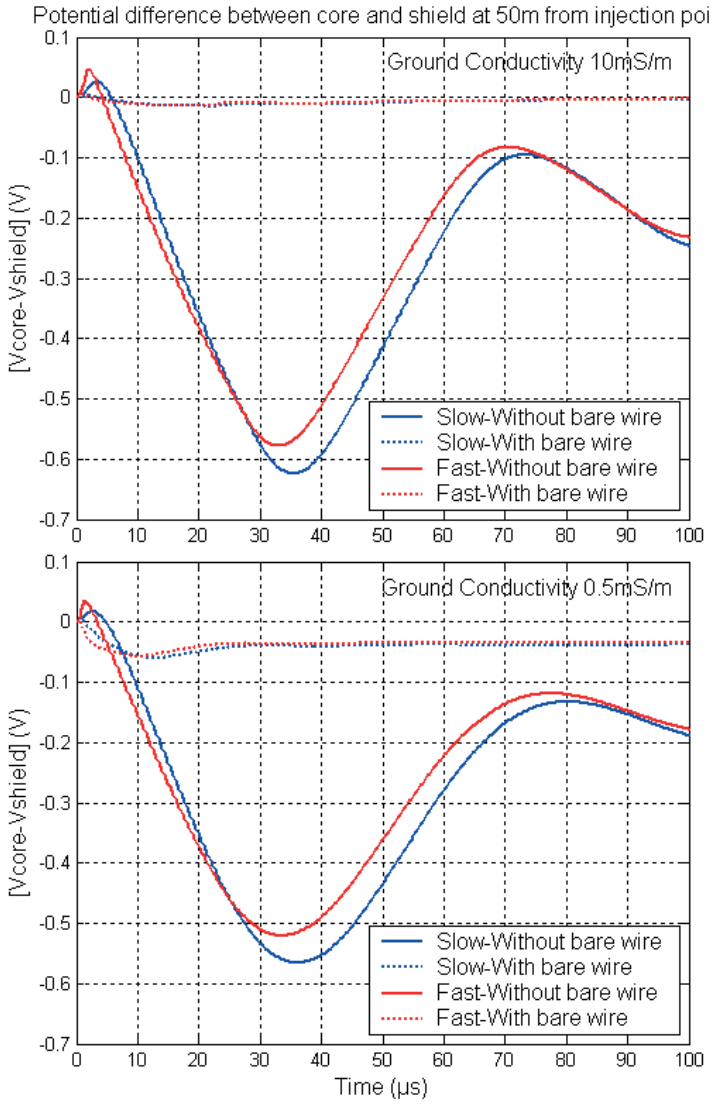

Figure 8.11: Example of 500m long cable showing the advantage of follow on earth wire for diverting the surge currents

8.5 Conclusions

In this Chapter it is shown in detail the coupling phenomena associated with the cable shields and armor for any multi-conductor cable configuration. The expressions for the impedance and admittance matrices are given based on the concept of tube impedances. A simple/approximate method of determining the capacitance and inductance matrix is shown. It is observed that shorting the unused pairs in the cable helps in reducing the induced voltages in cable core: this phenomenon requires further investigations. It is also shown how a follow on earth/bare wire running parallel to the cable helps in reducing the shield currents and the corresponding induced voltages. The model proposed in this Chapter is beneficial for the analysis of multi-conductor telecommunication cables in the future.

9. Transient response of booster transformer and track circuit equipment

Until now a lot has been dealt with the subject of transmission lines. Let's move a little away from that subject and have a closer look at some important equipment that are connected to overhead catenary wires, return conductors and the tracks of the Swedish railway system. Here, the examples considered are booster transformer as shown in Fig. 1.8, the rectifier unit as shown in Fig. 1.9 and the relay unit as shown in Fig. 1.10, and analyze their responses for lightning type of transients based on experiments and modeling. Note that all these devices exist on the MTLs system shown in Fig. 1.6 as some kind of termination on the lines. It is therefore necessary to model them so as to plug them appropriately into the transmission line equations. By doing so, more realistic estimates of voltages and currents on the MTLs system can be achieved for the future lightning interaction studies. Such devices have unique transfer functions, and estimating them is a difficult task. Consider booster transformers, they are very robust high voltage equipment and do not breakdown easily. They do not have any associated electronics with it. Since they are high withstand capacity equipment and they considerably affect the surge transfer characteristics, an attempt to model them is taken up in this Chapter. However, track circuits, such as relay and rectifier units, are fairly low voltage equipment and tend to breakdown at transient voltage levels of a few kV. Hence it is necessary mainly to know their breakdown voltages and failure modes, which can be tested in the laboratory. In this Chapter, let's first derive a circuit model for the booster transformer and later determine the withstand capabilities of relay and rectifier units.

9.1 Booster transformer ¶

Booster transformers are widely used in the traction power systems. They are used to collect the traction currents from the S-rail and return back to the feeding transformers via the return conductors. The use of booster transformer helps in reducing the rail currents to a minimum. Note that the booster transformer, nearest to the locomotive, responds in collecting the currents. The typ-

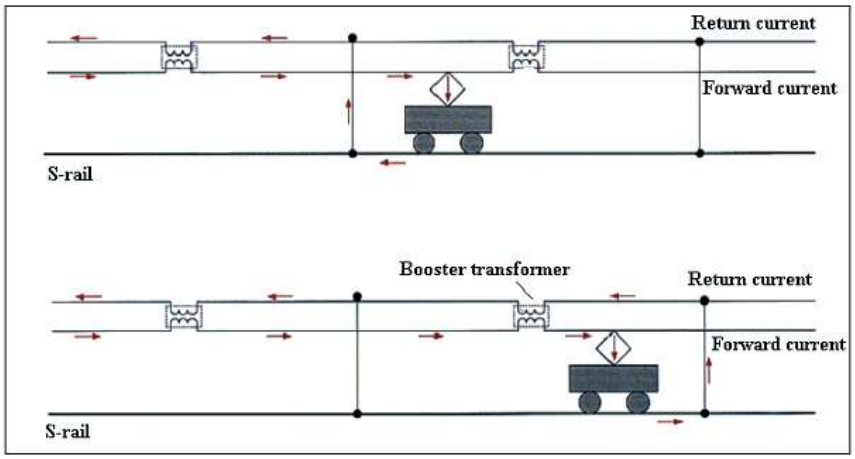

Figure 9.1: The booster transformer positions and connections

ical distance between two booster transformers is about $5km$. The schematic of the booster transformer connections with the contact wire and return conductors and the interconnection between the S-rail and the return conductors are shown in Fig. 9.1. Booster transformers are low impedance single-phase transformers with the ratio 1 : 1. The primary windings are connected in series with the contact wire and the secondary windings in series with the return conductors as shown in Fig. 9.1. The currents in the S-rail find the nearest S-rail-return conductor interconnection point. Note that there is always an interconnection between the S-rail and the return conductors as shown in Fig. 9.1 between two given booster transformers. This is necessary to maintain the proper current directions in the system.

9.1.1 Short circuit tests on booster transformer

In order to derive a simple model for the booster transformer, short circuit tests are to be performed. The experimental setup for the short circuit test on the transformer is shown in Fig. 9.2. An impulse voltage source is connected to the primary of the transformer with its secondary shorted. The voltage at the primary terminals, the current injected into the winding and the current in the secondary winding are shown in Fig. 9.3. The injected voltage impulse was a $1.2/50\mu s$ waveform. Due to the presence of a short circuit load the voltage tail decays faster. The current responses are very similar in the primary and secondary windings showing the dominance of 1 : 1 ratio. All the inter-turn winding capacitances, inductances, capacitance to tank, etc, become active leading to what are known as high frequency transformer models.

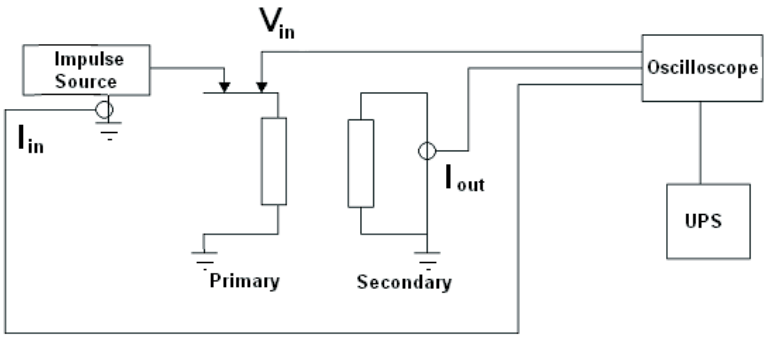

Figure 9.2: Schematic showing the setup for short circuit transformer tests

9.1.2 Terminal model for the booster transformer

Several researchers have worked to develop high frequency transformer models for three phase power distribution or generation or substation transformers. The author chose to adopt the model proposed by *Morched et al.* [136], called as the *RLC* model due to its simplicity. There exists other models in the literature. However, *Morched et al.* [136] classify them into two main categories known as detailed internal winding models and terminal models. In detailed internal winding models, a large network of capacitances and coupled inductances are derived from the complex electromagnetic field calculations and requires the physical layout and constructional details of the transformer, which is generally not available. In terminal models, the network of complex equivalent circuits is derived from the frequency and/or time domain characteristics at the terminals of the transformer. Thus the *RLC* model, implemented here, is a terminal model based on the concept of two-port network. *Høidalen* [137] has used an *RLCG* model (simple extension of *RLC* model) for modeling transformers in low voltage systems. *Manyahi* in [102] used a similar approach to model *XLPE* cable winding transformer.

The voltages and currents at the input and output ports are related through driving point admittances [138] as,

$$\begin{pmatrix} I_1 \\ I_2 \end{pmatrix} = \begin{pmatrix} y_{11} & y_{12} \\ y_{21} & y_{22} \end{pmatrix} \cdot \begin{pmatrix} V_1 \\ V_2 \end{pmatrix} \tag{9.1}$$

If a voltage source V_S is connected at the input port in series with a resistance R_S and the load at the output port is R_L, then the boundary conditions are given by (9.2).

$$V_2 = -R_L \cdot I_2 \tag{9.2a}$$

$$V_1 = V_S - R_S \cdot I_1 \tag{9.2b}$$

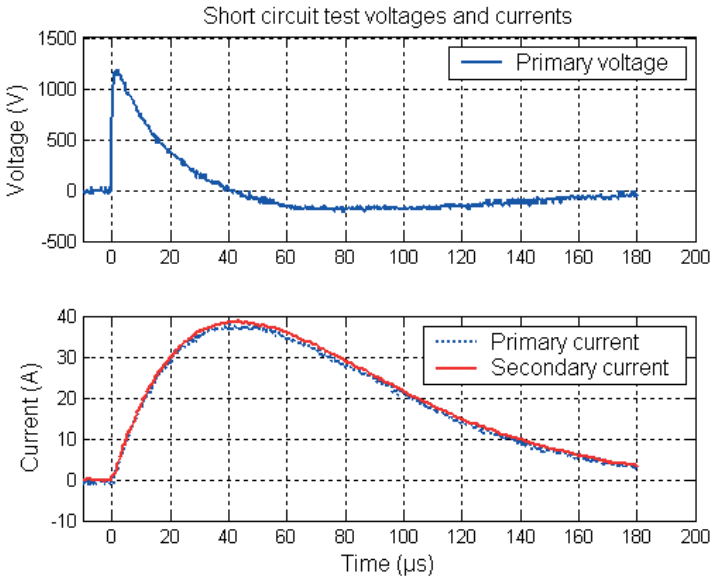

Figure 9.3: Experimentally measured currents and voltages at the primary and secondary of the booster transformer for voltage injection in the primary

Since short circuit tests based on (9.1) were made, one can get the driving point admittances. Note that the measured currents and voltages have to be *Fourier* transformed and the frequency response must be used for the determination of driving point impedances. Thus in *Laplace* domain the driving point admittances are given by (9.3).

$$y_{11}(s) = \left[\frac{I_1(s)}{V_1(s)}\right]_{V_2(s)=0} \tag{9.3a}$$

$$y_{22}(s) = \left[\frac{I_2(s)}{V_2(s)}\right]_{V_1(s)=0} \tag{9.3b}$$

$$y_{12}(s) = y_{21}(s) = \left[\frac{I_2(s)}{V_1(s)}\right]_{V_2(s)=0} \tag{9.3c}$$

Note that for the booster transformer, if the voltage were injected from the secondary side one gets the same behavior as shown in Fig. 9.3. The control system toolbox of *Matlab* was employed here for transfer function analysis [45]. The approximate driving admittance functions are (9.4).

$$y_{11}(s) = y_{22}(s) = \frac{(2.545\times10^{6})s^2 + (3.607\times10^{12})s + (2.205\times10^{17})}{443s^3 + (1.953\times10^{9})s^2 + (9.504\times10^{13})s + (1.163\times10^{18})} \tag{9.4a}$$

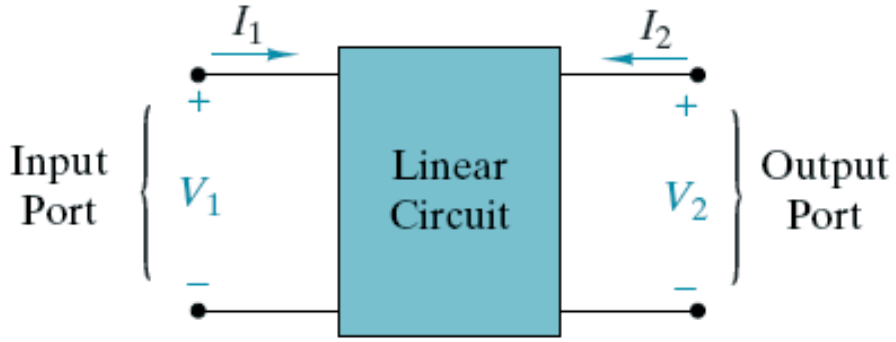

Figure 9.4: Schematic of a linear two-port network

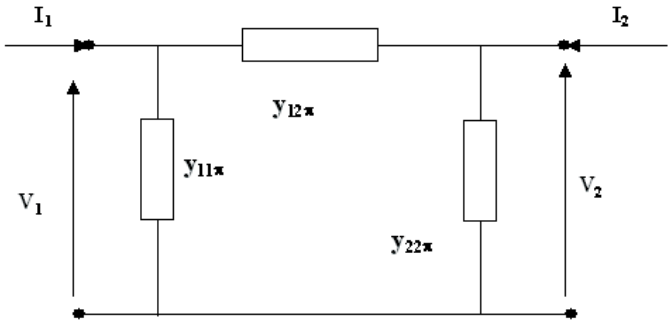

Figure 9.5: π model of the booster transformer used for modeling

$$y_{12}(s) = y_{21}(s) = \frac{(2.705 \times 10^6)s^2 + (3.833 \times 10^{12})s + (2.343 \times 10^{17})}{443s^3 + (1.953 \times 10^9)s^2 + (9.504 \times 10^{13})s + (1.163 \times 10^{18})} \tag{9.4b}$$

Fig. 9.5 shows the π model [138] representation of the transformer. It is possible to relate the π model admittances in Fig. 9.5 to the driving point admittances using the conditions given in (9.3).

$$y_{11} = y_{11\pi} + y_{12\pi} \tag{9.5a}$$

$$y_{22} = y_{22\pi} + y_{12\pi} \tag{9.5b}$$

$$y_{12} = y_{21} = -y_{12\pi} \tag{9.5c}$$

$$y_{11\pi} = y_{11} + y_{12} \tag{9.6a}$$

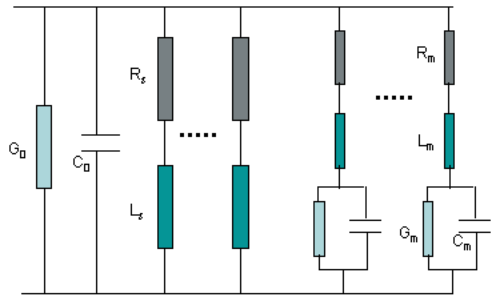

Figure 9.6: The RLCG model of the transformer adapted from [102, 136, 137]

$$y_{22\pi} = y_{22} + y_{12} \tag{9.6b}$$

$$y_{12\pi} = -y_{21} \tag{9.6c}$$

Thus, the π model admittance values and the corresponding *RLCG* model can be obtained if the circuit components can be extracted using vector-fitting method [69]. The method of extraction of circuit components is discussed in [136, 137, 102].

9.1.3 Fitting admittance functions

Note that interesting methods for fitting admittance functions are discussed by authors like *Gustavsen and Semlyen* [69], *Morched et al.* [136], *Høidalen* [137]. The orientation of all fitting techniques is in solving a least squares problem and then solving a *Jacobian* matrix as a result of *Newton's* method [137]. In vector fitting [69], the fitted response in pole and residue form is (9.7).

$$y_{fit}(s) = \sum_{i=1}^{n} \frac{c_i}{s - a_i} + s \cdot e + d \tag{9.7}$$

The series summation represents the well-known rational fitting in pole and residue form and n represents the number of poles (order of approximation). The additional terms e and d are negligible and can be neglected for the case treated here. The admittance matrix is realized in circuit form as in Fig. 9.6.

Note that if there are n poles out of which p_r are real poles and p_c represents the complex poles, then there will be p_r number of only *RL* branches and $\frac{p_c}{2}$ number of *RLCG* branches. Why one has only half the number of branches corresponding to the complex poles is because the other half of the complex poles are conjugates. This will be demonstrated by an example later. Comparing each branch of Fig. 9.6 to equation (9.7), the circuit components of each

branch, as derived by the author, is shown below.

$$G_0 = d \tag{9.8a}$$

$$C_0 = e \tag{9.8b}$$

Corresponding to all the p_r number of real poles, the parameters for *RL* branches are given by (9.9).

$$Y_s = \sum_{i=1}^{p_r} \frac{\frac{1}{L_{si}}}{s + \frac{R_{si}}{L_{si}}} = \sum_{i=1}^{p_r} \frac{c_i}{s - a_i} \tag{9.9}$$

The following equations give the parameters directly for the *RLCG* branch corresponding to half the number of complex poles.

$$Y_m = \sum_{i=1}^{\frac{p_c}{2}} \frac{\frac{s}{L_{mi}} + \frac{G_{mi}}{C_{mi} \cdot L_{mi}}}{s^2 + 2 \cdot s \cdot \Xi + (\Xi^2 + \varpi^2)} = \sum_{i=1}^{\frac{p_c}{2}} \frac{c_i}{s - a_i} + \frac{c_i^*}{s - a_i^*} \tag{9.10aa}$$

$$Y_m = \sum_{i=1}^{\frac{p_c}{2}} \frac{\frac{s}{L_{mi}} + \frac{G_{mi}}{C_{mi} \cdot L_{mi}}}{[s - (-\Xi - j\varpi)][s - (-\Xi + j\varpi)]} = \sum_{i=1}^{\frac{p_c}{2}} \frac{c_i[s - a_i^*] + c_i^*[s - a_i]}{[s - a_i][s - a_i^*]} \tag{9.10ab}$$

$$2\Xi = \frac{G_{mi}}{C_{mi}} + \frac{R_{mi}}{L_{mi}} \tag{9.10ba}$$

$$\Xi^2 + \varpi^2 = \frac{G_{mi}}{C_{mi}} \cdot \frac{R_{mi}}{L_{mi}} + \frac{1}{L_{mi} \cdot C_{mi}} \tag{9.10bb}$$

$$\Xi = -\Re[a_i] \tag{9.10bc}$$

$$\varpi = -\Im[a_i] \tag{9.10bd}$$

$$L_{mi} = \frac{1}{c_i + c_i^*} \tag{9.11a}$$

$$R_{mi} = L_{mi} \cdot [2\Xi + (c_i \cdot a_i^* + c_i^* \cdot a_i) \cdot L_{mi}] \tag{9.11b}$$

$$C_{mi} = \frac{1}{L_{mi}[\Xi^2 + \varpi^2 + R_{mi} \cdot (c_i \cdot a_i^* + c_i^* \cdot a_i)]} \tag{9.11c}$$

$$G_{mi} = -L_{mi} \cdot C_{mi} \cdot (c_i \cdot a_i^* + c_i^* \cdot a_i) \tag{9.11d}$$

Consider the admittance function y_{11} (9.4). This function was fitted using vec-

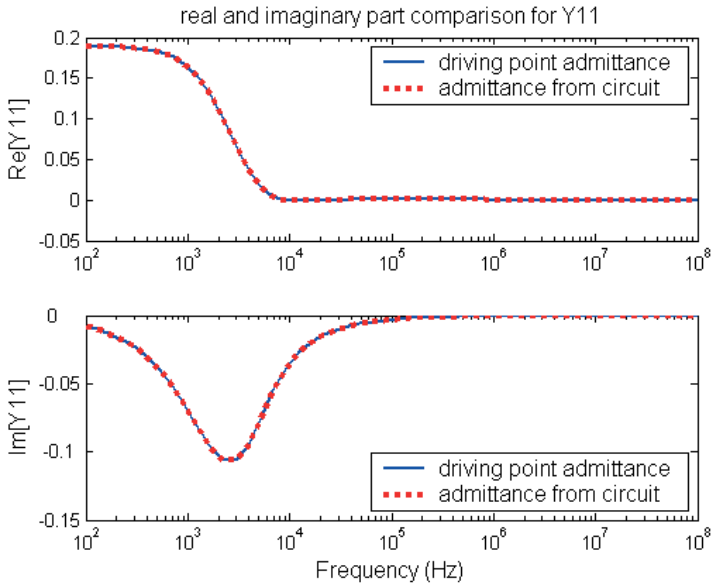

Figure 9.7: Comparison between the actual driving point admittance function and its corresponding circuit representation in frequency domain

tor fitting with three poles. This gave one real pole and two complex conjugate poles. Therefore, by the above analogy, there will be two branches: one *RL* branch and one *RLCG* branch. The values of the components for *RL* branch are, $R_{s1} = 1.1k\Omega$ and $L_{s1} = 0.25mH$, and for *RLCG* branch, it is $R_{m1} = -7.87\Omega$, $L_{m1} = 0.55mH$, $C_{m1} = 1.2\mu F$ and $G_{m1} = 75mS$. Now, the total admittance of this circuit should give the appropriate driving point admittance y_{11} (9.4), which is compared as shown in Fig. 9.7. It can be seen that the circuit representation indeed agrees well with the actual driving point admittance. Similarly, the circuit representation of y_{12} is for *RL* branch $R_{s1} = 1.0k\Omega$ and $L_{s1} = 0.24mH$, and for *RLCG* branch it is $R_{m1} = -7.4\Omega$, $L_{m1} = 0.52mH$, $C_{m1} = 1.3\mu F$ and $G_{m1} = 80mS$. The parameter values for $-y_{12}$ are the same as y_{12} but with corresponding negative signs[27]. Using this circuit representation in the π model as shown in Fig. 9.5 and using (9.6) one can solve the circuit under short circuit conditions for comparison with experiment in Fig. 9.3. The simulations are shown in Fig. 9.8. It has good correlation with the experiments. The author has performed the frequency domain calculations based on the assumption that the same primary measured voltage as in Fig. 9.3 is

[27] In [139, 140] it is mentioned that one can have negative circuit elements and that transient simulation software like ATP-EMTP [119, 122] accepts negative values for the components. The author has not investigated these aspects using any commercial software as the solution to the problem was carried out in frequency domain using Kirchoff's current law with the above said circuit components and later transformed to time domain using inverse Fourier transforms.

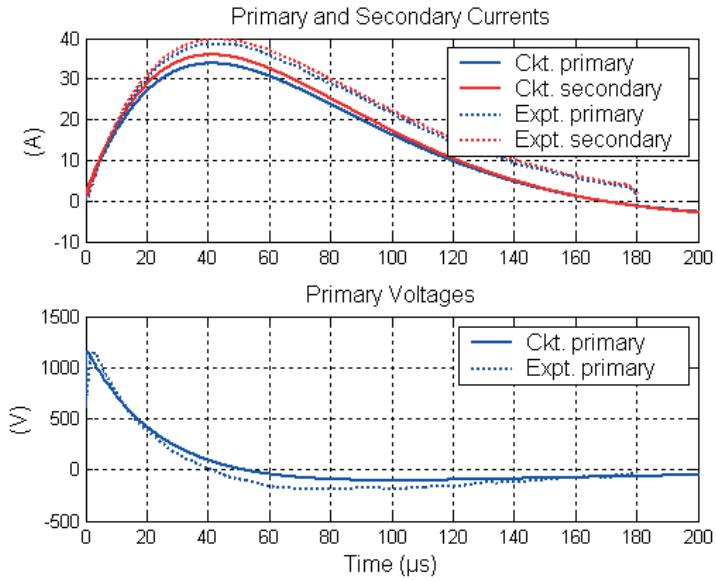

Figure 9.8: Comparison between the experiment and the simulations based on the π model circuit for the short circuit test

injected into the primary winding with negligible source resistance and the secondary is short-circuited. The generator is not modeled because it is the input output surge transfer through the transformer that is of interest for the moment. The circuit was solved using simple *Kirchoff's* current law. The short circuit conditions are to be modeled because it can be seen that in real situation the secondary terminals are shorted to the S-rail as shown in Fig. 9.1. Thus a simple circuit model has been developed for the booster transformer, which will be used in the MTLs model for future studies.

9.2 Track circuit withstand tests

From the simulations presented in Chapter-5 and based on simulations by *Theethayi et al.* [74 **Paper-C**] it is certain that there will be large common mode and differential mode voltages that would be appearing along and across the auxiliary power conductors and the rails/tracks. Therefore it becomes necessary to identify the failure modes of various equipments connected along the above ground lines and tracks. Here let's discuss the failure modes of two important devices connected to the tracks, they are the relay unit and the rectifier unit. Their connections to the tracks are shown in Fig. 1.2. Since the relay and rectifier sections are connected in parallel across the tracks, it was decided that the best way to test the system would be to test the two sections indepen-

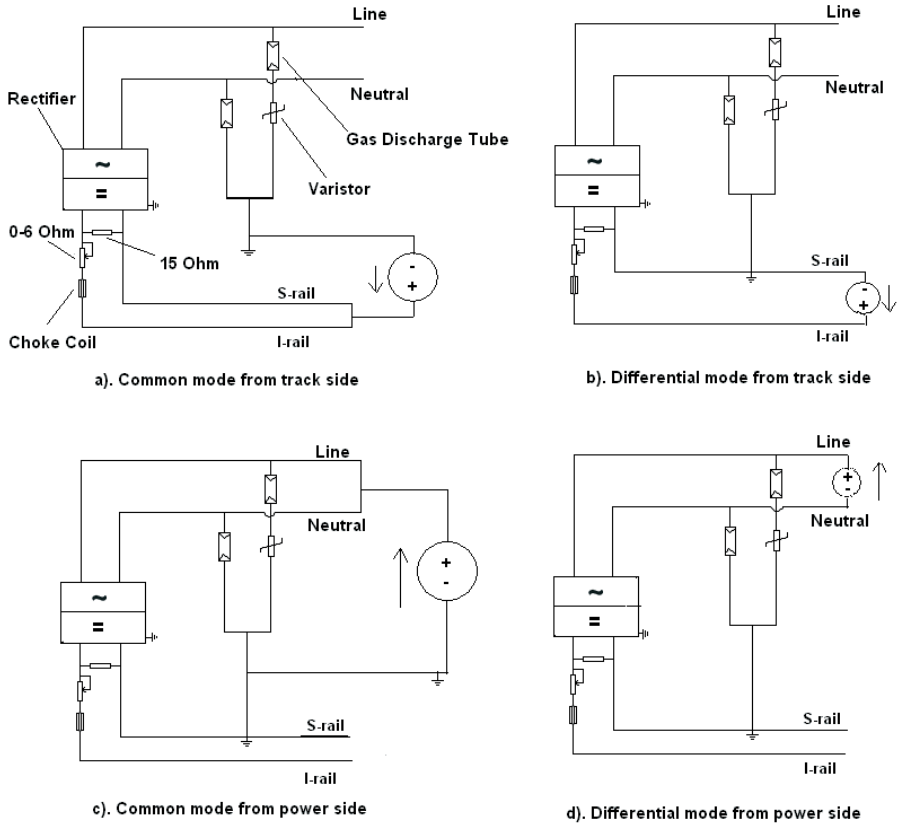

Figure 9.9: Configurations of tests conducted on the rectifier unit

dently and identify the most vulnerable components in each section that can fail.

The rectifier section, which has a power supply section, consisting of overvoltage protection, the rectifier unit, a choke coil and an adjustable resistor $(0-6\Omega)$, was tested and documented in a previous report [11]. The unit was subjected to lightning type of surges in four different configurations: a) Common mode from trackside, b) Differential mode from track side, c) Common mode from auxiliary power supply side and d) Differential mode from auxiliary power supply side. The schematic of the test configurations are shown in Fig. 9.9. The injected voltage was increased from $200V$ to $6kV$ using the *Schaffner* generator [135]. The existing protection design that consists of the series choke, gas discharge tubes, varistors and diodes, work very well with for the first three cases of the tested surge voltage of $1.2/50\mu s$ up to $6kV$. For the fourth case, that is differential mode injection from the auxiliary power side, the diodes failed at about $3kV$. Since an additional rectifier unit was available, series of impulse tests were again carried out and it was found that the diodes

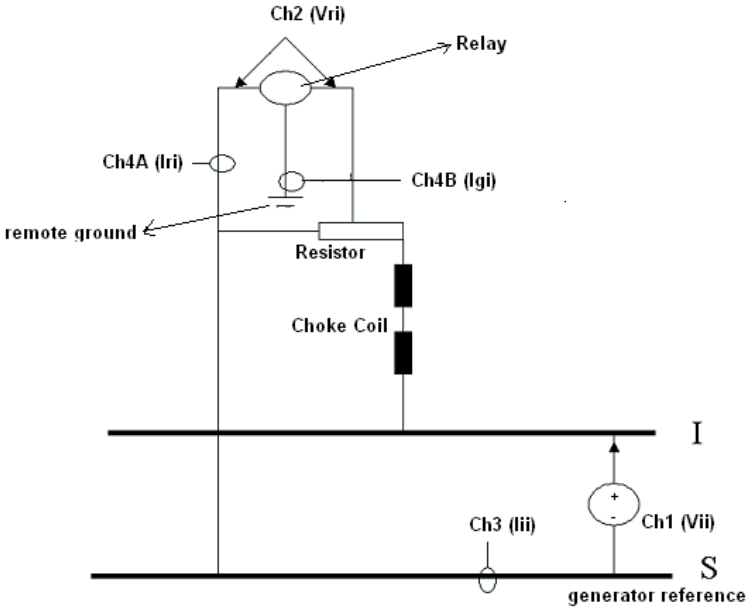

Figure 9.10: Experimental setup for the I-Rail injection tests for the relay

are most likely to breakdown. It was also observed that the diodes change their characteristics when the amplitude of the injected voltage or current impulses is increased. The damage/breakdown was usually found to occur at voltage levels of $3-3.5kV$. A breakdown on the capacitor was also observed. Thus the failure mode was identified. The most vulnerable components in the rectifier section were the diodes and the capacitor, both in the rectifier unit as shown in Fig. 1.9. Thus the levels of protection already existing in the rectifier section and power supply units are to be reconsidered with regard to lightning protection. Banverket authorities have observed that the rectifier units were getting damaged during thunderstorms.

The relay withstand tests were carried out in two stages: one is the injection to the I-Rail with respect to the S-rail as reference and the second is injection to the S-rail with I rail as the reference. This is because in the event of lightning strikes the S-rail and I-rail could be at different potentials [74 **Paper-C**]. Therefore it is necessary to simulate both environments in the laboratory. The connection for the I-Rail injection is shown in Fig. 9.10.

The voltages and currents were measured for the above said test for different injected voltage from $500V$ and $6kV$ respectively. The test was conducted in steps by increasing the injection voltage or current. No breakdown in any part of the device was observed for the I-Rail injection. The setup for the S-Rail injection is similar to Fig. 9.9 but the source is injected to the S-Rail. The injected voltage was increased from $500V$ in steps. No breakdown was observed

until $5kV$. When the voltage was increased above $6kV$, then a breakdown was observed. The test with this injection voltage was repeated more than twice and it was found that there was a breakdown all the time. The breakdown was happening either between the relay coil and the body or between the relay contacts and mounting rod. Thus the failure mode of the relay unit under the S-rail injection conditions in differential mode is between $5-6kV$. With higher voltage or current injections, there could be heavy arcing, which can burn the relay contacts and relay coils. Banverket have also observed these features in their damaged relays.

It is found that the choke coil, whose purpose is to filter out the AC traction current, offers a certain amount of protection to the relay unit from the high voltages inflicted on the system when transients enter via the I-rail. When the transient was applied to the S-rail, the relay unit is exposed to the full force of the impulse voltage. The relay unit is not robust enough to withstand transient currents of this magnitude. A possible solution might be to include an inductor between the S-rail and the relay unit, so that the unit has a similar level of protection from lightning transients irrespective of its port of entry.

9.3 Conclusions

In this Chapter it is shown in detail how various lumped devices on the MTLs system behave when transients enter them. A detailed booster transformer modeling is presented. It was found that for a voltage injection in the primary with secondary shorted, the transformer still shows a $1:1$ behavior under transient conditions. A simple π model of the transformer and its circuit parameter extraction is presented. The failure modes of the rectifier and relay units of the track circuits have been identified. It is seen that the differential mode lightning induced voltages from the power side to the rectifier unit can cause damage to the diodes and capacitor of the rectifier unit and hence, the existing protection scheme in the rectifier unit has to be reconsidered. The relay unit has the only protection through a choke coil, which is not sufficient if the S-rail potentials due to lightning induced voltages exceed $6kV$. Additional protection for the relay unit has to the considered. It is very probable that induced voltages can be higher on the rails due to large contribution from the horizontal component from lightning electric and magnetic fields as shown in the Chapter-5.

10. My thesis: What else?

One may wonder towards the end of this thesis as to what is the use of simulations and modeling presented in the thesis or in various other literatures, which still has the scope of application in the kind of problem dealt in this thesis? The author had personally observed and experienced, that many interesting and useful works by various researchers with regard to simulation, theory and mathematical models, very much suitable for industrial application, are gathering dust on university bookshelves and/or perhaps hidden in the archives. Therefore, a mutually beneficial relationship should be developed between the academy and the industry. The strength of such a relationship depends on the bond of togetherness between the engineers of the industry and the researchers of the university.

The Division for Electricity and Lightning Research of Uppsala university has been quiet successful in establishing such a feeling of togetherness with research partners like Banverket and Bombardier Transportation on studying EMC problems of railway industry. The EMC group at the division started a focused development of a simulation software for engineers of the railway industry [141 **Paper-L**]. It is hoped that the software could assist engineers in solving problems related to lightning protection and EMC to a great extent, which they might encounter in the field. The heart of the software is a computer simulation program that will utilize the state of the art knowledge in lightning protection and EMC. Mathematical models for the behavior of complex distributed electrical systems when subjected to lightning transients and other electromagnetic interferences, are required for this software.

This thesis marks the beginning of such a software development. However, making versatile software is always dependant on models, its validity and development and, more importantly, the knowledge of the systems being studied. All these will be a result of the knowledge and experience of Uppsala University and the associated research partners in lightning protection and EMC research.

Salient features of the proposed software are,

- Modular approach - The railway system is broken down into different sub-systems. For example, above the earth conductor system that includes catenery, tracks, power lines etc., train positioning and signaling circuits etc. Model for each module will be tested experimentally. As the software

develops, more modules can be included and updated.

- Clickable interface screen - An engineer can see schematic diagrams of the system on a screen and control the simulation using mouse and keyboard. The main simulation window of the present version of the software is shown in Fig. 10.1(top window).
- Details of models at different levels - To start with there will be an overall schematic diagram of the system. Behind this there will be detailed models of the subsystem, which can be accessed by a few clicks on the mouse. If required, detailed models of basic components can be included. For example, models for EMC characteristics of different types of cables, different types of surge protection components, etc.
- Simulation in time domain (for wide frequency range) - Non-linearity such as action of surge arresters and insulator flashovers can be easily included. Provisions will be made for simulation in frequency domain for some systems and there will be smooth integration of both types of simulations in the software.
- Facility to include documentation - On-line documentation in the form of guidelines for using the model, recommendations for interpreting simulation results and solving the EMC problem, internal standards, general articles for providing information etc.
- Facility for future improvements - The software and computer programs will be structured in such a way that future improvements to the software can be done with reasonable efforts. Additional modules, representing new sub-systems can be added.
- Remote simulation via internet - This feature is based on Client - Server approach. The server can be at any convenient place and the client (engineers) can get access to the software from his work place. The Client - Server approach employed in this program is shown in Fig. 10.1 (bottom sketch).
- Some of the inputs to the software - Location of lightning (or lightning electromagnetic fields, current amplitudes and their wave shapes), any other EMI signal and the position of its source and editing of the system geometry like heights and lengths and inputting material properties. The windows for data entry are shown in 10.2.
- Output from the model - Currents and voltages at any terminal in the system included in the model, warnings about components exceeding its rated capacity, electric and magnetic fields at different distances from tracks, recommendation on solutions to EMC problems through on-line documentation. The instruments and a typical result window are shown in Fig. 10.3.
- User-friendly interface and improvement - The software will have a user-friendly interface and documentation on its use will be provided. The software and the underlying simulation programs will be continuously de-

bugged, improved and checked for its validity.

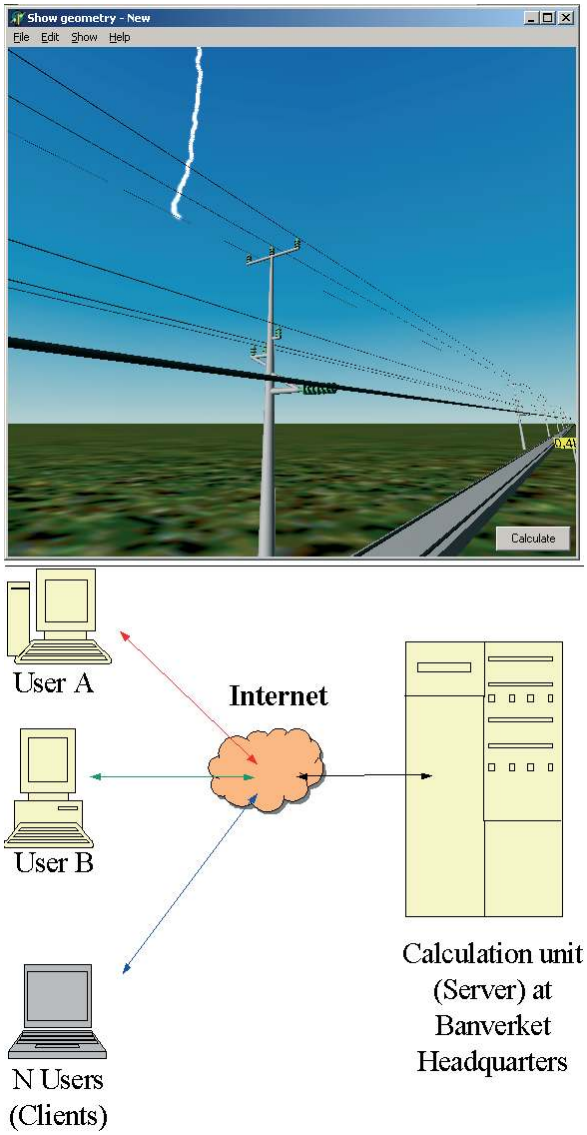

Figure 10.1: Client user interface window (top) and a typical client-server system

It should be noted that the present version of the software has included only some of the above mentioned features such as surge propagation in the conductor system, with ground losses, insulator flashovers and soil ionization and interconnections between conductors. As mentioned earlier it is yet to grow and more and more features will be included and updated in the future.

The scope of this thesis is not large enough to include simulations and ex-

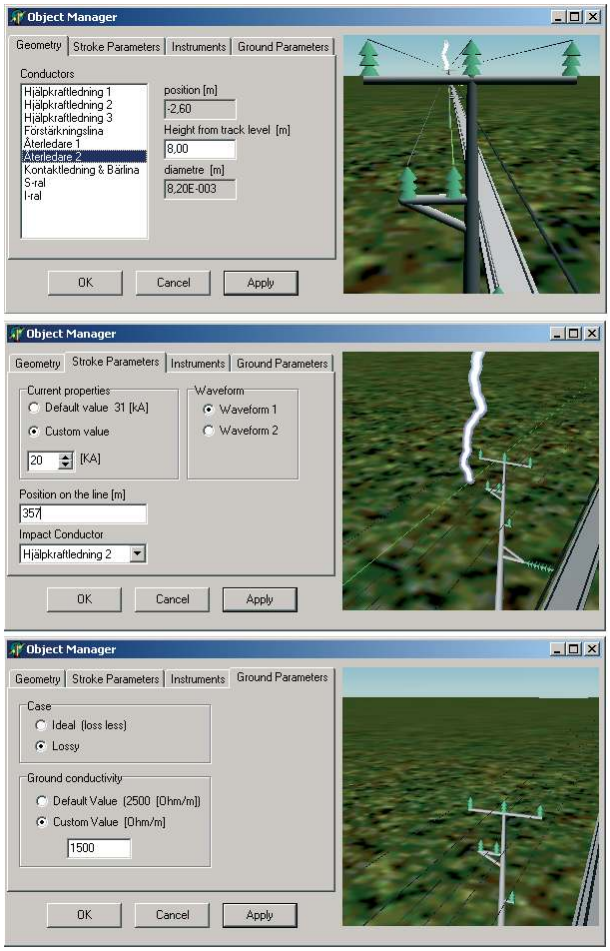

Figure 10.2: Edit geometry window, location and positioning the stroke, ground properties

periments for several other important problems, which indeed would form a package for future research. They are too many to explain here. A few of them are given below:

- Is earth truly homogeneous? How sure one can be about the multi-layer earth even though *Sunde* [58] mentions that because of the poor knowledge of soil structure, one could commit an error $> 20\%$? If the inhomogenity in the soil were correctly determined, how much would it effect the various ground impedance and admittance expressions? More importantly, can one prove them experimentally?
- What would be the effect of various static devices, like track circuits, booster transformers, auto transformers, feeding transformers, step down transformers at auxiliary power, cable termination to technical houses

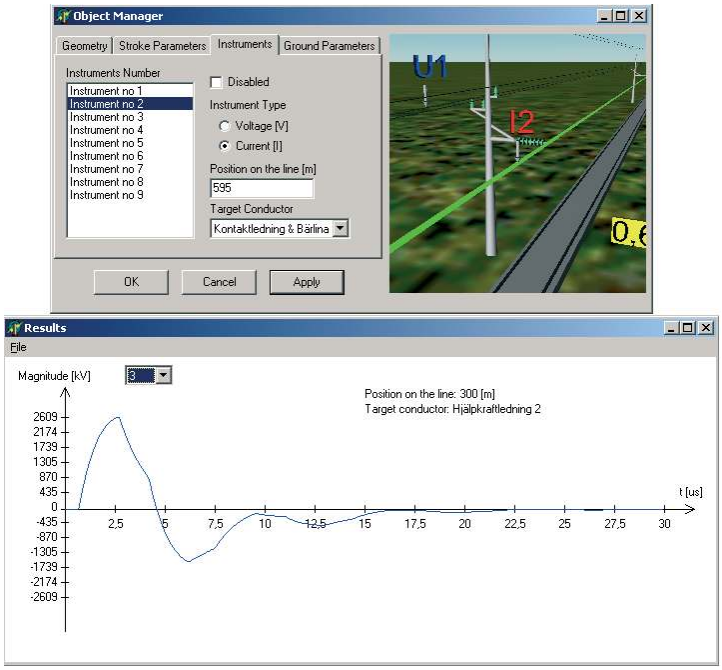

Figure 10.3: The window showing the instruments and a typical simulation result

at auxiliary power, etc. connected to the MTLs in the surge propagation characteristics?

- How are the track Balises affected in the event of lightning strikes?
- Is the existing surge protection design sufficient for the track circuits, power supply systems in the technical houses feeding telephone networks?
- How do various system grounds and references oscillate in potentials in the event of lightning strikes and also under normal operations?
- How valid are the models for non-linear phenomena like insulator flashover and soil ionization at the pole footing? Can these be validated using experiments? How do polluted or damaged insulators influence the flashover mechanism? How does the soil ionization in the grounding conductors causes variations in the local and S-rail potentials. How does arcing between the conductors, like tracks and other close overhead conductors behave if large differential voltages appear between them?
- How is the pulse propagation in buried cables are affected if the communication equipments and terminations are incorporated? How effective are the surge protection for the communication equipments?
- Can an outage analysis be carried out coupling the lightning statistics and system configurations? This perhaps will give a broader picture of the threat levels within the railway systems.

To conclude, asking questions like **how?** and **what?** will lead you (if you do not approximate things too much) to another important question, **why?**. The moment you ask **why?**, you will be led to a very important person whom the author has mentioned in the beginning of this thesis, and he is *James Clarke Maxwell*. By answering the question **why?**, you are partly into the answers to **how?** and **what?**.

11. Sammanfattning

Denna avhandling behandlar problemet med elektromagnetisk kompabilitet (EMC) för distribuerade elektriska nätverk, med fokus på elektromagnetisk interferens orsakad av blixtnedslag i elektriska nätet för den elektrifierade järnvägen. Järnvägen har utvecklats kraftigt under åren och försöker utnyttja framsteg gjorda inom integrerade kretsar, telekommunikation och trådlös teknologi samt kontrollsystem. Ett problem som uppstår är att dessa moderna system klarar mindre påkänningar än de elektromekaniska apparater som de ersatt. Därför måste säkerhetsaspekter och tillgängligheten för dessa moderna system undersökas. I de sektioner utav nätverken som har uppgraderats med modern utrustning är det vanligt med problem från transienter och EMC, orsakade utav otillräcklig skydd mot Blixnedslag. Åskoväder är ett oförutsägbart vanligt förekommande naturfenomen, som orsakar kända problem med transienter. Konsekvenserna utav dessa åsktransienter i järnvägsnätet är skador på systemen som kontrollerar tågens färd och därför orsakar långa förseningar. Det är därför av vikt att förstå växelverkan, och associerade kopplingsmekanismer, för hur de moderna kontrollsystemen påverkas av åsktransienter. Det är också viktigt att utveckla beräkningsmodeller som kan simulera hur olika delar av järnvägsnätet påverkas av blixtnedslag för att bedöma olika system för åskskydd samt ta hänsyn till EMC. En del utav modellerandet kan äga rum genom utförandet av kontrollerade experiment. Denna avhandling behandlar växelverkan mellan åsknedslag och den elektrifierade järnvägen. Det svenska järnvägsnätet valdes att studeras.

I ledningsnätet för järnvägen är både räls och luftledare utsatta för starka elektromagnetiska fält från de inducerade spänningar och strömmar som uppstår från ett blixtnedslag. Liknande allvarliga fenomen förekommer också när luftledaren träffas direkt av ett blixtnedslag, något som är vanligt förekommande. Alla elektriska nätverk på och över marken modelleras som överföringsledare med många ledare för att kunna beräkna inducerade spänningar och strömmar och hur dessa överförs i systemet. I distribuerade nätverk för utomhusbruk, såsom järnvägsnätet, är de elektriska parametrarna för den omkringliggande jordarten viktig för generering och överföring utav elektromagnetiska transienter. De elektriska egenskaperna hos jordarten för de svenska förhållandena varierar från 0.01 S/m till 0.0001 S/m i olika delar av landet. Föregående modeller som uppställts för att studera jorden

i förhållande till transienter i kraftledningsnätet är inte direkt tillämpbara på den låga konduktiviteten och stora variation i höjd på kraftledarna som gäller för Svenska förhållanden. Därför har befintliga modeller för jorden modifierats för att gälla för ett stort spann av konduktiviteter, så låg som 0.0001 S/m, samt för ett brett spektra av frekvenser mellan ett fåtal hertz till några tiotal megahertz. Vidare har modellerna även modifierat för att ta hänsyn till ledningshöjder på mindre än en meter till ett flertal meter. En detaljstudie har utförts för hur olika jordkonduktiviteter, laster samt ledningshöjder påverkar åskinducerade pulser vid direkta och indirekta åsknedslag. Luftledarna i järnvägsnätet är stadgade med hjälp av isolatorer på stolparna. För att studera indirekta effekter utav ett blixtnedslag i järnvägsnätet har en modell som kan förutsäga avlägsna elektriska fält jämförbara med experimentella observationer även framtagits.

Det finns fotografier som registrerat långa ytljusbågar och ljusbågar som penetrerar marken. Eftersom ledningssystemet för järnvägen är högst sammankopplat så kommer det att uppstå potential skillnader mellan olika jordpunkter i nätet. Både ljusbågar och potentialskillnader kommer att påverka nedgrävda närliggande telekommunikation och signalkablar genom inducerade strömmar, då kabelskärmningen kan leda stora strömmar och i sin tur påverka de inre ledarna i kabeln. Dessa störningar kan propagera över avsevärda avstånd. Om dessa inducerade effekter är av större magnitud kan de påverka all kommunikations och signalutrustning anslutna till kabeln. Vidare så kan problem uppstå om spänningen mellan innerledare och kanelskärmen är större än den fältstyrka som isolationen kan tåla. För att förstå hur spänningar och strömmar propagerar i skärmade och oskärmade kablar har en detaljerad undersökning av vågutbredning i nedgrävda kablar med jordåterledare utförts. Förenklade och giltiga impedansuttryck som är beräkningsmässigt effektiva har föreslagits för både nedgrävda kablar och kablar som ligger på marken. En modell för kopplingen genom kabelskärmen för kablar med flera innerledare föreslås. Genom att använda den uppställda modellen för nakna och isolerade kablar, samt för kablar med flera innerledare och flera kabelskärmar, har några viktiga slutsatser och rekommendationer kunnat dras för hur inducerade fenomen kan begränsas eller undvikas. Vi anser att den uppställda kabelmodellen kommer att vara användbar för att analysera hur blixtnedslag interagerar med de komplexa telekablar som används vid järnvägen.

I järnvägsnätet finns ett stort antal ihopkopplad utrustning ansluten till antingen luftledare, kablar eller rälsen. I denna avhandling har felfall för två viktiga komponenter som används för tågets position och signalsystem samt relä och likriktarenheter för åsktransienter undersökts. Det har observerats att denna utrustning fungerar dåligt eller går sönder då transienter med spänningsfall på ett par kV uppstår över polerna. Därför föreslås att transientskyddet i dessa anläggningar bör modifieras. Det finns ett antal transformatorer

som används för drivningen utav tågsystemen. En av dem är den så kallade sugtransformatorn, som är installerad med ca 5 km mellanrum och ansluten mellan kontaktledningen och återledaren. Dessa transformatorer modifierar pulspropageringens karakteristika i luftledarna och därför har en högfrekvent kretsmodell för dessa transformatorer utvecklats. Denna modell kan komma att kopplas till luftledaren för ett mer realistiskt studium av åskskydd.

För första gången har experiment utförts på åskinducerade transienter hos den svenska järnvägens teknikhus. Metoden för att utföra och instrumentera experimentet beskrivs samt hur nedslaget korrelerar med de inducerade strömmarna. Dessa experiment kommer vara till stor hjälp för att verifiera beräkningsmodellerna. Data framtaget vid denna studie har använts för att ta fram en approximativ formel för att beräkna den inducerade spänningen mellan innerledare och nolledaren i förhållande till kraftförsörjningen i järnvägens relähus/teknikhus beroende på position och strömmens amplitud i nedslaget.

De framtagna simuleringsmodellerna kodas i användarvänliga program för att användas av ingenjörer vid järnvägen för att undersöka EMC-problem orsakade av blixtnedslag.

Acknowledgments

A tradition of over five centuries and a quarter, educational and research support, liberal attitude, national and international scientific and engineering research works, collaboration with industry: the Uppsala University has the right atmosphere for research students. The eight Nobel Laureates the University has produced inspire the students towards the highest achievement. Privileged am I that I could do my doctoral studies in this University.

For my thesis I worked under the guidance of Prof. Rajeev Thottappillil. The hallmark of his guidance is freedom - the freedom of thought and the freedom of work - with a clear focus on achieving the objective within the given time. I acknowledge to have gained a lot during the four years of our association. In fact, he has transformed me to be independent - a greatly desired quality for a researcher. I am indebted to Prof. Thottappillil.

Working very closely with Prof. Vernon Cooray in the area of lightning protection and return stroke modeling has led me to a better understanding of the subject. Discussion or work, he always leaves me more enlightened. His personality, on the one hand, and his research work, on the other, has given me the confidence to venture into unexplored areas of knowledge. Indeed I am grateful to Prof Cooray.

For my work, I have been benefited by the several rounds of technical discussions with Prof. Viktor Scuka. I am grateful to him.

I thank Prof. Mats Leijon, Chair, Division for Electricity and Lightning Research of the Uppsala University for all his encouragement and support during my studies.

To me Prof. Farhad Rachidi is a special person. Across time and space, he has been an asylum for technical intricacies on wave propagation in transmission systems. I recollect, with profound gratitude, our discussions and interactions on the sidelines of meetings and conferences. I am grateful to him for the encouragement and support he has given me, unstintingly. I also appreciate his critical review of my thesis.

I take this opportunity to thank Dr. Yaqing Liu in a special way for all the interesting discussions, experimental investigations and collaborative works carried out together.

I thank Mr. Raul Montano for his technical help and discussions in experiments for my work.

This work would not have been possible but for the financial support of the Swedish National Rail Administration (Banverket). I would like to thank Mr. Per Anders Lindeberg, Mr. Ulf Hellström, Mr. Roger Bystrom, Mr. Peter Deutschmann, Mr. Bertil Artelius and Mr. Malcolm Lundgren of Banverket for their interest, participation and support all through.

My thanks are also due to Bombardier Transportation for their support and interest in the project. Special thanks to Dr. Michael Zitnik and Mr. Georg Bohlin of Bombardier Transportation for several discussions on EMC practices in the Railways.

I thank Mr. Göran Unden of FMV, Dr. Mats Backstrom of FOI, Prof. Jan Carlsson of SP and Dr. Torbjörn Karlsson of EMICON for their useful discussions on EMC issues and practices.

I would like to express my sincere thanks to Prof. Goran Andersson, Prof. Vladimir Rakov, Prof. Marcos Rubinstein, Prof. Carlo Alberto Nucci, Dr. Gerhard Diendorfer, Dr. Takatoshi Shindo, Dr. Pierre Zweiacker, Dr. Anders Larsson, Prof. Rajeev Ahuja and Dr. Thomas Cease, whose advice I have been benefited from.

My work here was spread over a period of four years, 2001-2005. I made friends with many. They have been very supportive to me in more ways than one. My thanks are due to them: Mr. Marley Becerra, Mr. Daniel Månsson (also acknowledged for his timely help with the Swedish translations) and Mr. Surajit Midya for all the wonderful time I had with them; Mr. Paul Deglaire, Ms. Natalia Savenko and Mr. Adam Lindblom, my neighbors at work, for tolerating my noisy discussions; Ms. Gunnel Ivarsson, who helped me with various administrative issues; Mr. Ulf Ring for helping me in fixing up certain experimental setups; Mr. Thomas Götschl for all the technical support he gave me for the computer software and hardware installations; Dr. Marcus Berg and Mr. Mahbubur Rahman for interesting technical discussions.

I had the privilege of being master's thesis supervisor of Mr. Yves Gilliaret, Mr. Christian Nanchen, Mr. Tegene Yirdaw, Mr. Stephen Burt and Mr. Ziya Mazloom. I thank all of them for working with me in the area of EMC and lightning protection and appreciate their good work.

I thank my friends Dr. Abraham Rubinstein, Dr. Jose Bermudez, Mr. Davide Pavanello, Ms. Ana Vukicevic, Mr. Mahesh Edirisinghe, Mr. Prasanna Liyanage, Prof. Dragan Poljak, Mr. Vicko Doric and Prof. Fransisco Roman, whom I have met during my studies and had a lot of fun together.

My thanks are also due to my coffee friends Dr. Hans Bernhoff, Dr. Olov Ågren, Dr. Jan Isberg, Dr. Urban Lundin (also acknowledged for his timely help with the Swedish translations), Dr. Jan Sundberg, Ms. Karin Thorburn, Ms. Karin Nilsson, Ms. Sandra Eriksson, Mr. Erik Segergren, Mr. Björn Bolund, Mr. Oskar Danielsson, Mr. Mikael Eriksson, Mr. Andreas Solum, Mr. Richard Perers, Mr. Ludvig Lundström, Mr. Olle Svensson and all other mem-

bers of the division.

I thank my friend Dr. Mose Akyuz and the members of his family for all the beautiful time I had spent with them.

I would like to thank, in a special way, my friends Dr. Pradeep Kumar, Dr. Bharath Bhikkaji and Mr. Gopal Datta - the first three Indians I met in Uppsala. Being with them was an experience I cherish to remember. I also thank my other friends Dr. Mahalingam, Mr. Varghese Oommen, Ms. Jharna Barman, Dr. Kiran Mantripragada, Mr. Puneet Shrivastava, Dr. Chandrasekhar Kanduri and others who have made me feel at home.

By completing this work, I take yet another step towards fulfilling the expectations of my mother, father, uncle, brother and my dear sister Nisha. I thank them for supporting me in all that I do.

References

[1] Hill R. J., Carpenter D. C. and Tasar T., "Rail track admittance, earth leakage effects and track circuit operation," *Proceedings of IEEE/ASME joint Railroad Conference*, 1989, pp. 55-62.

[2] Carpenter D. C. and Hill R. J., "The effects of magnetic saturation, hysteresis and eddy currents on rail track impedance," *Proceedings of IEEE/ASME joint Railroad Conference*, 1989, pp. 73-79.

[3] Carpenter D. C. and Hill R. J., "FEM applied to track electrical impedance and adjacent track crosstalk modeling," *Proceedings of IEEE/ASME joint Railroad Conference*, 1991, pp. 87-95.

[4] Hill R. J. and Carpenter D. C., "Rail track distributed transmission line impedance and admittance: theoretical modeling and experimental results," *IEEE Transactions on Vehicular Technology*, Vol. 42, No. 2, 1993, pp. 225-241.

[5] Carson J. R., "Wave propagation in overhead wires with ground return," *Bell Systems Technical Journal*, Vol. 5, 1926, pp. 539-556.

[6] Carpenter D. C. and Hill R. J., "Railroad track electrical impedance and adjacent track crosstalk modeling using the finite element method of electromagnetic system analysis," *IEEE Transactions on Vehicular Technology*, Vol. 42, No. 4, 1993, pp. 555-562.

[7] Hill R. J., Brillante S., De Souza C. R. and Leonard P. J., "Electrical material data for railway track transmission line parameter studies," *IEE Proceedings on Electrical Power Applications*, Vol. 146, No.1, 1999, pp. 60-68.

[8] Ferrari P. and Pozzobon P., "Railway lines models for impedance evaluation," *8th international IEEE/PES and NTUA joint conference on harmonics and quality of power, ICHQP 98*, Athens, 1998, pp. 641-646.

[9] Equiluz. R. P., David. M. P., Roboam X. and Fornel B. D., "Pantograph detachment perturbation on a railway traction system," *Eighth International Conference on Power Electronics and Variable Speed Drives, London*, 2000, IEE Conference Publication No. 475, pp. 437-442.

[10] Equiluz. R. P., David. M. P., Roboam X. and Fornel B. D., "Dead time effect in railway traction system," *Proceedings of the IEEE International Symposium on Industrial Electronics, Puebla*, 2000, Vol. 1, pp. 151-156.

[11] "Lightning protection of the Swedish railway network, final technical report," *Division for Electricity and Lightning Research, Department of Engineering Sciences, Uppsala University*, Banverket project 2001-000282, 2001-03.

[12] Paul C. R., "*Analysis of Multiconductor Transmission Lines,*" John Wiley and Sons Incorporation, 1994.

[13] Stevenson W. D., "*Elements of Power system analysis,*" McGraw-Hill Book Company, 1988.

[14] Lagestam L., "*Kabelsystem - Huvud-/mellanortskabel för Banverkets telenät, Elektriska kvalitetskrav på par-och fyrskruskabel,*" BVF 518.1101, BVF 518.1002, Banverket, 2001.

[15] Personal communication with Lindeberg P. A. and Hellström U. of Banverket, 2002.

[16] Bulund A., Hellström U. and Varju G., "Changing from booster transformer system to autotransformer system in the Kiruna-Råtsi-Svappavaara line in Sweden," *EMC York International Conference and Exhibition, EMC York*, 2004 Presentations for download.

[17] EMMA Hand book (Elektromagnetisk miljö anvädarhandbok), Försvarets MaterielVerk (FMV), 2002.

[18] Thottappillil R., "*A review of lightning with emphasis on the properties important for the protection of ground based assets,*" document prepared for Försvarets MaterielVerk (FMV) under contract, 2000-2001.

[19] Thottappillil R., "Electromagnetic pulse environment of cloud-to-ground lightning for EMC studies," *IEEE Transactions on Electromagnetic Compatibility*, Vol. 44, No. 1, 2002, pp. 203-213.

[20] Cooray V. (Editor), "*The Lightning Flash,*" IEE power series; 34, published by the IEE, London, 2003.

[21] Rakov V. A. and Uman M. A., "*Lightning physics and effects,*" Cambridge University press, 2003.

[22] Cooray V., "Horizontal fields generated by return strokes," *Radio Science*, Vol. 27, 1992, pp. 529-537.

[23] Golde R. H. (Editor), "Lightning," Academic Press, 1977.

[24] Baldo G., "Lightning Protection and the Physics of Discharge," *Proceedings of 11th International Symposium on High Voltage Engineering, London*, 1999, Conference Publication No. 467, Paper No. 2.169.S0.

[25] Horvath T., "*Computation of Lightning Protection,*" Research Studies Press Limited, John Wiley and Sons Incorporation, 1991.

[26] Working Group on Lightning Performance of Transmission lines, "A Simplified Method for Estimating the Performance of Transmission Lines," *IEEE Transactions on Power Apparatus and Systems*, Vol. 104, No. 4, 1985, pp. 919-932.

[27] Rizk F., "Modeling of transmission line exposure to lightning strokes," *IEEE Transactions on Power Delivery*, Vol. 5, 1990, pp. 1983-1997.

[28] Personal communication with Zitnik M. of Bombardier Transportation, Stockholm (Signal), 2004.

[29] Personal communication with Lindeberg P. A. and Hellström U. of Banverket, 2003.

[30] Eriksson A. J., "Lightning and tall structures," *Transactions of South African IEE*, No. 69, 1978a, pp. 238-252.

[31] Rachidi F., "Formulation of the Field-to-Transmission Line Coupling Equations in Terms of Magnetic Excitation Field," *IEEE Transactions on Electromagnetic Compatibility*, Vol. 35, No. 3, 1993, pp. 404-407.

[32] Nucci C. A. and Rachidi F., "On the Contribution of the Electromagnetic Field Components in Field-to-Transmission Line Interaction," *IEEE Transactions on Electromagnetic Compatibility*, Vol. 37, No. 4, 1995, pp. 505-508.

[33] Agrawal A. K., Price H. J. and Gurbaxani S., "Transient response of a multiconductor transmission line excited by a nonuniform electromagnetic field," *IEEE Transactions on Electromagnetic Compatibility*, Vol. 22, No. 2, 1980, pp. 119-129.

[34] Taylor C. D., Sattenvhite R. S. and Harrison C. W., "The response of a terminated two-wire transmission line excited by a nonuniform electromagnetic field," *IEEE Transactions on Antennas and Propagation*, Vol. 13, No. 6, 1965, pp. 987-989.

[35] Technical Council of the IEEE Power Engineering Society "IEEE guide for the application of insulation coordination," IEEE Std. 1313.2, 1999.

[36] Sengupta D. L. and Sarkar T. K., "Maxwell, Hertz, the Maxwellians and the early history of electromagnetic waves," *IEEE Antennas and Propagation magazine*, Vol. 45, No. 2, 2003, pp. 13-19.

[37] Unz H., "Oliver Heaviside (1850-1925)," *IEEE Transactions on Education*, 1963, pp. 30-33.

[38] Lee T. H., "*Planar Microwave Engineering - A practical guide to theory, measurements and circuits,*" Cambridge University press, 2004.

[39] Wangsness R. K., "*Electromagnetic Fields,*" John Wiley and Sons Incorporation, 1986.

[40] Paul C. R. and Naser S. A., "*Introduction to Electromagnetic Fields,*" McGraw-Hill, 1987.

[41] Paul C. R., "*Introduction to Electromagnetic Compatibility,*" John Wiley and Sons Incorporation, 1992.

[42] Tesche F. M., Ianoz M. V. and Karlsson T., "*EMC Analysis Methods and Computational Models,*" John Wiley and Sons Incorporation, 1997.

[43] Degauque P. and Hamelin J. (Editors), "*Electromagnetic Compatibility,*" Oxford University Press, 1993.

[44] Dorf R. C. (Editor), "*The Electrical Engineering Handbook,*" CRC press, 1998.

[45] The Math Works, Incorporation, USA.

[46] Jeans J., "*The Mathematical Theory of Electricity And Magnetism,*" Cambridge University Press, 1958.

[47] Ramo S. and Whinnery J. R., "*Fields and Waves in Modern Radio,*" John Wiley and Sons Incorporation, 1953.

[48] Schelkunoff S. A., "The Electromagnetic Theory of Coaxial Transmission Lines and Cylindrical Shields," *Bell Systems Techcnical Journal,* Vol. 13, 1934, pp. 532-579.

[49] Schelkunoff S. A., "*Electromagnetic Waves,*" D. Van Nostrand Company Incorporation, 1943.

[50] Nahman N. S. and Holt D. R., "Transient analysis of coaxial cables using the skin effect approximation," *IEEE Transactions on Circuit Theory,* Vol. 19, No. 5, 1972, pp. 443-451.

[51] Wedepohl L. M. and Wilcox D. J., "Transient analysis of underground power-transmission systems: system-model and wave propagation characteristics," *Proceedings of IEE,* Vol. 20, No. 2, 1973, pp. 253-260.

[52] Rachidi F., Nucci C. A., Ianoz M. and Mazzetti M., "Influence of a lossy ground on lightning induced Voltages on overhead lines," *IEEE Transactions on Electromagnetic Compatibility,* Vol. 38, No. 3, 1996, pp. 250-264.

[53] Tesche M., "Comparison of the transmission line and scattering models for computing the HEMP response of overhead cables," *IEEE Transactions on Electromagnetic Compatibility,* Vol. 34, No. 2, 1992, pp. 93-99.

[54] Theethayi N., Liu Y., Montano R. and Thottappillil R., "On the influence of conductor heights and lossy ground in multiconductor transmission lines for lightning interaction studies in railway overhead traction systems," *Journal of Electric Power Systems Research,* Vol. 71, No. 2, 2004, pp. 186-193.

[55] Semlyen A., "Ground Return Parameters of Transmission Lines an Asymptotic Analysis for very High frequencies," *IEEE Transactions on Power Apparatus and Systems,* Vol. 100, No. 3, 1981, pp. 1031-1038.

[56] Wang Y. J. and Liu S. J., "A review of methods for calculation of frequency dependent impedance of overhead power transmission lines," *Proceedings of National Science Council. ROC (A),* Vol. 25, No. 6, 2001, pp. 329-338.

[57] Deri A., Tevan G., Semlyen A. and Castanheira A., "The complex ground return plane a simplified model for homogeneous and multilayer earth Return," *IEEE Transactions on Power Apparatus and Systems,* Vol. 100, No. 8, 1981, pp. 3686-3693.

[58] Sunde E. D., "*Earth conduction effects in the transmission systems,*" Van Nostrand, New York, 1949.

[59] Wait J. R., "Theory of wave propagation along a thin wire parallel to an interface," *Radio Science,* Vol. 7, No. 6, 1972, pp. 675-679.

[60] Essex E. A., "Hertz vector potentials of electromagnetic theory," *American Journal of Physics,* Vol. 45, No. 11, 1977.

[61] Chen K. C. and Damrau K. M., "Accuracy of approximate transmission line formulas for overhead wires," *IEEE Transactions on Electromagnetic Compatibility,* Vol. 31, No. 4, 1989, pp. 396-397.

[62] Rachidi F., Nucci C. A. and Ianoz M., "Transient analysis of multiconductor lines above lossy ground," *IEEE Transactions on Power Delivery,* Vol. 14, No. 1, 1999, pp. 294-302.

[63] Vance E. F., "*Coupling to Cable Shields,*" Wiley Interscience, New York, 1978.

[64] Timotin A. L., "Longitudinal transient parameters of a unifilar line with ground return," *Rev. Roum. Science Technical - Electrotechn. et Energ,* Vol. 12, No. 4, 1967, pp. 523-535.

[65] Orzan D., "Time domain low frequency approximation for the off-diagonal terms of the ground impedance matrix," *IEEE Transactions on Electromagnetic Compatibility,* Vol. 39, No. 1, 1997, pp. 64.

[66] Araneo R. and Celozzi S., "Direct time domain analysis of transmission lines above a lossy ground," *IEE Proceedings on Science and Measurement Technology.,* Vol. 148, No. 2, 2001, pp. 73-79.

[67] Rachidi F., Loyka S. L., Nucci C. A. and Ianoz M., "A new expression for ground transient resistance matrix elements of multiconductor overhead transmission lines," *Journal of Electric Power Systems Research,* Vol. 65, No. 1, 2003, pp. 41-46.

[68] Taflove A. (Editor), "*Computational electrodynamics: the finite difference time domain method,*" Artech House, Boston, 1995.

[69] Gustavsen B. and Semlyen A., "Rational approximation of frequency domain responses by vector fitting," *IEEE Transactions on Power Delivery,* Vol. 14, No. 3, 1999, pp. 1052-1061.

[70] Nielsen H. B., "Damping Parameter in Marquardt's Method," Report IMM-REP-1999-05, Department of Mathematical Modeling, 1999, Technical University of Denmark.

[71] Rachidi F., Nucci C. A., Ianoz M. and Mazzetti C., "Response of multicondcutor power lines to nearby lightning return stroke electromagnetic Fields," *IEEE Transactions on Power Delivery,* Vol. 12, No. 3, 1997, pp. 1404-1411.

[72] Theethayi N., Thottappillil R., Liu Y. and Montano R., "Parameters that influence the crosstalk in multiconductor transmission line," *Conference Proceedings of the 2003 IEEE Bologna Powertech, Bologna,* Italy, paper No. 68.

[73] Theethayi N., Thottappillil R., Liu Y. and Montano R., "Importance of ground impedance in the study of parameters that influence crosstalk in multiconductor transmission lines," *Paper in review at Journal of Electric Power Systems Research, 2005.*

[74] Theethayi N., Liu Y., Montano R., Thottappillil R., Zitnik M., Cooray V. and Scuka V. "A theoretical study on the consequence of a direct lightning strike to electrified railway system in Sweden," *Journal of Electric Power Systems Research,* Vol. 74, No. 2, 2005, pp. 267-280.

[75] Nucci C. A., Deindorfer G., Uman M. A., Rachidi F., Ianoz M. and Mazzetti C., "Lightning return stroke current model with specified channel-base current: A review and comparison," *Journal of Geophysical Research, 95,* 1990, pp. 20395-20408.

[76] Rubinstein M., Tzeng A. Y., Uman M. A., Medelius P. J. and Thomson E. M., "An experimental test of a theory of lightning-induced voltages on an overhead wire," *IEEE Transactions on Electromagnetic Compatibility,* Vol. 31, No. 4, 1989, pp. 376-383.

[77] Rubinstein M., Uman M A., Medelius P. J. and Thomson E. M., "Measurements of the voltage induced on an overhead power line 20 m from triggered lightning," *IEEE Transactions on Electromagnetic Compatibility,* Vol. 36, No. 2, 1994, pp. 134-140.

[78] Nucci C. A., Rachidi F., Ianoz. M, and Mazzetti C., "Comparison of Two coupling models for lightning-induced over Voltage calculations," *IEEE Transactions on Power Delivery,* Vol. 10, No. 1, 1995, pp. 330-339.

[79] Jankov V., "Estimation of the maximal Voltage induced on an overhead line due to the nearby lightning," *IEEE Transactions on Power Delivery,* Vol. 12, No. 1, 1997, pp. 315-324.

[80] Borghetti A., Gutierrez J. A, Nucci C. A., Paolone M., Petrache E. and Rachidi F., "Lightning-induced voltages on complex distribution systems: models, advanced software tools and experimental validation," *Journal of Electrostatics,* Vol.60, No. 2-4, 2004, pp. 163-174.

[81] Paolone M., Nucci C. A., Petrache E. and Rachidi F., "Mitigation of lightning-induced overvotlages in medium Voltage distribution lines by means of periodical grounding of shielding wires and of surge arresters: modeling and experimental validation," Vol. 19, No. 1, 2004, pp. 423-431.

[82] Lin Y. T., Uman M. A., Tiller J. A., Brantley R. D., Beasley W. H., Krider E. P. and Weidman C. D., "Characterization of lightning return stroke electric and magnetic fields from simultaneous two-station measurements," *Journal of Geophysical Research,* Vol. 84, 1979, pp. 6307-6314.

[83] Weidman, C. D., and Krider E. P., "The Fine Structure of Lightning Return Stroke Wave Forms," *Journal of Geophysical Research Letters,* Vol. 7, 1980, pp. 955-958.

[84] Rakov V., "Lightning discharges triggered using rocket- and wire techniques," *Recent Research Developments in Geophysics,* Vol. 2, 1999, pp. 141-171.

[85] Nucci C. A., Rachidi F., Ianoz M. and Mazzetti C., "Lightning-Induced voltages on overhead lines," *IEEE Transactions on Electromagnetic Compatibility,* Vol. 35, No. 1, 1993, pp. 75-86.

[86] Cooray V., "Some considerations on the "Cooray-Rubinstein" formulation used in deriving the horizontal electric field of lightning return strokes over finitely conducting ground," *IEEE Transactions on Electromagnetic Compatibility,* Vol. 44, No. 4, 2002, pp. 560-566.

[87] Thomson E. M., Medelius P. J., Rubinstein M., Uman M. A., Johnson J. and Stone J. W., "Horizontal electric fields from lightning return strokes," *Journal of Geophysical Research,* Vol. 93, No. D3, 1988, pp. 2429-2441.

[88] Uman M. A. and McLain D. K., "Magnetic field of the lightning return stroke," *Journal of Geophysical Research,* Vol. 74, No. 28, 1969, pp. 6899-6910.

[89] Rachidi F. and Nucci C. A., "On the Master, Uman, Lin, Standler and the modified transmission line lightning return stroke current models," *Journal of Geophysical Research,* Vol. 95, No. D12, 1990, pp. 20389-20394.

[90] Rakov V. and Dulzon A. A., "Calculated electromagnetic fields of lightning return strokes," *Tekhnicheskaya Elektrodinamika,* No.1, 1987, pp. 87-89.

[91] Thottappillil R., Schoene J. and Uman M. A., "Return stroke transmission line model for stroke speed near and equal that of light," *Journal of Geophysical Research,* Vol. 28, No. 18, 2001, pp. 3593-3596.

[92] Thottappillil R., Uman M. A. and Theethayi N., "Electric and magnetic fields from a semi-infinite antenna above a conducting plane," *Journal of Electrostatics,* Vol. 61, No. 3-4, 2004, pp. 209-221.

[93] Theethayi N. and Cooray V., "On the representation of the lightning return stroke process as a current pulse propagating along a transmission line," *IEEE Transactions on Power Delivery,* Vol. 20, No. 2, 2005, pp. 823-837.

[94] Theethayi N. and Cooray V., "Representation of the return stroke as a transmission line: the apparent return stroke velocity," *Proceedings of International Conference on Lightning Protection,* 2004, Avignon, France.

[95] Thottappillil R. and Uman M. A., "Comparison of lightning return-stroke models," *Journal of Geophysical Research,* Vol. 98, No. D12, 1993, pp. 22903-22914.

[96] Fano R. M., Chu L. J. and Adler R. B., "*Electromagnetic fields, energy and forces,*" John Wiley and Sons Incorporation, 1960.

[97] Engel T. G., Donaldson A. L. and Kristiansen M., "The pulsed discharge arc resistance and its functional behavior," *IEEE Transactions on Plasma Science,* Vol. 17, No. 2, 1989, pp. 323-329.

[98] Theethayi N., Liu Y., Thottappillil R., Götschl T., Montano R., Lindeberg P. A. and Hellström U., "Measurements of Lightning Transients Entering a Swedish Railway Facility," *Proceedings of International Conference on Lightning Protection,* 2004, Avignon, France.

[99] Theethayi N., Yirdaw T., Liu Y., Götschl T. and Thottappillil R., "Experimental Investigation of Lightning Transients Entering a Swedish Railway Facility," *Paper in review at IEEE Transactions on Power Delivery, 2005.*

[100] Blomqvist A., Danielsson J. and Petersson P., "Project Lightning Flashes," *a project work,* submitted at the Physics Department of Uppsala University, for the course on Computer Based Measuring Techniques, 2003.

[101] Silfverskiöld S., Thottappillil R., Ye M., Cooray V. and Scuka V., "Induced voltages in a low-Voltage power installation network due to lightning electromagnetic fields: An experimental study," *IEEE Transactions on Electromagnetic Compatibility,* Vol. 41, No. 3, 1999, pp. 265-271.

[102] Manyahi M. J., "*Characteristics of surge transfer through transformers. Study of conventional distribution transformer and XLPE cable winding transformer (Dryformer),*" Ph.D. Thesis, ISBN 91-554-5398-8, Uppsala University, 2002.

[103] Bewley L. V., "Theory and tests of the counterpoise," *Electrical Engineering,* Vol. 53, 1934, pp. 1163-1172.

[104] Anderson J. G., "Lightning performance of EHV-UHV lines," *Chapter - 12 in the book: Transmission line reference book 345 kV and above,* Electric Power Research Institute, Fred Weidner and Son printers Incorporation, 1975.

[105] Lee C. H. and Meliopoulos A. P. S., "Comparison of touch and step voltages between IEEE Std 80 and IEC 479 - 1," *IEE Proceedings on Generation, Transmission and Distribution,* Vol. 146, No. 5, 1999, pp. 593-601.

[106] Deindorfer G. and Schulz W., "Lightning incidence to elevated objects on mountains," *Proceedings of International Conference on Lightning Protection,* 1998, Birmingham, England.

[107] Personal communication with Unden G. of FMV, 2003.

[108] Thottappillil R., Scuka V., Zitnik M., Liu Y. and Lövstrand K. G., "Grounding of communication towers for lightning protection," *Proceedings of International Conference on Lightning Protection,* Cracow, Poland, 2002.

[109] Thottappillil R. and Theethayi N., "Lightning strikes to tall towers, with implications to electromagnetic interference," *Proceedings of RVK 05 conference,* 2005, Linköping, Sweden.

[110] Theethayi N. and Thottappillil R., "Lightning current pulse propagation in underground wires - a transmission line analysis: Part I- Simple expressions for external wire impedance and admittance," *Paper in review at IEEE Transactions on Power Delivery, 2004.*

[111] Theethayi N. and Thottappillil R., "Lightning current pulse propagation in underground wires - a transmission line analysis: Part II- Time domain simulations for sensitivity analysis," *Paper in review at IEEE Transactions on Power Delivery, 2004.*

[112] Theethayi N. and Thottappillil R., "Pulse propagation in underground wires - A transmission line analysis," *Proceedings of RVK 05 conference,* 2005, Linköping, Sweden.

[113] Bridges G. E., "Fields generated by bare and insulated cables buried in a lossy half-space," *IEEE Transactions on Geoscience and Remote Sensing,* Vol. 30, No.1, 1992, pp.140-146.

[114] Petrache E., "*Lightning electromagnetic field coupling to overhead transmission line networks and to buried cables,*" Ph. D thesis, No. 3024, Swiss Federal Institute of Technology, Lausanne, Switzerland, 2004.

[115] Pollaczek F., "Über das feld einer unendlich langen wechsel stromdurchflossenen Einfachleitung," *Electrishe Nachrichten Technik,* Vol. 3, No. 9, 1926, pp. 339-360.

[116] Pollaczek F., "Sur le champ produit par un conducteur simple infiniment long parcouru par un courant alternatif," *Review of General Electric,* Vol. 29, 1931, pp. 851-867.

[117] Saad O., Gaba G. and Giroux M., "A closed-form approximation for ground return impedance of underground cables," *IEEE Transactions on Power Delivery* Vol. 11, No. 3, 1996, pp. 1536-1545.

[118] Dommel H. W., "Overhead line parameters from handbook formulas and computer programs," *IEEE Transactions on Power Apparatus and Systems,* Vol. 104, 1985, pp. 366-372.

[119] Dommel H. W., "*Electromagnetic transients program (EMTP theory book),*" Bonneville Power Administration, 1986.

[120] Chen K. C., "Transient Response of an Infinite Wire in a Dissipative Medium," *Interaction notes on EMP and related subjects,* Dr. C. E. Baum, Editor, IN453, 2001.

[121] Wait J. R., "Electromagnetic wave propagation along a buried insulated wire," *Canadian Journal of Physics,* Vol. 50, 1972, pp. 2402-2409.

[122] Meyer W. S. and Liu T., "*Alternative Transient Program (ATP) rule book,*" by Canadian/American EMTP user group, 1987-1992.

[123] Geri A. and Visacro S. F., "Grounding systems under surge conditions: comparison between a field model and circuit model," *Proceedings of International Conference on Lightning Protection,* 2002, Cracow, Poland.

[124] Grcev L. D., "Computer analysis of transient voltages in large grounding systems," *IEEE Transactions on Power Delivery,* Vol. 11, No. 2, 1996, pp. 815-823.

[125] Liu Y., "*Transient response of grounding systems caused by lightning: Modeling and Experiments,*" PhD Thesis, ISBN 91-554-6041-0, Uppsala University, 2004.

[126] Dawalibi F. P. and Southey R. D., "Analysis of electrical interference from power lines to gas pipe lines. I. Computational methods," *IEEE Transactions on Power Delivery,* Vol. 4, No. 3, 1989, pp. 1840 - 1846.

[127] Farag A. S., Cheng T. C. and Penn D., "Grounding terminations of lightning protective systems," *IEEE Transactions on Dielectrics and Electrical Insulation,* Vol. 5, No. 6, 1998, pp. 869-877.

[128] http://www.elfa.se, March 2005.

[129] Stern R. B., "Time domain calculation of electric field penetration through metallic shields," *IEEE Transactions on Electromagnetic Compatibility,* Vol. 30, No. 3, 1988, pp. 307-311.

[130] General Radio 1658 RLC Digibridge, Form: 1658-0120-D.

[131] http://www.draka.se, March 2005

[132] Mazloom Z., "*Transfer impedance and transmission line parameters of multi-conductor cables,*" ISSN: 1401-5757, UPTEC F05 055, Teknisk - naturvetenskaplig fakultet UTH - enheten, Uppsala University, 2005.

[133] Agrawal A. K., Lee K. M., Scott L. D and Fowles H. M., "Experimental characterization of multicondcutor transmission lines in the frequency domain," *IEEE Transactions on Electromagnetic Compatibility,* Vol. 21, No. 1, 1979, pp. 20-27.

[134] Agrawal A. K., Scott L. D and Fowles H. M., "Experimental characterization of multicondcutor transmission lines in inhomogeneous media using time domain techniques," *IEEE Transactions on Electromagnetic Compatibility,* Vol. 21, No. 1, 1979, pp. 28-32.

[135] Schaffner Holding AG, Switzerland.

[136] Morched A., Marti L. and Ottevangers J., "A high frequency transformer model for EMTP," *IEEE Transactions on Power Delivery,* Vol. 8, No.3, 1993, pp. 1615-1626.

[137] Høidalen H. K., "*Lightning-induced over voltages in low-voltage systems,*" PhD Thesis, ISBN 82-471-0177-7, NTNU Trondheim, 1997.

[138] Bobrow L. S., "*Elementary linear circuits analysis*" Oxford University Press, Oxford University Press Incorporation, 1987.

[139] Cipparrone F. A. M., "Discussion on Enforcing passivity for admittance matrices approximated by rational functions," *IEEE Transactions on Power Delivery,* Vol. 16, No. 4, 2001, pp. 954-955.

[140] Gustavsen B. and Semlyen A., "Closure to discussion of Enforcing passivity for admittance matrices approximated by rational functions," *IEEE Transactions on Power Delivery,* Vol. 16, No. 4, 2001, pp. 955.

[141] Thottappillil R., Theethayi N., Liu Y., Scuka V., Lindeberg P. A. and Hellström U., "Computer simulation model for Swedish railway systems for evaluating the effects of lightning and EMI," *Poster presented at the World Congress on Railway Research, conference proceedings, topic. Interactive systems and environment, session. EMC,* abstract no. P 070, 2003, Edinburgh, England.

Acta Universitatis Upsaliensis

Digital Comprehensive Summaries of Uppsala Dissertations from the Faculty of Science and Technology 76

Editor: The Dean of the Faculty of Science and Technology

A doctoral dissertation from the Faculty of Science and Technology, Uppsala University, is usually a summary of a number of papers. A few copies of the complete dissertation are kept at major Swedish research libraries, while the summary alone is distributed internationally through the series Digital Comprehensive Summaries of Uppsala Dissertations from the Faculty of Science and Technology. (Prior to January, 2005, the series was published under the title "Comprehensive Summaries of Uppsala Dissertations from the Faculty of Science and Technology".)

Distribution: publications.uu.se
urn:nbn:se:uu:diva-5889

ACTA
UNIVERSITATIS
UPSALIENSIS
UPPSALA
2005